Title
Development And Experimental Evaluation Of Autonomous Vehicles For Roadway/vehicle Cooperative Driving

Author
Ioannou, Petros

Publication Date
1998

CALIFORNIA PATH PROGRAM
INSTITUTE OF TRANSPORTATION STUDIES
UNIVERSITY OF CALIFORNIA, BERKELEY

Development and Experimental Evaluation of Autonomous Vehicles for Roadway/Vehicle Cooperative Driving

Petros Ioannou
University of Southern California

California PATH Research Report
UCB-ITS-PRR-98-9

This work was performed as part of the California PATH Program of the University of California, in cooperation with the State of California Business, Transportation, and Housing Agency, Department of Transportation; and the United States Department of Transportation, Federal Highway Administration.

Report for MOU 248

February 1998

ISSN 1055-1425

Development and Experimental Evaluation of Autonomous Vehicles for Roadway/Vehicle Cooperative Driving

by
Petros A. Ioannou
Final Report MOU# 248 (Former MOU# 164)
Sept. 26, 1997

Development and Experimental Evaluation of Autonomous Vehicles for Roadway/Vehicle Cooperative Driving

by
Petros A. Ioannou
Final Report MOU# 248 (Former MOU# 164)
Sept. 26, 1997

This work was performed as a part of the California PATH Program of the University of California, in cooperation with the State of California Business, Transportation, and Housing Agency, Department of Transportation; and the United States Department of Transportation, Federal Highway Administration.

Table of Contents

Executive Summary

This is the final report for the project entitled "Development and Experimental Evaluation of Autonomous Vehicles for Roadway/Vehicle Cooperative Driving" in response to the contractual requirements of the Memorandum of Understanding MOU# 164/248, between the Partners of Advanced Transit and Highways (PATH) and the University of Southern California, administered at the University of California at Berkeley.

The original MOU# 164 was a two year project and became MOU# 248 in the second year. A final report for MOU# 164 entitled "Vehicle Following Control Design for Automated Highway Systems" by H. Raza and P. Ioannou was submitted to PATH in July 1996. For the sake of completeness the final report for MOU# 164 is included as part I of this report in order to provide continuity since the division of the project into two MOU's was not based on technical factors.

The purpose of the project was to study the development and evaluation of Autonomous Intelligent Cruise Control (AICC) systems that could be used as a part of an intelligent roadway/vehicle system to improve traffic flow rates. The design, analysis and simulation parts of the project were performed at the Center of Advanced Transportation Technologies at the University of Southern California. The experiments with actual vehicles were performed at the PATH, Richmond fields facility, on I-15 North of San Diego and at the Crow's landing facility near Patterson, California.

The work performed under this project is presented in the form of three reports presented in part I, II, and III of this final report. In addition to these reports a video tape showing scenes of the vehicle following experiments performed is included. The video tape is not a professional one and is developed by students that participated in these experiments. Below we summarized the results and conclusions developed under this project. The details are presented in parts I to III.

In part I entitled "Vehicle Following Control Design for Automated Highway Systems" we present the work of the first year of the project that was referred to as MOU# 164. This work is an integral part of the second year of the project that was renamed MOU# 248. In this work we designed and tested a controller that provides the required intelligence for several modes of

operation of infrastructure managed vehicle following. The supervisory controller processes the inputs from the driver, the infrastructure, the surrounding vehicles and the on-board sensors and sends the appropriate commands to the brake and throttle controllers. It makes decisions about normal, emergency and transition operations so that the resulting motion of the vehicle is safe and efficient. The logic and throttle/brake control algorithms for normal and emergency AICC modes, roadway to vehicle and vehicle to vehicle communications as a part of a cooperative driving system are presented and simulated. Emphasis was put on the emergency situation assessment part and on the stability and performance of the overall system. Simulations are used to demonstrate the effectiveness of the proposed supervisory controller. Parts of this controller were successfully tested using two PATH vehicles on I-15. The vehicles were equipped with a throttle actuator and had vehicle to vehicle communication capability.

In part II a more extensive set of vehicle experiments performed at the Crow's landing facility near Patterson, California using three PATH vehicles is presented. The vehicles had both throttle and brake actuators and vehicle to vehicle communication capability. In this case a complete roadway/vehicle cooperative driving system was tested. The roadway to vehicle communication capability was simulated in the software since it was not available in the testing facility. In addition scenes from the vehicle experiments are presented in the attached video tape.

While parts I and II of the report concentrate on the microscopic aspect of a cooperative driving system, part III deals with the macroscopic aspect of the system. That is, it deals with the characteristics of traffic flow of vehicles in a cooperative driving system. Since traffic flow may be the result of different modes of operation a neural network technique is developed that continuously learns about the characteristics of traffic flow. Based on these learned characteristics a roadway controller is designed to control the flow of traffic by issuing speed commands to vehicles in the various sections of the highway. Even though the method is developed for a single lane its extension to multiple lanes is trivial. The method is very flexible and is applicable to different types of automated traffic and roadway geometries.

The conclusion of this project is that the design of autonomous vehicles for roadway/vehicle cooperative driving is feasible. Our analysis and simula-

tions suggest that the development of such a cooperative driving system will have significant beneficial effects on the characteristics of traffic flow especially during accidents and other traffic disturbances. The system is designed with reasonable safety constraints and with the appropriate logic to handle emergencies. The human factors issues, however, that may have a significant effect on safety were not studied since they were not part of the project.

Vehicle Following Control Design for Automated Highway Systems*

H. Raza and P. Ioannou
Dept. of Electrical Engineering-Systems
University of Southern California
Los Angeles, CA 90089-2562

Abstract.

Automatic vehicle following is an important feature of a fully or partially automated highway system (AHS). The on-board vehicle control system should be able to accept and process inputs from the driver, the infrastructure and other vehicles, perform diagnostics and provide the appropriate commands to actuators so that the resulting motion of the vehicle is safe and compatible with the AHS objectives. The purpose of this paper is to design and test a vehicle control system in order to achieve full vehicle automation in the longitudinal direction for several modes of operation, where the infrastructure manages the vehicle following. These modes include autonomous vehicles, cooperative vehicle following and platooning. The vehicle control system consists of a supervisory controller that processes the inputs from the driver, the infrastructure, other vehicles and the on-board sensors and sends the appropriate commands to the brake and throttle controllers. In addition, the controller makes decisions about normal, emergency and transition operations. Simulation results of some of the basic vehicle following maneuvers are used to verify the claimed performance of the designed controllers. Experiments on I-15 that demonstrate the performance of the throttle controller with and without vehicle-to-vehicle communications in an actual highway environment are also included.

Keywords: Vehicle Control, Automated Highway Systems, Automatic Vehicle Following, Supervisory Control.

*This work is supported by the California Department of Transportation through PATH of the University of California. The contents of this paper reflect the views of the authors who are responsible for the facts and accuracy of the data presented herein. The contents do not necessarily reflect the official views or policies of the State of California or the Federal Highway Administration. This paper does not constitute a standard, specification or regulation.

Executive Summary

In this paper the problem of design of on-board vehicle intelligence for achieving full vehicle automation in the longitudinal direction is addressed. The on-board intelligence is an essential part of any vehicle following scheme for a fully or partially automated highway system to provide the necessary interface between the vehicle subsystem controllers and the external agents.

A supervisory controller is designed to provide the required intelligence for several modes of operation of infrastructure managed vehicle following. The supervisory controller processes the inputs from the driver, the infrastructure, surrounding vehicle and on-board sensors and sends the appropriate commands to the brake and throttle controllers. It makes decisions about normal, emergency and transition operations so that the resulting motion of vehicle is safe and follows AHS objectives. Simulation results are used to test the performance of the designed controllers. Finally, the experimental results of a vehicle following test conducted on I-15 demonstrates the effectiveness of the controller in an actual highway environment.

Contents

1 Introduction

One of the objectives of Automated Highway Systems (AHS) is to meet the increasing demand for capacity by the efficient utilization of the existing infrastructure. Capacity is calculated by the simple formula:

$$C = \frac{V}{X_r + L} \tag{1}$$

where C is the capacity, measured in number of vehicles crossing a fixed point/unit time, V is the vehicular speed of flow, X_r is the inter-vehicle spacing and L is the vehicle length. The capacity formula (1) is derived by assuming that all vehicles have the same length L, keep the same inter-vehicle spacing X_r and follow the same speed V. The capacity C can

be viewed as the maximum possible flow rate q for a given speed V, inter-vehicle spacing X_r and vehicle length L. While the traffic flow rate may exceed C during transients by violating the maximum allowable V or minimum allowable X_r, in an AHS environment such violations have to be reduced or eliminated for safety considerations. Therefore in AHS q has to be kept less than or equal to C during transients and C should be the desired value q should converge to in steady state. These constraints give rise to the following requirements: (i) The system should be designed for maximum capacity under the constraints of safety. (ii) The system should be designed so that the actual traffic flow rates tend to the maximum capacity at steady state and transients are not excessive and are not due to the violation of safety constraints on the vehicle level.

The first requirement can be met by using the safety considerations to decide about the maximum allowable speed V and minimum inter-vehicle spacing X_r [1]. The second requirement can be met by designing the vehicle following control system properly, getting the infrastructure involved in managing traffic flow on the macroscopic level, minimizing disturbances due to lane changing and by choosing the appropriate configurations for the roadway system [2, 3, 5].

The purpose of this paper is to concentrate on the design of the vehicle longitudinal control system (VLCS) that will guarantee smooth and safe vehicle following. In an AHS environment the VLCS should be able to accept and process inputs from the driver, infrastructure, other vehicles in the vicinity as well as from its own sensors. The VLCS is designed for intelligent cruise control (ICC) applications, cooperative driving and platooning. In ICC the vehicle is autonomous in the sense that it does not communicate with the infrastructure and/or other vehicles. In cooperative driving the VLCS may accept inputs from the vehicles in front and the infrastructure, whereas in platooning the VLCS has to process inputs from the leader of the platoon as well as from the infrastructure and other vehicles. These three different modes of operation may be necessary in AHS and the design of a VLCS to operate in each chosen mode is therefore essential.

The VLCS consists of a supervisory controller which is the "brain" of the system and a throttle/brake controller. Since several throttle/brake controllers have already been proposed and tested [6-11], the emphasis of the paper is on the supervisory controller and its interaction with the various inputs and throttle/brake controller. The design of the supervisory controller is similar to the design concept of event driven state machine control. The design objective is to replace the human driver functions in the longitudinal direction. The throttle and brake controllers are used both in normal as well as in emergency situation to give complete automation in the longitudinal direction.

The emergency situation handling logic, as a part of the supervisory controller, is designed on the principles used by the human drivers to handle emergencies. It comprises a situation assessment logic to detect the presence of emergencies, and a compensation logic

to handle emergencies of different severities. The effectiveness of this scheme relies on the quality of the sensors and actuators that can provide low detection and actuation delays. In addition, the supervisory controller chooses the mode of operation and handles the transitions from manual to automatic and vice-versa.

The paper is organized as follows: Some of the possible AHS configurations are discussed in section 2. The concept of vehicle longitudinal control design and a detailed description of the design of supervisory controller is presented in section 3. The stability and performance analysis of the overall closed loop system is given in section 4. A sufficient condition for stability of platoon of vehicles is developed in the same seciton. In section 5, the simulation and experimental results for different vehicle following scenarios are discussed. The paper ends with the main results summarized in the conclusion section.

Basic Notation

AVF	automatic vehicle following
ICC	intelligent cruise control
VLCS	vehicle longitudinal control system
a	acceleration of the vehicle (m/sec^2)
h	time headway (sec)
V	speed of the vehicle (m/sec)
$\mathcal{B}_{sub}$	boolean variables, sub identifies each variable
h_{sub}	variables associated with headway
V_{sub}	variables associated with speed

2 AHS Configuration and Modes of Operation

A general AHS configuration that captures a wide class of AHS concepts is shown in Figure 1, where the infrastructure may issue speed and headway commands to the vehicles, in an effort to produce uniform and homogeneous traffic flow conditions, which in turn can guarantee stable and higher traffic flows [12]. In this configuration a distributed control is exercised, where the control loop contains part of the infrastructure as well as the vehicle itself. In terms of the classification defined in [13], the complete control hierarchical structure is shown in Figure 2. The structure is defined in terms of different layers, the network and link layer lies with the infrastructure, whereas the coordination, regulation and physical layers reside in the vehicle.

In terms of the structure shown in Figure 2, the infrastructure control consists of the network and link layer or roadway controller. The network controller optimizes the opera-

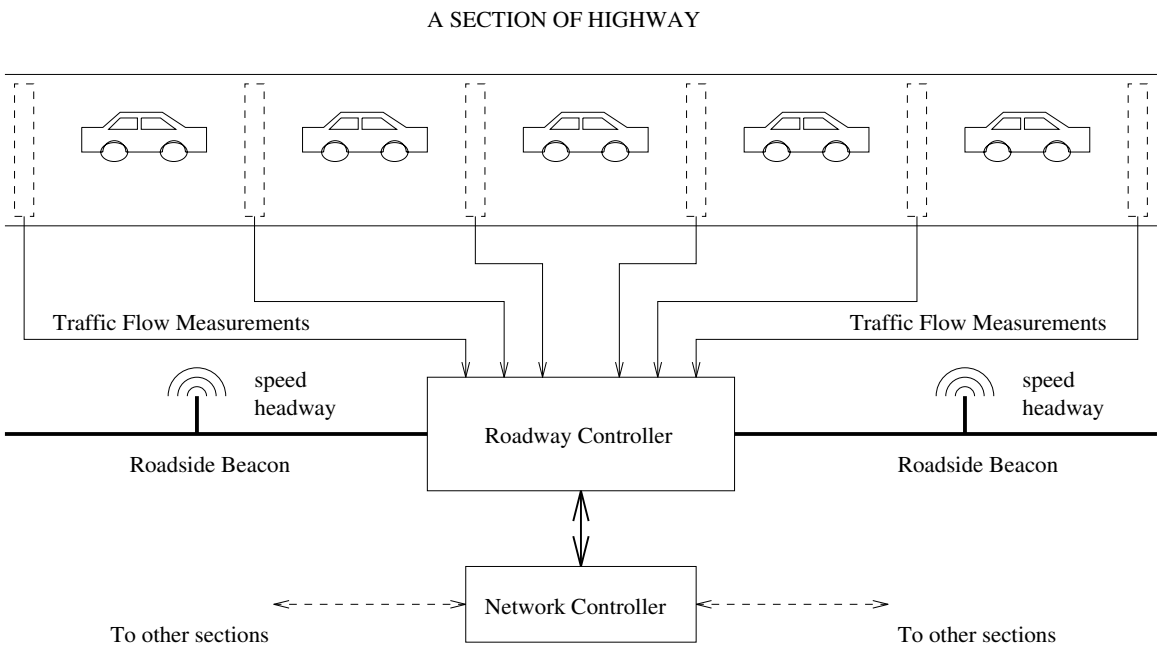

Figure 1: An AHS configuration.

tion of the traffic network by issuing routing instructions, traffic synchronization commands and by providing desired traffic distributions for the various branches of the network to the link layer or roadway controllers. The roadway controller manages a branch of the network such as a large section of the highway. It receives desired traffic density distributions from the network controller, traffic flow measurements from the section and issues speed and headway commands to the vehicles in its section, in order to change the traffic density to the desired one. The speed and headway commands can be transmitted by using the road side beacons (see Figure 1) or other communication techniques.

The vehicles operating in the AHS configuration of Figure 1 are equipped with the appropriate control systems that allow them to respond to the roadway commands as well as to the commands of the driver (during transitions). In addition the on-board control systems have to be able to process the information received from their own sensors and depending on the mode of operation communicate and coordinate maneuvers with other vehicles.

The on-board control system includes the coordination and regulation layers shown in Figure 2. The coordination layer consists of a supervisory controller that is responsible for self-diagnostics, recognizing the desired mode of operation, communicating with the link layer, other vehicles and the driver and issuing appropriate commands to the regulation layer. The regulation layer consists of the throttle, brake and steering controllers that are

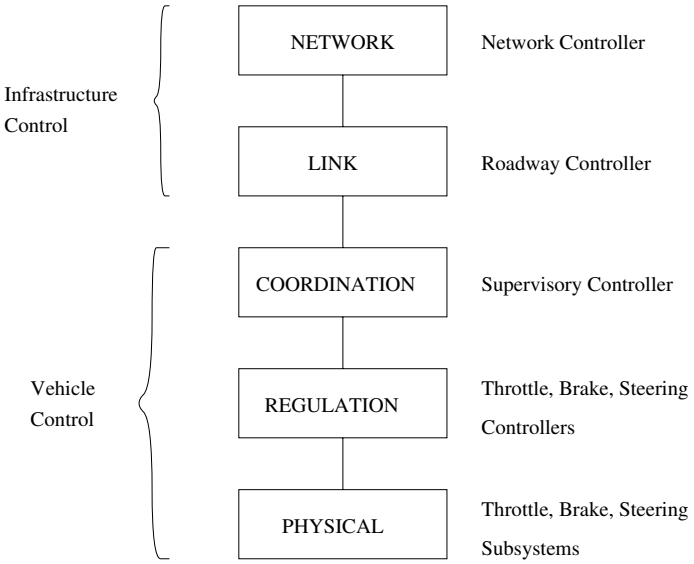

Figure 2: Distributed control structure for infrastructure managed vehicle control.

activated by the supervisory controller and generate the appropriate commands to the actuators that reside in the physical layer.

In this paper we concentrate on the coordination layer by designing the structure of the supervisory controller for longitudinal control that may be used for several modes of vehicle following operations described in the following subsections.

2.1 Intelligent Cruise Control (ICC)

Intelligent cruise control (ICC) is a near term device that will allow automatic vehicle following under the possible supervision of the driver. In this case the driver sets the desired speed and headway and passes the task of vehicle following to the ICC system. The driver is responsible for steering and for recognizing and responding to emergencies. The roadway in this case may issue desired speeds to the driver using road signs etc.

The supervisory controller accepts and responds to the driver inputs, it monitors its onboard sensors, performs diagnostics and sends the appropriate commands to the throttle and brake controllers.

2.2 Cooperative Driving (no v-v communication)

In this mode of operation, the roadway to vehicle communication capability is added to the ICC system. The roadway controller can now send speed commands to the supervisory controller directly in order to control the traffic density along the highway lanes. The

driver's role and responsibility remains the same as in the ICC mode, except that he/she is not allowed to set the desired speed.

With this mode of operation the supervisory controller should be able to communicate and respond to the roadway commands in addition to responding to the inputs associated with the ICC mode.

2.3 Cooperative Driving (with v-v communication)

The addition of vehicle to vehicle (v-v) communication capability allows the vehicles to communicate with the neighboring vehicles in order to negotiate and coordinate maneuvers, inform vehicles about braking capabilities, acceleration, deceleration maneuvers etc. This extra capability can be fully exploited if the ICC system is upgraded to detect and handle emergencies in the longitudinal direction. Since the control system becomes responsible for emergencies, the headway is no longer selected by the driver but is chosen by the on-board control system.

For this mode of operation the supervisory controller should be able to handle and interpret the communications with other vehicles, detect and handle emergencies in the longitudinal direction in addition to the tasks associated with cooperative driving without v-v communications. One of the important tasks of the supervisory controller is to process all the available inputs and information and select the appropriate headway in order to guarantee collision free vehicle following. In addition, the task of transition from automatic to manual is handled in a way that does not put the driver in a situation he/she cannot safely handle.

2.4 Platooning

When the vehicles are capable of communicating with each other and the roadway in addition to being able to follow each other in the longitudinal direction, it may make sense to organize them in a way that improves capacity without affecting safety. It has been proposed in [13] that the organization of vehicles in platoons of 10 to 20 with small intra-platoon but larger inter-platoon spacing (see Figure 3) will increase capacity considerably. The organization of vehicles in platoons allows the roadway to treat each platoon as a single entity and therefore eases the requirements on the bandwidth of roadway to vehicle communication system. Therefore, instead of communicating with each vehicle independently, it communicates with the leader of each platoon. The platoon leader in turn communicates with its vehicles in order to make sure the whole platoon operates as required according to the roadway commands and the traffic conditions. Since each vehicle could become a leader the supervisory controller should be designed to handle the case where the vehicle is a follower and a member of platoon as well as the case where the vehicle is a platoon leader.

The reasons for considering different modes of operation are the following:

1. The vehicle should be able to operate on non-AHS facilities. Since the ICC system is developed independent of AHS, the AHS vehicle should be able to operate as any other vehicle equipped with ICC on non-AHS facilities.
2. During certain failures or traffic conditions platooning may not be the most appropriate mode of operation and the system may have to operate in the cooperative driving or even ICC mode.

3 Vehicle Longitudinal Control Design

The block diagram of the Vehicle Longitudinal Control System (VLCS) is shown in Figure 4. The supervisory controller accepts inputs from the roadway, driver, other vehicles and its on-board sensors. It processes these inputs and performs some or all of the following tasks:

1) Determines the current mode of operation, i.e., ICC, cooperative driving, platooning etc.
2) Performs the transition operation, from manual to automatic and back to manual.
3) Selects the desired headway and speed for normal operating conditions.
4) Detects and handles emergency situations in cooperative driving and platooning.

The design objective of the supervisory controller is to smoothly execute these tasks without risking the safety and comfort of the occupants. The details of these tasks are given in the following subsections. A detailed block diagram of the proposed supervisory controller is shown in Figure 5.

3.1 Selection of AHS Mode

The different modes of operation of AHS are classified in terms of distribution of authority between the driver and external agents, such as infrastructure, platoon leader and surrounding vehicles. Since the vehicle will be using some means to communicate with the roadway and other vehicles, it is safe to assume that these signals will be tagged or labeled to identify the source of information. Hence the logical way for determining the mode of operation of AHS is to detect the presence or absence of certain input signals.

In case no speed and headway commands are received from the roadway or platoon leader and no communication is established from the leading vehicle, ICC mode is selected. In case speed commands are received from the roadway only and no communication is detected from the platoon leader/leading vehicle, cooperative mode with no v-v communication is selected. Similarly other operating modes are selected based on the presence of necessary commands from the external agents discussed in the previous section.

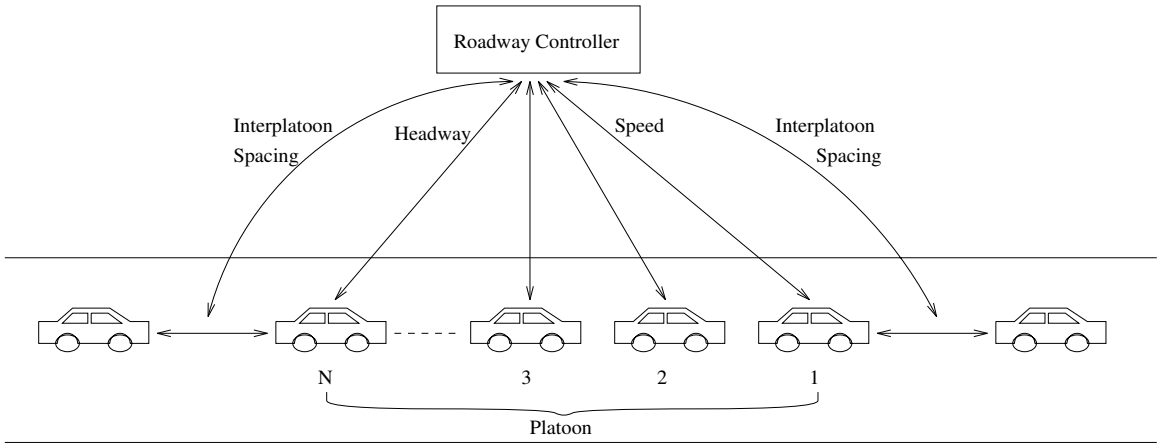

Figure 3: Platooning of vehicles as one possible mode of operation of AHS.

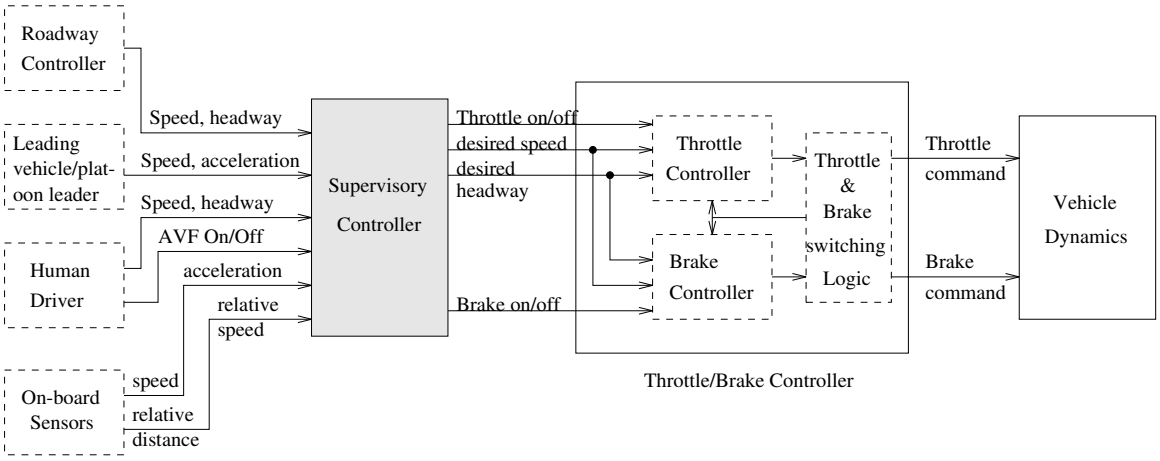

Figure 4: Vehicle longitudinal control system.

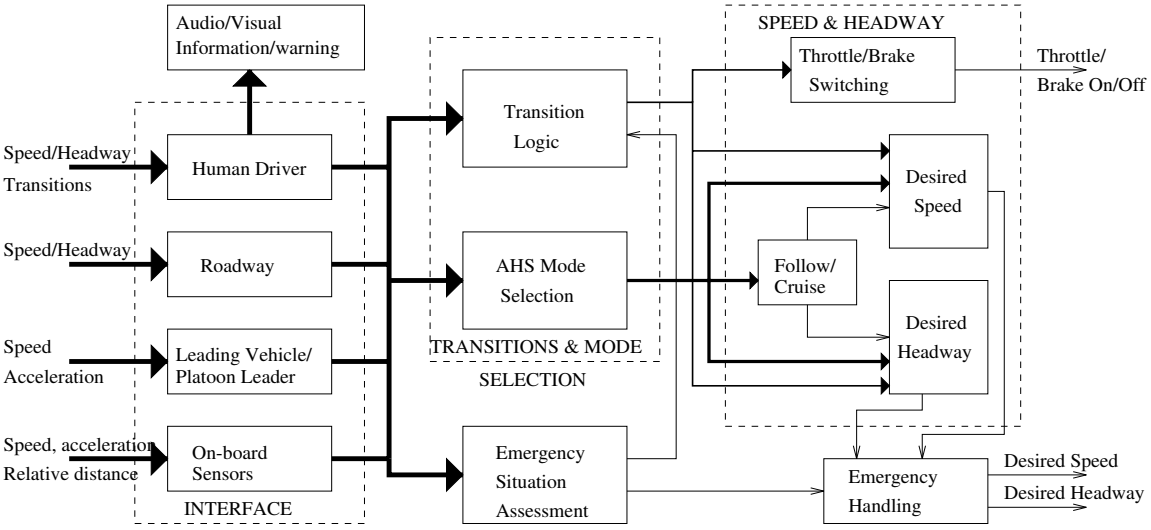

Figure 5: Detailed structure of the supervisory controller.

3.2 Transitions

The driver initiates the transition by giving the "automatic vehicle following (AVF) on" or "AVF off" input to the driver interface module of the supervisory controller. The driver interface module assigns a value to the signal $\mathcal{B}_{D_{on}}(.)$ to be used by the transition logic as shown by the flowchart in Figure 6.

The transition module uses two logical signals $\mathcal{B}_{D_{on}}(.)$, $\mathcal{B}_S(.)$ and on-board sensor readings to decide if the requested transition operation is safe to execute. For transition from manual to automatic, the driver selects the "AVF on" command that assigns a value of 1 to the signal $\mathcal{B}_{D_{on}}$. The transition module then checks the working status of all subsystems and assigns the value $\mathcal{B}_S = 1$ if the system is free of faults, otherwise $\mathcal{B}_S = 0$ is assigned. The checking of operating status of the system is a continuous process of self diagnostics using sensor measurements and fault detection algorithms, hence the automatic mode is transitioned to manual at any time a serious fault is detected.

At the end of trip, the driver initiates the automatic to manual transition process by giving "AVF off" command. This switching process involves the steps that are taken to make the driving conditions suitable for human capabilities. This is achieved by slowing down the vehicle and increasing the headway, so that the driver can easily drive the vehicle off the auto lane. The output of transition logic, $\mathcal{B}_{A_{on}}$, which shows the status of AVF, is

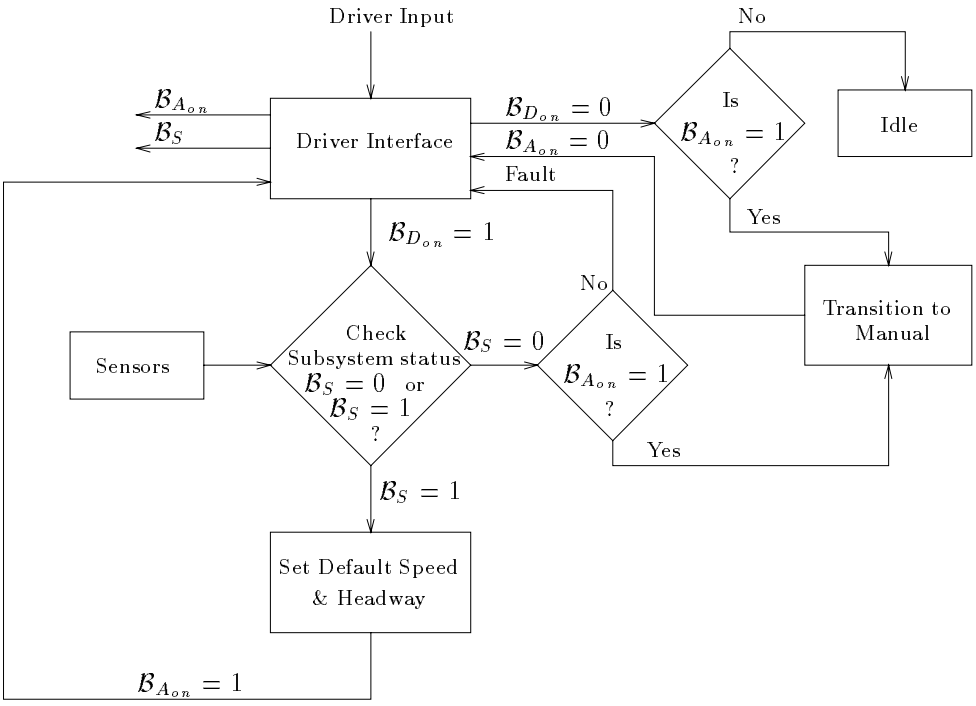

Figure 6: Logic for transitions.

a logical signal having values $\{1, 0\}$ and is given as:

$$\mathcal{B}_{A_{on}}(k) = \begin{cases} 1 & \text{if } \mathcal{B}_{D_{on}}(k) = 1 \text{ and } \mathcal{B}_S(k) = 1 \\ 0 & \text{if } (\mathcal{B}_{D_{on}}(k) = 0 \text{ or } \mathcal{B}_S(k) = 0) \text{ and } (h(k) \geq h_{max} \text{ and } V(k) \leq V_{max}), \end{cases} \tag{2}$$

where V, h are the vehicle speed and headway respectively, V_{max} and h_{max} are the design constants and k represents the sampling instant. As given in (2) the current speed and headway are checked against certain thresholds, speed and headway are progressively increased by speed and headway selection logic till they reach the required limits. It should be noted that the process of transition from manual to automatic is the same for all modes of AHS, however, the transition back to manual mode may be different for each mode. Such as the thresholds V_{max}, h_{max} will be different for ICC than the cooperative driving and platooning. The requirement of making the driving conditions suitable for human drivers is more strict in modes of AHS where the driver is not responsible for emergency handling, such as cooperative driving with v-v communication and platooning.

3.3 Automatic Vehicle Operation

After AVF is switched on, i.e., when the transition logic has the output $\mathcal{B}_{A_{on}} = 1$, the supervisory controller proceeds with the selection of the mode of automatic vehicle operation. Two different modes of automatic vehicle operation are possible and are determined by the presence or the absence of a valid target. If there is a vehicle or obstacle, referred to as target, within the designated sensing range then the supervisory controller will choose the follow mode and if there is no target the controller will choose the cruise mode as shown in Figure 7.

The conditions for a valid target are the following:

(i) The target is within a designated range that is chosen a priori based on safety considerations.
(ii) The speed of the target is less than the speed selected by the driver (in ICC mode), or the roadway/platoon leader commanded speed (in cooperative driving/platooning mode).

If either of these two conditions is violated, the vehicle in front is not considered to be a valid target to follow. The conditions given above can be combined to form a "follow target" condition $\mathcal{B}_F(.)$ as:

$$\mathcal{B}_F(k) = \begin{cases} 1 & \text{if } \mathcal{B}_{A_{on}}(k) = 1 \text{ and } [\{h(k) < h_t \text{ and } (V_l(k) < V_C(k) + \Delta_1)\} \text{ or} \\ & \{(V_l(k) < V_C(k) + \Delta_2) \text{ and } \mathcal{B}_F(k-1) = 1\}] \\ 0 & \text{else,} \end{cases} \tag{3}$$

where h_t is the threshold for headway calculated from the sensing range, V_l is the speed of the leading vehicle, V_C is the roadway or driver commanded speed and Δ_1, $\Delta_2 > 0$ are

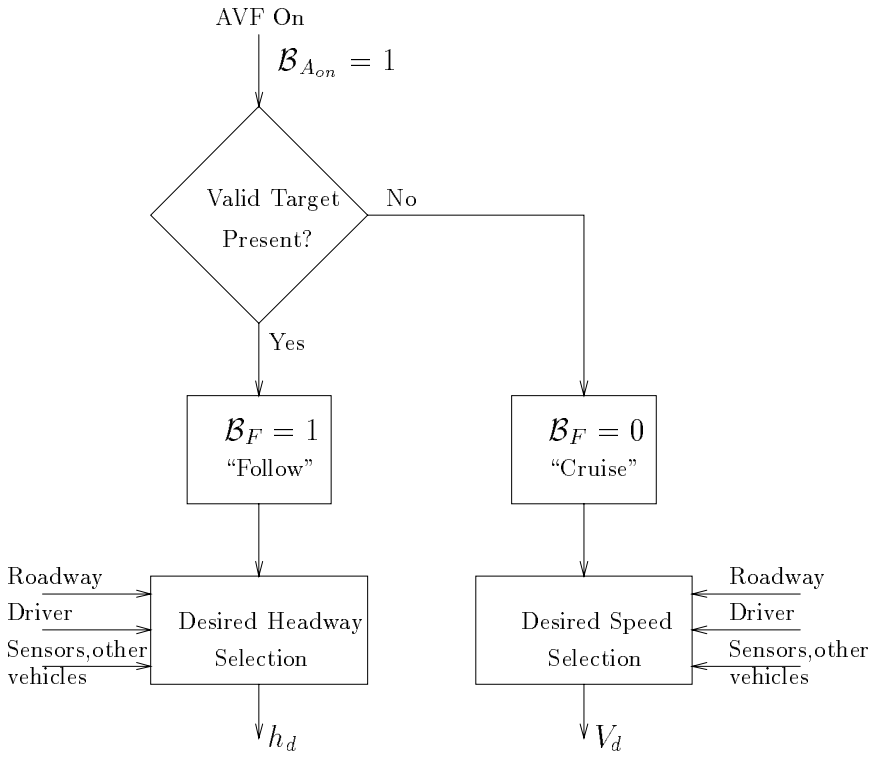

Figure 7: Operating mode selection logic.

design constants. In (3) $\Delta_2 > \Delta_1$ is used to avoid the unnecessary switching of the targets caused by the transients and/or sensor noise, hence if the target was previously being followed, then a larger fluctuation in target speed is tolerated. The design constants Δ_1, Δ_2 may be different for different modes of AHS, similarly the commanded speed V_C is different for each mode, e.g., V_C is the speed commanded by the driver in ICC mode and so on.

As shown in Figure 7, if the vehicle is in follow mode the supervisory controller has to select a safe headway. The calculation of the safe headway is done by the headway selection logic, which uses the inputs from the driver, roadway and other vehicles for different modes of AHS. In the follow mode the desired speed is the speed of the leading vehicle. Similarly if the vehicle is cruising, the safe cruising speed is calculated by the speed selection logic. The process of safe headway and speed selection is explained in the following subsections.

3.4 Desired Headway Selection

After AVF is switched on and the vehicle is operating in the follow mode, the desired headway selection logic has to initialize the system with a safe headway. This initializing value is taken to be the same as the actual headway $h(.)$, irrespective of the mode of

operation of AHS. After this initialization sequence, the headway selection logic allows the driver or the external agents to change the desired headway as long as this change does not risk the safety of the system. A logical structure of this selection process in shown in Figure 8. The switching logic shown in Figure 8 contains all of the decision making process for desired headway calculation. It generates the desired headway h_i as a nonlinear function of its inputs. A filter $D(z)$ is used to generate the filtered version of the desired headway h_d. The details of different tasks performed by the headway selection module are given below. These tasks are different for each mode of operation of AHS and will be defined separately.

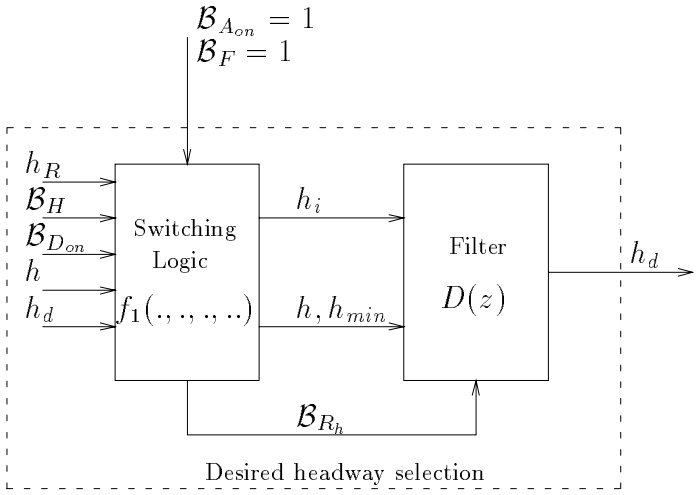

Figure 8: Block diagram of the desired headway calculation.

ICC and Cooperative Driving without v-v Communication

The state diagram of switching logic for this case is shown in Figure 9. A "headway reset" operation is performed during initialization or whenever the "follow" mode is switched on. During this the value of $h_d(.)$ is chosen to be the current headway $h(.)$ as long as it is greater than the minimum allowable headway h_{min}. This task is performed irrespective of the mode of operation of AHS and ensures that there are no large transients, even though the conditions at switching are not close to the desired ones. Hence the value of $h_d(.)$ during reset operation is:

$$h_d(k) = \max(h(k), h_{min}) \quad \text{if} \quad \mathcal{B}_{R_h}(k) = 1, \tag{4}$$

where $\mathcal{B}_{R_h}(.)$ is the condition used to trigger the headway reset operation. As pointed out before that a resetting operation is performed by the switching logic whenever the AVF is switched on or a valid target appears in the cruise mode. The reset headway command

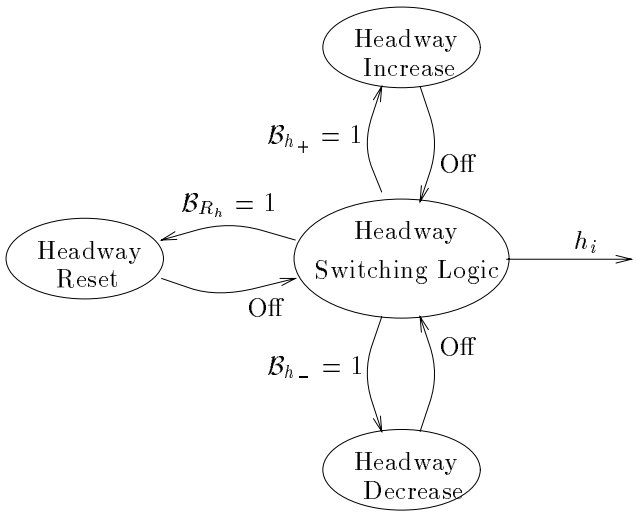

Figure 9: State diagram for headway switching logic.

$\mathcal{B}_{R_h}(.)$ is calculated as:

$$\mathcal{B}_{R_h}(k) = \begin{cases} 1 & \text{if } (\mathcal{B}_{A_{on}}(k) = 1 \text{ and } \mathcal{B}_{A_{on}}(k-1) \neq 1) \text{ or } (\mathcal{B}_F(k) = 1 \text{ and } \mathcal{B}_F(k-1) \neq 1) \\ 0 & \text{else.} \end{cases} \tag{5}$$

Since in ICC and cooperative driving without v-v communication, the driver is allowed to adjust the headway according to his/her comfort level, the requests for headway changes are processed by using the "headway increase" and "headway decrease" operations shown in Figure 9. The headway is increased/decreased by a predefined step size Δh and this change is accomplished through the output signal $h_i(.)$ from the switching logic given below:

$$h_i(k) = \begin{cases} \Delta h & \text{if } \mathcal{B}_{h_+}(k) = 1 \\ -\Delta h & \text{if } \mathcal{B}_{h_-}(k) = 1 \\ 0 & \text{else,} \end{cases} \tag{6}$$

where, $\mathcal{B}_{h_+}(.)$, $\mathcal{B}_{h_-}(.)$ are the conditions for starting the headway increase and headway decrease operations respectively. The headway decrease operation is triggered only after detecting a headway decrease command from the driver. On the other hand, headway increase operation can also be started by "transition to manual" operation. As shown in Figure 6, a transition to manual operation is performed whenever the driver wants to switch off the AVF or a fault is detected in any critical subsystem. However, as given in (2), the transition operation requires that the headway be greater than certain threshold h_{max} and the speed less than V_{max}. All of these conditions are formulated in the form of logical signals

$\mathcal{B}_{h_+}(.)$ and $\mathcal{B}_{h\_}(.)$ given below:

$$\mathcal{B}_{h_+}(k) = \begin{cases} 1 & \text{if } (\mathcal{B}_F(k) = 1 \text{ and } \mathcal{B}_H(k) = 0) \text{ or } \mathcal{B}_{A_{off}}(k) = 1 \\ 0 & \text{else} \end{cases} \tag{7}$$

$$\mathcal{B}_{h\_}(k) = \begin{cases} 1 & \text{if } \mathcal{B}_F(k) = 1 \text{ and } \mathcal{B}_H(k) = 1 \text{ and } \mathcal{B}_{A_{off}}(k) = 0 \\ 0 & \text{else,} \end{cases} \tag{8}$$

where $\mathcal{B}_H(.)$, $\mathcal{B}_{A_{off}}(.)$ are the conditions for processing the headway commands from the driver and transition to manual operation respectively. The condition used by the switching logic to process the headway commands form the driver, $\mathcal{B}_H(.)$, ensures that $h \in [h_{min}, h_{max}]$ and is given below:

$$\mathcal{B}_H(k) = \begin{cases} 0 & \text{if } \mathcal{B}_{D_h}(k) = 0 \text{ and } h(k) < h_{max} \text{ and } h_d(k-1) < h^d_{max} \\ 1 & \text{if } \mathcal{B}_{D_h}(k) = 1 \text{ and } h(k) > h_{min} \text{ and } h_d(k-1) > h_{min}, \end{cases} \tag{9}$$

where h^d_{max} is a design constant and $\mathcal{B}_{D_h}(.)$ is an output signal from the driver interface to process the headway changes requested by the driver, $\mathcal{B}_{D_h} = 0$ when the driver wants to increase the headway and $\mathcal{B}_{D_h} = 1$ otherwise. As pointed out before that the signal $\mathcal{B}_{A_{off}}(.)$ tests the conditions at the time of transition to manual mode and is given as:

$$\mathcal{B}_{A_{off}}(k) = \begin{cases} 1 & \text{if } \{\mathcal{B}_{A_{on}}(k) = 1 \text{ and } (\mathcal{B}_{D_{on}}(k) = 0 \text{ or } \mathcal{B}_S(k) = 0) \text{ and } (h(k) < h_{max} \\ & \quad \text{or } V(k) > V_{max}) \text{ and } h_d(k-1) < h^d_{max}\} \\ 0 & \text{else.} \end{cases} \tag{10}$$

As shown in Figure 8, the headway command generated by the switching logic $h_i(.)$ is filtered to avoid excessive transients. The filtered desired headway command h_d is given as:

$$h_d(k) = h_d(k-1) + Th_i(k), \tag{11}$$

where T is the sampling time and $h_i(.)$ is given in (6).

Cooperative Driving with v-v Communication and Platooning

The state diagram of switching logic for this case is shown in Figure 10. As pointed out before that the "headway reset" task is same for each mode of operation of AHS, hence the relations in this case are the same as given in (4) and (5). However, the design constant h_{min} may be different for each mode of AHS.

In ICC and cooperative driving mode without v-v communication, the actual headway h is taken as the desired headway command from the driver, with the assumption that the driver will switch on the AVF when the vehicle is following the preceding vehicle at a

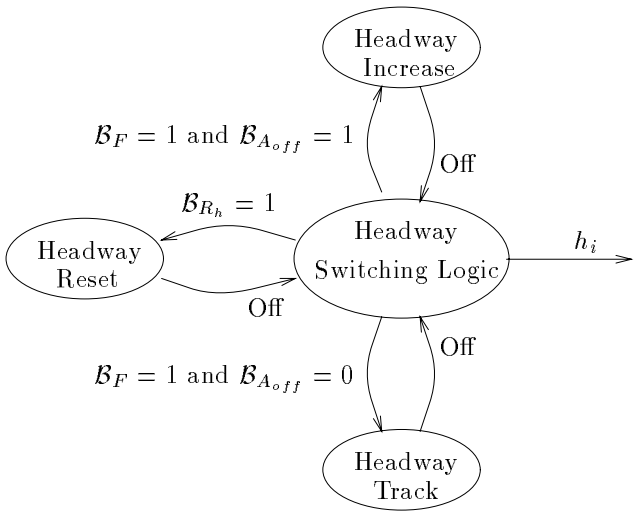

Figure 10: State diagram for headway switching logic.

comfortable distance. However, in cooperative driving with v-v communication and platooning modes the headway h at the time of resetting can be different than the roadway commanded headway h_R, (in the case of platooning h_R is received indirectly through the platoon leader). The desired headway in this case is smoothly changed to h_R by using the "headway track" operation shown in Figure 10. Also shown in Figure 10 is the "headway increase" task, which is performed only when the transition to manual mode is required. The output of the switching logic $h_i(.)$ in this case is:

$$h_i(k) = \begin{cases} k_p(h_R(k) - h_d(k-1)) & \text{if } \mathcal{B}_F(k) = 1 \text{ and } \mathcal{B}_{A_{off}}(k) = 0 \\ \Delta h & \text{if } \mathcal{B}_F(k) = 1 \text{ and } \mathcal{B}_{A_{off}}(k) = 1 \\ 0 & \text{else,} \end{cases} \tag{12}$$

where k_p is a design constant and $\mathcal{B}_{A_{off}}(.)$ is the same as given in (10). In (12) it is assumed that $h_R \in [h_{min}, h_{max}]$. Again the filter $D(z)$ given in (11) is used in this case too. For reference a complete expression for the desired headway command $h_d(.)$ is given below:

$$h_d(k) = \begin{cases} \max(h(k), h_{min}) & \text{if } \mathcal{B}_{R_h}(k) = 1 \\ h_d(k-1) + Th_i(k) & \text{else,} \end{cases} \tag{13}$$

where $h_i(.)$ is given by either (6) or (12) depending on the mode of operation of AHS.

3.5 Desired Speed Selection

If the vehicle is operating in the cruise mode, the speed selection logic calculates a desired speed to be given to the throttle/brake controller. If the vehicle is operating in ICC the

desired speed is selected by the driver while in cruise mode. In this case the vehicle is traveling without any valid target in front. In the case of cooperative driving and platooning, desired speed is issued by the roadway. While platooning the vehicle can be in the cruise mode only if it is a platoon leader. The structure of the desired speed selection logic is the same as that of the desired headway, shown in Figure 8. The functions performed by the switching logic in this case are given below.

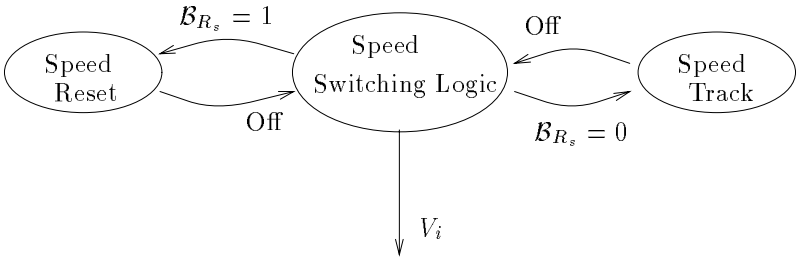

Figure 11: State diagram for the speed switching logic.

The state diagram for speed switching logic is shown in Figure 11. For the desired speed selection we are assuming a different kind of driver interface in which the speed command from the driver is available in exact numbers instead of increase/decrease command considered for headway selection. Hence the state diagram shown in Figure 11 is same for each mode of AHS, the only difference is that the speed command for "speed track" operation has different sources.

A "speed reset" operation is performed whenever the AVF is switched on and the desired speed V_d is taken as the current speed of the vehicle V. This resetting condition avoids large speed transients at the time when the AVF is switched on. Hence

$$V_d(k) = V(k) \quad \text{if} \quad \mathcal{B}_{R_s}(k) = 1, \tag{14}$$

where, $\mathcal{B}_{R_s}(.)$ is the speed reset command and is generated as:

$$\mathcal{B}_{R_s}(k) = \begin{cases} 1 & \text{if } \mathcal{B}_{A_{on}}(k) = 1 \text{ and } \mathcal{B}_{A_{on}}(k-1) \neq 1 \\ 0 & \text{else.} \end{cases} \tag{15}$$

After initialization, the desired speed V_d is made to track the speed command V_C through "speed track" operation. The speed switching logic generates a signal $V_i(.)$ which is passed through a filter $D_1(z)$ designed with comfort constraints. The speed command V_i generated by the switching logic is given as:

$$V_i(k) = \begin{cases} k_i Sat_1(r(k-1) - V_d(k-1)) & \text{if } \mathcal{B}_{A_{off}}(k) = 1 \\ k_i Sat_2(r(k-1) - V_d(k-1)) & \text{else,} \end{cases} \tag{16}$$

where, k_i is a design constant, $Sat_1(.)$, $Sat_2(.)$ are saturation functions and $\mathcal{B}_{A_{off}}(.)$ is the same as given in (10), which is used to determine if the speed and headway at the time of transition to manual mode are within the specified limits. In (16), $r(.)$ is given as:

$$r(k) = \begin{cases} V_s & \text{if } \mathcal{B}_{A_{off}}(k) = 1 \\ s(k) & \text{else,} \end{cases} \tag{17}$$

where, $V_s > 0$ is a design constant and is the vehicle speed when the control is finally transferred to the driver after transition, usually taken to be equal to the nominal highway speed. The signal $s(.)$ in (17) chooses the source of desired speed command for different modes of AHS and is given as:

$$s(k) = \begin{cases} V_l(k) & \text{if } \mathcal{B}_F(k) = 1 \\ V_C(k) & \text{else,} \end{cases} \tag{18}$$

where V_l is the speed of the leading vehicle and V_C is the speed command provided by the driver or infrastructure. As discussed before, in ICC mode V_C is issued by the driver, whereas in cooperative driving and platooning $V_C = V_R$. However, in platooning mode, only the platoon leader can operate in the cruise mode and hence can receive speed commands from the roadway. The rest of the platoon takes the desired speed and headway commands through the platoon leader. It will be shown later in the simulation section that the conditions for following a target given in (3) and switching the desired speed from the leader speed to the roadway speed, as given in (18), prevents excessive overshoot when the platoon executes a slowing down maneuver. The speed command $V_i(.)$ is passed through a filter $D_1(z)$ which is given as:

$$V_d(k) = V_d(k-1) + TV_i(k). \tag{19}$$

It should be noted that $(r(k-1) - V_d(k-1))$ in (16) at the input of the integrator (19) is an acceleration term. Therefore the comfort constraints imposed in terms of maximum allowable acceleration and deceleration are given in (16) as saturation functions, $Sat_1(.)$ and $Sat_2(.)$, where

$$Sat_1(r - V_d) = \begin{cases} A_{max} & \text{if } (r - V_d) \geq A_{max} \\ A_{min} & \text{if } (r - V_d) \leq A_{min} \\ r - V_d & \text{else} \end{cases} \tag{20}$$

$$Sat_2(r - V_d) = \begin{cases} A'_{max} & \text{if } (r - V_d) \geq A'_{max} \\ A'_{min} & \text{if } (r - V_d) \leq A'_{min} \\ r - V_d & \text{else} \end{cases} \tag{21}$$

where $A_{max}, A'_{max} > 0$ and $A_{min}, A'_{min} < 0$ are design constants. The limits for maximum allowable acceleration and deceleration are different during transition to manual mode,

which is obvious from (20) and (21), where $A_{max} \leq A'_{max}$ and $A_{min} \geq A'_{min}$. For reference, a complete expression for the desired speed command $V_d(.)$ is give below:

$$V_d(k) = \begin{cases} V_d(k-1) + TV_i(k) & \text{if } \mathcal{B}_{R_s}(k) = 0 \\ V(k) & \text{else.} \end{cases} \tag{22}$$

3.6 Emergency Operation

In cooperative driving and platooning modes, the recognition and handling of emergencies is one of the tasks performed by the supervisory controller. The recognition of emergencies requires that the input signals be continuously monitored for detecting the presence of any abnormal pattern or behavior. Once an emergency situation is detected, a set of actions is performed by an emergency handling logic. The recognition and handling of emergencies is discussed in subsections below.

3.6.1 Emergency Situation Assessment

The presence of a potential emergency situation is estimated by detecting an unusual pattern in the input signals. The common kind of emergencies encountered while driving in the automatic following mode are:

1) subsystem failure,
2) potentially dangerous target in cruise/follow mode.

For detecting subsystem failure, the assessment logic receives operating status of all the major subsystems of the vehicle. In case a failure is detected in any critical subsystem by the failure detection logic, an emergency situation is declared to be present.

The presence of a potentially dangerous target while operating in the cruise or follow mode can be determined by comparing the measured time to collision (TTC) against a minimum time for stopping the vehicle safely. At any time t, the relative distance X_r between the vehicles can be written as:

$$X_r(t) = X_r(t_0) + [V_l(t_0) - V_f(t_0)](t - t_0) + \int_{t_0}^{t} \int_{t_0}^{\tau} [a_l(s) - a_f(s)] ds \, d\tau, \tag{23}$$

where, V_l and V_f are the speeds of leading and following vehicles respectively, a_l and a_f are the accelerations of leading and following vehicle respectively and t_0 is the time at which the measurement of TTC is required. If for some time $t > t_0$ $X_r(t) = 0$, then TTC $= t - t_0$. Since the calculation of TTC requires prediction of the deceleration profiles for the leading and following vehicle for the time interval $[t_0, t]$, different assumptions can be made to approximate its value. For a rough cut estimate of TTC, we can assume that $a_f(\tau) = a_l(\tau)$ $\forall \tau \in [t_0, t]$. Also with the assumption that the ranging sensor provides both

the relative distance and speed information, the TTC can be calculated as:

$$TTC = \frac{\Delta X}{\Delta V} \tag{24}$$

where $\Delta X = X_r(t_0)$ and $\Delta V = V_f(t_0) - V_l(t_0)$ are the measured relative distance and speed respectively at time t_0. For TTC to have any significance it is required that $\Delta V > 0$. For a more conservative estimate of TTC, we can assume that the leading vehicle is decelerating with the maximum possible deceleration allowed in emergency condition and the trailing vehicle is braking with maximum deceleration allowed in the automatic following mode, i.e., $a_l(\tau) = a_{l_{min}}$, $a_f(\tau) = a_{min}$ $\forall \tau \in [t_0, t]$, then:

$$(a_{l_{min}} - a_{min})(t - t_0)^2 - \Delta V(t - t_0) + \Delta X = 0, \tag{25}$$

where a_{min} is the maximum deceleration allowed in the automatic following mode and $a_{l_{min}}$ is the maximum possible deceleration of the leading vehicle. From (25), TTC can be written as:

$$TTC = \frac{-\Delta V + \sqrt{\Delta V^2 + 4\Delta X \Delta a}}{2\Delta a}, \tag{26}$$

where, $\Delta a = a_{min} - a_{l_{min}} > 0$. The actual value of TTC lies between that given in (24) and (26), however, from the safety point of view, we will use the more conservative estimate given in (26).

The calculation of the minimum stopping time of the vehicle, t_{min}, however, involves some of the most un-deterministic parameters of the vehicle, i.e., the surface friction coefficient and the effective braking force on the wheels. However, with the assumption of a fairly constant braking capabilities, we can use different scenarios explored in [1] to estimate the minimum stopping time.

To calculate t_{min}, we use the scenario shown in Figure 12. After time delay t_d, which includes processing and actuator delays, the brakes are applied with the maximum jerk J_{max}, $(t_b - t_d)$ is the time it takes to reach the maximum deceleration a'_{min}, then:

$$t_d = T_1 + \tau, \tag{27}$$

$$t_b = \frac{a'_{min}}{J_{max}} + t_d, \tag{28}$$

where T_1 and τ are the processing and actuator delays respectively. The value of t_{min} is calculated by using the condition given below:

$$V(t_d) + \int_{t_d}^{t_{min}} a(t)dt = 0. \tag{29}$$

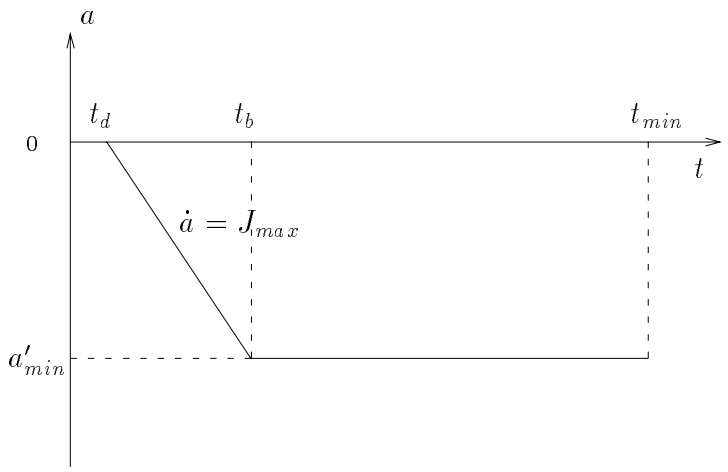

Figure 12: Scenario for calculation of minimum stopping time.

Hence,

$$V(t_d) - \frac{1}{2}J_{max}(t_b - t_d)^2 - a'_{min}(t_{min} - t_b) = 0,$$
$$\Rightarrow \; t_{min} = \frac{V(t_d) - \frac{1}{2}J_{max}(t_b - t_d)^2}{a'_{min}} + t_b, \tag{30}$$

where $a(.)$ is the acceleration and $V(.)$ is the speed of the vehicle.

However, since the comparison of TTC with the stopping time require measurements from the sensors and calculations, it introduces a certain amount of delay, which in some cases may prove to be the bottleneck of the emergency situation handling scheme. That is the reason for requiring v-v communication for detection of emergency situation. Since with the existence of v-v communication, presence of emergency in most cases can be estimated without significant delay by receiving the acceleration/deceleration commands from the preceding vehicle. Hence the triggering point for the detection of an emergency situation is that the deceleration of the leading vehicle a_l is more than a threshold, i.e.,

$$\text{if } a_l < a_{min} \Rightarrow \text{emergency exists},$$

where, $a_{min} < 0$ is the maximum deceleration allowed in the normal automatic following mode. Hence the presence of emergency is estimated as:

$$\mathcal{B}_E(k) = \begin{cases} 1 & \text{if } a_l < a_{min} \text{ or } TTC < t_{min} \\ 0 & \text{else.} \end{cases} \tag{31}$$

3.6.2 Emergency Situation Handling

Two major functions performed by the supervisory controller are the desired speed and headway calculation, hence are affected by the presence of an emergency situation. The desired values given earlier are modified to take into account the prevailing emergency situation.

The set of actions taken to handle subsystem failures depends on the level of redundancy provided in the system design. If redundancy is available for all critical subsystems, such as throttle, brake, steering actuators and sensors, then in the case of failure a warning is issued and AVF is switched off. This transition procedure is completed with the help of redundant sensors or actuators. As discussed before, the desired speed and headway selection logics use the signal $\mathcal{B}_{A_{off}}(.)$ in (10) to detect if the driver wants to switch to manual mode or if there is any failure in the system. In the case of failure $\mathcal{B}_{A_{off}} = 1$, then as given in (6), (12) and (17) the desired headway is increased and the desired speed is decreased till the actual headway and speed reach a safe value. However, in case no redundancy is available, the driver is instructed to complete the transition process manually and to drive the vehicle out of the auto lane.

A target can be declared potentially dangerous while the vehicle is operating in either the cruise or follow mode. The steps taken to handle the emergency situation in this case is to modify the desired speed and headway commands calculated for normal operating mode. In order to formulate the modification of the desired headway and speed commands (13), (22), we define the relative magnitude of emergency as:

$$M_E(k) \triangleq min\left[max\left\{\left(1-\frac{TTC}{t_{min}}\right),\left(\frac{a_{min}-a_l}{a_{min}-a'_{min}}\right),0\right\},1\right], \tag{32}$$

where a'_{min} is the maximum possible deceleration of the vehicle. It should be noted that $M_E(k) \in [0,1]$. We further define the maximum change in the vehicle speed, ΔV^b_{max}, and hence the maximum change in the headway Δh^b_{max} in one sampling interval due to the application of maximum allowable braking force f^b_{max}.

$$\Delta V^b_{max} \triangleq -\frac{f^b_{max}}{M}T, \tag{33}$$

$$\Delta h^b_{max} \triangleq \frac{f^b_{max}}{VM}Th, \tag{34}$$

where, M is the mass of the vehicle, V, h are the current speed and headway of the vehicle respectively. Hence the change in desired headway, Δh_d, and the desired speed, ΔV_d, can be calculated by scaling down their maximum values Δh^b_{max} and ΔV^b_{max} respectively, i.e.,

$$\Delta h_d = \Delta h^b_{max}\left[1-e^{-\frac{M_E}{1-M_E}}\right], \tag{35}$$

$$\Delta V_d = \Delta V^b_{max}\left[1-e^{-\frac{M_E}{1-M_E}}\right]. \tag{36}$$

Hence with the existence of an emergency, the calculation of the desired headway and speed can be changed as:

$$h'_d(k) = \begin{cases} h_d(k) + \Delta h_d(k) & \text{if } \mathcal{B}_E(k) = 1 \\ h_d(k) & \text{else,} \end{cases} \tag{37}$$

$$V'_d(k) = \begin{cases} V_d(k) + \Delta V_d(k) & \text{if } \mathcal{B}_E(k) = 1 \\ V_d(k) & \text{else.} \end{cases} \tag{38}$$

The simulation results for an emergency situation in which the leading vehicle slows down with a constant deceleration of 0.3g is shown in Figure 13.

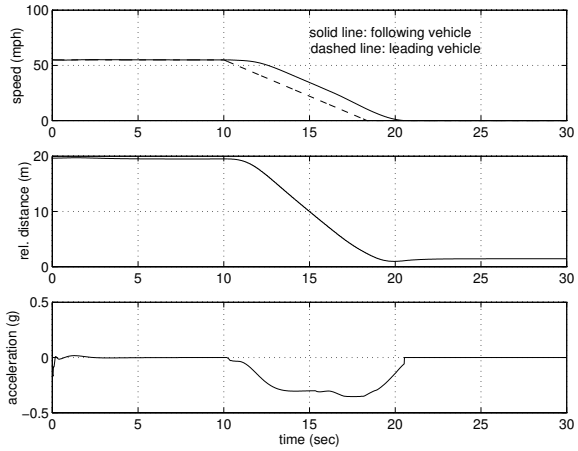

Figure 13: At $t_0 = 10$ sec the leading vehicle slows down at a constant rate of -0.3g. The following vehicle with $X_r(t_0) = 19.5$ m (corresponding to time headway of 0.8 sec) manages to stop without collision.

4 Stability and Performance Analysis

In this section we will analyze the stability of the overall closed loop system shown in Figure 4. For analysis purpose the block diagram is redrawn in Figure 14, showing all the states and input/output for each block separately. For completeness sake we will briefly describe the vehicle dynamics model here, a complete study can be found in [10, 14, 15].

Two control inputs, the throttle angle and the braking torque, are used to control the motion of the vehicle in the longitudinal direction. The speed of the vehicle V is a nonlinear function of the throttle angle θ, i.e.,

$$V = F(\theta, t, \tau). \tag{39}$$

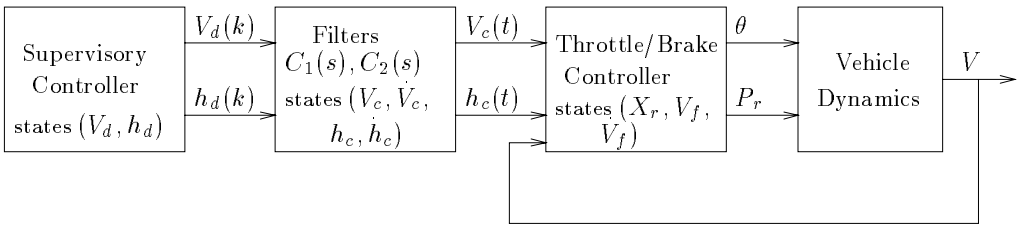

Figure 14: Closed loop system for stability analysis.

Various expressions for the nonlinear function $F(\theta, t, \tau)$ exist in the transportation literature and can be found in [14, 15]. For normal vehicle operation, the nonlinear model (39) can be approximated by a linearized model given below:

$$\frac{\bar{V}}{\bar{\theta}} \approx \frac{\hat{b}}{s + \hat{a}}, \tag{40}$$

where, $\bar{V} = V - V_0$ and $\bar{\theta} = \theta - \theta_0$ are the deviations of (V, θ) from the operating point (V_0, θ_0) and the model coefficients, $\hat{a}$, $\hat{b}$ are function of operating point. The model (40) can be rewritten as:

$$\dot{\bar{V}} = -\hat{a}\bar{V} + \hat{b}\bar{\theta} + d, \tag{41}$$

where the disturbance term, d, accounts for the neglected dynamics in (40). Similarly, the dynamic equation of the braking torque to the vehicle speed is given as:

$$\dot{V} = \frac{1}{M}\left(-c_1 T_b - f_0 - c_2 V - c_3 V^2\right), \tag{42}$$

where T_b is the braking torque, M is the vehicle mass, f_0, $c_2 V$, $c_3 V^2$ represent the static friction force, rolling friction force and air resistant force respectively. The term $c_1 T_b$ in (42) is the braking force and is proportional to the brake line pressure P_r shown in Figure 14 as a control input. For this study we will use the nonlinear PID throttle controller and the brake controller designed with feedback linearization in [10] to represent the throttle/brake controller in Figure 14. Since the throttle/brake controller requires continuous signals as the desired speed and headway, the discrete time signals $V_d(k)$ and $h_d(k)$ are filtered to generate continuous signals $V_c(t)$ and $h_c(t)$ respectively, shown in Figure 14. For throttle controller, the dynamic equations of the vehicle following are:

$$\begin{aligned}
\dot{X}_r &= V_l - V_f, \\
\dot{V}_f &= -\hat{a}(V_f - V_l) + \hat{b}\bar{\theta}_f + d, \\
\delta &= X_r - hV_f - S_0, \\
V_r &= V_l - V_f,
\end{aligned} \tag{43}$$

where δ is the deviation from the desired spacing, V_l is the speed of the leading vehicle (desired speed), V_r is the relative speed, S_0 is a constant and $\bar{\theta}_f = \theta_f - \theta_0$ is the throttle angle to be generated by the control law. For PID controller $\bar{\theta}_f$ is given as:

$$\bar{\theta}_f = k_1 V_r + k_2 \delta + \int_0^t (k_3 V_r + k_4 \delta) d\tau. \tag{44}$$

The gains $k_1 \ldots k_4$ are chosen to place the closed loop poles at the desired locations. In [10] it is shown that the control law (44) guarantees that with constant h and V_l, δ, $V_r \to 0$ (exponentially). Similarly for the brake controller the closed loop system after feedback linearization is:

$$\begin{aligned} \dot{X}_r &= V_l - V_f, \\ \dot{V}_f &= k_5 V_r + k_6 \delta, \\ \delta &= X_r - h V_f - S_0, \\ V_r &= V_l - V_f, \end{aligned} \tag{45}$$

where k_5 and k_6 are the gains to be selected to make the closed loop system stable and to guarantee that δ, $V_r \to 0$ for constant h and V_l. However, with the supervisory controller in the loop the desired speed and headway $V_c(t)$ and $h_c(t)$ cannot be assumed to be constant. Hence some analysis is required to show the closed loop stability with time varying desired speed and headway commands. In the analysis to follow, we will use the following Lemma [16].

Lemma 4.1 *If the linear system:*

$$\dot{x} = A(t)x \qquad \text{where } A \text{ is continuous } \forall t \geq t_0,$$

is uniformly asymptotically stable (u.a.s.) then the system:

$$\dot{x} = [A(t) + B(t)]x,$$

is also u.a.s. if $B(t)$ is continuous $\forall t \geq t_0$ and if $B(t) \to 0$ as $t \to \infty$.

Using Lemma 4.1, the following Theorem establishes the stability of the closed loop system shown in Figure 14.

Theorem 4.1 *(i) All the signals in closed loop system of Figure 14 are bounded.*

(ii) if $V_d(k) \to c_1$ and $h_d(k) \to c_2$, where c_1, $c_2 > 0$ are constants then δ, $V_r \to 0$.

Proof: (i) The boundedness of the closed loop signals will be shown in two steps.

Step 1. As shown in Figure 14, the supervisory controller with the filters generate the desired trajectory, hence in first step we will show that $V_c(t)$ and $h_c(t)$ are bounded. The

switching logic in the speed and headway selection logic guarantees that $V_i(k) \in [V_{min}, V_{max}]$ and $h_i(k) \in [h_{min}, h_{max}]$. From (22) and (13) we have that $V_d(k)$, $h_d(k) \in l_\infty$. Also the filters $D_1(z)$ and $D(z)$ in (22), (13) are designed so that $\Delta V_d(k)$, $\Delta h_d(k) \in l_\infty$, where $\Delta f(k) = f(k) - f(k-1)$. Since $V_c(s) = C_1(s)V_d(k)$ and $h_c(s) = C_2(s)h_d(k)$ with $V_d(k)$, $h_d(k) \in l_\infty$, filters $C_1(s)$ and $C_2(s)$ can be designed such that V_c, $\dot{V}_c \in \mathcal{L}_\infty$ and h_c, $\dot{h}_c \in \mathcal{L}_\infty$.

Step 2. Before analyzing the stability of throttle/brake system, we consider the possible variations in the headway signal $h_c(t)$. Since the headway changes occur only at finite number of instants, on requests issued by the driver or roadway, the signal $h_c(t)$ is mainly constant with finite number of transitions. Without loss of generality, we can assume that one such transition occurs at t_0, then $h_c(t)$ can be represented as, $h_c(t) = h(t_0) + h_j(1 - e^{-\alpha(t-t_0)})$, where h_j is the jump in headway at time t_0 and α is a constant determined by the filter $C_2(s)$. Hence

$$h_c(t) = \bar{h}_c + h_\Delta, \tag{46}$$

where $\bar{h}_c = h(t_0) + h_j$ is constant and $h_\Delta = -h_j e^{-\alpha(t-t_0)}$. Then for $t \geq t_0$ the closed loop system (43), (44) becomes:

$$\begin{aligned}
\dot{X}_r &= V_c - V_f, \\
\ddot{V}_f &= -(\hat{a} + \hat{b}k_1 + \hat{b}k_2\bar{h}_c)\dot{V}_f - (\hat{b}k_2 + \hat{b}k_3 + \hat{b}k_4\bar{h}_c)V_f - (\hat{a} + \hat{b}k_1)\dot{V}_c \\
&\quad +(\hat{b}k_2 + \hat{b}k_3)V_c + \hat{b}k_4 X_r - (\hat{b}k_4 h_\Delta V_f + \hat{b}k_2 \dot{h}_\Delta V_f + \hat{b}k_2 h_\Delta \dot{V}_f), \\
\delta &= X_r - \bar{h}_c V_f - h_\Delta V_f, \\
V_r &= V_c - V_f.
\end{aligned} \tag{47}$$

The terms S_0 and d in (43) are constants and have no effect on the current analysis, hence are neglected in (47). The closed loop system (47) can also be written as:

$$\begin{aligned}
\dot{X} &= [A + D_1(t)]X + Bu, \\
Y &= [C + D_2(t)]X + Du,
\end{aligned} \tag{48}$$

where $X = [X_r, V_f, \dot{V}_f]^\top$, $u = [V_c, \dot{V}_c]^\top$, $Y = [\delta, V_r]^\top$. The matrices A, B, C, D, $D_1(t)$ and $D_2(t)$ in (48) are given as:

$$A = \begin{bmatrix} 0 & -1 & 0 \\ 0 & 0 & 1 \\ \hat{b}k_4 & -\hat{b}(k_2 + k_3 + k_4\bar{h}_c) & -(\hat{a} + \hat{b}k_1 + \hat{b}k_2\bar{h}_c) \end{bmatrix}; B = \begin{bmatrix} 1 & 0 \\ 0 & 0 \\ \hat{b}(k_2 + k_3) & -(\hat{a} + \hat{b}k_1) \end{bmatrix},$$

$$C = \begin{bmatrix} 1 & -\bar{h}_c & 0 \\ 0 & -1 & 0 \end{bmatrix}; D = \begin{bmatrix} 0 & 0 \\ 1 & 0 \end{bmatrix},$$

$$D_1(t) = \begin{bmatrix} 0 & 0 & 0 \\ 0 & 0 & 0 \\ 0 & -\hat{b}(k_4 h_\Delta + k_2 \dot{h}_\Delta) & -\hat{b}k_2 h_\Delta \end{bmatrix}; D_2(t) = \begin{bmatrix} 0 & -h_\Delta & 0 \\ 0 & 0 & 0 \end{bmatrix}.$$

It should be noted that (A, B, C, D) from (48) are the same as that for the closed loop system (43), (44) with $h = \bar{h}_c$ and $V_l = V_c$. Now consider the homogeneous part of the LTV system (48):

$$\dot{X} = [A + D_1(t)]X. \tag{49}$$

Since $\dot{X} = AX$ is an exponentially stable system, $D_1(t)$ is continuous $\forall t \geq t_0$ and $D_1(t) \to 0$ as $t \to \infty$, then by Lemma 4.1 we have that (49) is u.a.s. Now (49) is u.a.s. if and only if $\exists\ \lambda_0,\ \alpha_0 > 0 \ni \|\Phi(t,\tau)\| \leq \lambda_0 e^{-\alpha_0(t-\tau)}$, for $t_0 \leq \tau \leq t < \infty$, where $\Phi(.,.)$ is the state transition matrix for (49). Since in step 1 we have proved that $u = [V_c, \dot{V}_c]^\top \in \mathcal{L}_\infty$, by solving the LTV system (48) for X and Y, we have that:

$$\begin{aligned} \|X\|_\infty &\leq \frac{\lambda_0 a_1}{\alpha_0}\|u\|_\infty + \epsilon, \\ \|Y\|_\infty &\leq \left(\frac{\lambda_0 a_1 a_2}{\alpha_0} + a_3\right)\|u\|_\infty + \epsilon, \end{aligned} \tag{50}$$

where $a_1 = \|B\|_\infty$, $a_2 = \sup_t \|C + D_2(t)\|$, $a_3 = \|D\|_\infty$ and ϵ is an exponentially decaying to zero term due to $X(t_0) \neq 0$. Hence $X, Y \in \mathcal{L}_\infty$. The same analysis can be shown for the brake controller (45). Since the throttle/brake switching logic designed in [10] guarantees that the throttle and brake controller are not acting together at the same time, all the signals and states in the closed loop system in Figure 14 are bounded.

(ii) To show that $\delta, V_r \to 0$ when $V_d(k), h_d(k) \to$ constant, we will use another representation of the closed loop system. From (43) and (44) we can get the transfer function from $\dot{V}_l$ to δ and V_r as:

$$\begin{aligned} \delta &= \frac{(1 - \hat{a}h - \hat{b}k_1 h)s - \hat{b}k_3 h}{\Delta(s)}\dot{V}_l, \\ V_r &= \frac{s^2 + \hat{b}k_2 hs + \hat{b}k_4 h}{\Delta(s)}\dot{V}_l, \end{aligned} \tag{51}$$

where $\Delta(s) = s^3 + (\hat{a} + \hat{b}k_1 + \hat{b}k_2 h)s^2 + \hat{b}(k_2 + k_3 + k_4 h)s + \hat{b}k_4$. With supervisory controller in the loop (51) becomes:

$$\begin{aligned} \dot{e} &= [A_1 + D_3(t)]e + B_1\dot{V}_c, \\ Y &= [C_1 + D_4(t)]e, \end{aligned} \tag{52}$$

where $e \in \mathcal{R}^3$, (A_1, B_1, C_1) is a state space representation of (51) in the controller canonical form, $D_3(t)$ and $D_4(t)$ are exponentially decaying to zero disturbance matrices obtained by replacing h with $h_c(t)$ given in (46). Since $D_3(t)$ follows the conditions stated in Lemma 4.1, $\dot{e} = [A_1 + D_3(t)]e$ is u.a.s. Now as $V_d(k) \to c_1 \Rightarrow \dot{V}_c \to 0$, (52) is a u.a.s. system with a bounded input which goes to zero, hence $Y = [\delta, V_r]^\top \to 0$. The same result can be shown for the brake controller (45). □

The simulation results in Figures 17-18, where the desired speed and headway commands are made to change, support the claim asserted in Theorem 4.1. In the following subsection we will develop a sufficient condition for stability of platoon of vehicles.

4.1 Platoon Stability

In this section we will establish the conditions the supervisory and regulation layer controllers have to follow to guarantee the stability of platoon of vehicles. We will use the following definition for platoon stability.

Definition 4.1 *A platoon of vehicles of length n is called stable if $\|\delta_i(t)\|_\infty \leq \|\delta_{i-1}(t)\|_\infty$ and $\|V_{r_i}(t)\|_\infty \leq \|V_{r_{i-1}}(t)\|_\infty$, $i = 2 \ldots n$, where δ is the deviation from the desired spacing and V_r is the relative speed between two vehicles.*

Before we analyze the stability of platoon, we will make the following assumption.

Assumption:

A–I Speed fluctuations between any two successive vehicle in the platoon are within the limit Δ_2 defined for the leading vehicle to be a valid target, i.e., $V_{c_i} = V_{i-1}$.

By using Definition 4.1 and assumption **A–I**, the following theorem establishes the conditions for platoon stability.

Theorem 4.2 *Under assumption* **A–I**, *a platoon of vehicles is stable if:*

$$\lambda_0(\max\{1, \hat{b}(k_2 + k_3)\}) \leq \alpha_0.$$

Where λ_0, α_0, $\hat{b}$, k_2 and k_3 are as defined in Theorem 4.1.

Proof: With supervisory controller in the loop we have, $\delta_i(s) = G_\delta(s)V_{c_i}$, using assumption **A–I** we have, $\delta_i(s) = G_\delta(s)V_{i-1}$. The transfer function relating δ_i and δ_{i-1} can be found as:

$$\begin{aligned} \frac{\delta_i(s)}{\delta_{i-1}(s)} &= \frac{\delta_i(s)}{V_{i-1}(s)} W_1(s) \frac{V_{i-2}(s)}{\delta_{i-1}(s)}, \\ &= W_1(s), \end{aligned} \tag{53}$$

where $V_i(s) = W_1(s)V_{i-1}(s)$. Similarly, we can show that $\frac{V_{r_i}(s)}{V_{r_{i-1}}(s)} = W_1(s)$. Hence a sufficient condition for platoon stability is that:

$$\|w_1(t)\|_1 \leq 1. \tag{54}$$

From the closed loop system (47) we have:

$$\begin{aligned}
\dot{X}_{r_i} &= V_{i-1} - V_i, \\
\ddot{V}_i &= -(\hat{a} + \hat{b}k_1 + \hat{b}k_2\bar{h}_c)\dot{V}_i - (\hat{b}k_2 + \hat{b}k_3 + \hat{b}k_4\bar{h}_c)V_i - (\hat{a} + \hat{b}k_1)\dot{V}_{i-1} \\
&\quad +(\hat{b}k_2 + \hat{b}k_3)V_{i-1} + \hat{b}k_4 X_{r_i} - (\hat{b}k_4 h_\Delta V_i + \hat{b}k_2 \dot{h}_\Delta V_i + \hat{b}k_2 h_\Delta \dot{V}_i).
\end{aligned} \tag{55}$$

Since $W_1(s)$ is the transfer function between V_i and V_{i-1}, (55) can be written as:

$$\begin{aligned}
\dot{X}_1 &= [A + D_1(t)]X_1 + b_1 u_1, \\
y_1 &= c_1 X_1,
\end{aligned} \tag{56}$$

where $X_1 = [X_{r_i}, V_i, \dot{V}_i]^\top$, $u_1 = V_{i-1}$ and $y_1 = V_i$. The matrices A, $D_1(t)$ are the same as defined in (48). The vectors b_1 and c_1 are:

$$b_1 = \begin{bmatrix} 1 & 0 & \hat{b}(k_2 + k_3) \end{bmatrix}^\top; \; c_1 = \begin{bmatrix} 0 & 1 & 0 \end{bmatrix}.$$

As proved in Theorem 4.1 that $\dot{X}_1 = [A + D_1(t)]X_1$ is u.a.s. and

$$\|y_1\|_\infty \leq \frac{\lambda_0 a_1}{\alpha_0}\|u_1\|_\infty + \epsilon. \tag{57}$$

Since $\|w_1\|_1 = \|T\|_\infty$, where T is the map, $T : u_1 \to Tu_1 = y_1$, we have:

$$\|w_1\|_1 \leq \frac{\lambda_0 a_1}{\alpha_0}. \tag{58}$$

Since $a_1 = \|b_1\|_\infty = \max\{1, \hat{b}(k_2 + k_3)\}$, the sufficient condition for platoon stability is:

$$\lambda_0(\max\{1, \hat{b}(k_2 + k_3)\}) \leq \alpha_0. \tag{59}$$

□

It should be noted that the condition (59) puts a limit on the closed loop poles of PID controller and the choice of filter $C_2(s)$.

5 Simulation and Experimental Results

The automatic vehicle following (AVF) controller designed in section three is simulated using the PID throttle/brake controller designed in [10] and a nonlinear longitudinal vehicle model [10]. The values chosen for different design constants in the supervisory controller are given below:

$h_t = 2$ sec, $\Delta_1 = 2.5$ mph, $\Delta_2 = 5$ mph. (see (3)),

$h_{max} = 1.2$ sec, $h_{min} = 0.25$ sec, $h^d_{max} = 1.5$ sec, $V_{max} = 65$ mph. (see (9), (10)),

$k_p = 0.1$, $\Delta h = 0.02$, $k_i = 10.$ (see (12), (6) and (16)),

$A_{max} = 0.7$, A_{min} = -0.4, $A'_{max} = 0.7$, A'_{min} = -2. (see (20) and (21)),

$V_s = 55$ mph. (see (17)).

The design constants for the throttle/brake controller [10] and the constraints for maximum acceleration, deceleration and jerk are chosen as:

$\omega_n = 0.1$, $\zeta = 1$, $\lambda_0 = 1.2$,

$k_5 = 1$, $k_6 = 0.25$,

$a_{max} = 0.2$g, a_{min} = -0.2g, $j_{max} = 10\ m/sec^3$.

The logic switch designed for throttle and brake controller [10] requires three parameters, X_{min}, X_{max} and V_1. The values chosen for these parameters are:

$X_{min} = 6$ m, $X_{max} = 40$ m, $V_1 = 13.4$ m/sec.

Three different tests are simulated to investigate the performance of the designed controller under different operating conditions, these are given in the subsections below. Finally, the test results of automatic vehicle following demonstrated in an actual highway environment are briefly discussed in subsection 5.4.

5.1 Test 1: Leader-Follower Scenario

In this test the cooperative driving mode is simulated, only two vehicles are used and are designated as the leader and follower. The effect of different initial conditions while switching on the AVF is studied. In this scenario the leader is assumed to be in the AVF mode at $t = 0$ sec, and is traveling at a speed of 55 mph, which is the roadway commanded speed, i.e., $V_l = V_R = 55$ mph. The follower, however, switches on the AVF with different initial conditions. The cases used for simulation are:

T1–I $V_f = 45$ mph $< V_l$, $h_f = h_R = 0.8$ sec.

T1–II $V_f = V_R$, $h_f = 0.6$ sec. $< h_R$.

The simulation results for these cases are shown in Figures 15-16. It can be seen that the following vehicle manages to operate in the automatic following mode even though starting from significantly different initial conditions. The magnitude of the transients are quite small, maximum acceleration and deceleration are limited to 0.16g and -0.15g respectively. The maximum jerk is observed in Figure 16, where the following vehicle executes a slowing down maneuver to increase the headway, the value of maximum jerk is 3.6 m/sec^3.

5.2 Test 2: Leader-Follower Scenario: Effect of Roadway Commands

In this test the same leader-follower scenario of Test 1 is assumed, i.e., the leader and follower are traveling at roadway commanded speed, $V_l = V_f = V_R = 55$ mph, and $h_f = h_R = 0.8$ sec. In the following cases it is assumed that at $t = 60$ sec, the roadway changes speed and/or headway commands. The cases are:

T2–I $V_R(k_0) = 65$ mph $> V_R(k_0 - 1)$, where $k_0 T = 60$ sec.

T2–II $h_R(k_0) = 1.0$ sec $> h_R(k_0 - 1)$

The simulation results for these cases are shown in Figures 17-18. In Figure 17, both vehicles accelerate from a steady speed of 55 mph to 65 mph, following the roadway command issued at $t = 60$ sec. The maximum acceleration for both vehicles is limited to about 0.05g. In Figure 18, the following vehicle decreases its speed momentarily to increase the headway from 0.8 sec to 1.0 sec. It should be noted that a change in the desired headway at $t = 60$ sec, creates a negative position error, the throttle/brake controller uses this new headway command to decrease the position error.

5.3 Test 3: Platoon Maneuvers

In the third set of simulations, a platoon of six vehicles is used to demonstrate the process of platoon formation and deformation. Furthermore, the effects of acceleration and deceleration on the platoon stability is also analyzed. The cases used for simulations are:

T3–I Platoon formation: Five vehicles join the leader at a consecutive interval of 5 sec.

T3–II Platoon deformation: Vehicles exit from the end of the platoon at a consecutive interval of 5 sec.

T3–III Platoon acceleration/deceleration: In steady state at 55 mph, platoon accelerates/decelerates to 65/45 mph.

The results of these simulations are shown in Figure 19-22. In the platoon formation maneuver, Figure 19, the incoming vehicles were made to join the platoon with monotonically increasing negative position error. The magnitude of speed overshoot is reasonably small even with large negative position error. In the case of platoon deformation, Figure 20, at the time the AVF is switched off, the headway is gradually increased from $h_R = 0.8$ sec to $h_{max} = 1.2$ sec at a rate of 0.02 sec for each sampling interval. Hence at a speed of 55 mph it creates a position error of about -1.2 m during this period of time. The position error goes to zero as the AVF is switched off.

When the platoon executes an acceleration maneuver, Figure 21, the speed increases from 55 mph to 65 mph, with no slinky type effect. For the deceleration maneuver, as pointed out earlier, the condition for following target given in (3) and switching the desired speed from the leader speed V_l to the roadway speed V_R in (20), if the former is significantly different than the later, helps in uniform deceleration of platoon. Hence all of the vehicles uniformly decelerate till the speed of the leading vehicles is within $\Delta_1 = 2.5$ mph of V_R, at which point the leading vehicles are treated as valid targets.

5.4 Experiments on I-15

In this experiment, two vehicles were used. Each of the two vehicles were equipped with ranging sensors, which can measure relative distance up to about 20 meters, and v-v communication devices. Through the communication, the leading vehicle passes its speed, acceleration, and other information to the following vehicle. The vehicles were equipped with the throttle actuators only, hence the desired speed profiles were chosen so that the required deceleration can be achieved without using brakes (by using engine torque only).

For each controller designed in [10], tests were conducted with two kind of time headway, 0.25 seconds and 0.4 seconds. There were 3 speed profiles for the leading vehicle. The first speed profile was starting at 30 mph, going to 60 mph with small acceleration, staying at 60 mph for a while, decreasing to 40 mph slowly, going back to 60 mph slowly, and then staying at 60. For simplicity, we use 30-60-40-60 to indicate this speed profile. The second speed profile is 40-50-40-50 or 40-50 with large acceleration. The third speed profile is that the leading vehicle was driven manually following some sinusoidal speed curve. The experimental results of some of the tested controllers are included here, for a detailed description of this test conducted on I-15 the reader is referred to [17].

The test results of nonlinear PID throttle controller and no v-v communication are shown in Figures 23-24. It can be seen from Figure 24 that the negative position error is within 1 m, which allows the following vehicle to travel close to the leading vehicle without any collision. The speed profiles in Figure 23 show that the following vehicle tracks the speed profile of the leading vehicle closely except near transitions, where a sudden change in speed of the leading vehicle creates a large position error which is reduced by making the speed of the following vehicle greater than that of the leading vehicle during that interval. In this test the headway is set to be 0.25 seconds, hence as shown in Figure 24 the actual headway is smoothly reduced from an initial value of 0.265 seconds to the desired value of 0.25 seconds. As pointed out earlier that the controller design ensures that the acceleration of the vehicle is within the specified bounds. The claim is obvious from the acceleration profiles shown in Figure 23, where the acceleration of the following vehicle is less than the set limit of 1 m/sec^2, even though the leading vehicle accelerates beyond the set limit.

The test results of PID controller with communication for a speed profile of 40-55-40-55 are shown in Figures 25-26. By comparing Figure 25 with Figure 23 it is obvious that

the addition of v-v communication has helped the following vehicle to closely track the speed profile of the leading vehicle. Hence transmission of the acceleration of leading vehicle reduces the time delay incurred by assessing the same information through the sensor measurements. Similarly Figure 26 shows that the maximum negative position error is close to 1 m, which is satisfactory considering the fact that no brake actuator was used in the experiment and the required deceleration was obtained by the engine torque only.

Figures 27-28 and 29-30 show the experimental results for adaptive controller without and with v-v communication respectively. In both cases sinusoidal speed profile, which represents typical manual driving, was chosen. The time headway in both cases was selected to be 0.25 seconds. Again by comparison of Figures 27 and 29 it is obvious that addition of v-v communication improves the performance of the vehicle following controller.

6 Conclusion

In this paper we have designed and tested a vehicle control system for achieving full vehicle automation in the longitudinal direction. The vehicle control system is an interconnection of a supervisory controller and a throttle/brake controller. The supervisory controller is designed so that it can operate in different configurations of AHS, allowing the vehicle to operate with varying distribution of authority between the driver and external agents. The supervisory controller helps the driver during transitions and generates the desired trajectory of the vehicle based on available inputs. Overall system safety is improved by inclusion of emergency situation handling algorithm as a part of supervisory controller. The simulation results of some of the basic vehicle following maneuvers are used to test the performance of the designed controllers. Finally, the experimental results of a vehicle following test conducted on I-15 verifies the system performance in an actual highway environment.

Acknowledgment:

We thank Dr. Z. Xu for his useful comments and help for this study.

References

[1] Y. Sun, P. Ioannou, "A Handbook for Inter-Vehicle Spacing in Vehicle Following," California PATH Research Report, UCB-ITS-PRR-95-1

[2] D. B. Maciuca, J. K. Hedrick, "Brake Dynamics Effect on AHS Lane Capacity," Systems and Issues in ITS, SAE, Warrandale, PA, pp. 81-86, 1995.

[3] V. Sarakki, J. Kerr, "Effectiveness of IVHS Elements on Freeway/Arterial Capacity: Concepts and Case Studies," 64th Meeting of Institute of Transportation Engineers, Dallas, Compendium of Technical Papers, Institute of Transportation Engineers, Washington D.C., pp. 303-307, 1994.

[4] M. Shannon, et al., "Precursor Systems Analyses of Automated Highway Systems: AHS Safety Issues," vol. 9, Federal Highway Administration, Washington D.C., Report no. FHWA-RD-95-105, 1995.

[5] A. Hitchcock, "Configuration and Maneuvers in Safety-Consciously Designed AHS Configuration," California PATH Program, University of California at Berkeley, UCB-ITS-PWP-95-2, 1995.

[6] K. S. Chang, J. K. Hedrick, W. B. Zhang, P. Varaiya, M. Tomizuka, S. E. Shladover, "Automated Highway System Experiments in the PATH Program", *IVHS Journal*, vol 1, no. 1, pp. 63-87, Apr. 1993.

[7] C. C. Chien, P. Ioannou, "Automatic Vehicle Following", *Proc. of 1992 American Control Conference*, Chicago, IL, pp. 1748-1752. June 1992.

[8] J. K. Hedrick, et. al, "Control Issues in Automated Highway Systems", *IEEE Control Systems*, vol. 14, no. 6, pp. 21-32, Dec. 1994.

[9] P. Ioannou, C. C. Chien, "Intelligent Cruise Control", *IEEE Transactions on Vehicular Technology*, vol. 42, no. 4, pp. 657-672, Nov. 1993.

[10] P. Ioannou, Z. Xu, "Throttle and Brake Control System for Automatic Vehicle Following", *IVHS Journal*, vol. 1(4), pp. 345-377, 1994.

[11] S. E. Shladover, et. al, "Automatic Vehicle Control Developments in the PATH Program", *IEEE Transactions on Vehicular Technology*, vol. 40, no. 1, pp. 114-130, Feb. 1993.

[12] C. C. Chien, Y. Zhang, A. Stotsky, S. R. Dharmasena, P. Ioannou, "Macroscopic Roadway Traffic Controller Design", California PATH Research Report, UCB-ITS-PRR-95-28.

[13] P. Varaiya, "Smart Cars on Smart Roads: Problems of Control", *IEEE Transactions on Automatic Control*, vol. 38, no. 2, pp. 195-207, Feb. 1993.

[14] J. K. Hedrick, D. McMahon, V. Narendran, D. Swaroop, "Longitudinal Vehicle Controller Design for IVHS System," *Proc. of ACC*, vol. 3, pp. 3107-3112, June 1991.

[15] A. S. Hauksdottir, R. E. Fenton, "On the Design of a Vehicle Longitudinal Controller," *IEEE Trans. on Vehicular Technology*, vol. VT-34, no. 4, pp. 182-187, Nov. 1985.

[16] W. A. Coppel, "Stability and Asymptotic Behavior of Differential Equations", D. C. Heath and Company, Boston, pp. 64-70, 1965.

[17] P. Ioannou, Z. Xu, H. Raza, "Report on I-15 Vehicle Following Test", USC-CATT Report #96-3-01.

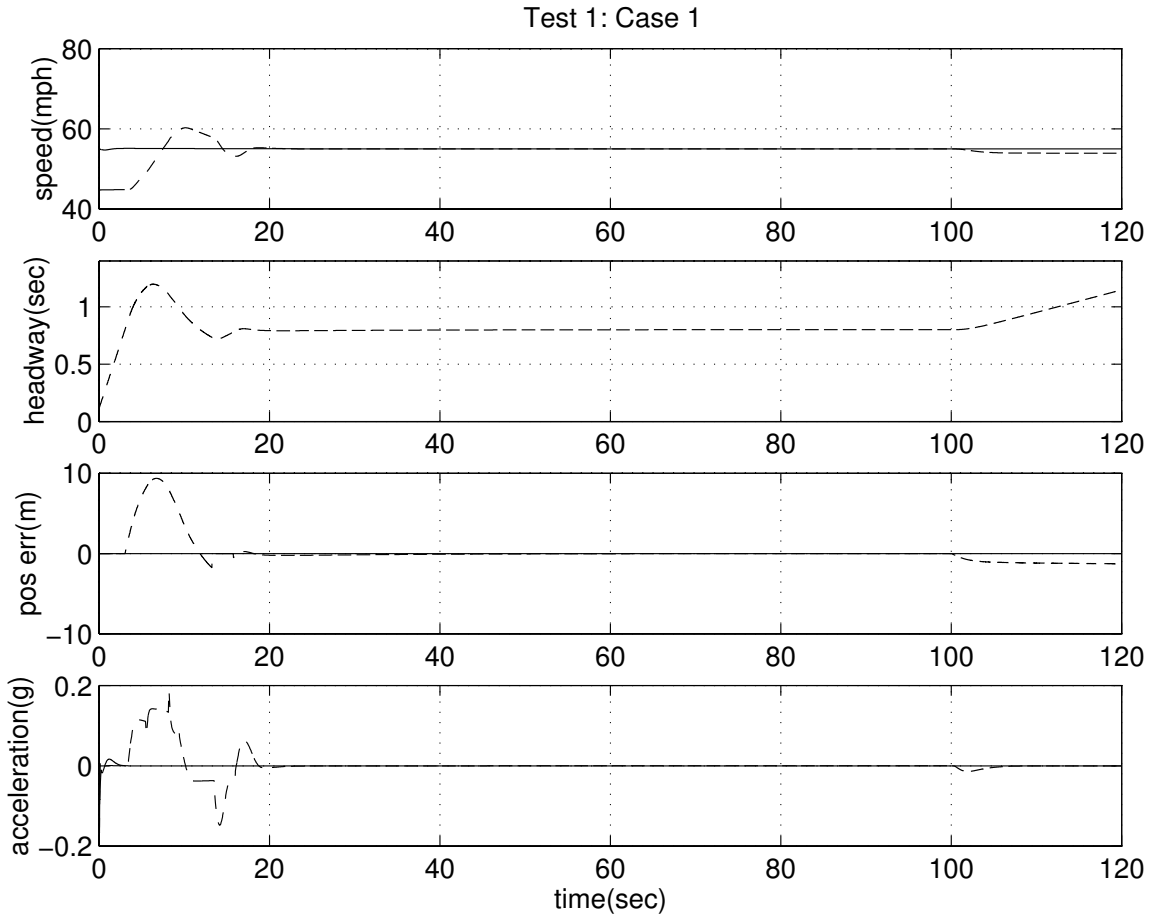

Figure 15: Follower switches on AVF at $t = 3$ sec with $V_f = 45$ mph and $h_f = h_R = 0.8$ sec. AVF is switched off at $t = 100$ sec.

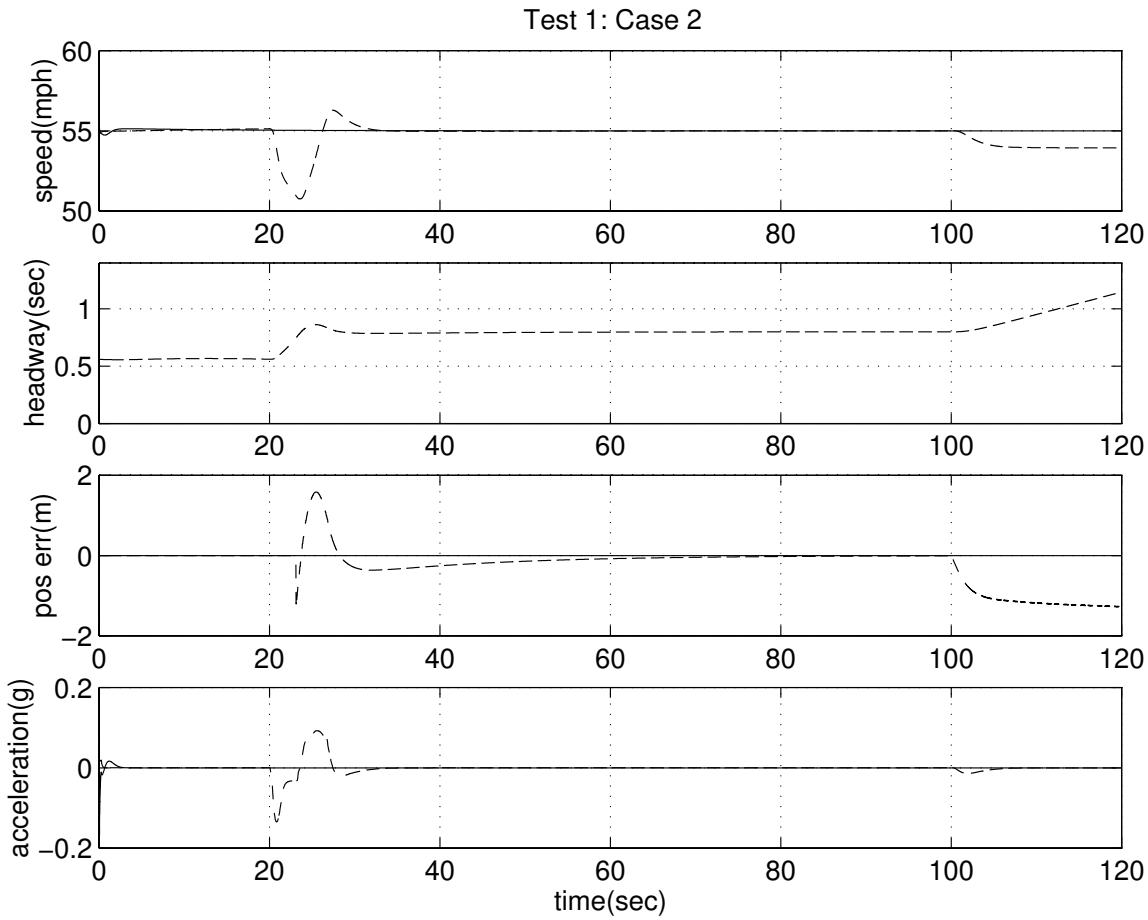

Figure 16: Follower switches on AVF at $t = 20$ sec with $V_f = 55$ mph and $h_f = 0.6$ sec. AVF is switched off at $t = 100$ sec.

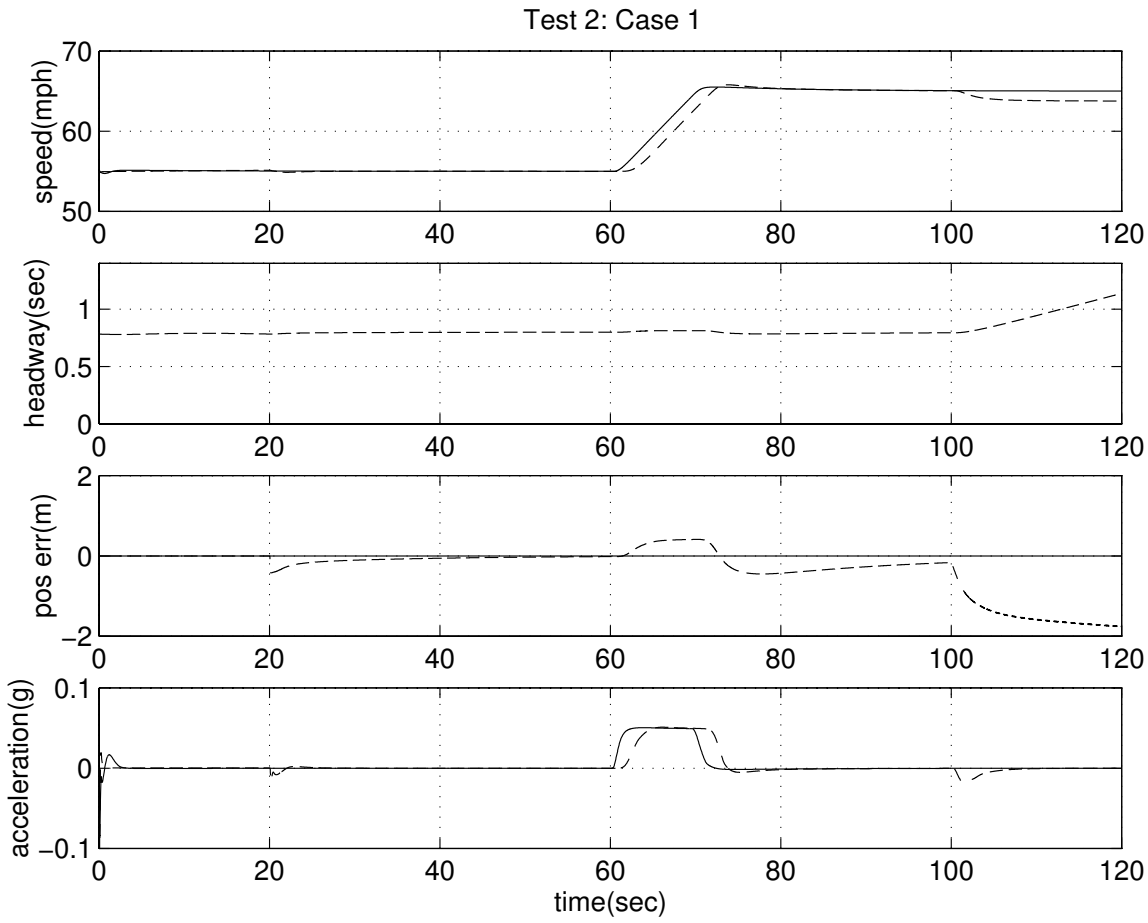

Figure 17: At $t = 60$ sec V_R changes from 55 to 65 mph.

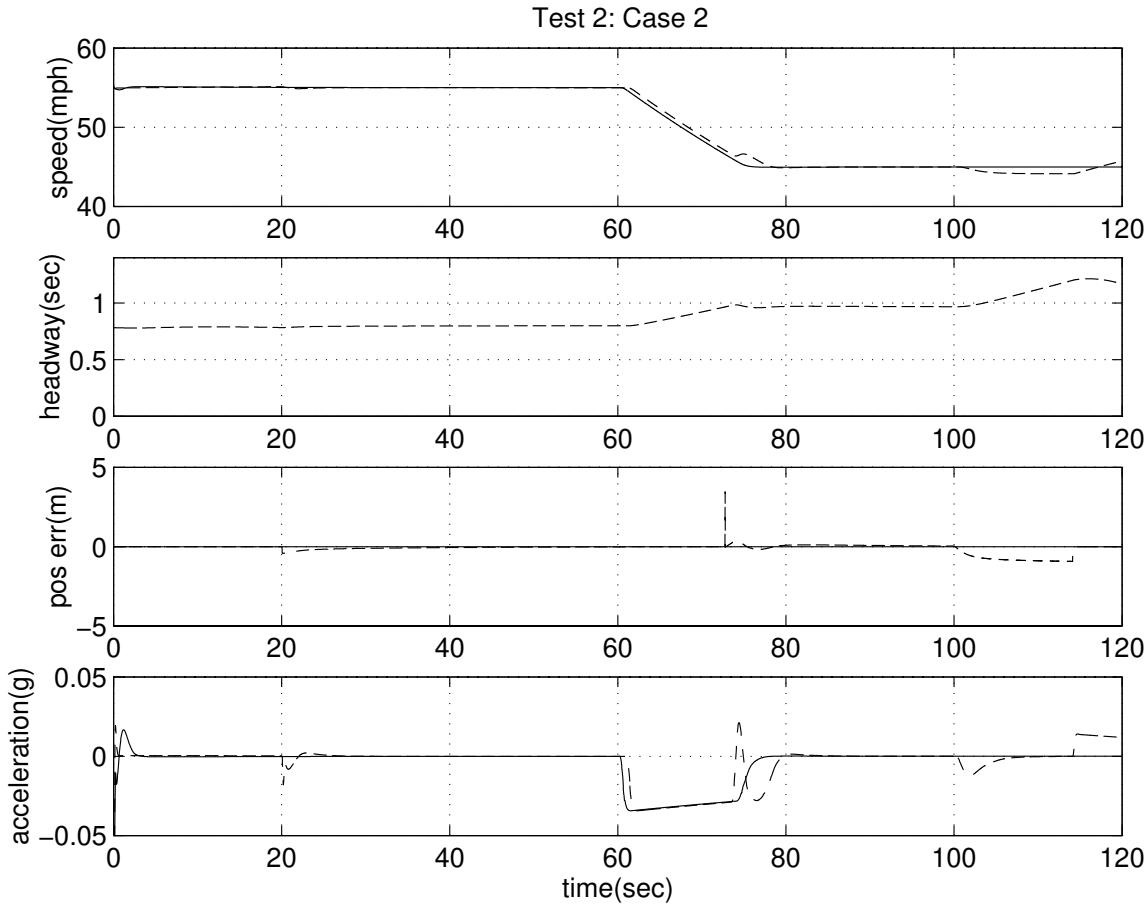

Figure 18: At $t = 60$ sec, h_R changes from 0.8 to 1.0 sec.

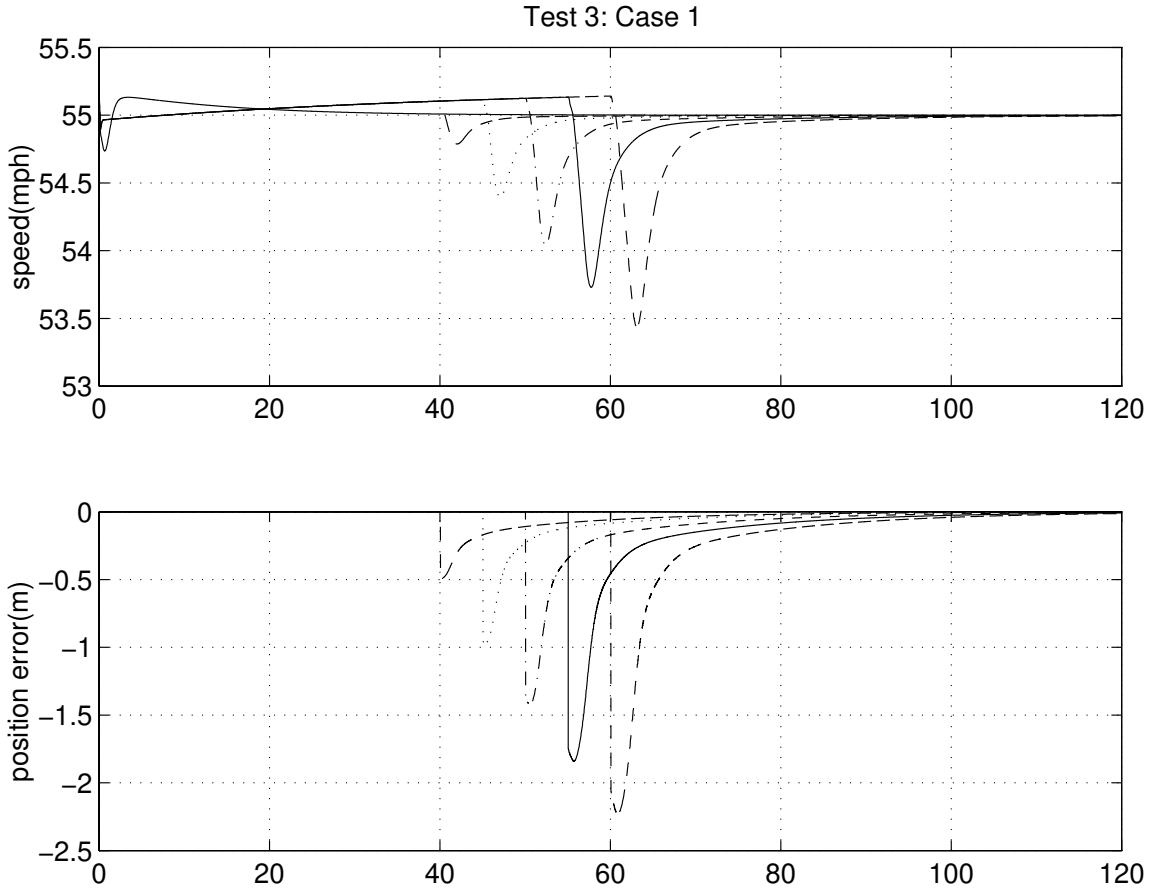

Figure 19: Platoon formation: At $t = 40$ sec, first vehicle joins the leader of the platoon. Four more vehicles join the platoon at a consecutive interval of 5 sec. Platoon formation was stable even though the starting position error was quite large.

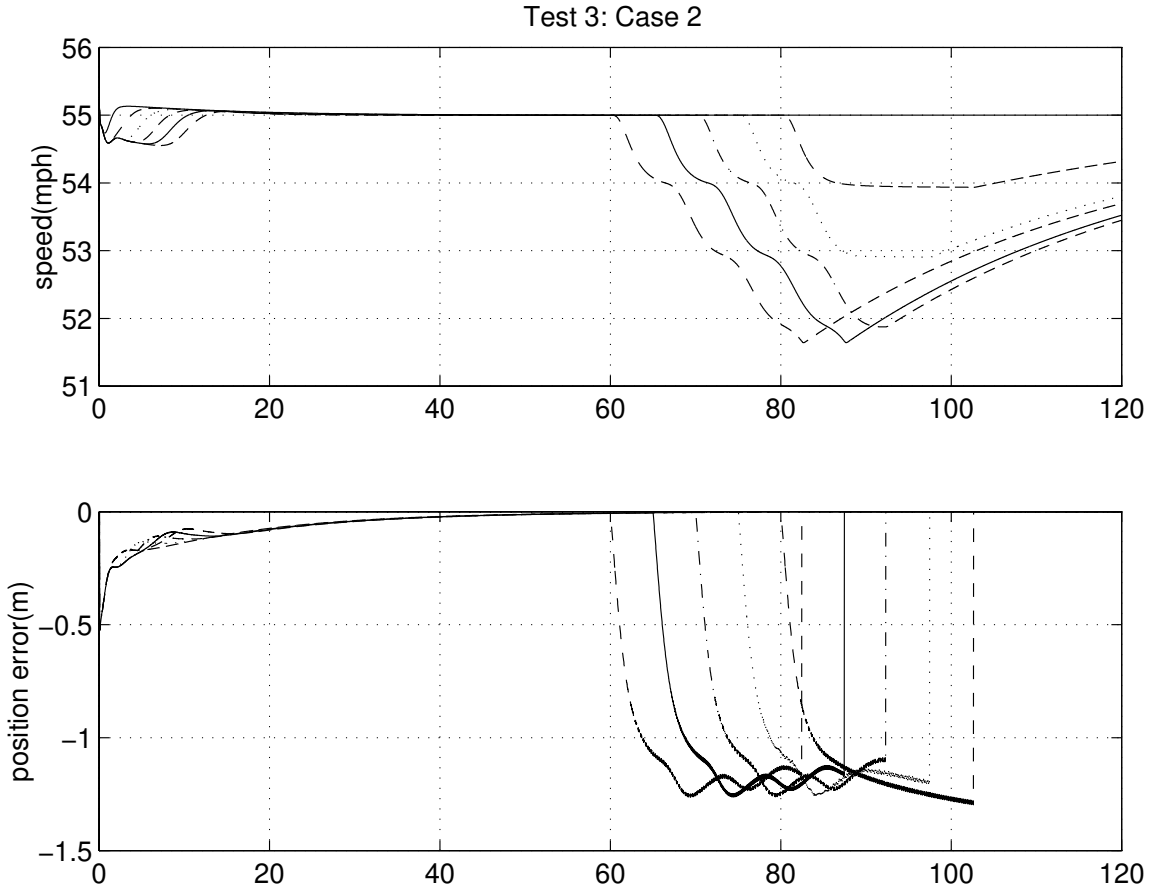

Figure 20: Platoon deformation: At $t = 60$ sec, vehicles start exiting at a consecutive interval of 5 sec. A negative position error is due to transition to manual operation, where the headway is increased till it reaches the specified value.

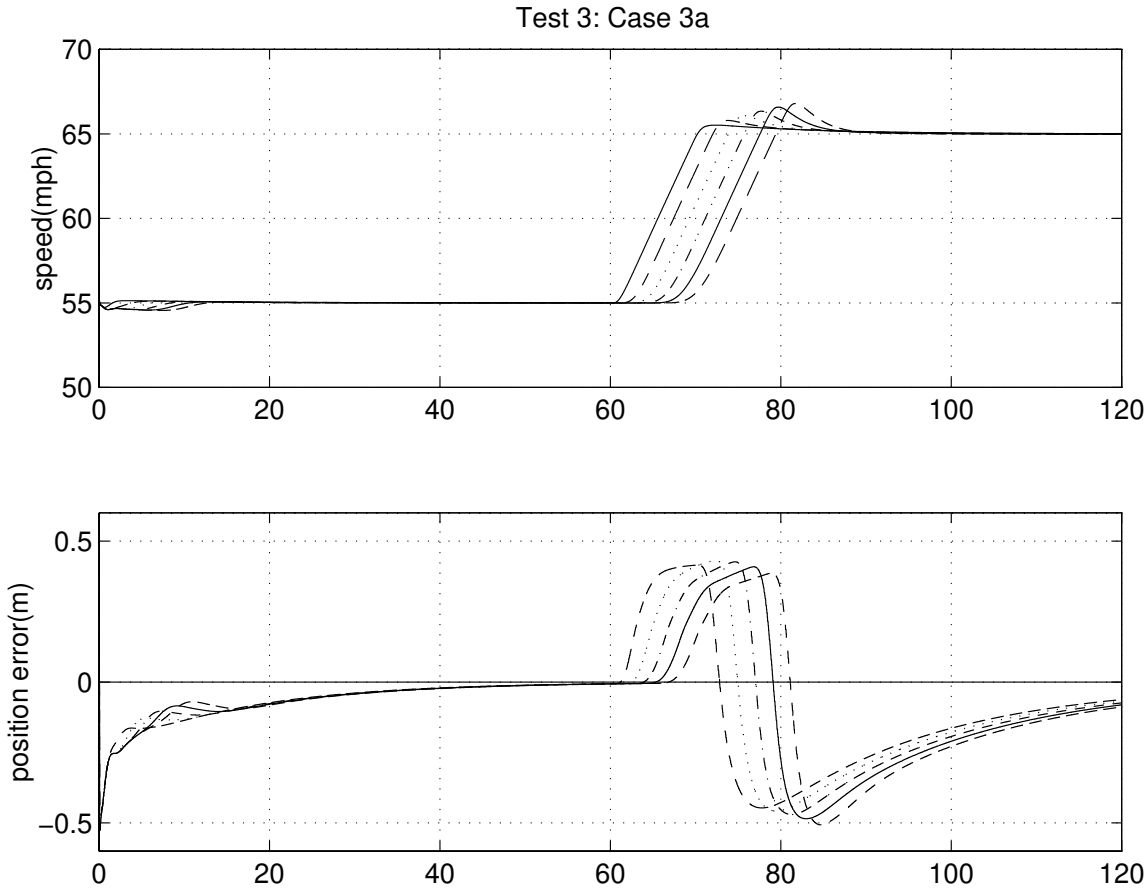

Figure 21: At $t = 60$ sec, platoon accelerates to 65 mph.

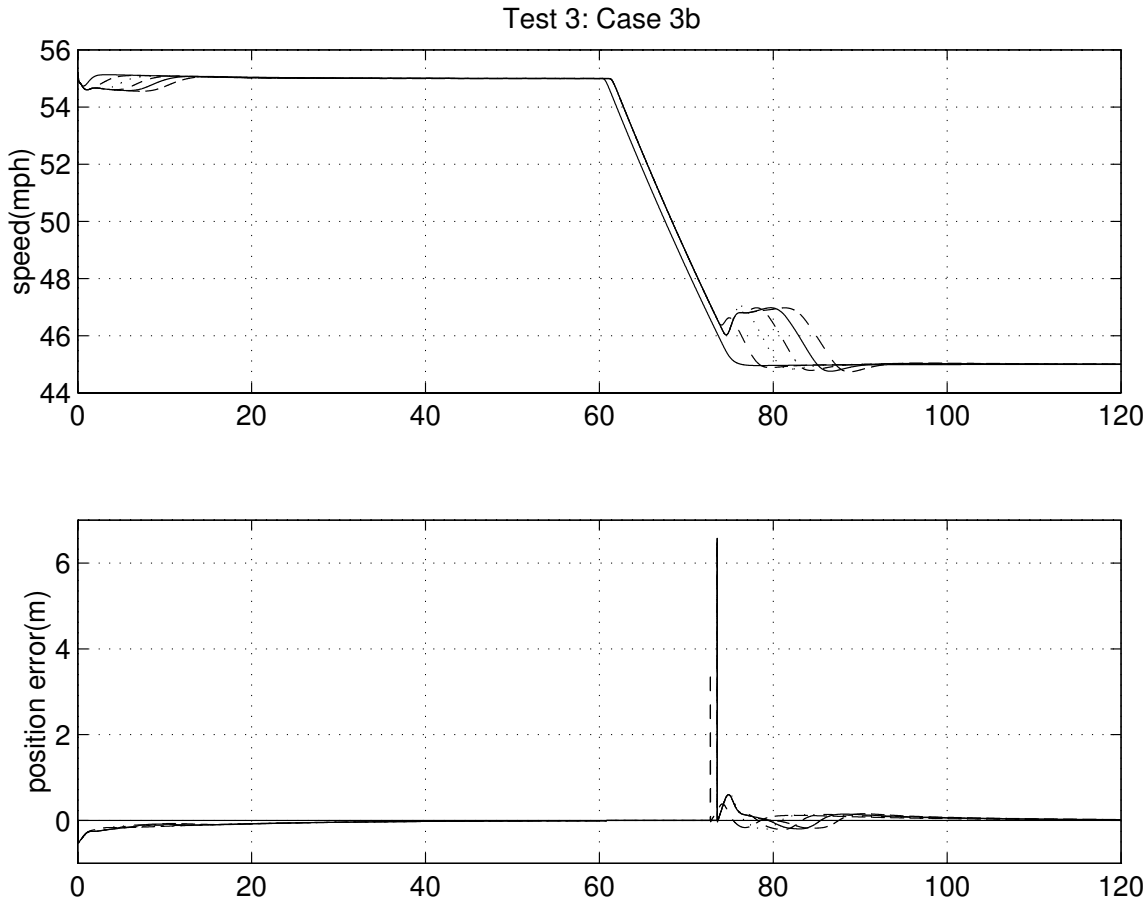

Figure 22: At $t = 60$ sec, platoon decelerates to 45 mph.

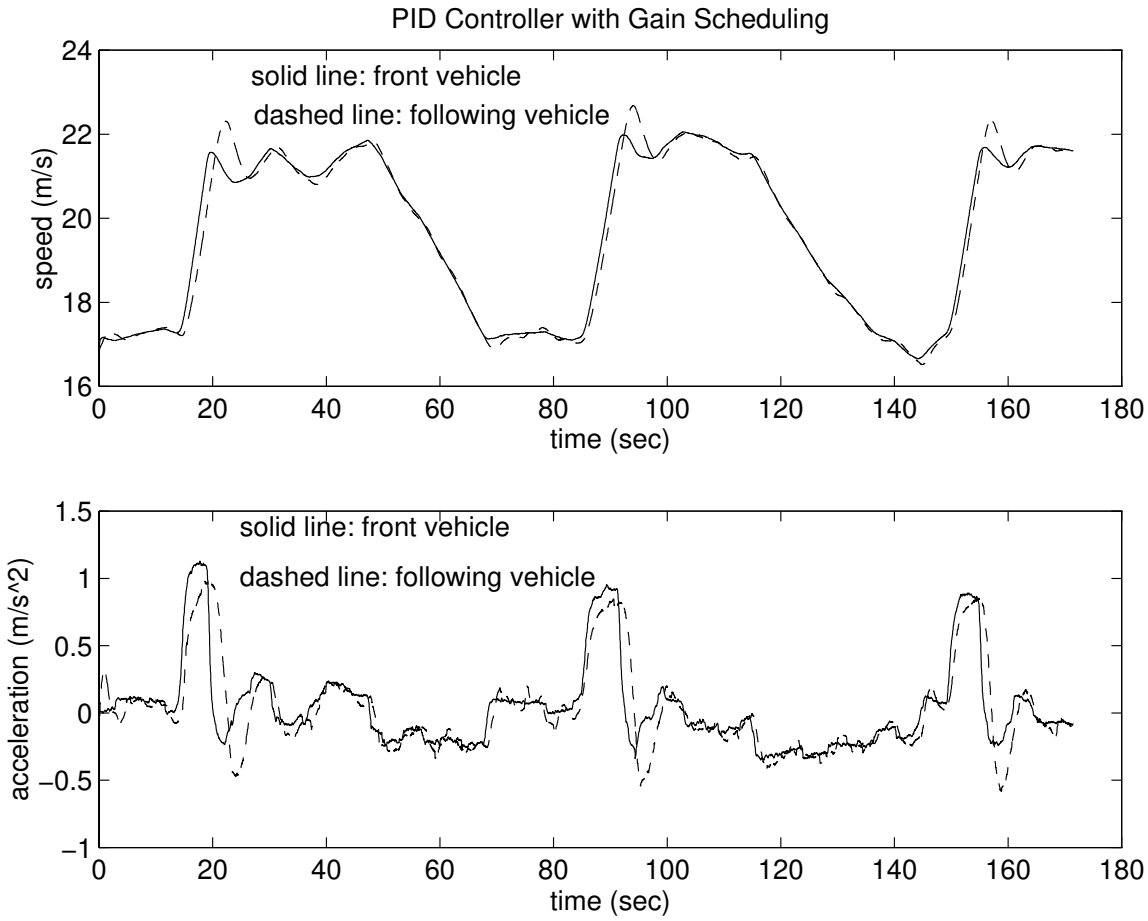

Figure 23: The speed and acceleration profiles for nonlinear PID controller with no v-v communication. The desired speed profile is 40-50-40-50 with large acceleration.

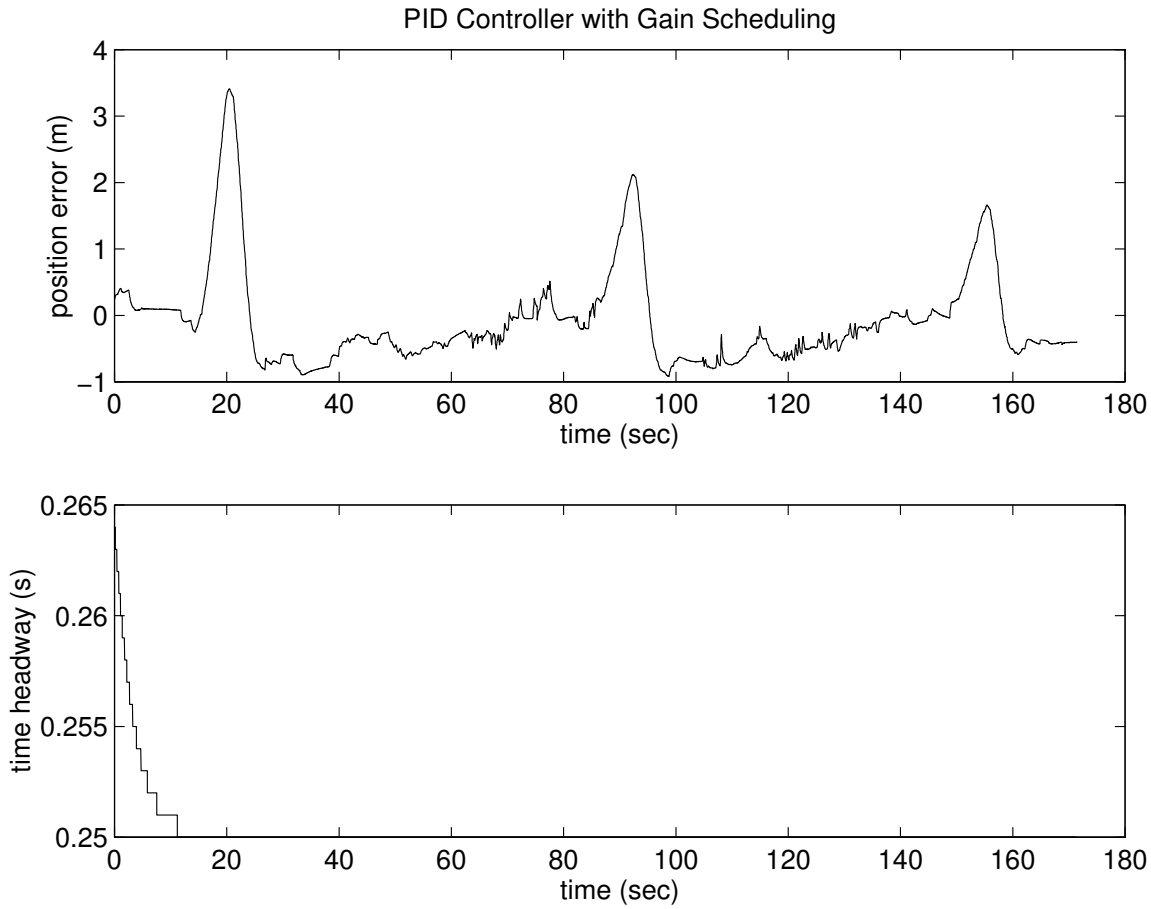

Figure 24: The position error and time headway for nonlinear PID controller with no v-v communication.

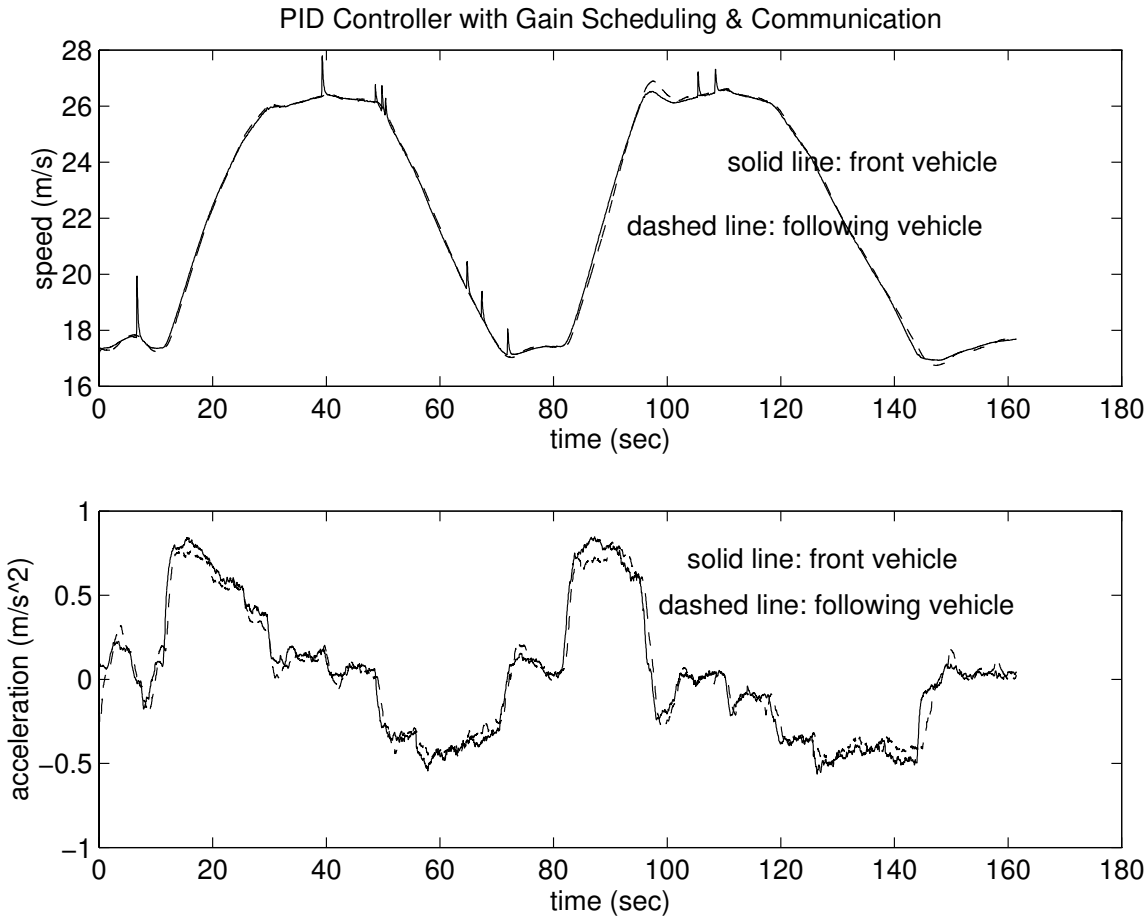

Figure 25: The speed and acceleration profiles for nonlinear PID controller with v-v communication. The desired speed profile is 40-55-40-55 with large acceleration.

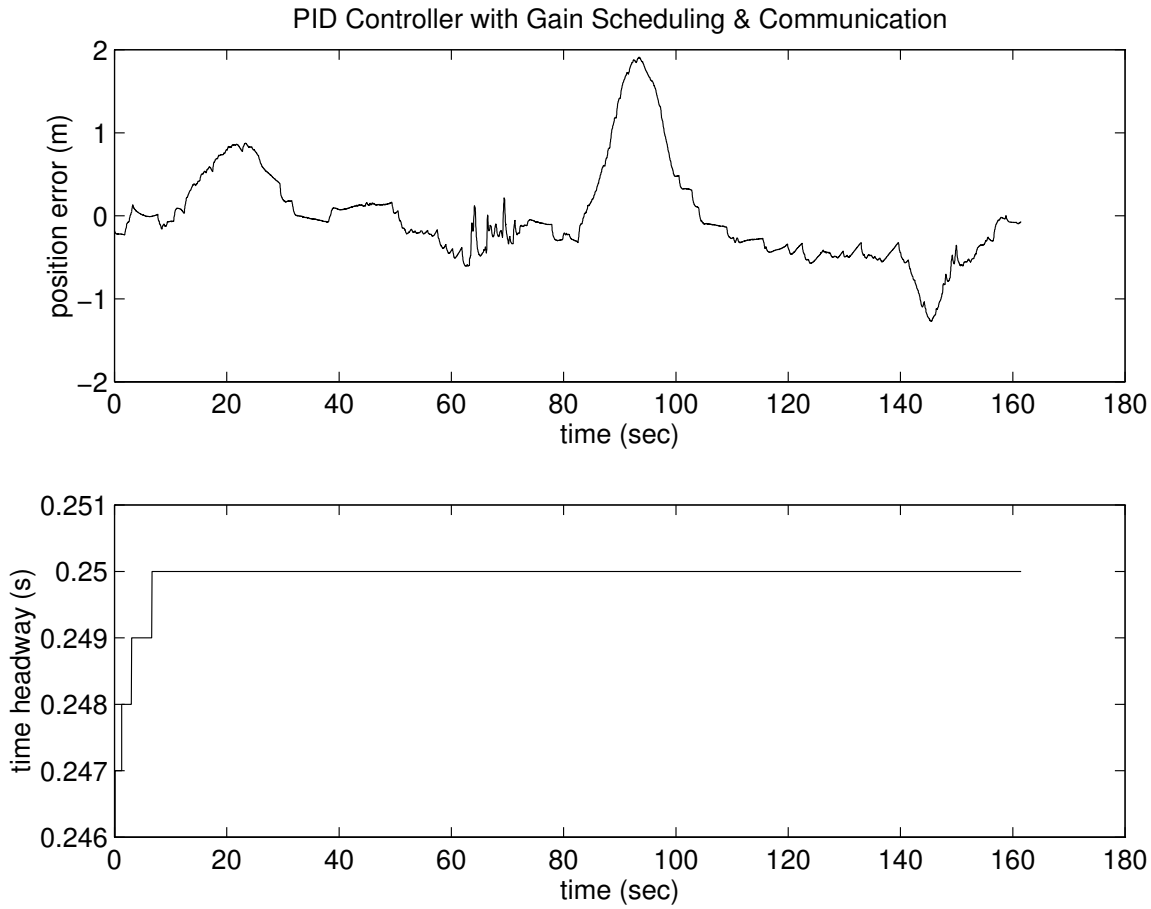

Figure 26: The position error and time headway for nonlinear PID controller with v-v communication.

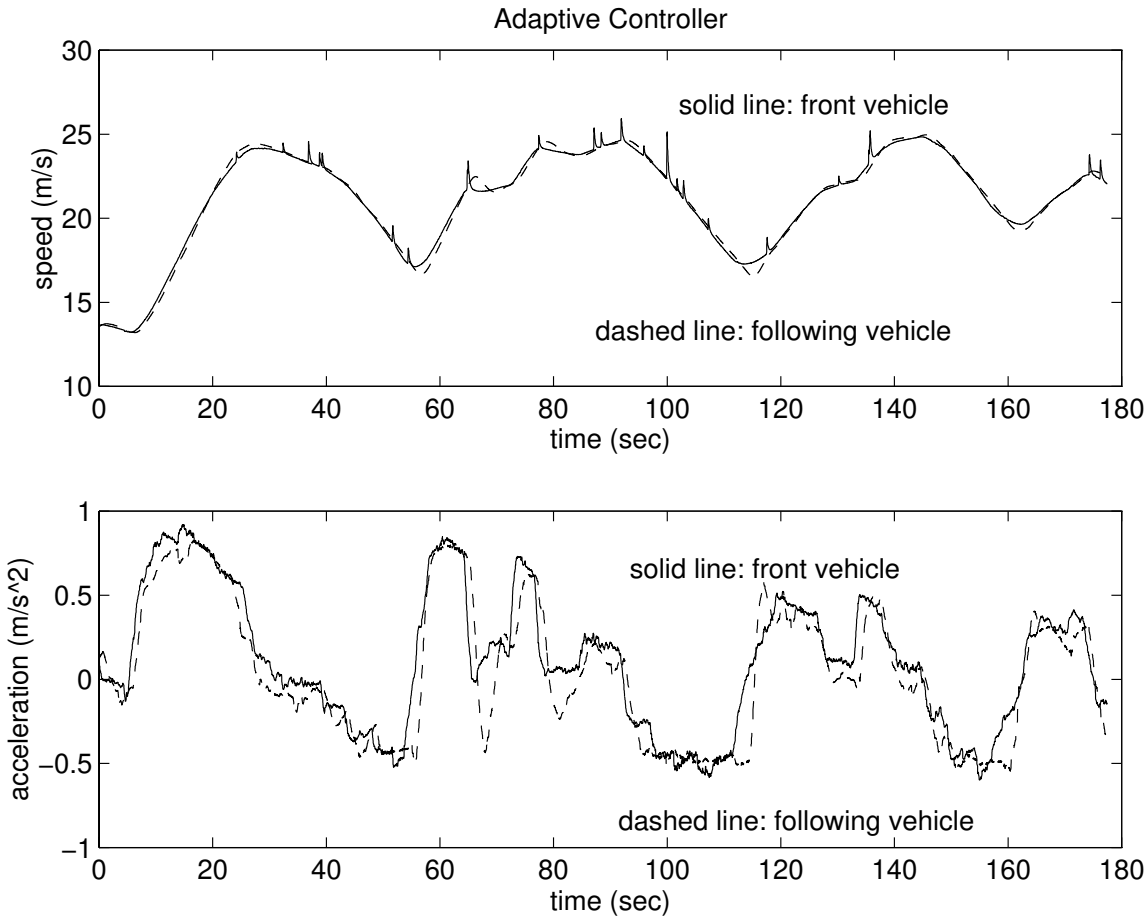

Figure 27: The speed and acceleration profiles for adaptive controller without v-v communication. The sharp spikes in leading vehicle speed are due to sensor noise.

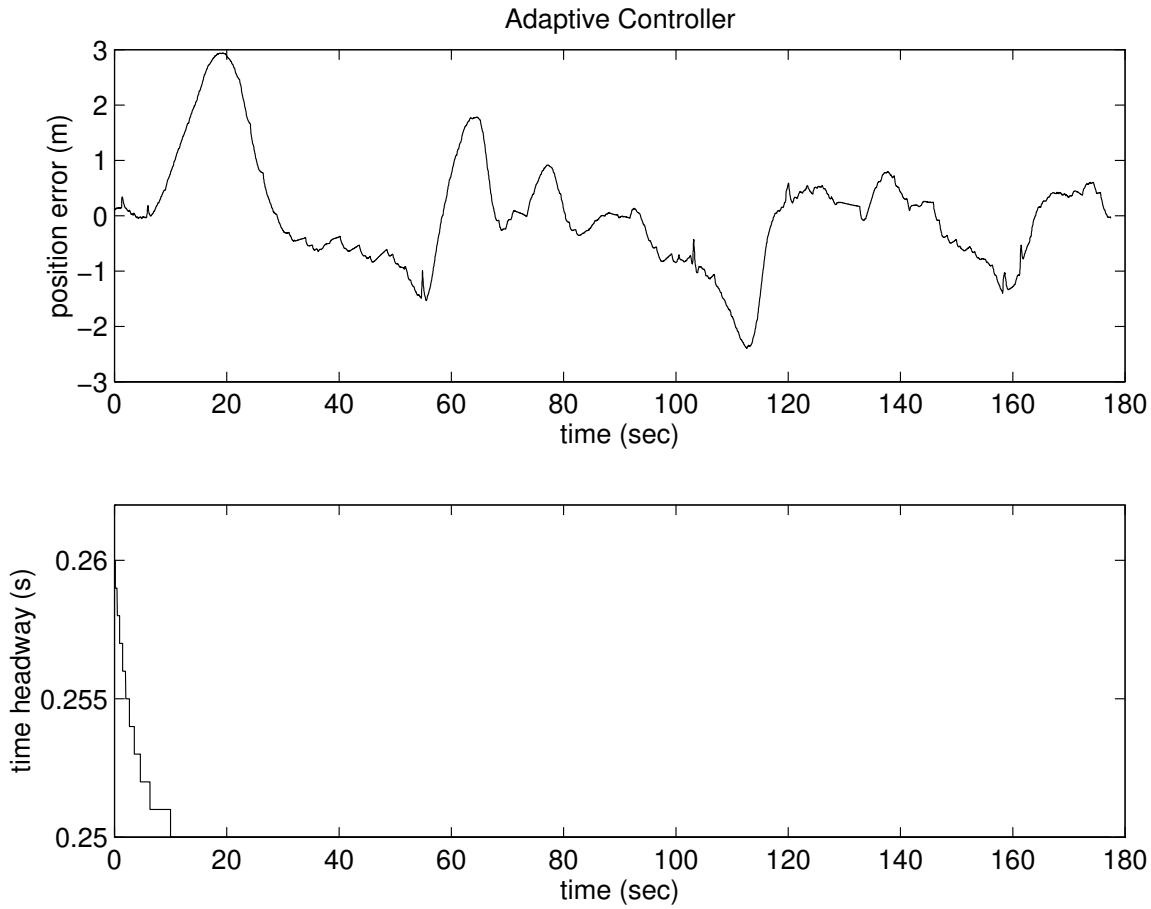

Figure 28: The position error and time headway for adaptive controller without v-v communication.

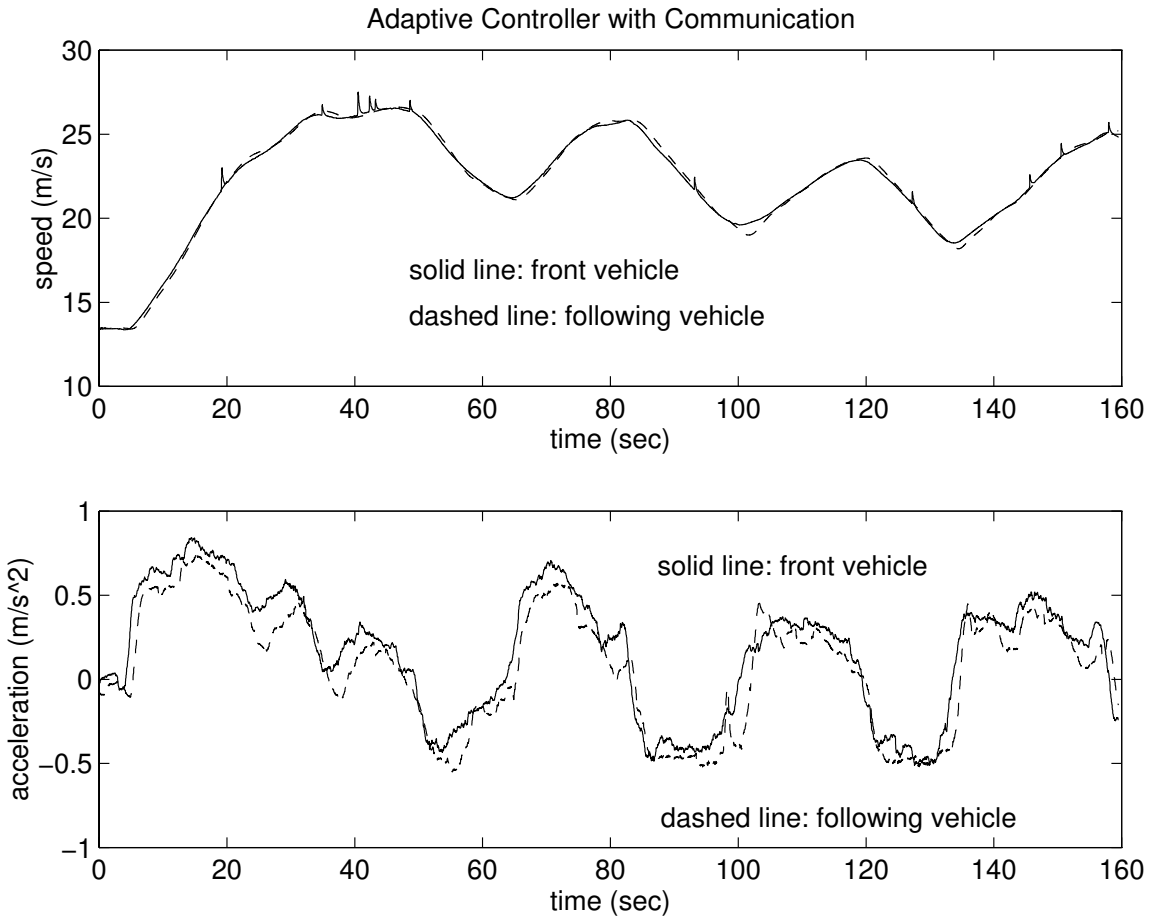

Figure 29: The speed and acceleration profiles for adaptive controller with v-v communication. The sharp spikes in leading vehicle speed are due to sensor noise.

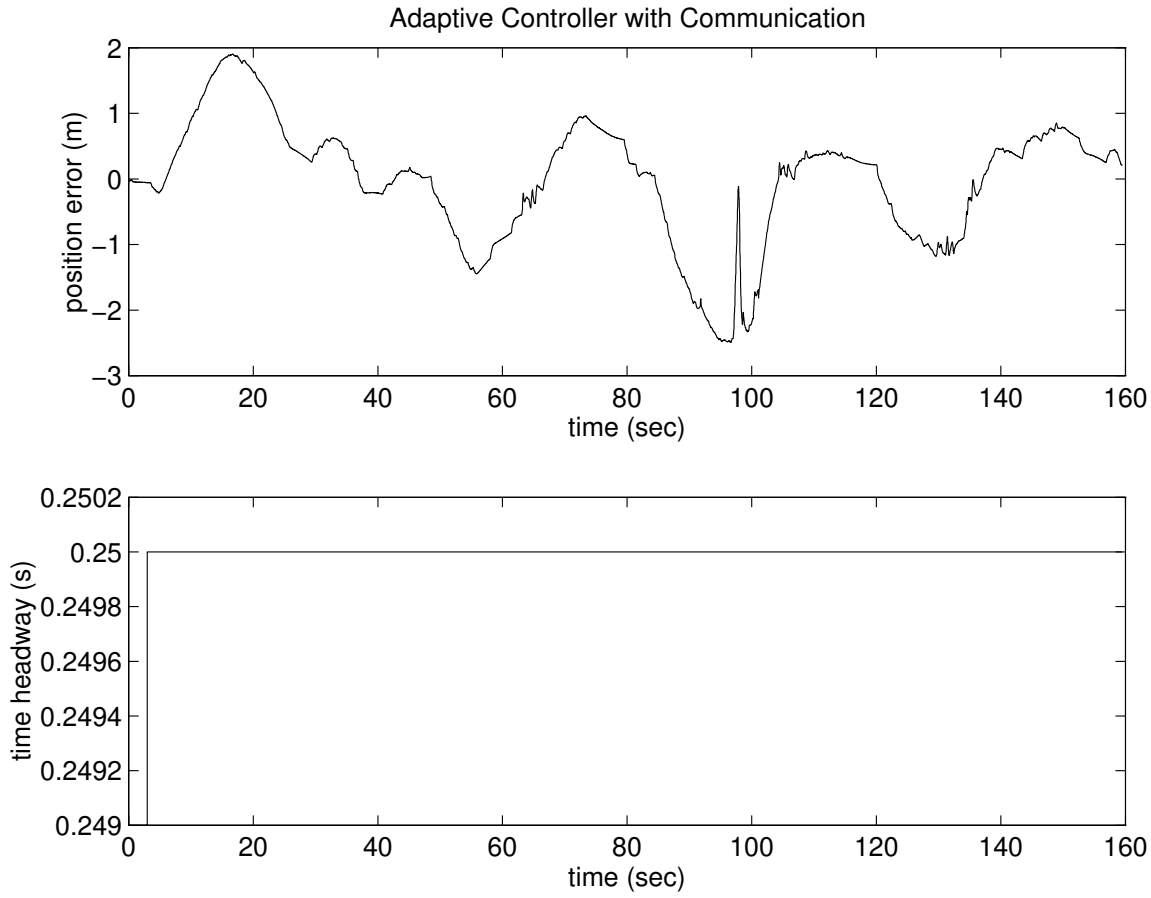

Figure 30: The position error and time headway for adaptive controller with v-v communication.

Experimental Evaluation of Cooperative Driving System[1]

by

H. Raza, Z. Xu, P. Ioannou

Report 97-7-01 July 1997

[1]This work is supported by the California Department of Transportation through PATH of the University of California. The contents of this paper reflect the views of the authors who are responsible for the facts and accuracy of the data presented herein. The contents do not necessarily reflect the official views or policies of the State of California or the Federal Highway Administration. This paper does not constitute a standard, specification or regulation.

Contents

Experimental Evaluation of Cooperative Driving System

H. Raza, Z. Xu, P. Ioannou
Center for Advanced Transportation Technologies
EE - Systems, EEB 200B
University of Southern California
Los Angeles, CA 90089-2562

Abstract

This report describes the experimental results of the vehicle tests conducted for PATH project MOU248. The complete testing was done in two phases. In the first phase, the vehicle tests were conducted in HOV lanes of I-15 (near San Diego, California) on February 7 — 8, 1995, using two vehicles provided by PATH. In this phase the vehicles were equipped only with the throttle actuators, hence the testing was restricted only to the throttle controllers. The second phase of experiments were conducted on Crow's Landing near Patterson, California on March 25th and April 24, 1997 using three vehicles provided by PATH. In this phase both throttle and brake controllers were tested. The testing was completed in several steps, with new features being added in each step. Finally a complete roadway/vehicle cooperative driving system was demonstrated by including roadway controller in the test loop. The required objective of the control design pursued in this study is supported by test results summarized in this report.

1 Introduction

Longitudinal control is an important part of advanced vehicle control system (AVCS). Some of the objectives of longitudinal control in AVCS are: to increase safety, to reduce the headway, to increase the traffic flow. Longitudinal control involves the throttle and brake control, and it can be accomplished with only on-board sensors, computers, and actuators, or with the aid of vehicle-to-vehicle (v-v) communications and/or roadway-to-vehicle (r-v) communications. If the vehicle following is achieved without v-v communication, it is called autonomous. The autonomous intelligent cruise control (AICC) is one of such configurations. In the AICC system, ranging sensor provides the information about the relative distance and relative speed of the vehicle in-front. Based on these measurements and other other on-board sensor measurements such as vehicle's own speed, engine speed, the on-board computer calculates and sends proper commands to throttle and brake actuators. The advantage of AICC is its simplicity. Its implementation does not requires any change

in infrastructure, and each vehicle operates independently. It has been shown that intelligent cruise can achieve smaller headway and larger traffic throughput than manual control because the ranging sensors and computers have faster response than drivers [1]. To further increase the response speed and reduce the minimum safety headway, v-v communication can be employed. On of the functions of v-v communication is to transfer the information about the acceleration of front vehicle, which is hard to be measured by the on-board sensor due to noise. With the front vehicle's acceleration information, the on-board computer can easily know its **intention** and hence respond promptly.

While conducting research on projects from PATH, our research group has designed several longitudinal vehicle following controllers and tested them on test track with Ford's vehicles. In those tests, two vehicles were used and no acceleration information was used in the controllers (which means no v-v communication was needed). The purpose of this study is to extend these simple AICC controllers so that they can be used in a roadway/vehicle cooperative driving system. In this environment the vehicle controllers have the capability to react not only to the commands issued by the driver, as in AICC, but also to the external commands issued by the roadway controller and/or surrounding vehicles.

The design objective was achieved by augmenting the AICC controller, which consists of throttle and brake controller, with additional outer loop controller, referred to as the supervisory controller. The supervisory controller ensures that the necessary commands are executed with guaranteed performance. The performance is dictated in terms of safety, comfort and stability of the local as well as the global system. A complete roadway/vehicle cooperative driving system was obtained by designing a roadway controller at the infrastructure level. The roadway controller issues speed and/or headway commands to vehicles in a section to attain the desired objective of optimal flow.

A significant portion of this study is to experimentally evaluate the performance of the designed controllers as they operate in a cooperative driving environment. The final objective of demonstrating a complete roadway/vehicle cooperative driving system is preceded by a group of tests each of which is aimed at testing a separate component of the complete system. The results obtained in these preliminary tests were used to gauge the performance of the system at each step and to tune the controllers before they can be used in the demonstration.

The initial phase of the testing was completed at I-15 near San Diego, California. The purpose of these test was to compare performance of different throttle controllers designed by our group and to choose an appropriate controller for the final demonstration. The second phase of tests was conducted on March 25th and April 24, 1997 at Crow's Landing near Patterson, California. Different test setups were used to test the basic components of the automatic vehicle following before demonstrating the cooperative driving system. The performance of the designed controllers was found to be satisfactory and fulfills the

requirements of this study. In the following we will describe the test results with appropriate discussion and recommendations.

2 Test 1: Evaluation of Throttle Controllers

The purpose of this test is to evaluate the performance of different throttle controllers developed by our research group while conducting research on projects from PATH. Based on the results of this test an appropriate throttle controller will be selected for final demonstration. Another objective of this test is to compare the performance of these controllers with and without v-v communication.

2.1 Test Setup

This test was conducted on HOV lanes of I-15 near San Diego with two vehicles provided by PATH. Each of the two vehicles were equipped with ranging sensor which can measure relative distances up to about 20 meters and v-v communication devices. Through the communication, the leading vehicle passes its speed, acceleration, and other information to the following vehicle. The vehicles were equipped with the throttle actuators but no brake actuators were available at the time this test was conducted. The whole setup is shown in Figure 1.

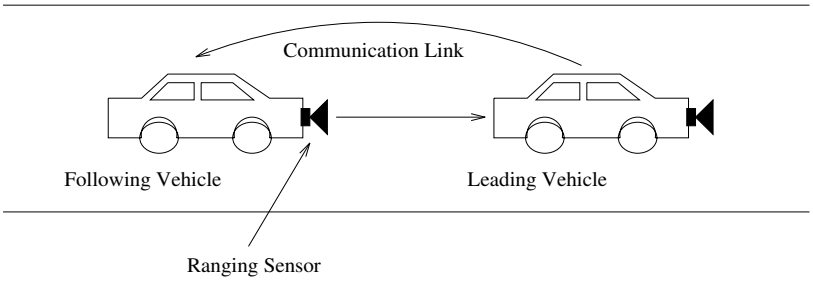

Figure 1: Two-vehicle-following setup for the test.

In the following, we will briefly describe the design of throttle controllers being tested. For details, the reader is referred to [2].

2.2 Tested Controllers

Before presenting controller algorithms to be tested, we first present the longitudinal vehicle model related to the throttle subsystem.

The vehicle speed is a nonlinear function of throttle, gear state, air/fuel ratio, engine speed, etc [3, 4, 5, 6]. With the help of Ford Motor Company, we obtained a validated vehicle model which describes this nonlinear dynamics. Based on this validated model, we developed a linearized model around an operating point (V_0, θ_0) where V_0 is the steady state

vehicle speed corresponding to a constant throttle angle input θ_0. Define $\bar{V} \stackrel{\triangle}{=} V - V_0$ as the deviation of the vehicle speed V from V_0, and $\bar{\theta} \stackrel{\triangle}{=} \theta - \theta_0$ as the throttle deviation from θ_0. Then the linearized model that relates $\bar{V}$ and $\bar{\theta}$ over a wide range of speed V_0 (from 0 to 36 m/s), has the form:

$$\frac{\bar{V}}{\bar{\theta}} = \frac{b_0}{s^3 + a_2 s^2 + a_1 s + a_0} = \frac{b_0}{(s+p_1)(s+p_2)(s+p_3)} \tag{1}$$

where the coefficients b_0, a_0, a_1, a_2 are functions of the operating point (V_0, θ_0), i.e., b_0 and a_i have different values for different V_0 or θ_0.

For all operating points considered, however, we found that $b_0 > 0$, $p_1 > 0$, and p_2 and p_3 (which may be either conjugate complex or real numbers) have positive real parts. Furthermore, $Re(p_2), Re(p_3) >> p_1$ and $0 < p_1 \leq 0.2$. A measure of how far apart $Re(p_2)$ and $Re(p_3)$ are from p_1 can be given by the value of a variable μ defined as

$$\mu \stackrel{\triangle}{=} \sup_{\theta_0 \in \Theta} \max \left[\frac{p_1}{Re(p_i)}, \; i = 2,3 \right] \tag{2}$$

where Θ is the full range of θ_0. Our simulation results show that $\mu < 0.05$ which indicates that $-p_1$ is the dominant pole and that fast modes associated with p_2 and p_3 can be neglected, leading to the simpler model

$$\frac{\bar{V}}{\bar{\theta}} = \frac{b}{s+a} \tag{3}$$

where a and b vary with V_0. The effects of the fast mode terms and uncertainties neglected in the linearization procedure may be modeled as a disturbance term d, leading to the model

$$\dot{\bar{V}} = -a\bar{V} + b\bar{\theta} + d \tag{4}$$

or equivalently,

$$\dot{V} = -a(V - V_0) + b\bar{\theta} + d. \tag{5}$$

Adding the position variable X to the vehicle model, we obtain the complete dynamic equations of the throttle angle to vehicle speed and position and are:

$$\begin{aligned} \dot{X} &= V \\ \dot{V} &= -a(V - V_0) + b\bar{\theta} + d. \end{aligned} \tag{6}$$

The important point to note is that the parameters a, b, d are functions of operating points (V_0, θ_0). For details of the development, reader is referred to [2].

Based on this simple model, we have designed six throttle controllers. Five of them were tested in this test phase and are presented below. In the following the subscript l denotes the leading vehicle, subscript f denotes the following vehicle.

2.3 Controllers without Communication

As pointed out earlier, the vehicles are equipped with ranging sensors which can measure only the relative distance between vehicles. The relative speed between two vehicles, which is required to calculate the throttle input, is not available directly from sensors. Hence in this set up the speed and acceleration of the leading vehicle is transmitted to the following vehicle through communication. In this way, the speed of the leading vehicle, available through communication, can be used to calculate the relative speed between two vehicles and compensates for the non-availability of the same information through sensors.

However, in this part of the test we will not use the acceleration information from the leading vehicle. The acceleration information can be considered as a mean to assess the intention of the leading vehicle and hence to modify the control input of the following vehicle accordingly. This absence of acceleration information of the leading vehicle in the control input will be regarded as the case with no v-v communication, even though there may or may not be an active communication link available to transfer other information. In the following we will present the design of throttle controllers which do not rely on acceleration information and hence require no v-v communication.

2.3.1 Nonlinear PID Controller

Based on the linearized model (6), we designed the control algorithm of the following form:

$$\theta_f = \theta_0 + k_1 V_r + k_2 \delta + \int_0^t (k_3 V_r + k_4 \delta) d\tau. \tag{7}$$

where V_r is the relative speed between the front vehicle and the following vehicle, i.e. $V_r = V_l - V_f$; δ is the position deviation from the desired one, i.e, $\delta = X_l - X_f - hV_f$, (where h is the time headway); θ_0 comes from a look-up table describing the relationship between θ_0 and the steady state vehicle speed V_0, i.e.

$$\theta_0 = f^{-1}(V_0). \tag{8}$$

In this controller, k_2 is the proportional gain for position deviation, k_1 is the proportional gain for speed deviation, and k_3, k_4 are the gains for integration. Since V_r is the derivative of the relative distance, we treat $k_1 V_r$ as the derivative term and the whole controller is called proportional-integral-derivative (PID) controller.

Because the parameters a, b and d in the linearized model (6) depend on the operating point (V_0, θ_0), we also change the gains k_1 — k_4 based on the operating speed V_0. In other words, we schedule the gains based the operating speed V_0. The controller designed in this way is called the PID controller with gain scheduling on nonlinear PID controller.

Because V_0 is the operating speed and V_l is the speed to track, it makes sense to let $V_0 = V_l$, which is exactly what we did. In other words, we schedule the gains based on the

speed of the front vehicle.

In our experiment, the function $f^{-1}(V_0)$ or $f^{-1}(V_l)$ and parameters a, b vs V_l are shown in Figures 2 and 3 respectively. By ignoring the disturbance d from (6), the gains k_1 — k_4 are calculated based on the following equations:

$$\begin{aligned} k_4(V_l) &= \frac{pole1 \times pole2 \times pole3}{b(V_l)} \\ k_3(V_l) &= 2 \times k_4 \\ k_2(V_l) &= \frac{pole1 \times pole2 + pole1 \times pole3 + pole2 \times pole3}{b(V_l)} - k_3 - k_4 \times h \\ k_1(V_l) &= \frac{pole1 + pole2 + pole3 - a(V_l)}{b(V_l)} - k_2 \times h \end{aligned} \tag{9}$$

which give the poles (pole1, pole2, pole3) for the closed loop system.

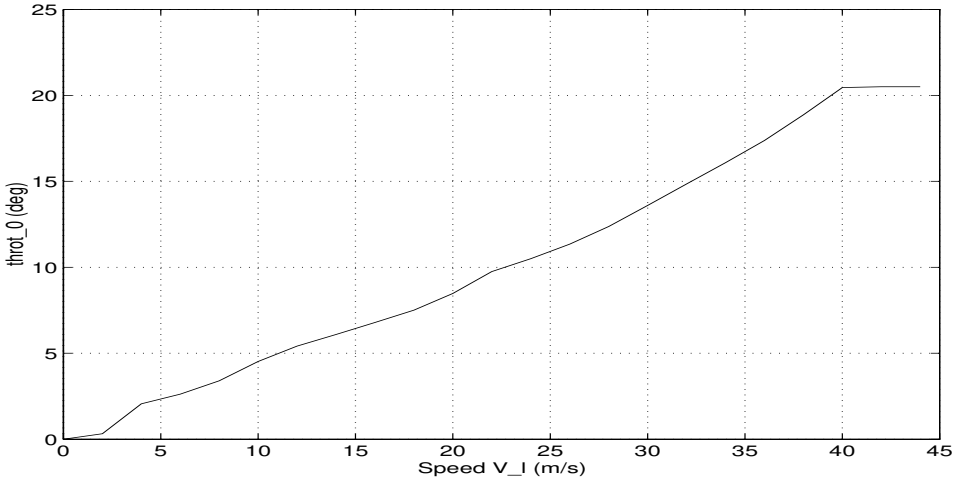

Figure 2: Throttle angle (θ_0) vs V_l

2.3.2 Adaptive Throttle Controller

The second controller we tested is the adaptive throttle controller. In this controller, we updated the gains on-line instead of using look-up tables. The control algorithm is described as follows.

$$\begin{aligned} \theta_f &= f^{-1}(V_l) + k_1 V_r + k_2 \delta + k_3 \\ \dot{k}_i &= \begin{cases} 0 & \text{if } k_i \geq k_{u_i} \text{ and } g_i > 0 \\ 0 & \text{if } k_i \leq k_{\ell_i} \text{and } g_i < 0 \\ g_i(\epsilon, V_f, \delta) & \text{otherwise} \end{cases} \end{aligned}$$

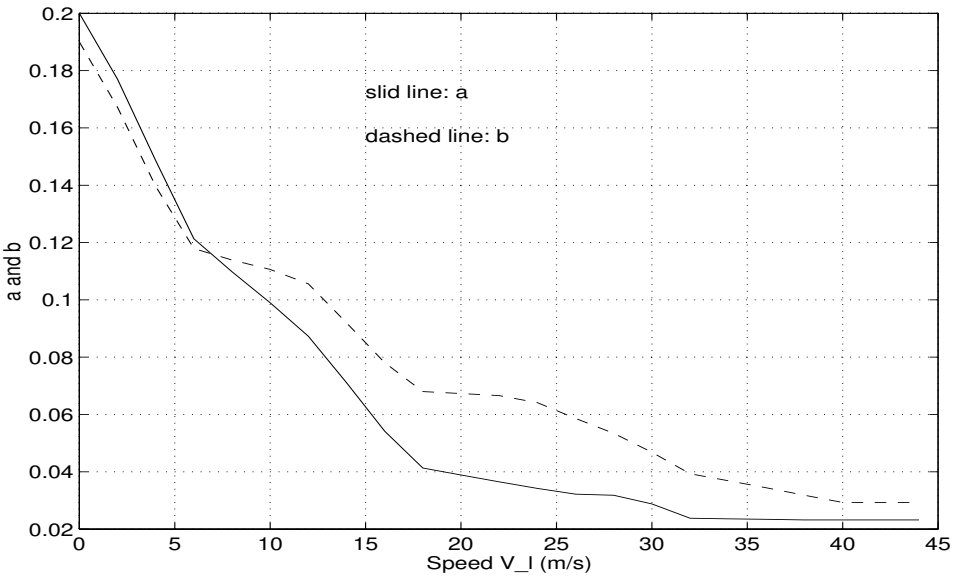

Figure 3: Parameters a, b vs V_l

$$\begin{aligned} \epsilon &= e_1 - \frac{1}{s+a_m}\lambda\epsilon m^2 \\ e_1 &= V_f - \frac{a_m}{s+a_m}[V_l + k\delta] \\ m^2 &= \delta^2 + V_r^2 \end{aligned} \tag{10}$$

where k_{u_i}, k_{ℓ_i} are upper and lower bounds for k_i respectively, ϵ is the modified error, λ is a design constant, and $g_1 = -\sigma_1(k_1 - k_{10}) - \gamma_1 V_r\epsilon$, $g_2 = -\sigma_2(k_2 - k_{20}) - \gamma_2\delta\epsilon$, and $g_3 = -\gamma_3\epsilon$ where $\sigma_i > 0$ $(i = 1, 2)$ are small design constants and k_{i0} is the initial estimate of k_i^* for $i = 1, 2$.

In the experiment, the actual parameters were set to be as follows:

$$a_m = 0.75, \quad \sigma_1 = 0.025, \quad \gamma_1 = 0.8, \quad k_{10} = 10, \quad , k_{u_1} = 40, \quad , k_{\ell_1} = 2,$$

$$k_{20} = 4, \quad , k_{u_2} = 20, \quad k_{\ell_2} = 0.3, \quad \sigma_2 = 0.005, \gamma_2 = 0.25,$$

$$\gamma_3 = 0.35, \quad k_{u_3} = 70, \quad k_{\ell_3} = -70, \lambda = 0.05.$$

The details of the derivation of the above two controllers can be found in [2]. In these two controllers, we have only used vehicle speed, relative distance and speed of front vehicle which are measurable by on-board sensors. Thus no v-v communication is required for these controllers. The following three controllers use the acceleration of front vehicle, and hence need the v-v communication.

2.4 Controllers with v-v Communication

The following controllers were tested with a communication link from the leading to the following vehicle, i.e., the acceleration information from the leading vehicle was used to modify the controllers (7) and (10).

2.4.1 Nonlinear PID Controller with v-v Communication

This controller is exactly the same as controller (7) described above except that it has an extra term due to the front vehicle acceleration. The controller is given as:

$$\theta_f = \theta_0 + k_1 V_r + k_2 \delta + \int_0^t (k_3 V_r + k_4 \delta) d\tau + k_5 a_l \tag{11}$$

where θ_0, k_1 — k_4 are the same as those in the PID controller with gain scheduling (7), and k_5 is given by the following equation:

$$k_5(V_l) = 0.9/b(V_l). \tag{12}$$

The choice of the parameter 0.9 is obtained from extensive simulations on the validated model. Note that $k_5 b a_l$ is part of the desired acceleration of the following vehicle. Hence addition of acceleration information of the leading vehicle a_l results in $0.9a_l$ being added to the acceleration of the following vehicle. Also note that $a_l \neq 0$ only during transients, and $k_5 a_l$ can be thought of as the feed forward term. Thus, $k_5 a_l$ can increase the response speed, but it does not affect the steady state performance of the controller.

2.4.2 Adaptive Controller with v-v Communication

This controller is the same as controller (10) described above except that it has an extra term due to the front vehicle's acceleration. The control input is given by the following equation:

$$\theta_f = f^{-1}(V_l) + k_1 \; V_r + k_2 \delta + k_3 + k_a \; a_l \tag{13}$$

where $f^{-1}(V_l)$, k_1, k_2, k_3 are the same as those in the above adaptive controller (10), and k_a is chosen as 18. This choice of gain k_a is again from extensive simulations on the validated model. Since $k_a a_l \neq 0$ only during transients, we did not change the adaptive algorithms for k_1 — k_3.

2.4.3 Fixed gain PID Controller with v-v Communication

This controller is the same as controller (11) except that the gains k_1 — k_5 are some constants. In the experiment, these gains were chosen as follows:

$$k_1 = 14.54, \quad k_2 = 3, \quad k_3 = 0.56, \quad k_4 = 0.25, \quad k_5 = 15.$$

This choice of the gains is also from extensive simulations on the validated model.

Remarks

- Because $a_l \neq 0$ only during transient, we use ka_l instead of $k(a_l - a_f)$ in controllers 11-13. In fact, our simulations show that using $k(a_l - a_f)$ will reduce the response speed of the following vehicle.

- Note that in [2], we designed a fixed gain PID controller without using the front vehicle's acceleration. Simulations and experiments shows that it can give satisfactory performance when the time headway is larger than 0.5 seconds. Due to the sensor limit, we could only do the experiment with time headway less than 0.5 seconds. Thus we did not test this controller in this experiment.

2.5 Experimental Results

For each controller presented above, the tests were conducted with two values of time headway, 0.25 seconds and 0.4 seconds. Due to the limit of the ranging sensor, we could not test the controllers with larger time headway. There were 3 speed profiles for the platoon leader. The first speed profile was starting at 30 mph, going to 60 mph with small acceleration, staying at 60 mph for a while, decreasing to 40 mph slowly, going back to 60 mph slowly, and then staying at 60. For simplicity, we use 30-60-40-60 to indicate this speed profile. The second speed profile is 40-50-40-50 or 40-50 with large acceleration. The third speed profile is that the platoon leader was driven manually following some sinusoid speed curve.

Figure 5 is a typical response of the position error for the PID controller with gain scheduling. The corresponding time headway, speed and acceleration profiles are shown in Figures 4-5. It can be seen from Figure 5 that the negative position error is within 1 m, which allows the following vehicle to travel close to the leading vehicle without any collision. The speed profiles in Figure 4 show that the following vehicle tracks the speed profile of the leading vehicle closely except near transitions, where a sudden change in speed of the leading vehicle creates a large position error which is reduced by making the speed of the following vehicle greater than that of the leading vehicle during that interval. In this test the headway is set to be 0.25 seconds, hence as shown in Figure 5 the actual headway is smoothly reduced from an initial value of 0.265 seconds to the desired value of 0.25 seconds. As pointed out earlier that the controller design ensures that the acceleration of the vehicle is within the specified bounds. The claim is obvious from the acceleration profiles shown in Figure 4, where the acceleration of following vehicle is less than the set limit of 1 m/sec^2, even though the leading vehicle accelerates beyond the set limit.

The test results of PID controller with communication for a speed profile of 40-55-40-55 are shown in Figures 6-7. By comparing Figure 6 with Figure 4 it is obvious that the addition of v-v communication has helped the following vehicle to closely track the speed profile of the leading vehicle. Hence transmission of the acceleration of leading vehicle reduces the time delay incurred by assessing the same information through the sensor measurements. Similarly Figure 7 shows that the maximum negative position error is close to 1 m, which is satisfactory considering the fact that no brake actuator was used in the experiment and

required deceleration was obtained by releasing the throttle.

Figures 8-9 and 10-11 show the experimental results for adaptive controller without and with v-v communication respectively. In both cases sinusoid speed profile, which represents typical manual driving, was chosen. The time headway in both cases was selected to be 0.25 seconds. Again by comparison of Figures 8 and 10 it is obvious that addition of v-v communication improves the performance of the vehicle following controller.

The experimental results for fixed gain PID controller with v-v communication, using 30-60-40-60 speed profile, are shown in Figures 12-13. It can be seen from Figure 12 that the following vehicle tracks the speed commands perfectly due to relatively small acceleration magnitudes used in this experiment. From Figure 12 the relatively poor performance of fixed gain PID is obvious in the form of not so smooth acceleration profile of the following vehicle, which is resultant of using fixed gains while calculating the throttle input.

2.6 Discussions and Recommendations

- In the experiments, we saw some large negative position error (which means smaller relative distance) when the front vehicle was decelerating. This is because, the vehicles were not equipped with brake actuators at that time. The best following vehicle could do to decrease the speed was to release the throttle. Affected by the road surface and other factors, the speed of the following vehicle may be larger than that of front vehicle, leading to large negative position error.

- The driver and passenger comfort is an important factor in our controller design. During the test, we did not experience any uncomfortable ride. The jerk was small, and the ride was smooth for each of the tested controller.

- To make the vehicles in a platoon to have uniform performance, we introduced the acceleration limiter in our throttle controller design. This is done by limiting the position error and the slope of the speed to be tracked. In the controller implementation, instead of using actual V_l we used a filtered version of V_l. The derivative of the filtered version of V_l is always within a pre-determined range. For detail of the acceleration limiter, please see [2]. In this test, we set the maximum acceleration to be 1 m/s^2. Figure 4 shows that the acceleration of the following vehicle do falls within this limit.

From the experimental results it is obvious that the performance of nonlinear PID throttle controller with v-v communication is much better than the other tested controllers for all speed profiles. Hence nonlinear PID throttle controller with v-v communication will be used in the subsequent tests and the final demonstration.

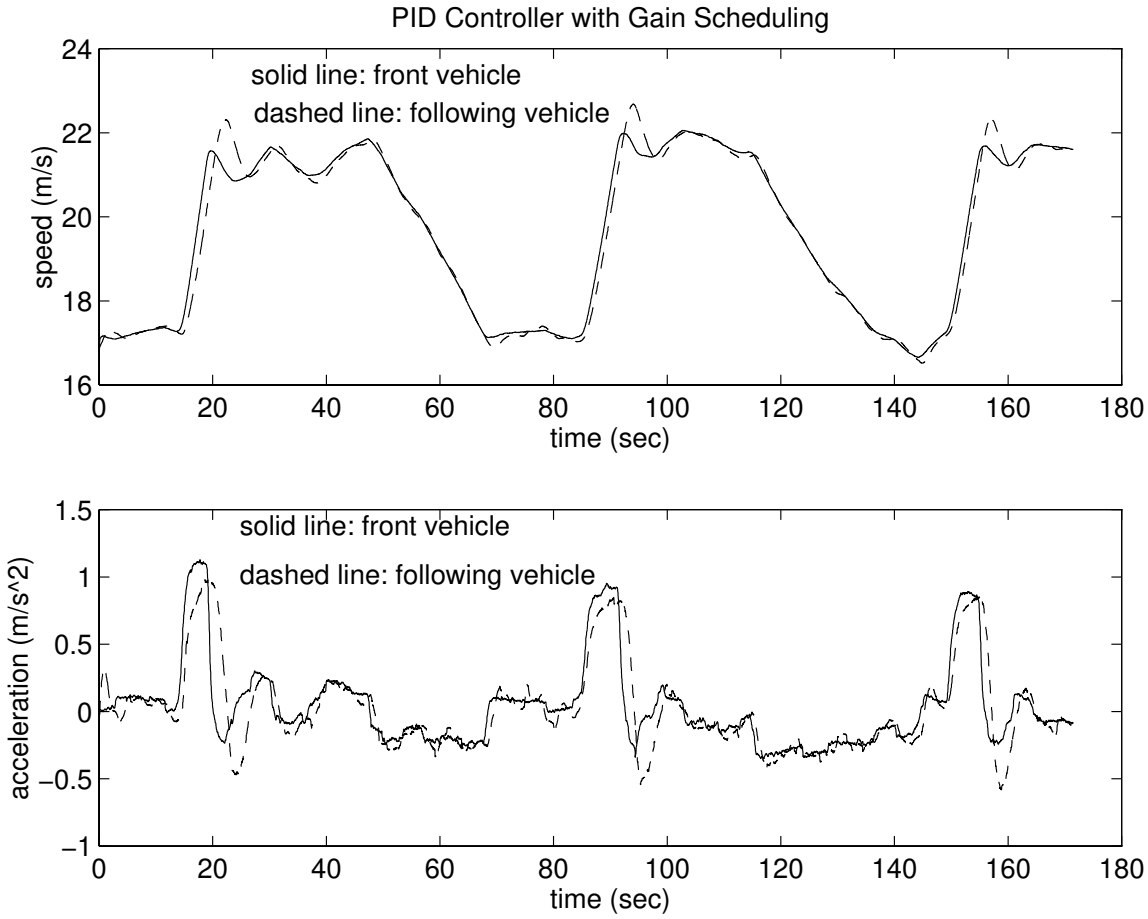

Figure 4: The speed and acceleration profiles for nonlinear PID controller with no v-v communication.

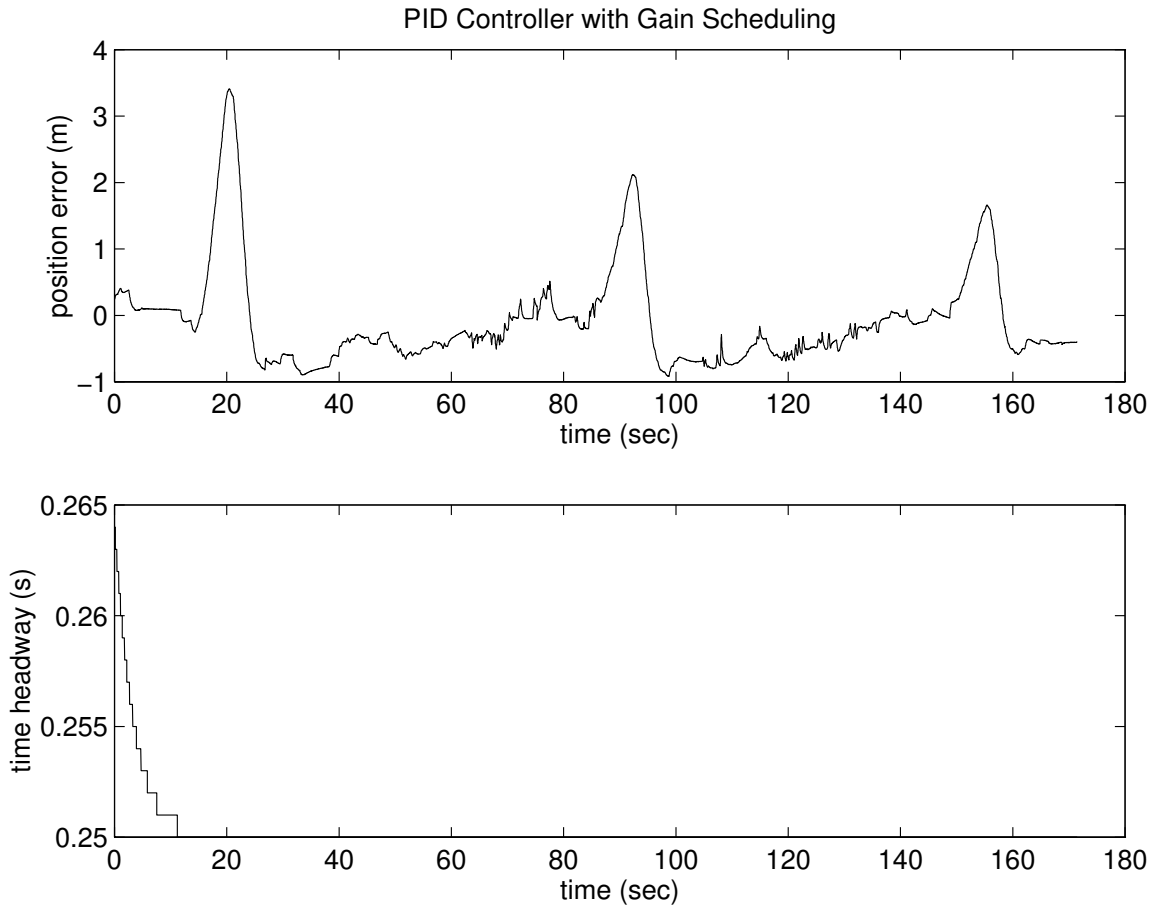

Figure 5: The position error and time headway for nonlinear PID controller with no v-v communication.

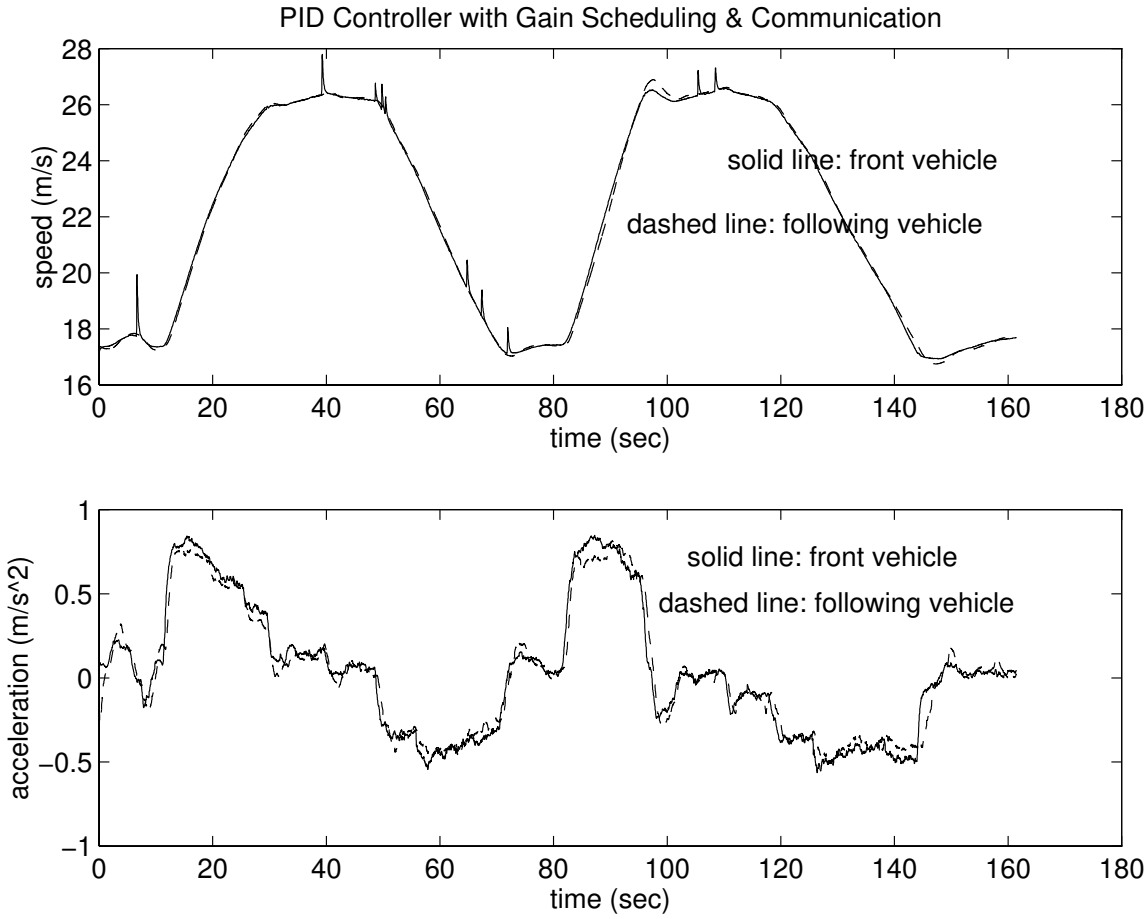

Figure 6: The speed and acceleration profiles for nonlinear PID controller with v-v communication.

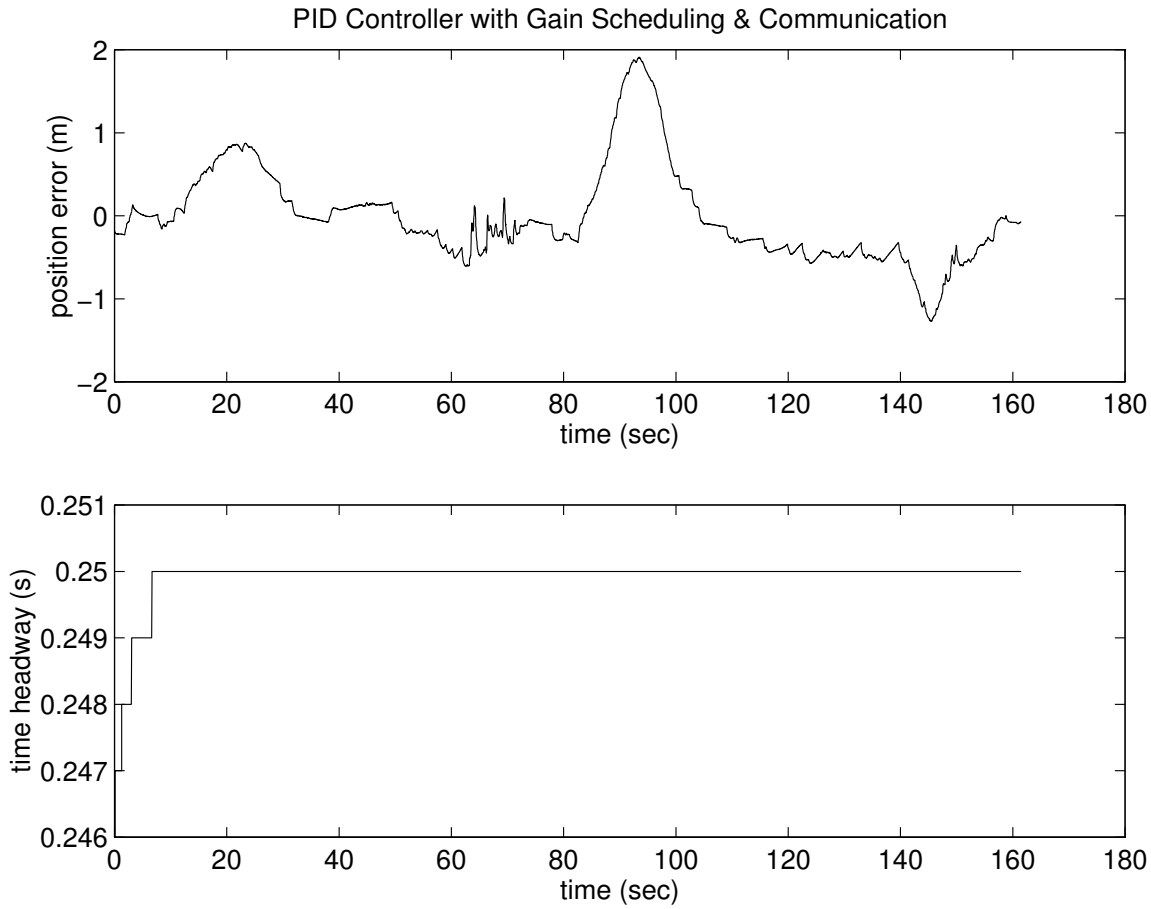

Figure 7: The position error and time headway for nonlinear PID controller with v-v communication.

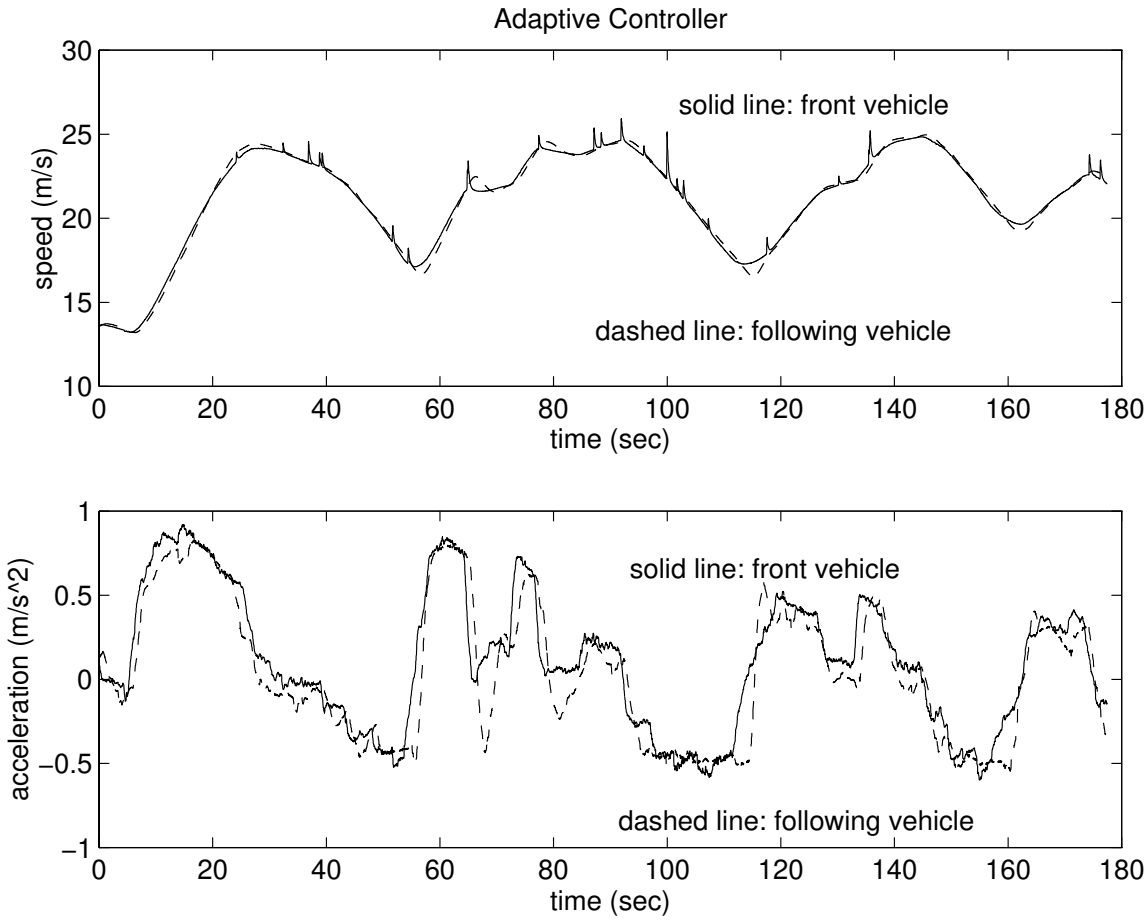

Figure 8: The speed and acceleration profiles for adaptive controller without v-v communication. The sharp spikes in leading vehicle speed are due to sensor noise.

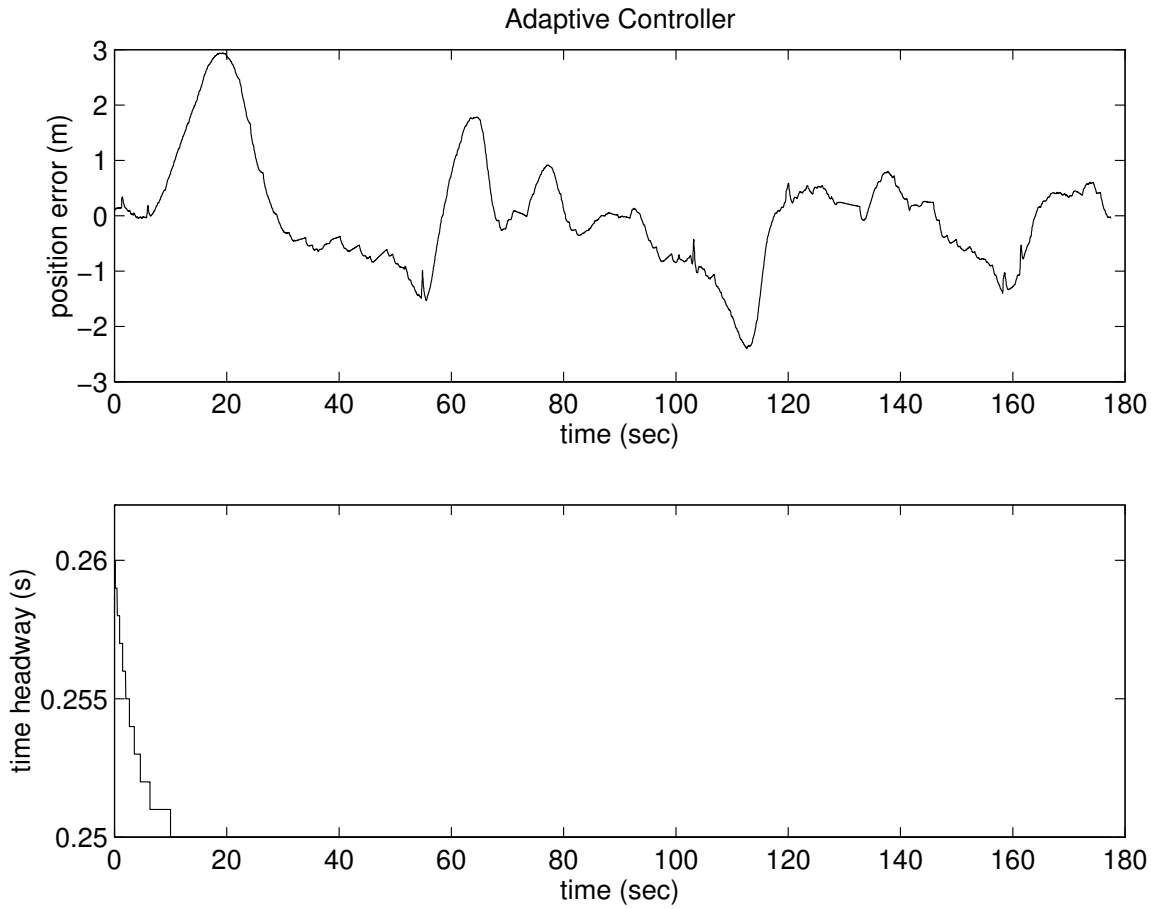

Figure 9: The position error and time headway for adaptive controller without v-v communication.

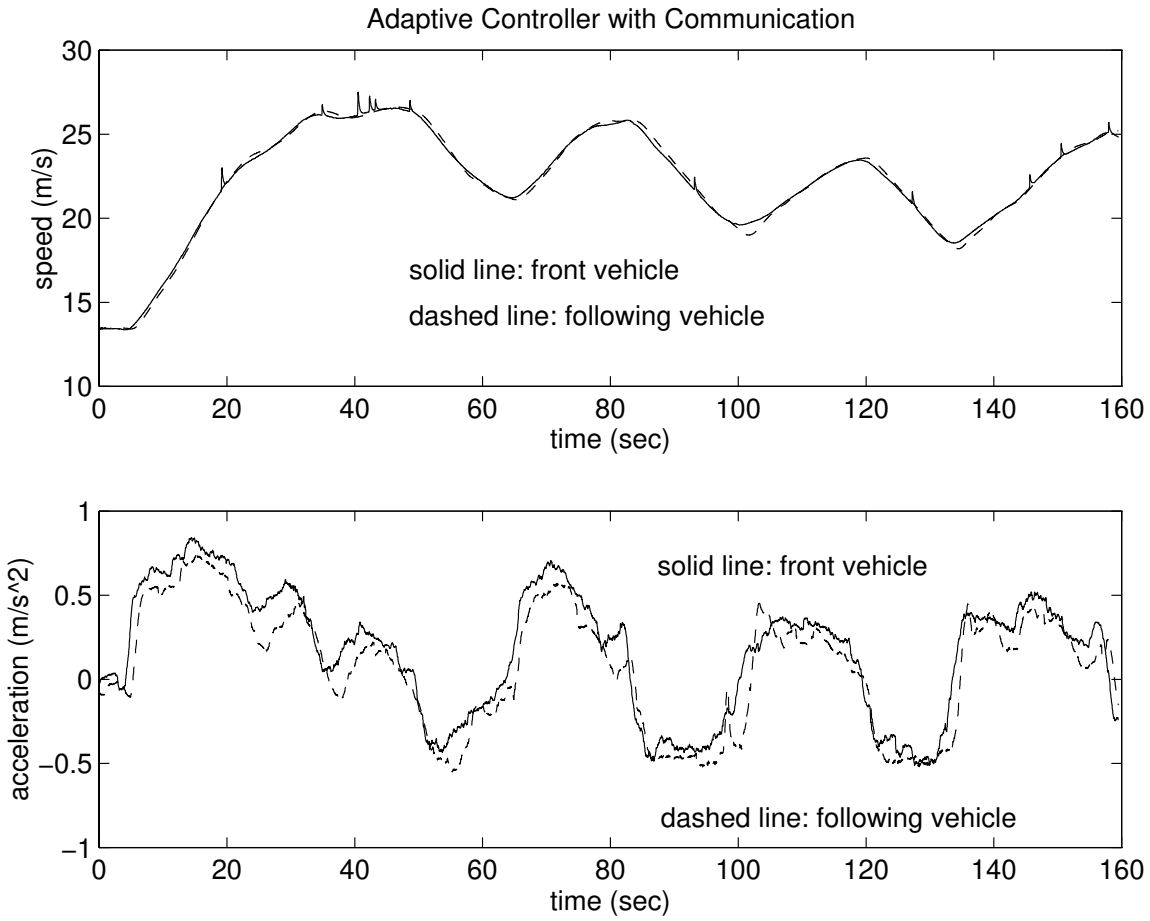

Figure 10: The speed and acceleration profiles for adaptive controller with v-v communication. The sharp spikes in leading vehicle speed are due to sensor noise.

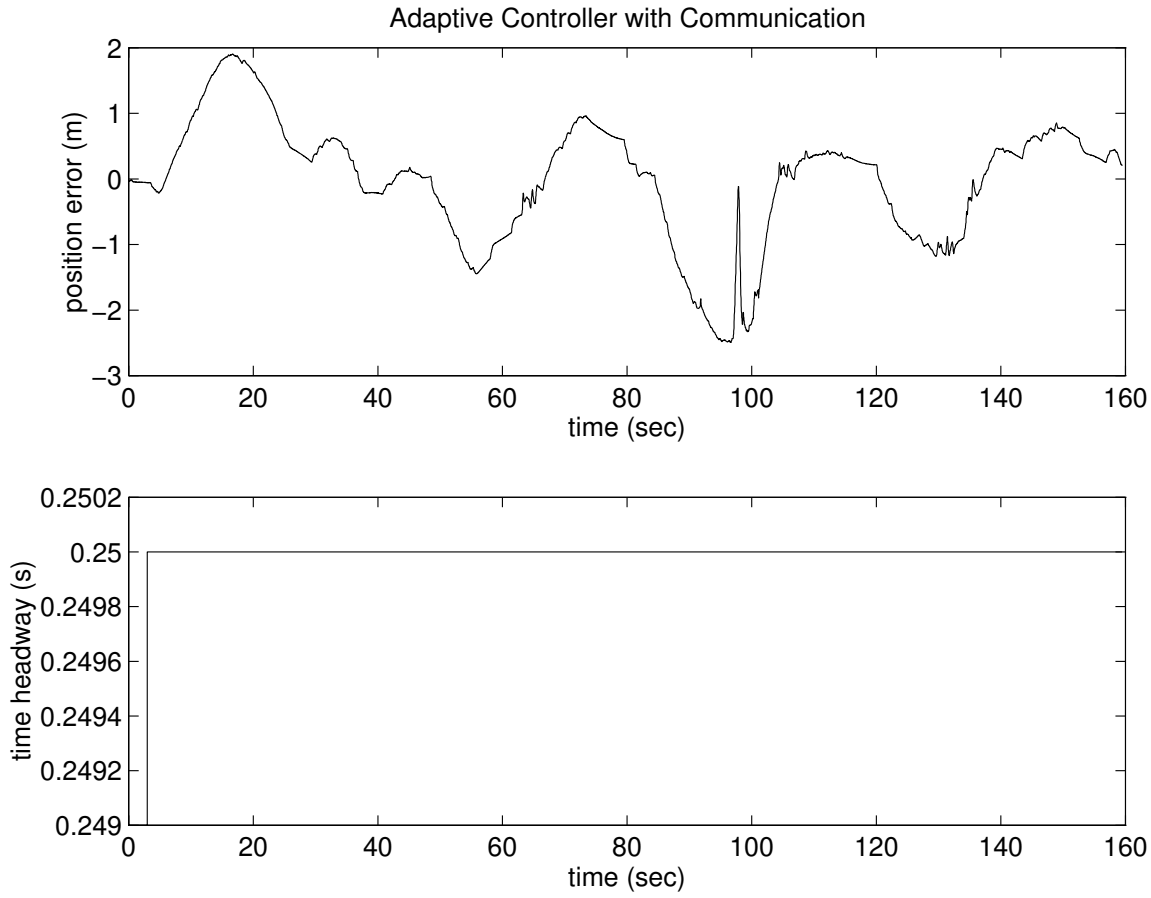

Figure 11: The position error and time headway for adaptive controller with v-v communication.

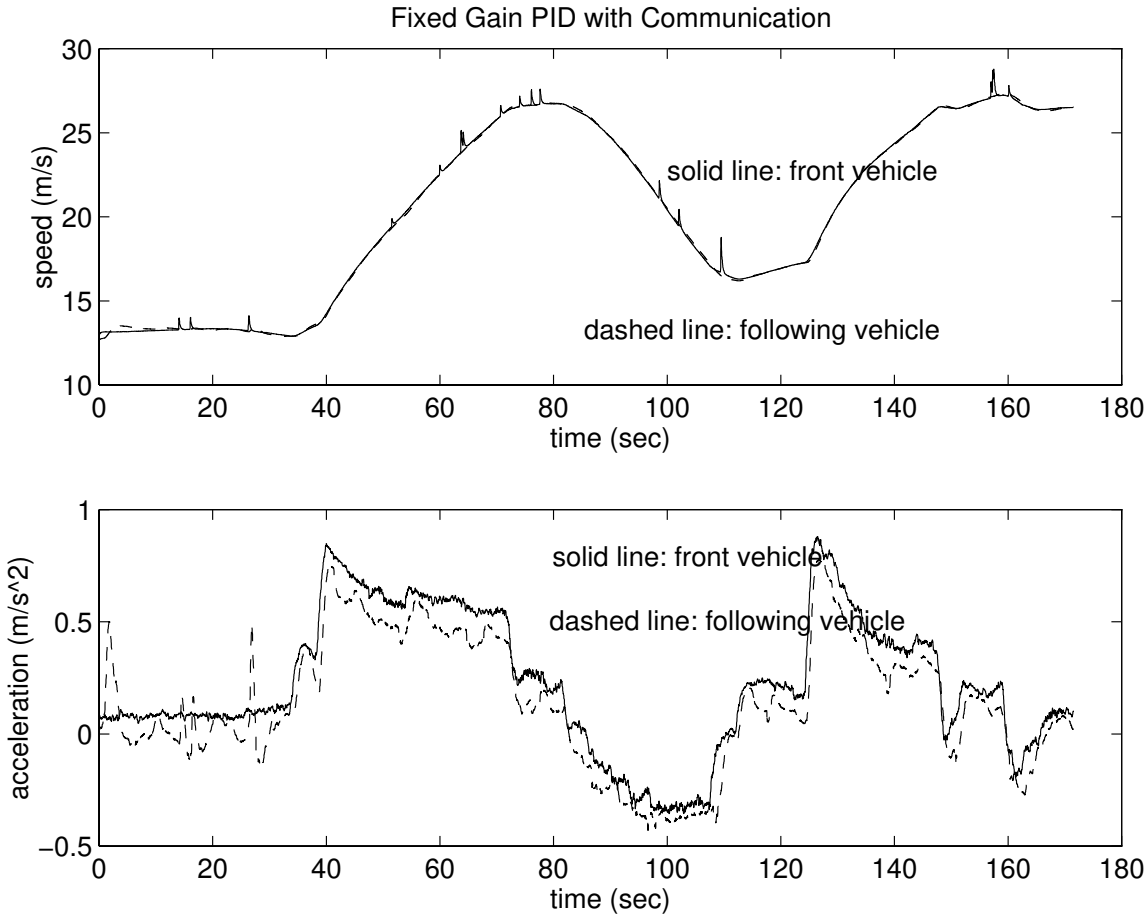

Figure 12: The speed and acceleration profiles for fixed gain PID controller with v-v communication.

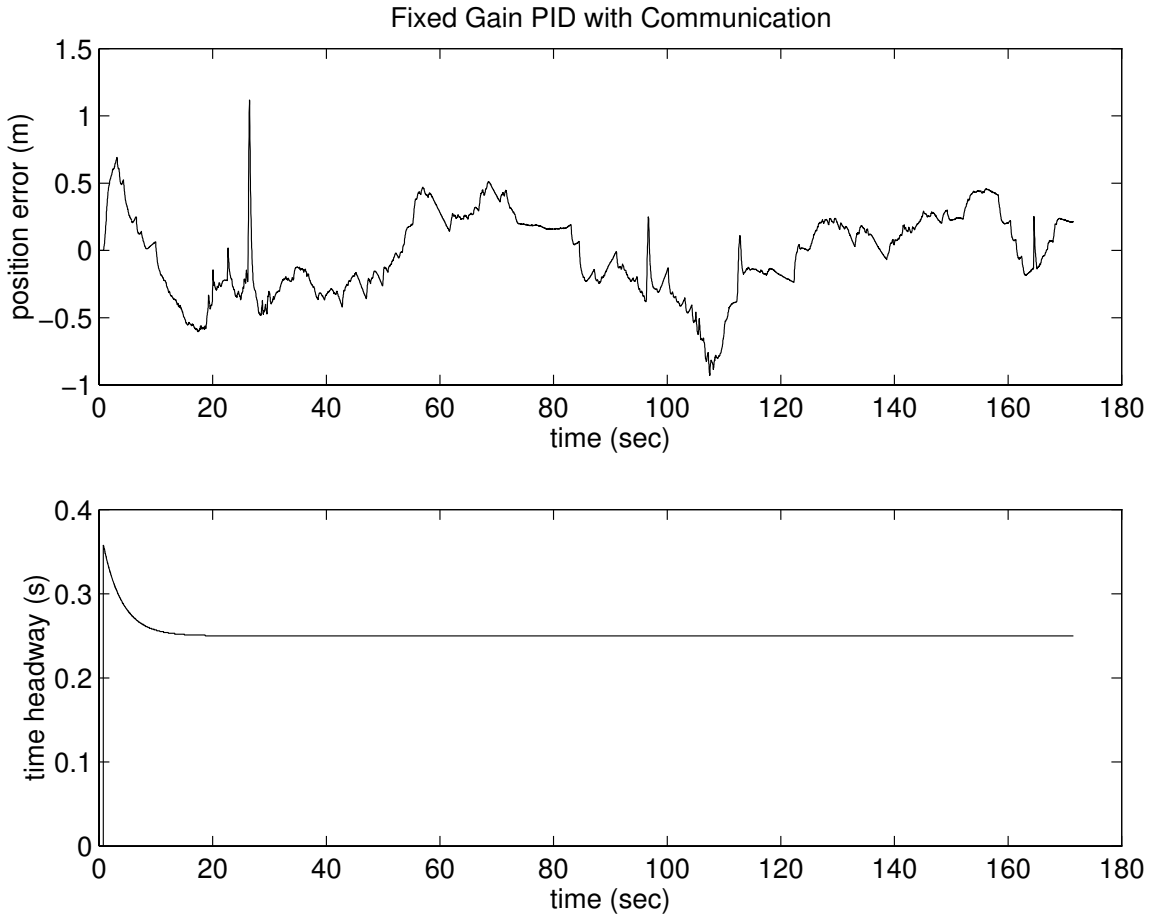

Figure 13: The position error and time headway for fixed gain PID controller with v-v communication.

3 Test 2: Evaluation of Throttle Controller with Modified Hardware and Software

The purpose of this test is to evaluate the performance of nonlinear PID throttle controller, selected in test 1, with the modified hardware and software installed in the vehicles. At the time test 1 was conducted no brake actuators were available in the vehicles, however, with the addition of these actuators some testing is necessary to make sure that the performance of throttle controller is not deteriorated.

3.1 Test Setup

In this test we will evaluate the performance of nonlinear PID throttle controller with v-v communication. Even though the brake actuators are available, no braking command is generated to track the desired speed profile. We have conducted this test using three vehicles at Crows Landing near Patterson, California.

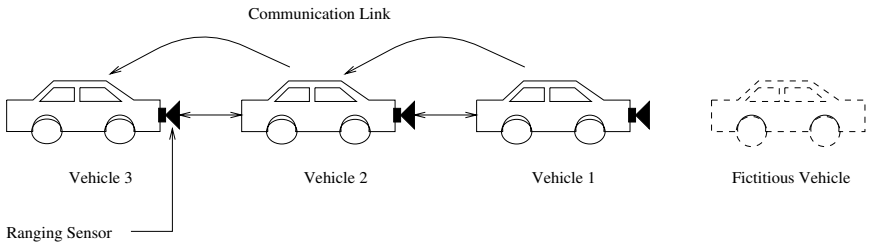

Figure 14: Setup for the vehicle following test 2.

The test set up is shown in Figure 14. The tested controller is the same as that described in section 2.4.1, however, some modifications are introduced to make it compatible with the existing hardware and software. We will rewrite the control law (11) to make it compatible with the multi-vehicle following case:

$$\theta_j = \theta_{0_j} + k_{1_j} V_{r_j} + k_{2_j} \delta_j + \int_0^t (k_{3_j} V_{r_j} + k_{4_j} \delta_j) d\tau + k_{5_j} a_{j-1}. \tag{14}$$

where $j = 1, \ldots, 3$ refers to the position of the vehicle, the rest of the terms have the same meaning as defined in (7). In this case, $V_{r_j} = V_{j-1} - V_j$ and $\delta_j = X_{r_j} - hV_j$, where $X_{r_j} = X_{j-1} - X_j$. The gains k_{ij}, $i = 1, \ldots, 5$ are calculated as given in (9) and (12), where V_l can be replaced with V_{j-1}. As shown in Figure 14, the required variables for the leading vehicle, $j = 1$, are calculated with respect to a fictitious target created inside that vehicle's computer.

In the following we will describe the experimental results.

3.2 Experimental Results

As shown in Figure 14, the desired trajectory for this test is provided by generating a fictitious target in front of the lead vehicle. The desired speed profile selected in this test starts from a constant speed of 45 mph, the speed smoothly increases to 56 mph and stays there for a while and then smoothly decreases to 45 mph again. Since only throttle controller is used in this test, the desired speed profile is quite smooth with the acceleration limited to $\pm 0.25\ m/s^2$. The desired headway in this test is set at 0.5 seconds.

Figure 15 shows the speed and acceleration profile for all the vehicles. The relative spacing error and actual time headway are shown in Figure 16. It can be seen from Figure 15 that all the vehicles closely track their desired speed profiles. The acceleration of all the vehicles are limited to $\pm 0.5\ m/s^2$. The relative spacing error is, $-0.7\ m \leq \delta \leq 0.5\ m$. The actual headway stays close to the desired one except during transients.

3.3 Discussions and Recommendations

The performance of the nonlinear PID throttle controller with v-v communication was found to be satisfactory with the modified hardware and software installed in the vehicles. The speed profiles of all the vehicles except the third vehicle were close to the desired ones. The speed tracking of vehicle 3 (Ford LTD) was not accurate due to problems in gear shifting and large tracking errors in the throttle command. The problem was sufficiently attenuated by reducing the desired acceleration, by smoothing out the desired speed profile. The maximum position error is limited to about 7 % of the desired spacing, which is adequate considering the fact that only throttle control is being used in this test.

4 Test 3: Basic Vehicle Following (Autonomous Vehicles)

The purpose of this test is to evaluate the performance of combined throttle and brake controllers for basic vehicle following maneuvers. Another objective of this test is to incorporate a supervisory controller, that operates above the throttle and brake controllers, to generate the desired trajectory for each vehicle. This test is necessary to check the performance of these combined controllers as they control each vehicle individually before testing them in cooperative driving environment. The test results will be used to tune the throttle and brake controllers and the logic for switching between these controllers.

4.1 Test Setup

In this test three vehicles were used. Each vehicle was equipped with the throttle and brake actuators, ranging sensors and v-v communication devices. The relative distance is provided by the ranging sensor, whereas the speed and acceleration of the vehicle in front is provided through communication link. The test setup is the same as shown in Figure 14.

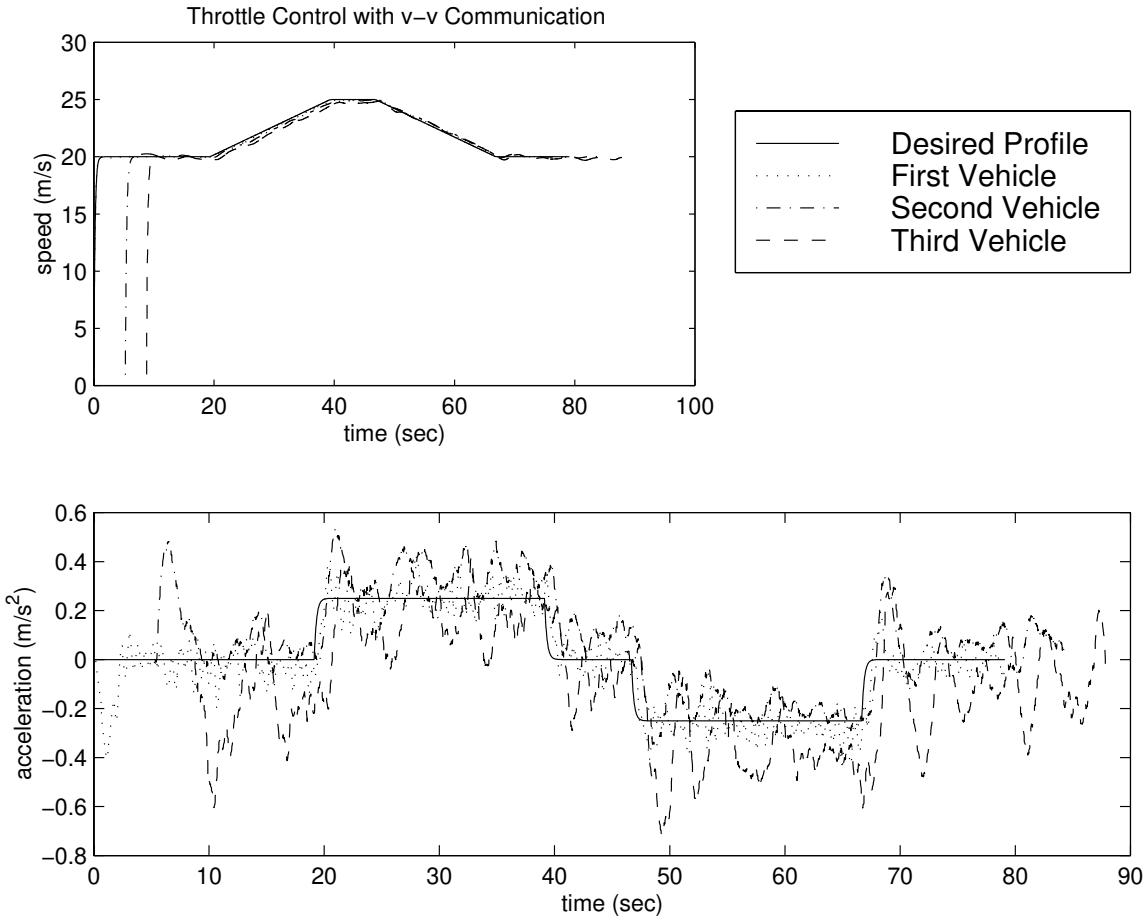

Figure 15: The speed and acceleration profiles for nonlinear PID throttle controller with v-v communication.

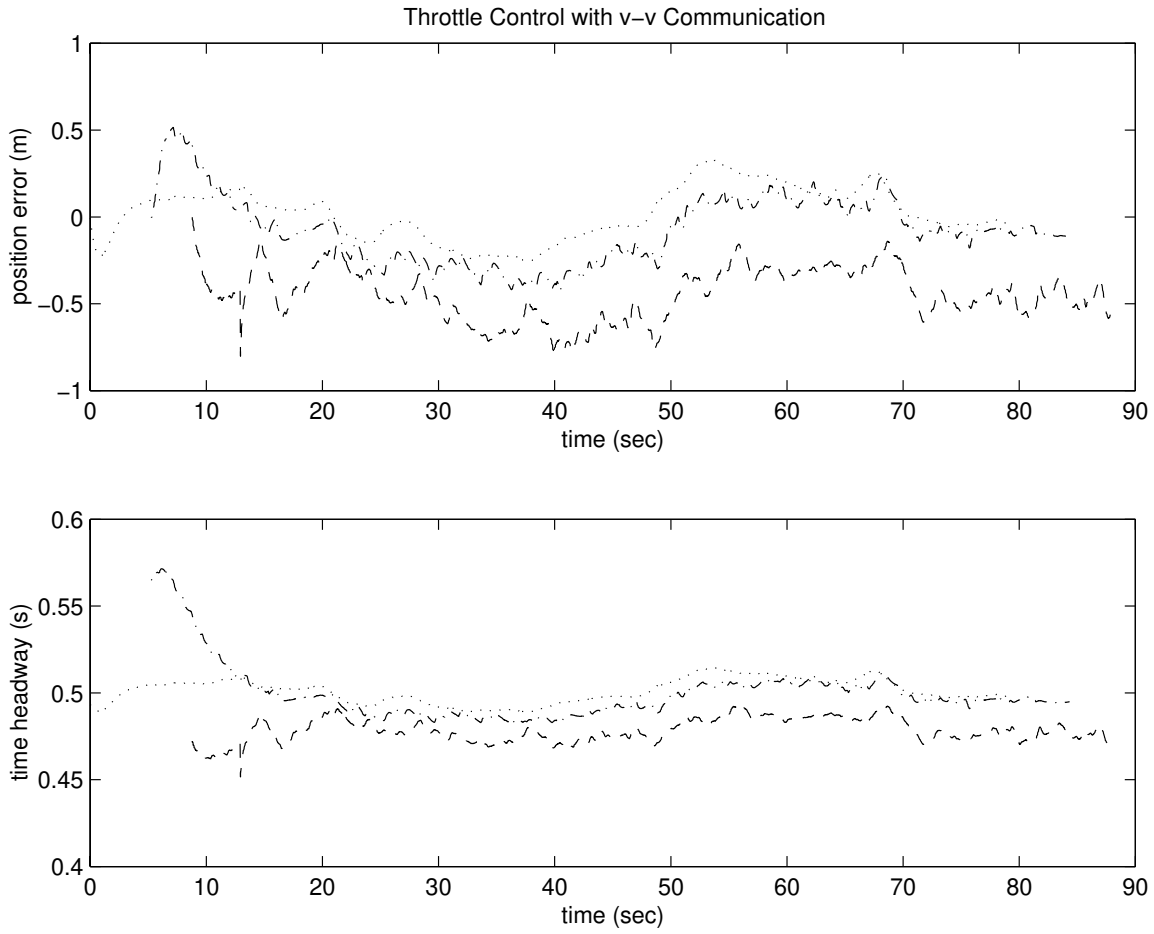

Figure 16: The position error and time headway for nonlinear PID throttle controller with v-v communication.

In this test we have used the nonlinear PID throttle controller with v-v communication, described in section 3.1, and a brake controller designed by using feedback linearization in [2]. For a safe and comfortable vehicle following, the desired trajectory has to follow certain constraints. These constraints are guaranteed by a supervisory controller which operates above the throttle and brake controllers. A design of such a supervisory controller is given in [7]. In the following we will briefly describe the features of this supervisory controller used in this test.

4.2 Supervisory Control Design

In order to guarantee the safety and comfort of the occupants, the supervisory controller performs certain tasks which are event driven. These events are described as combinations of the inputs to the supervisory controller. The tasks performed by the supervisory controller in this test are:

(i) Identify valid target.
(ii) Calculate a safe headway and speed.
(iii) Generate the desired acceleration based on the acceleration information of the vehicle in front.

The conditions used to check the validity of a target are the following:

(i) The target is within a designated range that is chosen a priori based on the sensing range and safety considerations.
(ii) The speed of the target is less than the desired speed.

If either of these two conditions is violated, the vehicle in front is not considered to be a valid target to follow. The conditions given above can be combined to form a "follow target" condition $\mathcal{B}_F(.)$ as:

$$\mathcal{B}_F(k) = \begin{cases} 1 & \text{if } \mathcal{B}_{A_{on}}(k) = 1 \text{ and } [\{h(k) < h_t \text{ and } (V_l(k) < V_d(k) + \Delta_1)\} \\ & \text{or } \{(V_l(k) < V_d(k) + \Delta_2) \text{ and } \mathcal{B}_F(k-1) = 1\}] \\ 0 & \text{else,} \end{cases} \tag{15}$$

where $\mathcal{B}_{A_{on}}$ is the signal to check the turning on of automatic following, h_t is the threshold for headway calculated from the sensing range, V_l is the speed of the leading vehicle, V_d is the desired speed and Δ_1, $\Delta_2 > 0$ are design constants. In (15) $\Delta_2 = 2.0\ m/s$ and $\Delta_1 = 1.0\ m/s$ is used to avoid the unnecessary switching of the targets caused by the transients and/or sensor noise, hence if the target was previously being followed, then a larger fluctuation in target speed is tolerated.

According to the condition given in (15), in case a valid target is present, the supervisory controller selects a safe desired headway and speed to be issued to the throttle and brake

controllers. The selection process of the safe headway is given below.

A "headway reset" operation is performed during initialization or whenever the "follow" mode is switched on. During this the value of desired headway, $h_d(.)$, is chosen to be the current headway $h(.)$ as long as it is greater than the minimum allowable headway h_{min}. Hence the value of $h_d(.)$ during reset operation is:

$$h_d(k) = \max(h(k), h_{min}) \quad \text{if} \quad \mathcal{B}_{R_h}(k) = 1, \tag{16}$$

where $\mathcal{B}_{R_h}(.)$ is the condition used to trigger the headway reset operation and is calculated as:

$$\mathcal{B}_{R_h}(k) = \begin{cases} 1 & \text{if } (\mathcal{B}_{A_{on}}(k) = 1 \text{ and } \mathcal{B}_{A_{on}}(k-1) \neq 1) \\ & \text{or } (\mathcal{B}_F(k) = 1 \text{ and } \mathcal{B}_F(k-1) \neq 1) \\ 0 & \text{else.} \end{cases} \tag{17}$$

After the headway reset operation the desired headway is generated by filtering the headway input, $h_i(.)$, provided to the supervisory controller. This filtering process avoids excessive transients and ensures the desired comfort. The filtered desired headway command h_d is given as:

$$h_d(k+1) = \begin{cases} \min[h_{max}, \max\{h_{min}, (h_d(k) + k_h * T(h_i(k) - h_d(k)))\}] & \text{if } \mathcal{B}_F(k) = 1 \\ h_d(k) & \text{else} \end{cases} \tag{18}$$

where $k_h = 0.6$, $h_{min} = 0.25$ seconds, $h_{max} = 0.75$ seconds are design constants and T is the sampling time interval.

Similarly, a "speed reset" operation is performed whenever the automatic vehicle following (AVF) is switched on and the desired speed V_d is taken as the current speed of the vehicle V. This resetting condition avoids large speed transients at the time when the AVF is switched on. Hence

$$V_d(k) = V(k) \quad \text{if} \quad \mathcal{B}_{R_s}(k) = 1, \tag{19}$$

where, $\mathcal{B}_{R_s}(.)$ is the speed reset command and is generated as:

$$\mathcal{B}_{R_s}(k) = \begin{cases} 1 & \text{if } \mathcal{B}_{A_{on}}(k) = 1 \text{ and } \mathcal{B}_{A_{on}}(k-1) \neq 1 \\ 0 & \text{else.} \end{cases} \tag{20}$$

After initialization, the desired speed V_d is made to track the speed input V_i through "speed track" operation. The supervisory controller generates the desired speed V_d by passing V_i through a filter designed with the comfort constraints. The desired speed command V_d is given as:

$$V_d(k+1) = V_d(k) + \min[a_{max}, \max\{a_{min}, (k_s * (V_i(k) - V_d(k)))\}] * T \tag{21}$$

where, $a_{max} = 1.0\ m/s^2$, $a_{min} = -3.0\ m/s^2$, $k_s = 12$ are design constants. The speed input V_i is generated as:

$$V_i(k) = \begin{cases} V_l & \text{if } \mathcal{B}_F(k) = 1 \\ V_C & \text{else.} \end{cases} \tag{22}$$

where V_l is the speed of the vehicle in front and V_C is the local speed command. Hence if the target is not suitable to follow a local speed command is provided to the filter (21).

The desired acceleration command for the vehicle can be generated to be used by the throttle and brake controllers. The acceleration information available from the vehicle in front, through v-v communication, can be filtered to comply with the desired jerk constraint. Hence the filtered desired acceleration command is given as:

$$a_d(k+1) = a_d(k) + \min[j_{max}, \max\{j_{min}, (k_a * (a_l(k) - a_d(k)))\}] * T \tag{23}$$

where a_l is the acceleration of the vehicle in front, $k_a = 6.0$, $j_{max} = 1.0\ m/s^3$ and $j_{min} = -2.0\ m/s^3$ are design constants.

With the addition of supervisory controller in the loop the terms V_{r_j} and δ_j in the throttle control law (14) can be rewritten as:

$$\begin{aligned} V_{r_j} &= V_{d_j} - V_j \\ \delta_j &= X_{r_j} - h_{d_j} V_j \end{aligned}$$

where V_{d_j} and h_{d_j} are given by (21) and (18) for each vehicle. Similarly, a_l in (14) can be replaced by a_d given in (23).

In the following, we will briefly describe the design of the brake controller and a logic that controls the region of operation of throttle and brake controllers.

4.3 Brake Controller Design

The dynamic equations relating the braking torque to the vehicle speed and position are given as:

$$\begin{aligned} \dot{X} &= V \\ \dot{V} &= \frac{1}{M}\left(-c_1 T_b - f_0 - c_2 V - c_3 V^2\right) \end{aligned} \tag{24}$$

where T_b is the braking torque, M is the vehicle mass, f_0, $c_2 V$, $c_3 V^2$ represent the static friction force, rolling friction force and air resistant force respectively. The assumptions used in deriving the model (24) are discussed in [2].

If the required deceleration in the automatic vehicle following cannot be generated by the engine alone, then to achieve the control objectives brake has to be applied. The dynamic equations for the brake subsystem are:

$$\begin{aligned}
\dot{X}_r &= V_d - V \\
\dot{V} &= \frac{1}{M}\left(-c_4 P_d - f_0 - c_2 V - c_3 V^2\right) \\
\delta &= X_r - h_d V - S_0 \\
V_r &= V_d - V
\end{aligned} \tag{25}$$

In (25), the brake line pressure, P_d has been chosen as a control input instead of brake torque T_b, used in (24). The brake line pressure is approximately proportional to the brake torque and is the quantity which is actually controlled in the brake subsystem. Feedback linearization is used to transform (25) into a linear system:

$$\begin{aligned}
\dot{X}_r &= V_d - V \\
\dot{V} &= u \\
\delta &= X_r - h_d V - S_0 \\
V_r &= V_d - V
\end{aligned} \tag{26}$$

where:

$$u = \frac{1}{M}\left(-c_4 P_d - f_0 - c_2 V - c_3 V^2\right) \tag{27}$$

The desired input u is selected such that it stabilizes the system given in (26) and forces δ, V_r to converge to zero. The desired line pressure P_d is then calculated from (27). The following feedback control law has been proposed:

$$u = k_6 V_r + k_7 \delta \tag{28}$$

Substituting (28) into (26), we have the following closed loop system.

$$\begin{aligned}
\dot{X}_r &= V_d - V \\
\dot{V} &= k_6 V_r + k_7 \delta \\
\delta &= X_r - h_d V - S_0 \\
V_r &= V_d - V
\end{aligned} \tag{29}$$

The system (29) can be solved for the outputs V_r and δ:

$$\begin{aligned}
V_r &= \frac{(s + k_7 h_d)s}{\Delta_b(s)} V_d + \frac{k_7 s}{\Delta_b(s)} S_0 \\
\delta &= \frac{(1 - k_6 h_d)s}{\Delta_b(s)} V_d - \frac{s + k_6}{\Delta_b(s)} S_0
\end{aligned} \tag{30}$$

where:

$$\Delta_b(s) = s^2 + (k_6 + k_7 h_d)s + k_7 \tag{31}$$

From equations (30) and (31), it is clear that the system is stable for any finite $k_6 > 0$ and $k_7 > 0$. In this test we have chosen $k_6 = 1.0$ and $k_7 = 0.25$ to have two real closed loop poles. Furthermore, if V_d is constant we have $V_r, \delta \to 0$. From the choice of values of k_6 and k_7 in (28) and using (27), we can calculate the desired line pressure as:

$$P_d = -\frac{1}{c_4}\left[M(k_6 V_r + k_7 \delta) + f_0 + c_2 V + c_3 V^2\right] \tag{32}$$

From (29), it is clear that $(k_6 V_r + k_7 \delta)$ is the desired deceleration of the vehicle, the saturation functions introduced in the supervisory controller design ensure that the deceleration of the vehicle satisfies the given constraint.

4.4 Switching Logic for Throttle and Brake Controllers

Since the throttle and brake controllers are not allowed to operate at the same time, a logic is needed to govern this switching operation. The logic design is based on the principle that a good driver never uses the brake and accelerator pedal together. Using the knowledge obtained from human driving, the three situations given below are investigated.

Situation 1: $X_r < X_{min}$ and $V > V_1$

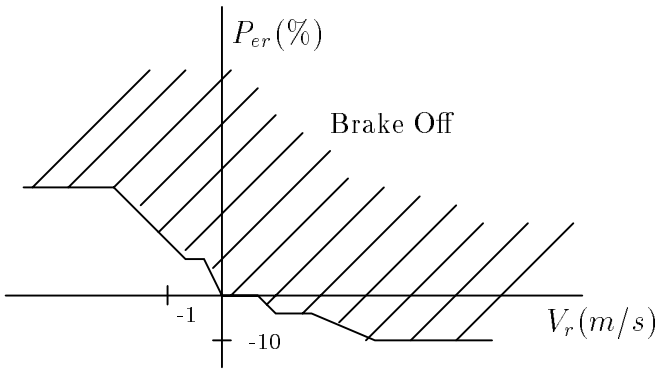

Figure 17: Logic switch for brake off when $X_r < X_{min}$ and $V > V_1$.

This situation occurs when the following vehicle is traveling at high speed and is relatively close to the preceding vehicle. Here X_{min} and V_1 are design variables and are chosen to match the braking capabilities of the vehicle. In this situation the brake is applied, and brake controller remains on until (V_r, P_{er}), where P_{er} is defined as the percentage position error, i.e., $P_{er} \triangleq \frac{\delta}{h_d V + S_0} \times 100$, is inside the shaded region shown in Figure 17. Once the

brake controller is switched off it remains off inside and outside the shaded region shown in Figure 17 until $X_r < X_{min}$ and $V > V_1$ again.

Situation 2: $X_r > X_{max}$

In this situation the relative distance is large enough and no braking is required.

Situation 3: $X_{min} \leq X_r \leq X_{max}$ or $X_r < X_{min}$ and $V \leq V_1$

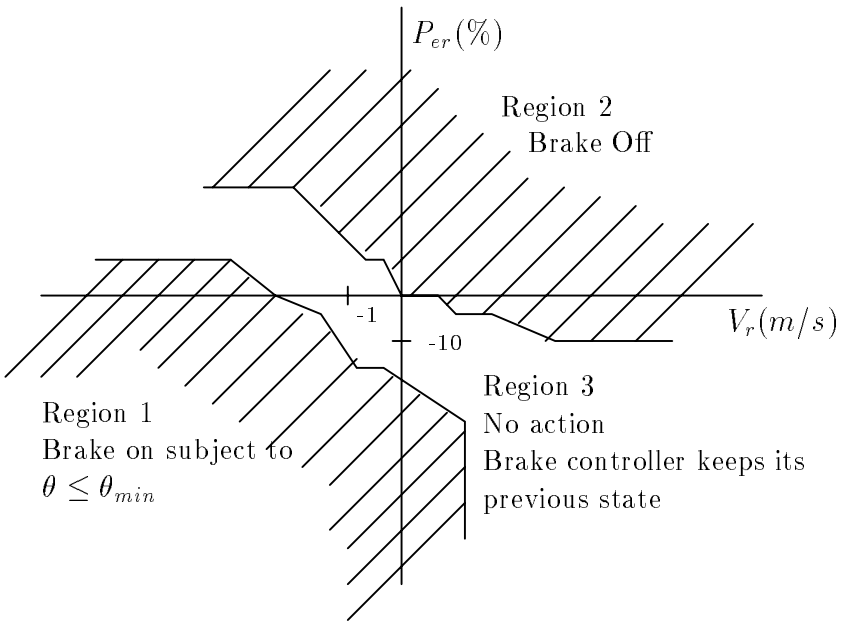

Figure 18: Logic switch for brake off when $X_{min} \leq X_r \leq X_{max}$ or $X_r < X_{min}$ and $V \leq V_1$.

In this case the switching of brake and throttle controller is determined by the values of V_r, P_{er} and θ, as shown in Figure 18. It should be noted that the Region 3 is a neutral region in which no change of state occurs, i.e., if the brake was on while in Region 1 then the brake would be switched off only in Region 2. The neutral region introduces a hysteresis to avoid chattering near switching boundary.

It should be noted that the threshold of switching logic, to turn on the brakes, depends on the measured V_r and P_{er}. These signals have low bandwidth due to inertial delays involved in the measurement of these signals. However, with the addition of v-v communication capabilities, this delay can be avoided by suitable modifications in the switching logic.

These modifications are:

$$b_{on}(k) = \begin{cases} 1 & \text{if } b'_{on}(k) = 1 \text{ and } (a_d(k) < A'_{min} \text{ and } u(k) < A_{min}) \text{ or} \\ & (b_{on}(k-1) = 1 \text{ and } u(k) < 0.0) \\ 0 & \text{else} \end{cases} \tag{33}$$

where $b_{on}(.)$ is the modified signal to turn on the brake controller, $b'_{on}(.)$ is the output of the switching logic described above, $u(.)$ is the desired deceleration given in (28), $A'_{min} = -0.1\ m/s^2$ and $A_{min} = -0.2\ m/s^2$ are design constants. Hence through the communication the braking intentions of the vehicle in front can be used as a signal to turn on the brakes of the vehicle without a significant amount of delay. Similarly, with the addition of v-v communication the desired deceleration command given in (28) can be modified to compensate for the acceleration of the vehicle in front:

$$u = k_6 V_r + k_7 \delta + k_8 a_d \tag{34}$$

where a_d is the desired acceleration command generated by the supervisory controller and $k_8 = 0.5$ is a design constant.

In the following, we will describe the results of this test.

4.5 Experimental Results

Three different speed profiles were selected for this test. The desired speed profiles start from a constant speed of 40 mph, the speed smoothly increases to 56 mph. The acceleration for all profiles is kept constant at 0.5 m/s^2. The speed stays constant at 56 mph for 10 seconds and then decreases to 40 mph. The three profiles differ in the desired deceleration during slowing down process. The desired decelerations of -0.7, -0.9 and -1.2 m/s^2 are used for these three profiles. The desired headway in this test is set at 0.5 seconds. The test results for profiles with decelerations of -0.9 and -1.2 m/s^2 are shown in Figures 19-21 and 22-24 respectively.

The speed and acceleration profiles for all the vehicles are shown in Figures 19 and 22 for the two desired speed profiles. The maximum deceleration occur in the hard braking case in Figure 22. The acceleration of all the vehicles are well below the maximum allowable acceleration limited by the filter (21) in the supervisory controller. The relative spacing error is limited to -0.7 m for medium braking and that for hard braking is -0.8 m.

4.6 Discussions and Recommendations

The performance of the combined throttle and brake controllers was found to be satisfactory when the vehicles are autonomously following each other. The addition of supervisory controller helps to satisfy the required acceleration and jerk constraints for comfort. The acceleration tracking is improved than in test 2 due to addition of the brake controller.

Again due to limited acceleration capabilities of the third vehicle, large positive errors in the relative spacing were observed, which are not critical from the safety point of view but result in poor speed tracking. The infimum of the relative spacing error was 8 %, which occurred in the hard braking case.

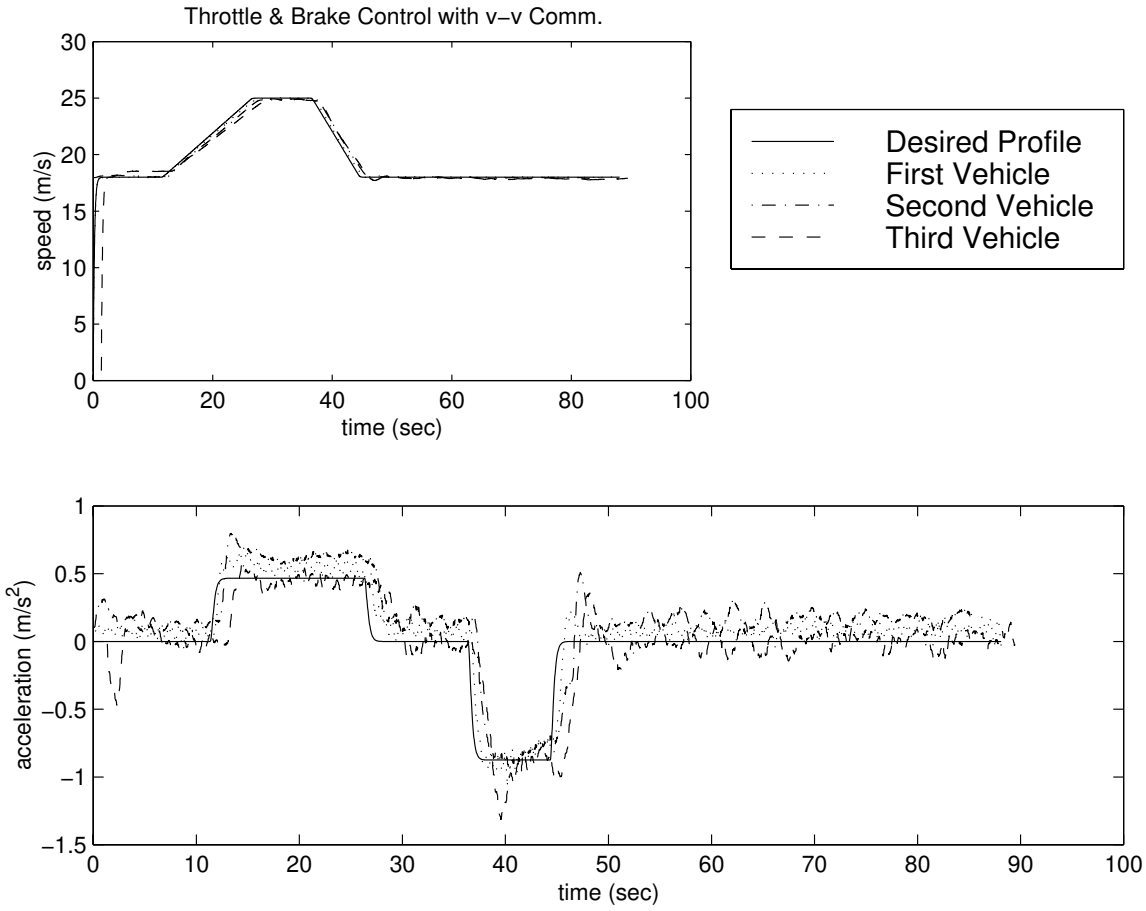

Figure 19: The speed and acceleration profiles for combined throttle and brake controllers with v-v communication (soft braking).

5 Test 4: Effect of v-v Communication on the Braking Performance

The purpose of this test is to compare the performance of the brake controller with and without v-v communications. This comparison will provide guidelines to enhance the braking performance of vehicles in autonomous as well as cooperative driving modes.

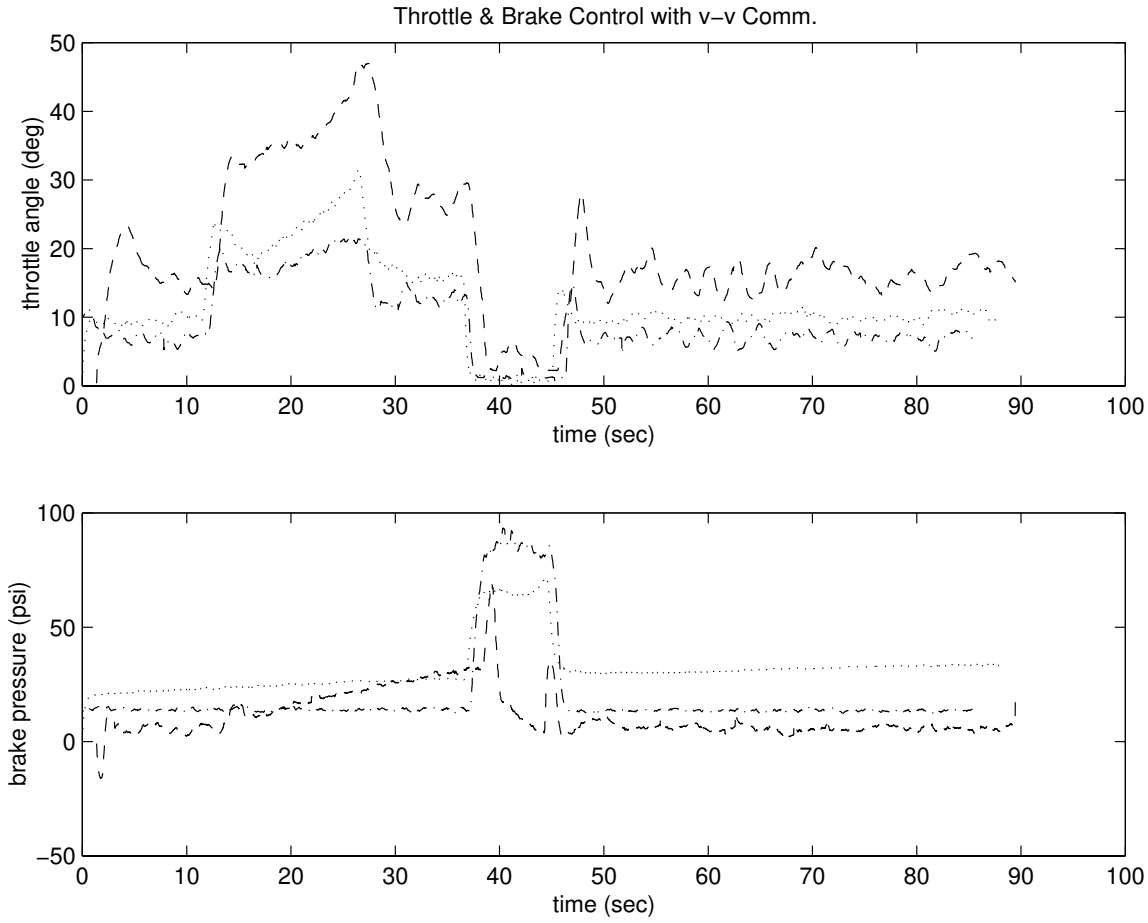

Figure 20: The throttle angle and brake pressure commands for test 3.

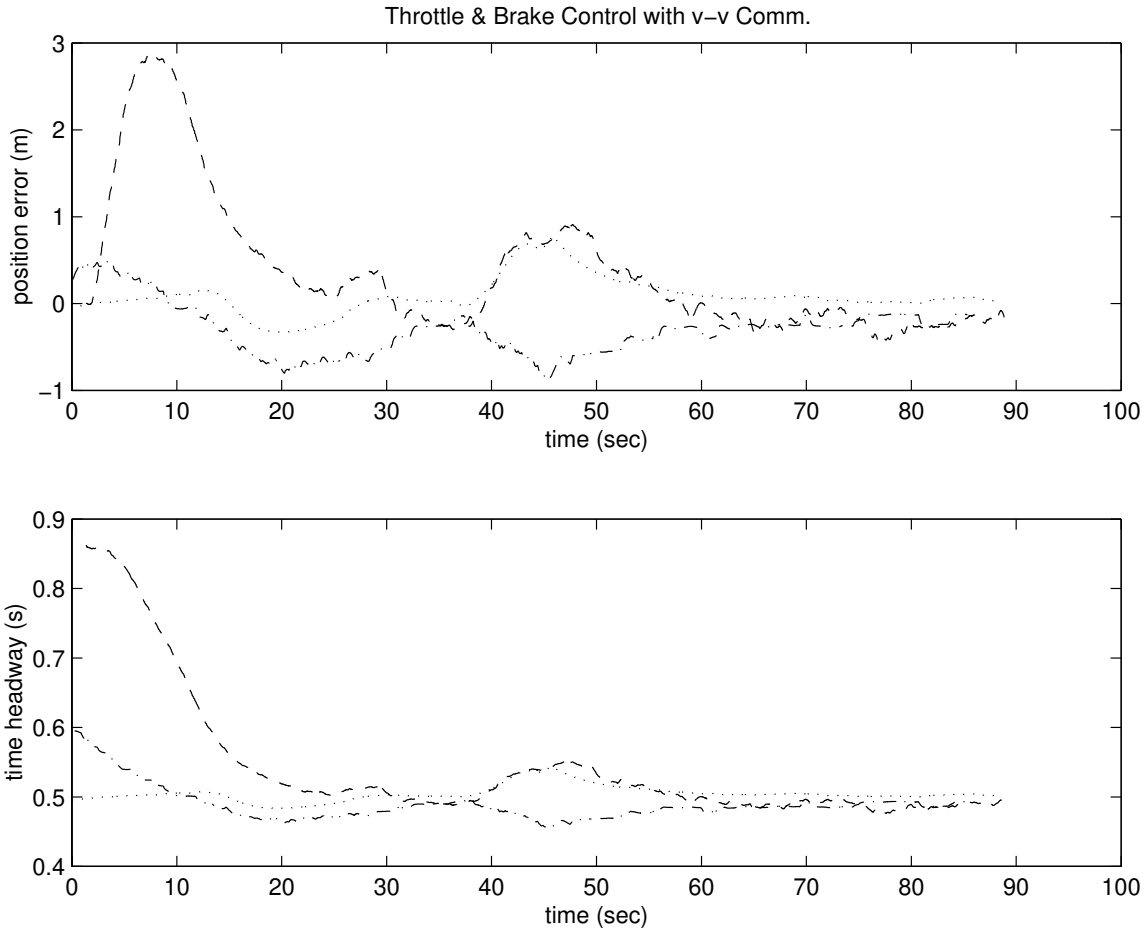

Figure 21: The position error and time headway for combined throttle and brake controllers with v-v communication (soft braking).

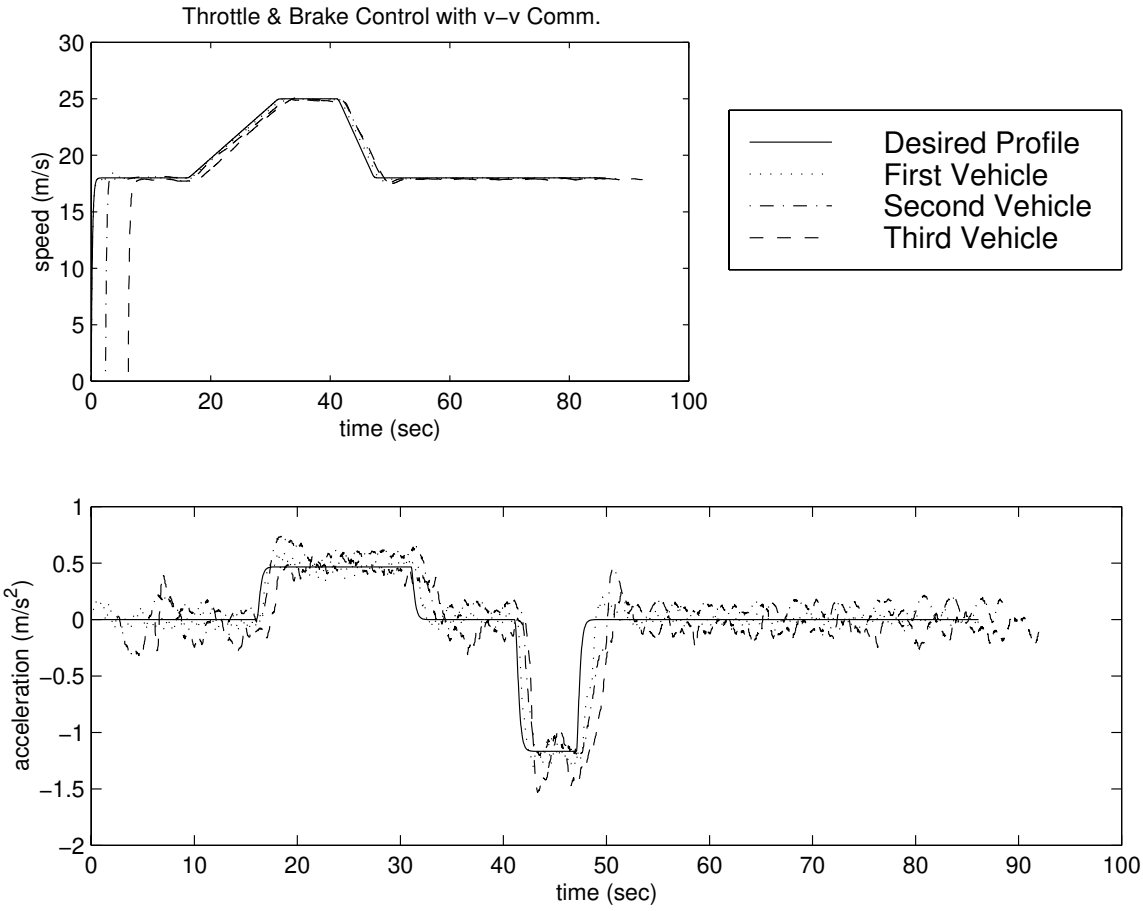

Figure 22: The speed and acceleration profiles for combined throttle and brake controllers with v-v communication (hard braking).

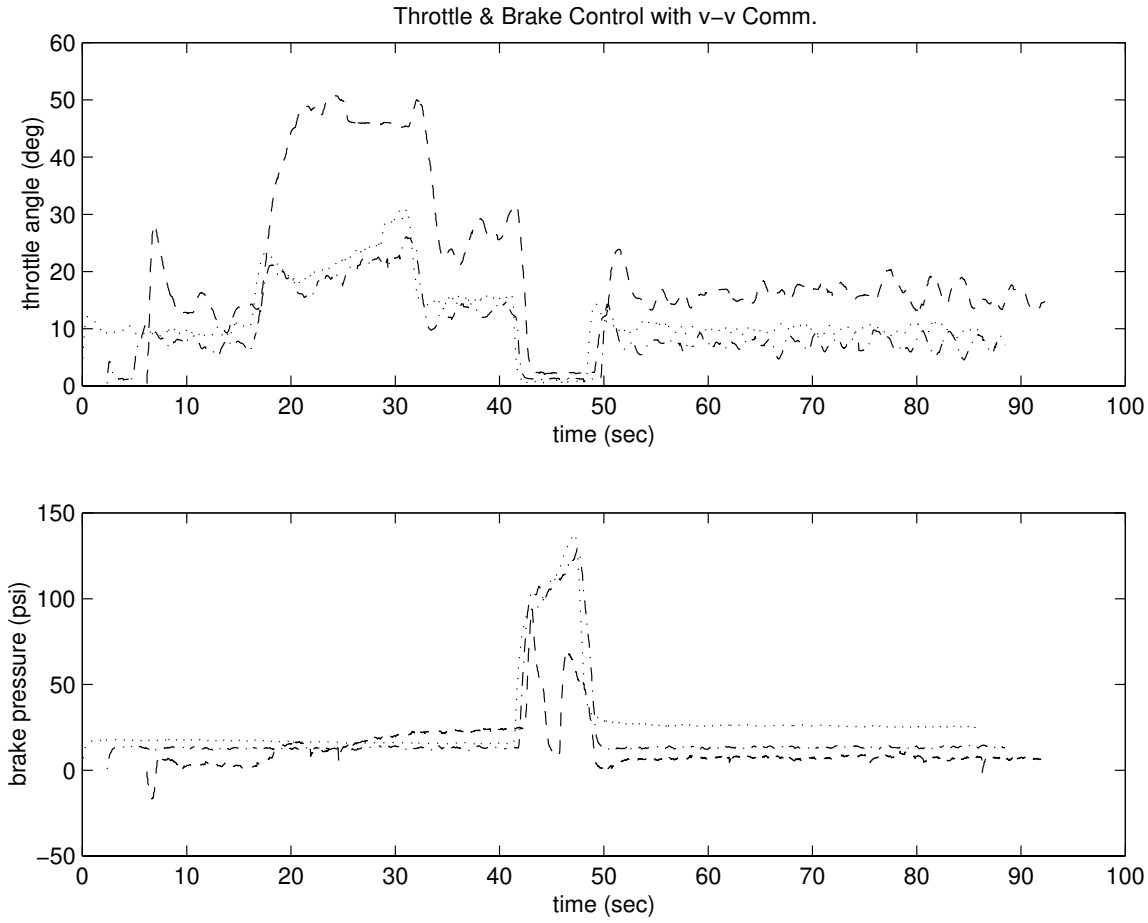

Figure 23: The throttle angle and brake pressure commands for test 3.

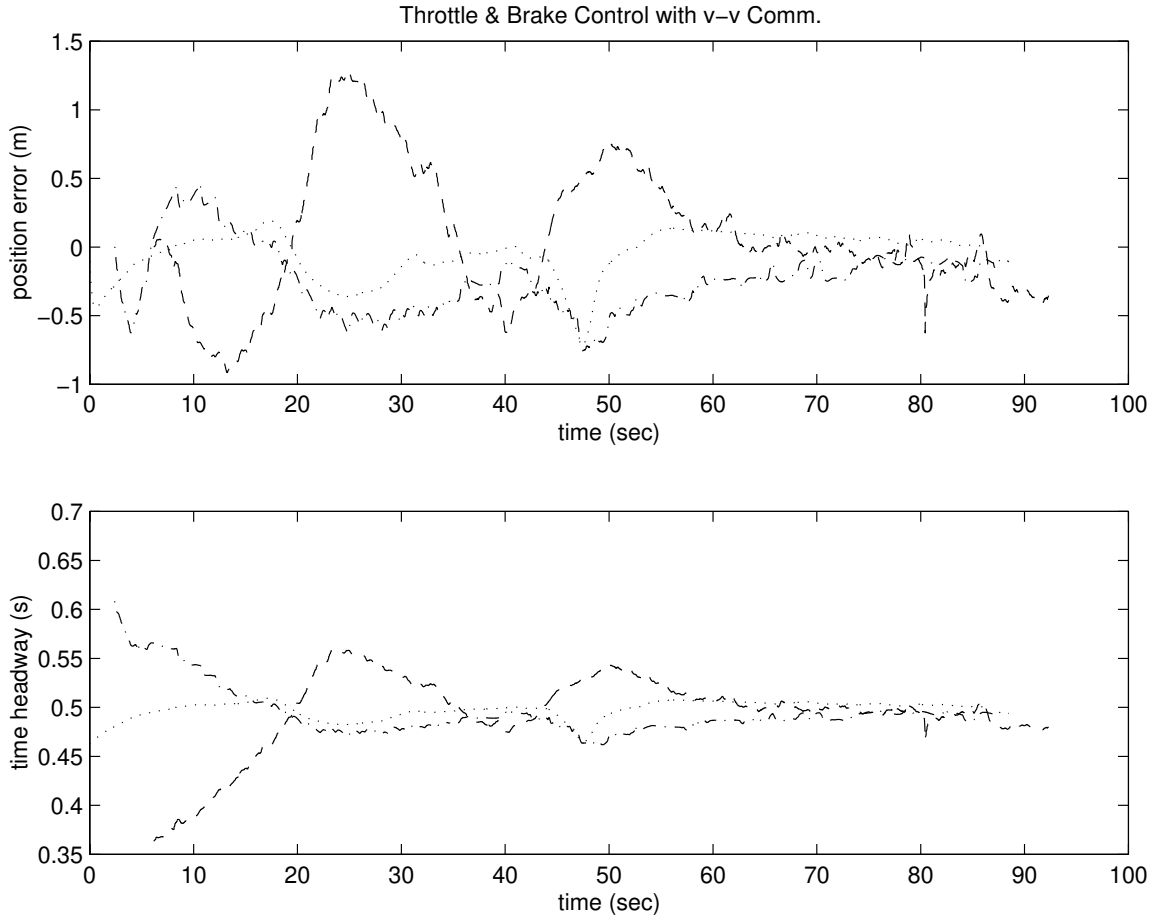

Figure 24: The position error and time headway for combined throttle and brake controllers with v-v communication (hard braking).

5.1 Test Setup

The test setup is similar to that shown in Figure 14, except that the acceleration information from the vehicle in front is not used in the throttle and brake controllers. Similarly the modifications introduced in the switching logic for the throttle and brake controllers, which depends on the acceleration information from the vehicle in front are not used in this test. Hence the switching operation is controlled only by the measurements of V_r and P_{er}.

5.2 Experimental Results

In this test we have used the desired speed profile 3 of the test 3. The acceleration part of the profile is relatively smooth, however, the deceleration of -1.2 m/s^2 requires hard braking. The desired headway in this test is set at 0.5 seconds. The speed and acceleration profiles are shown in Figures 25-27.

As shown in Figure 25, in this case, relatively large overshoots in the acceleration and speed are observed. The relative spacing error shown in Figure 27 grows as large as -2 m. The headway remains close to the desired one except during transients.

5.3 Discussions and Recommendations

As expected the addition of v-v communication results in much faster braking response. Since the switching of controllers based on the relative distance measurement introduces an excessive amount of delay which results in large relative spacing error. The relative spacing error in this case is about 21 % compared to 8 % for the same desired speed profile in test 3, where v-v communication is used in braking process. Similarly comparing Figures 19 and 25, we see that the case with no v-v communication results in large acceleration overshoots; These large overshoots results in relatively poor speed tracking. This test concludes that the v-v communication is necessary to demonstrate the cooperative driving system.

6 Test 5: Cooperative Driving Demonstration

The purpose of this test is to demonstrate a fully cooperative driving environment in which vehicles are capable of coordinating their maneuvers through communication with roadway and surrounding vehicles. This demonstration will support the key aspect of this proposal, which is the development and evolution of AICC systems into cooperative driving systems that could be used as a part of an intelligent roadway/vehicle system to improve traffic flow rates. Another objective of this test is to document the effect of roadway to vehicle communication and hence the roadway commands on the stability of the longitudinal vehicle following. Finally this demonstration will prove the guaranteed performance of the designed controllers.

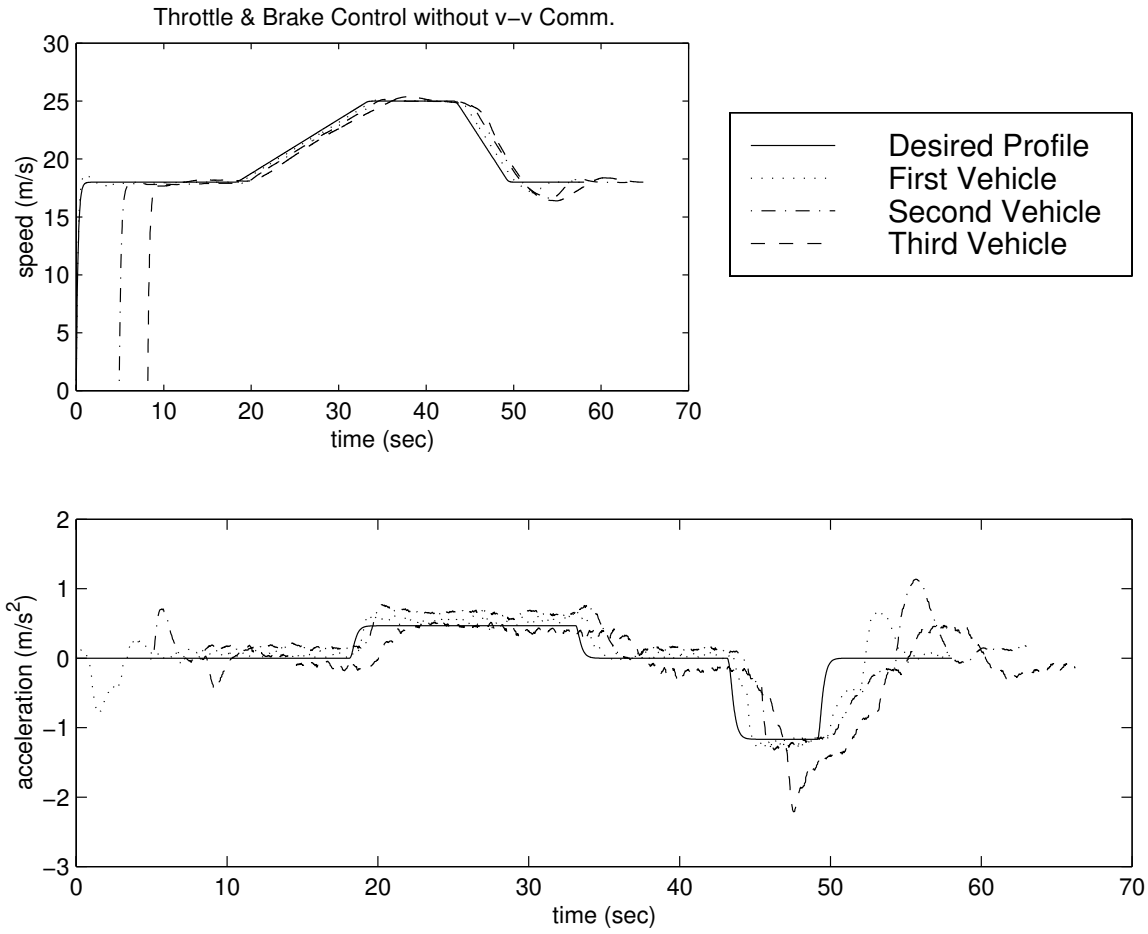

Figure 25: The speed and acceleration profiles for combined throttle and brake controllers without v-v communication.

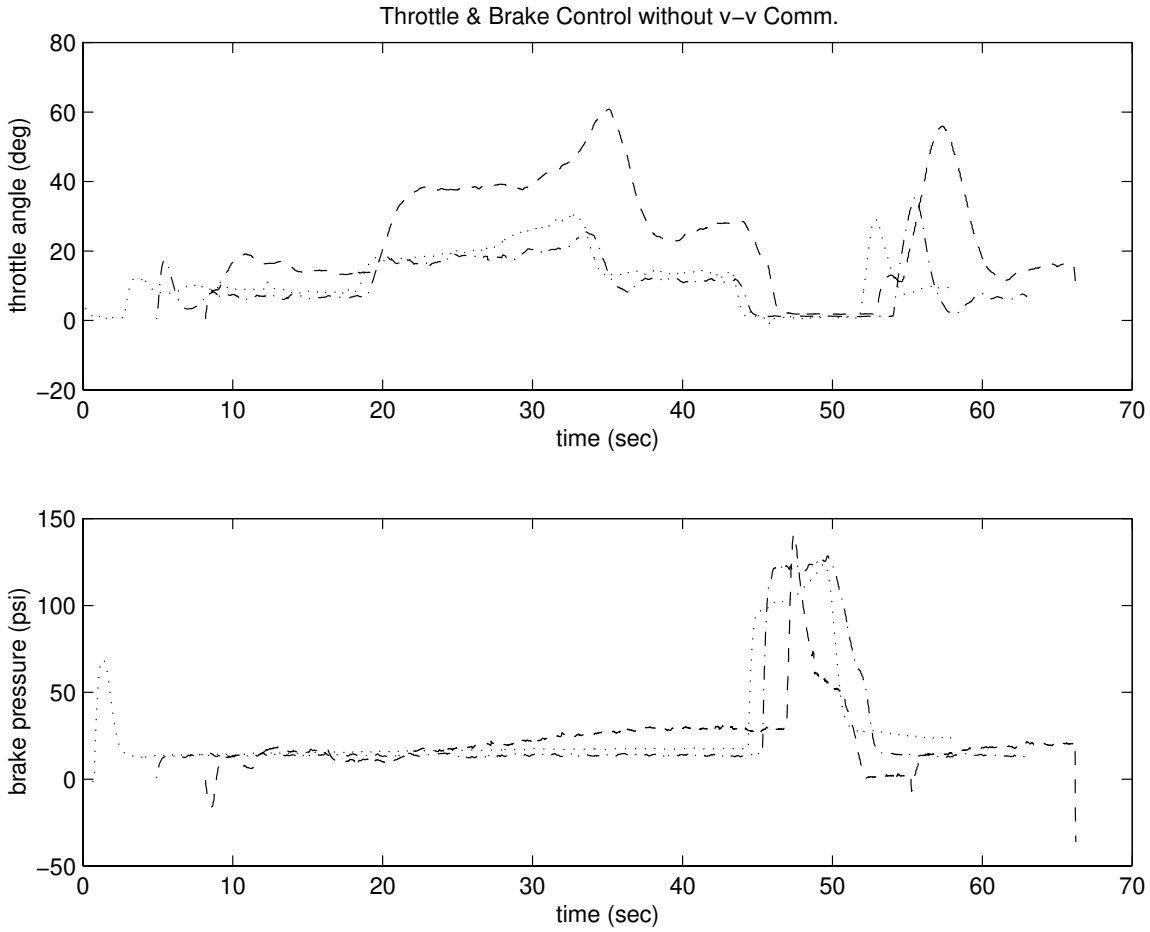

Figure 26: The throttle angle and brake pressure commands for test 4.

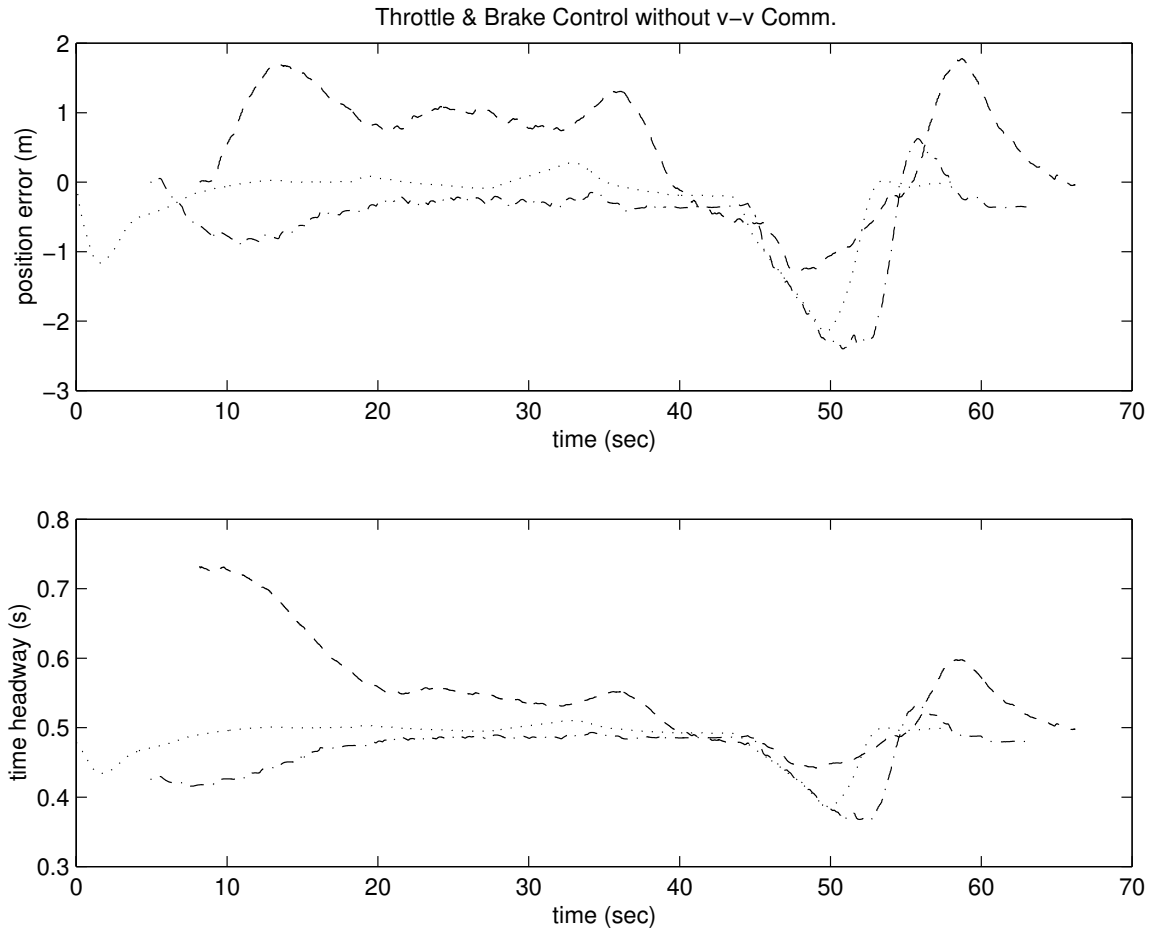

Figure 27: The position error and time headway for combined throttle and brake controllers without v-v communication.

6.1 Test Setup

The test setup used for this demonstration is shown in Figure 28. This demonstration of cooperative driving system requires active involvement of the roadway to control the trajectory and hence the flow of vehicles used in this test. However, due to non-availability of any infrastructure support on the test site, the roadway controller is simulated through the lead vehicle. Hence the computer in the leading vehicle plays a dual role, being a lead vehicle as well as the roadway controller.

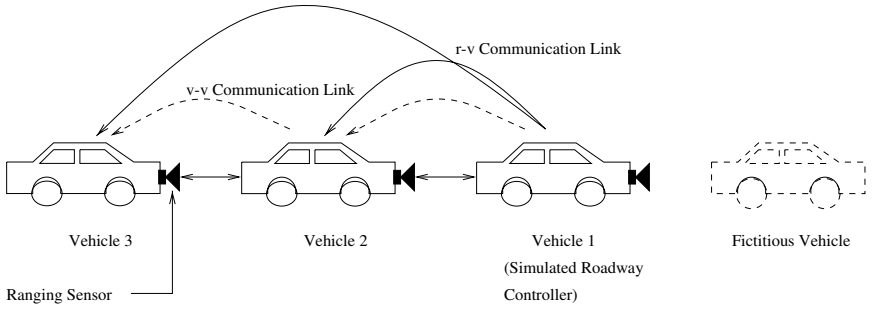

Figure 28: Setup for the cooperative driving demonstration.

Similarly at the time of this testing no true roadway to vehicle communications capability existed at the test site. This limitation was circumvented by using the communications capabilities of the lead vehicle. The current set up provides a broadcast channel, in addition to v-v communication, which was used to issue roadway to vehicle commands. The setup, however, is limited to only one user programmable channel with broadcast capabilities. Hence only a limited amount of testing can be performed.

The control inputs provided by the roadway controller to track the desired density profile are the speed and headway. The speed command indirectly controls the density of traffic flow by selectively slowing down or speeding up the vehicles in a section. During transients caused by incidents, the speed command generated by the roadway controller can be used to reduce the impact of such disturbance. However, in some cases the headway command can be issued by the roadway to increase or decrease the gap between the vehicles. The instances in which the headway commands are issued are relatively fewer than those which require speed commands. Similarly, there are cases when both of these commands are required. For example the merging of incoming traffic or a bad weather condition may require a minimum allowable headway in addition to a maximum allowable speed.

As described earlier due to hardware and software limitations imposed by the current setup the roadway controller cannot be implemented to issue the required commands in a feedback loop. The capability of the designed controllers to operate in a cooperative driving environment is, however, demonstrated in a virtual manner. In the case of longitudinal

vehicle following, the response of the roadway controller, when presented with any scenario, can be expressed in terms of the required speed and/or headway commands. In this demonstration, we have used these basic commands, which represent the response of the roadway controller for a particular cooperative maneuver, to control the trajectory of the vehicles. In the following, we will present the results of this demonstration.

6.2 Experimental Results

The purpose of this demonstration is to exhibit the capability of the designed AICC controllers to accommodate the extra commands necessary to allow a fully cooperative driving system. We have tested several scenarios which can exist in a cooperative driving environment to validate the performance of the designed controllers. The results of one such scenario will be described in this section.

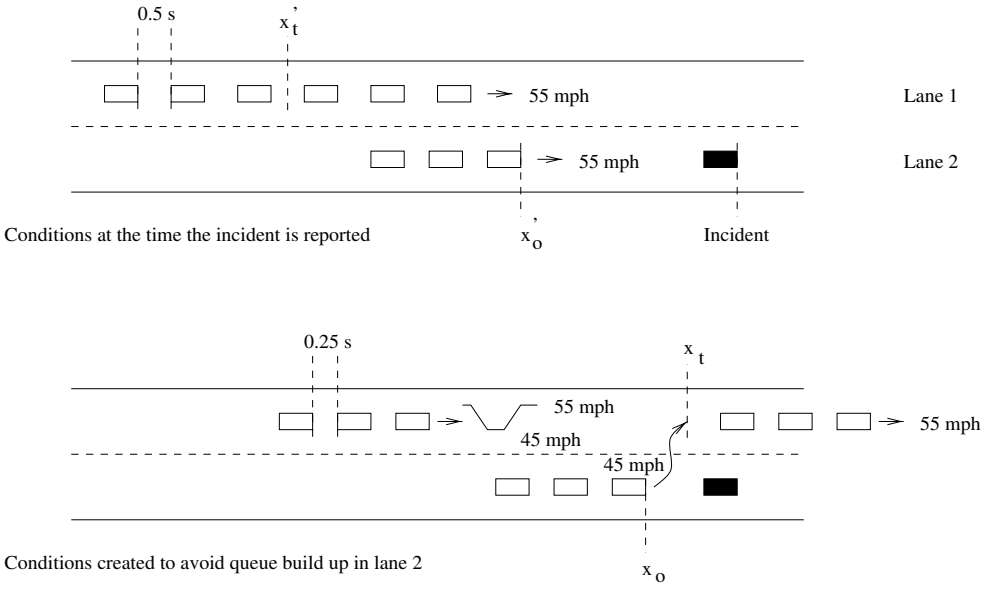

Figure 29: A scenario used for the demonstration of cooperative driving system.

As shown in Figure 29, it is assumed that an incident has occurred in lane 2. The roadway has to create suitable conditions in lane 1, so that the vehicles upstream the incident location in lane 2 can safely change lane and merge into the stream in lane 1. The strategy selected in this case is to:
i) Reduce the headway upstream and downstream the location x_t' in lane 1, to create gap for the merging vehicles.
ii) Reduce the speed upstream at the location x_o' in lane 2.

This strategy will create sufficient gap in lane 1 such that the group of vehicles with

their leader located at x_o in lane 2 can occupy the position x_t in lane 1. The merging process should be executed such that the safe spacing condition is not violated at any time. Furthermore, to guarantee stability in the stream of vehicles in lane 1, the vehicle upstream the location x_t are commanded to reduce their speed during this merging process. After the incident location is passed these vehicles can resume their normal operating speed and headway.

As described earlier due to limited availability of resources, the whole scenario is broken down into atomic maneuvers required to execute this coordination. Since only three vehicles are available and only one use selected (roadway) command can be broadcasted to all the vehicles, the whole maneuver is tested in two steps, which are described below.

Some remarks are in order

- Incident management through lane changes is a multi-variable optimization problem which depends on the speed, density and the relative speed, density in the adjacent lanes, among other factors. The scenario described here is not a global solution of this optimization problem, but results in improved overall flow in both lanes after the incident.
- (i) The selection of x_0' is a function of the nominal speed and the platoon size (given x_0).

  (ii) Selection of platoon split is a bit tricky. It depends not only on the selection of x_0' but also on the speed differential between the lanes and the size of the platoon changing the lane. In our case, for simplicity, both lanes have a nominal speed of 55 mph and the speed at x_0 and x_t is 45 mph, so it resulted in the shown x_t'. However in general if v_1 and v_2 are different, it is more complex to calculate the optimal platoon split point. For example if $v_1 > v_2$ then x_t' can be selected farther upstream.

6.2.1 Step 1

In this step vehicles downstream the location x_t' are instructed to reduce their headway from a nominal value of 0.5 seconds to 0.25 seconds. The vehicles are operating at a nominal speed of 55 mph before and after this command. The same test is repeated for these three vehicles assuming them to be upstream the location x_t'. The experimental results are shown in Figures 30-32.

6.2.2 Step 2

In the second step the speed command upstream the location x_t is modified to create extra space and to guarantee minimum speed differential between the joining vehicles and vehicles upstream the merging location. In this case the vehicles are commanded to reduce their speed to 45 mph (equal to the speed of the merging vehicles) before the start of the merging process. The speed of these vehicles remain at 45 mph during the merging process, which

is assumed to be completed within 10 seconds. The vehicles resume their normal speed afterwards. The test results are shown in Figures 33-35.

6.3 Discussions and Recommendations

In this test we have successfully demonstrated the capability of the designed AICC controllers to operate in a cooperative driving environment. The additional capability was introduced by designing a supervisory controller which operates above the regulation layer controllers to accommodate the commands issued by external agents. The external agents are the infrastructure, the surrounding vehicles and the driver. The supervisory controller is designed so that it can expect necessary commands from these external agents and modify the trajectory of individual vehicles so that they can operate in a cooperative driving environment without risking the safety and comfort of the occupants of these vehicles.

The complementary part of the supervisory controller, to achieve the objective of cooperative driving, is the roadway controller. However, due to limited availability of resources, at the time of testing, the roadway controller is restricted to its very basic for. The infrastructure assistance required to accomplish the cooperative driving was achieved through the lead vehicle of the test setup. Different scenarios were virtually created and were presented to the roadway detection making logic. This logic operated on these virtual situations and created a set of commands necessary to execute the chosen strategy. These commands were then issued to vehicles. The experimental results indicate that the performance of the designed controllers is adequate to operate in a cooperative driving environment. These controllers can react to the commands issued by the external agents and guarantee local and global stability.

Due to hardware and software limitations in the current test setup the complete scenario can be tested in several steps. With the availability of more resources, the current demonstration can be extended to include the complex maneuvers required to establish the feasibility and applicability of the designed roadway/vehicle cooperative driving system.

7 Conclusion

In this report we have documented the experimental results of the roadway/vehicle cooperative driving system. The design of a complete cooperative driving system is pursued in an evolutionary manner. We have augmented the basic vehicle following controller, designed in an earlier part of this study, with additional outer loop controllers so that the complete system can operate in a cooperative driving environment. The testing of the designed controllers is also done in a step-wise manner. Each new test setup adds an extra feature to the previously tested system. In the final step we have demonstrated a roadway/vehicle cooperative driving system, in which the vehicle following controllers have the capability of reacting to the commands issued by the infrastructure as well as the surrounding vehicles.

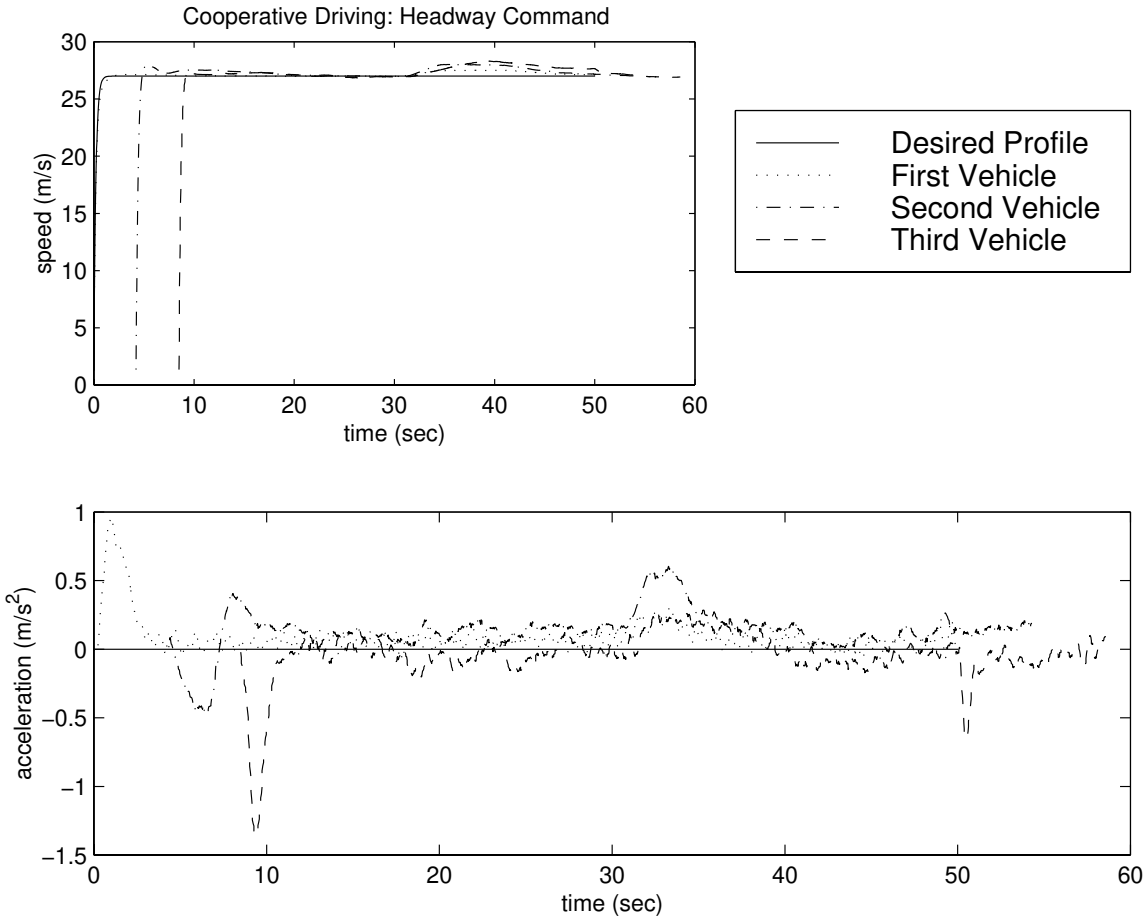

Figure 30: The speed and acceleration profiles for cooperative driving demonstration: Tracking of headway command.

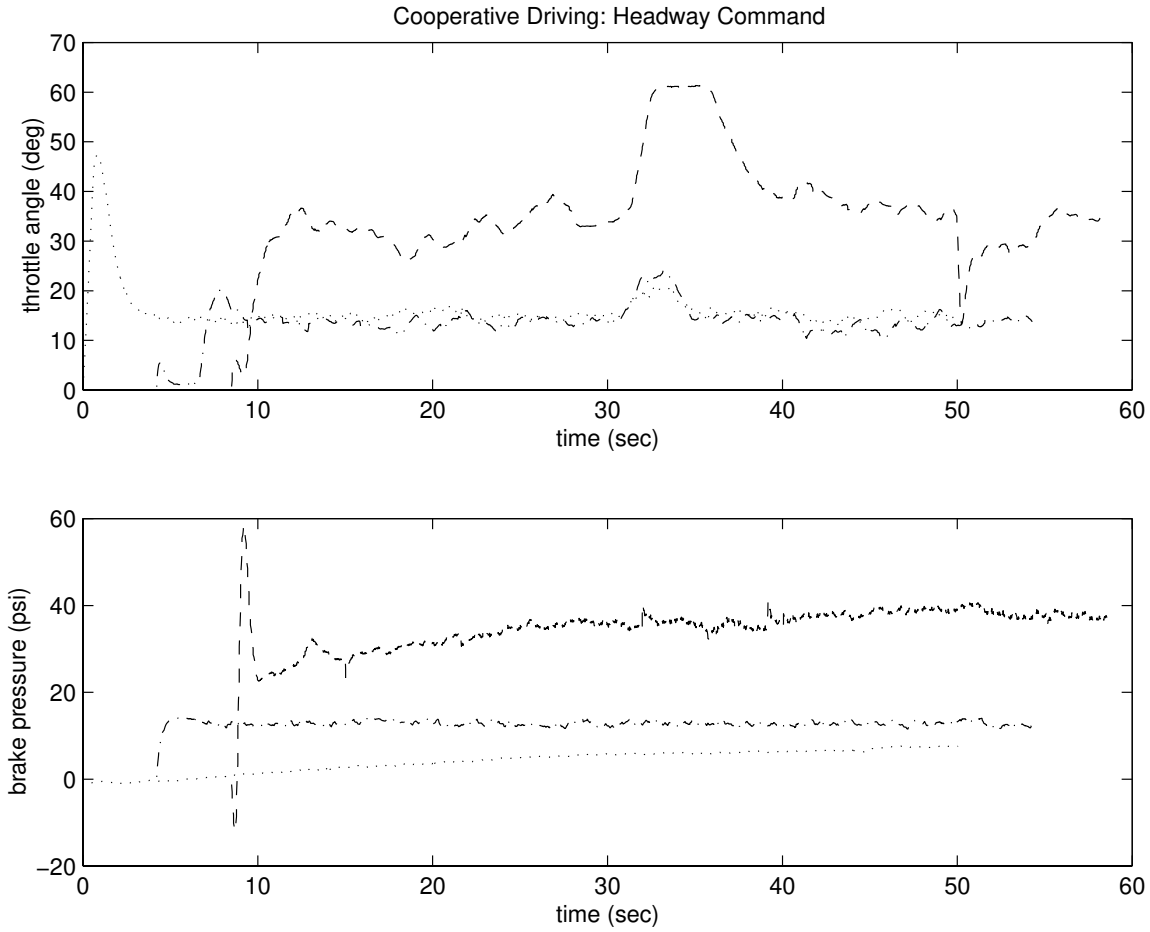

Figure 31: The throttle angle and brake pressure commands for test 5.

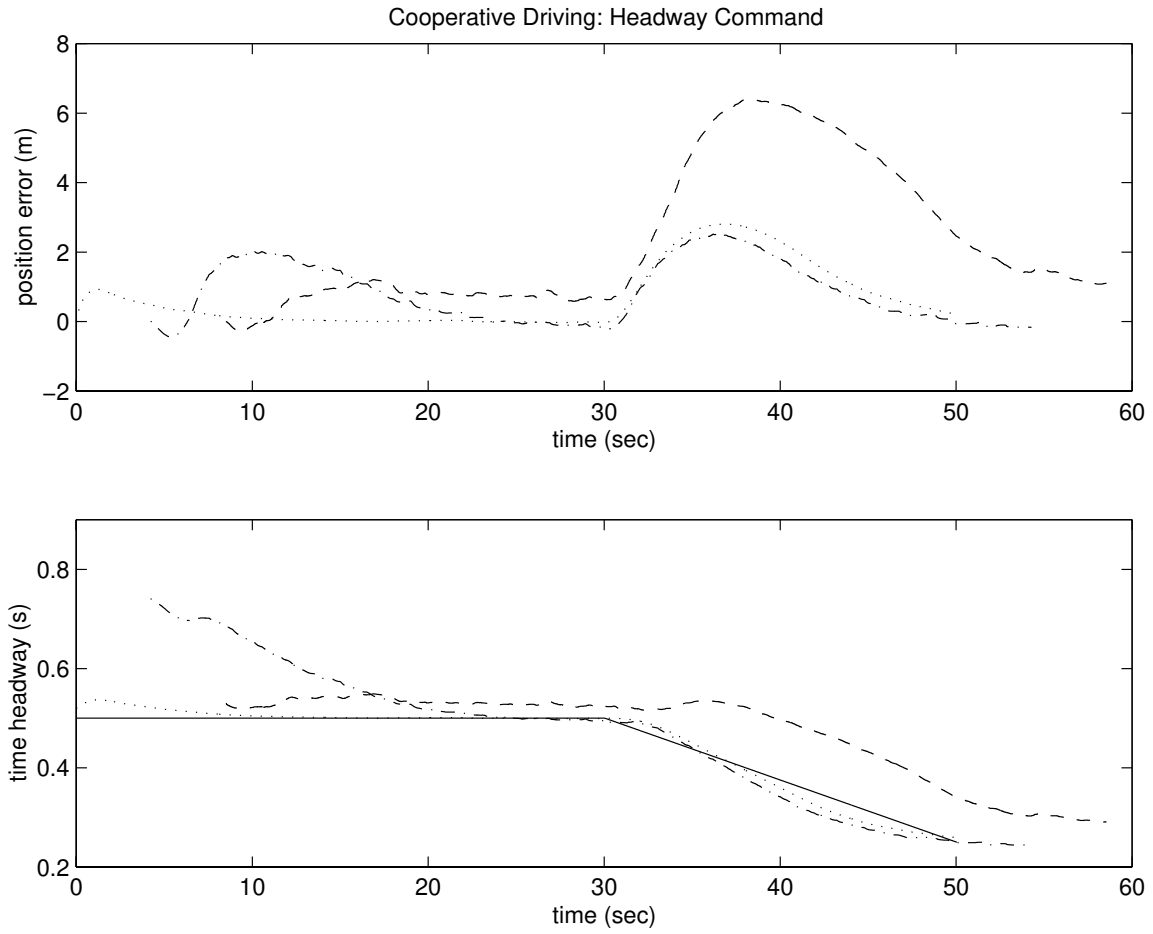

Figure 32: The position error and time headway for cooperative driving demonstration: Tracking of headway command.

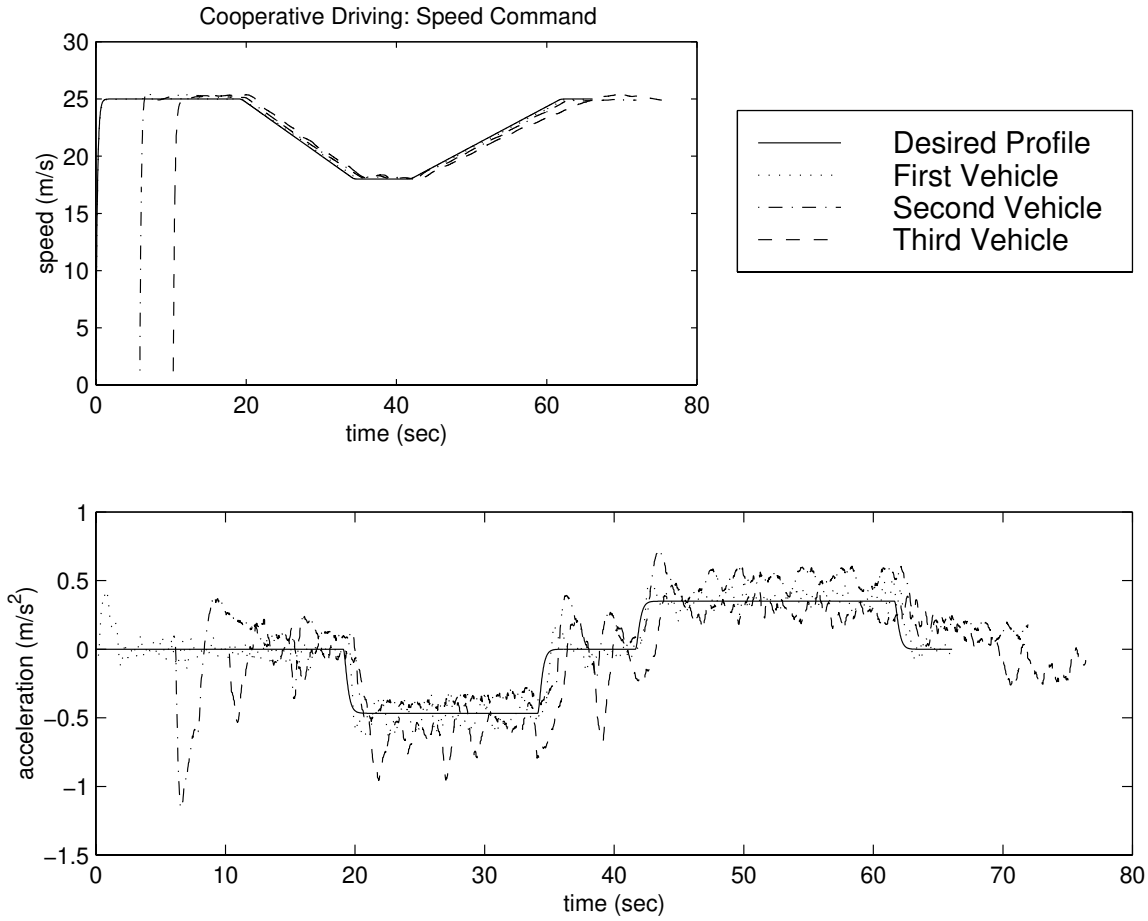

Figure 33: The speed and acceleration profiles for cooperative driving demonstration: Tracking of speed command.

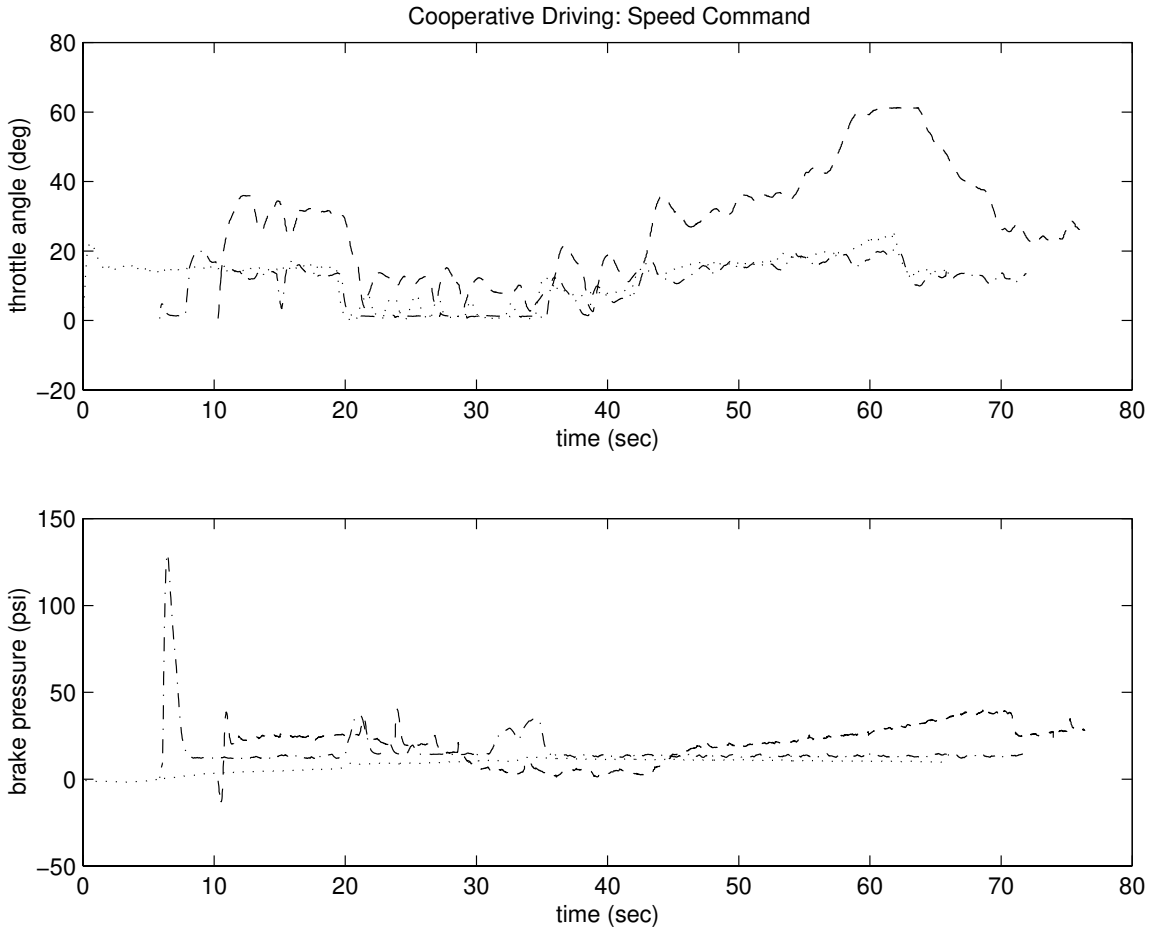

Figure 34: The throttle angle and brake pressure commands for test 5.

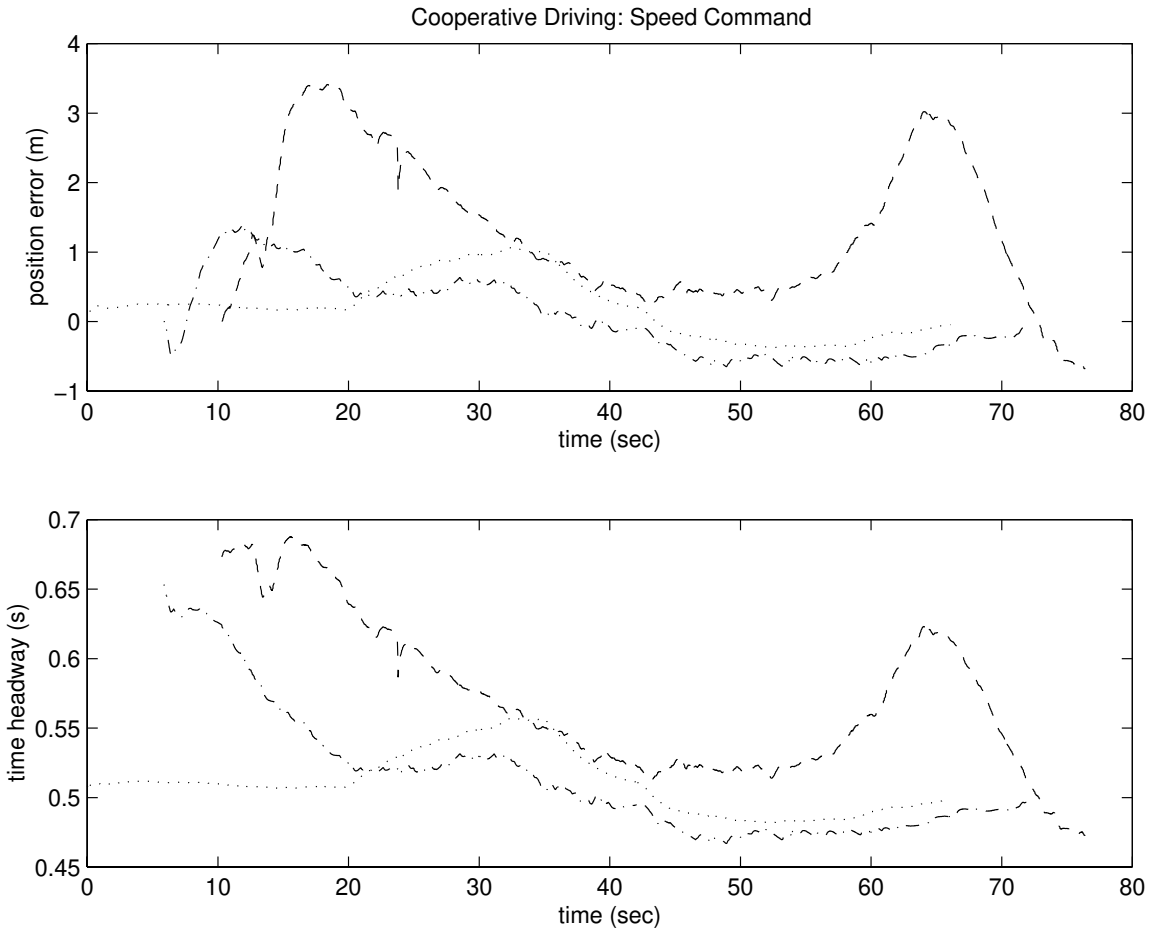

Figure 35: The position error and time headway for cooperative driving demonstration: Tracking of speed command.

Due to limited availability of resources at the time of this testing, the demonstration is broken down in several steps each of which is necessary to execute different maneuvers required in a cooperative driving system. The performance of the designed controllers was found to be satisfactory enough to permit their application in a real cooperative driving environment.

Acknowledgments:

We would like to thank the research team at PATH, particularly Steve Shladover, for providing necessary technical assistance to conduct these experiments. We gratefully appreciate the help provided by Jay Kniffen, Benedicte Bougler, Sonia Mahal and Robert Prohaska, throughout the course of these experiments.

References

[1] P. Ioannou, C. C. Chien, "Autonomous Intelligent Cruise Control", IEEE Transactions on Vehicular Technology, Vol. 42, pp. 657-672, Nov. 1993.

[2] P. Ioannou and Z. Xu, "Throttle and Brake Control System for Automatic Vehicle Following", *IVHS Journal*, Vol. 1(4), 1994, pp. 345-377.

[3] B. K. Powell and J. A. Cook, "Nonlinear Low Frequency Phenomenological Engine Modeling and Analysis", *Proc. of ACC*, Minneapolis, MN, pp. 332-340, June 1987.

[4] M. Würtenberger, St. Germann and R. Isermann, "Modeling and Parameter Estimation of Nonlinear Vehicle Dynamics", DSC-Vol. 44, *ASME Transportation Systems*, pp. 53-63, 1992.

[5] A. S. Hauksdottir, R. E. Fenton, "On the Design of a Vehicle Longitudinal Controller," *IEEE Trans. on Vehicular Technology*, vol. VT-34, no. 4, pp. 182-187, Nov. 1985.

[6] J. K. Hedrick, D. McMahon, V. Narendran, D. Swaroop, "Longitudinal Vehicle Controller Design for IVHS System," *Proc. of ACC*, vol. 3, pp. 3107-3112, June 1991.

[7] H. Raza, P. Ioannou, "Vehicle Control Design for Infrastructure Managed Vehicle Following", California PATH Research Report, UCB-ITS-PRR-96-29, 1996.

Modeling and Roadway Control of Traffic Flow Using Artificial Neural Networks *

Fu-Sheng Ho and Petros Ioannou
Center for Advanced Transportation Technologies
University of Southern California
Los Angeles, CA 90089-2562

Abstract. In this paper we use an artificial neural network technique to model and control highway traffic in a single lane. The developed controllers generate the speed commands for each section of the lane that vehicles need to follow in order to achieve a desired traffic flow density distribution along the lane. In an automated highway environment the speed commands could be communicated to the computer control system of the vehicle and followed directly without human errors and delays. For example vehicles equipped with intelligent cruise control (ICC) could follow each other automatically in the longitudinal direction and accept speed commands from the roadway via simple roadway to vehicle communication.

In this paper we simulated an automated highway environment and designed roadway neural network controllers to improve traffic flow characteristics. We use simulations to demonstrate that the use of feedback control on the macroscopic level could bring dramatic improvements on the characteristics of traffic flow. The same methodology could be applied to traffic in multiple lanes with on and off ramps.

*This work was supported by the California Department of Transportation through PATH Program of the University of California. The contents of this report reflect the views of the authors who are responsible for the facts and the accuracy of the data presented herein. The contents do not necessarily reflect the official views or policies of the State of California or the Federal Highway Administration. This paper does not constitute a standard, specification or regulation. The work of the first author was also supported in by the office of the senior Vice Minister of Ministry of Economic Affairs, Republic of China and in part by the California Department of Transportation.

1 Introduction

In most metropolitan areas, highway driving is the dominant mode of urban transportation. With the increasing demand of automobile and highway usage, highway traffic will continue to be an important social and economic problem. The current consensus of most traffic engineers and researchers is that highway capacity will be greatly increased if the facilities can be designed to be more intelligent and efficient by using advanced technologies. It has been argued that the use of smart sensors, actuators, computers and software tools, etc. is more practical and economically advantageous than building new highways. One of the outcomes of these arguments and debates is the concept of automated highway systems (AHS) where automation techniques are applied to vehicles and roadway in order to increase the capacity and efficiency of existing facilities.

Congestion is one of the most serious problems in highway traffic. The instability inherent in traffic flow due to the behavior of human drivers is one of the main causes of congestion. With vehicle automation such as intelligent cruise control (ICC) [7] (an initial step towards AHS) that allows vehicles to follow each other automatically, the roadway may be able to control traffic density and eliminate congestion by commanding the average speed of vehicles along lanes. One way of designing such controllers is to use a mathematical model that describes the flow of traffic.

The average behavior of vehicles at a specific location and time instant in a lane can be expressed by the flow variables defined for traffic. The three most important traffic flow variables used to describe the state of traffic flow are flow rate (q), concentration or density (k) and speed (v). There is a fundamental relationship among these variables called the fundamental equation of traffic flow which is written as $q = kv$ and is analogous to that of water flow studied in hydromechanics. An earlier attempt to describe the particular characteristics of traffic flow led to Greenshields' linear mathematical formula for speed-density relationship [5] followed by several nonlinear formulas proposed by Greenberg, Pipes, Munjal, Drew and Drake et. al. [4, 17, 12, 3, 8]. These relationships that describe the steady-state behavior of traffic flow are called traffic stream models. A volume-density relationship $Q(k)$, which is the well-known fundamental diagram of traffic engineering, can be derived based

upon these formulas and the fundamental equation. Based upon this understanding, Lighthill and Whitham [11] first proposed a model that explains kinematic waves phenomena in traffic flow. By assuming that the fundamental diagram is applicable, they formulated the continuity equation, a partial differential equation with density as the only state variable. Since this model is established based upon the analogy with incompressible fluid flow, it has certain limitations in describing traffic flow. Built upon the model of Lighthill and Whitham, several models have been proposed as modifications or extensions in an attempt to overcome these limitations. Payne proposed a space increment in which the mean speed adjusts to downstream traffic density. Also, the assumption of stationary mean speed-density relationship that mean speed adjusts instantaneously to traffic density was removed by introducing a small time delay [16]. These changes led to a model with two state variables. Papageorgiou et al. [15] proposed an extension to this model by considering weaving phenomena. Recently, a modified model was proposed by Karaaslan, Varaiya and Walrand [10] in order to eliminate some unrealistic phenomena observed in Payne's model. Generally speaking, mathematical modeling of traffic flow results in a nonlinear dynamic system. Because of the inconsistencies of driver behavior and variations in traffic flow patterns, one model validated in one area or one time may be inaccurate in another area and/or another time.

A potential method for modeling and controlling traffic flow is one that employs learning so that dynamic changes in traffic are learned on-line and accommodated with the proper use of identification and control techniques. One such method is based on the use of Artificial Neural Networks (ANNs).

Due to their capability to classify patterns, ANNs have been proposed to passively control traffic flow on freeways; namely, to monitor the traffic flow and detect non-recurring congestion caused by incidents [20, 1]. Spatial and temporal traffic patterns of lane-blocking incidents are recognized by ANNs and this information can be used to formulate effective countermeasures which may involve provision of real-time traveler information, timely dispatch of emergency services and incident removal crews and real-time control of traffic entering and on the freeway.

ANNs have also been proposed for identification and control of nonlinear dynamic systems by several researchers [13, 18]. The learning capability and universal approx-

imation property of ANNs make them suitable for modeling and control of uncertain nonlinear and time varying dynamic systems such as vehicular traffic.

In this paper we consider the modeling and control of traffic flow in a single highway lane using ANNs. The ANNs are first trained to accurately model the dynamics of the traffic flow. The ANN model is then used to control the traffic density and force it to follow a desired one. The objective of the controller is to eliminate congestion caused by inhomogeneous traffic density distributions along the lane. Computer simulations are used to demonstrate the effectiveness of the use of ANN techniques to model and control traffic flow.

2 Macroscopic Traffic Flow Models

Analogous to real fluid, traffic involves flows, concentrations and speeds. There is a natural tendency to attempt to describe traffic in terms of fluid behavior. The macroscopic view of traffic flow is based upon this hydrodynamic analogy. This point of view is more concerned with the overall average behavior of traffic than with the interactions between individual vehicles.

Treating traffic flow as a fluid analogue with density $k(x,t)$ and volume $q(x,t)$ at location x and time t, we obtain using the law of conservation of mass, the continuity equation

$$\frac{\partial k}{\partial t} + \frac{\partial q}{\partial x} = r - s \tag{1}$$

where r and s represent exogenous on-ramp and off-ramp sources respectively.

We discretize the above equation as follows: We consider a highway lane which is subdivided into N sections with length L_i, $(i = 1, \cdots, N)$ each having at most one on-ramp and one off-ramp as shown schematically in Figure 1.

For a discrete time instant nT, where T is the sample time interval, we introduce space-time-discretized traffic flow variables as follows.

$k_i(n)$: density in section i at time nT.

$v_i(n)$: space mean speed in section i at time nT.

$q_i(n)$: traffic flow leaving section i entering section $i+1$ at time nT.

L_i: length of freeway in section i.

Based upon these variables, a space-time-discretized form of the continuity equation (1) is given by

$$k_i(n+1) = k_i(n) + \frac{T}{L_i}[q_{i-1}(n) - q_i(n) + r_i(n) - s_i(n)] \tag{2}$$

The traffic volume $q_i(n)$ between two sections is usually modeled as a weighted sum of the traffic volumes corresponding to the densities of the two sections, expressed by the equation

$$q_i(n) = \alpha k_i(n) v_i(n) + (1-\alpha) k_{i+1}(n) v_{i+1}(n) \tag{3}$$

where $v_i(n)$ is the average speed at section i at time nT and $0 < \alpha < 1$ is the weighting factor. A density model of traffic flow is therefore given by

$$\begin{aligned} k_i(n+1) &= k_i(n) + \frac{T}{L_i}[\alpha k_{i-1}(n) v_{i-1}(n) + (1-\alpha) k_i(n) v_i(n) - \alpha k_i(n) v_i(n) \\ &\quad -(1-\alpha) k_{i+1}(n) v_{i+1}(n) + r_i(n) - s_i(n)] \end{aligned} \tag{4}$$

By assuming different velocity-density relationships, a hierarchy of velocity models of traffic flow with different accuracy can be derived. In Lighthill and Whitham's [11] model , velocity is an algebraic function of density which is written as

$$v(x,t) = V[k(x,t)]$$

However, it would be more realistic to assume that the mean speed adjusts to downstream density with a time delay according to

$$v(x, t+\Delta t) = V[k(x+\Delta x, t)]$$

which describes dynamic phenomena.

Based upon this assumption, a freeway traffic model, originally derived by Payne [16] and modified by Papageorgiou [14] and Cremer and May [2], is given for a single-lane freeway by

$$\begin{aligned} v_i(n+1) &= v_i(n) + \frac{T}{\Delta t}\{V_e[k_i(n)] - v_i(n)\} + \frac{T}{L_i} v_i(n)[v_{i-1}(n) - v_i(n)] \\ &\quad - \frac{\mu T}{\Delta t L_i} \frac{k_{i+1}(n) - k_i(n)}{k_i(n) + \kappa} \end{aligned} \tag{5}$$

where μ and κ are positive constants, V_e is the equilibrium mean speed and the $2nd$, $3rd$ and $4th$ terms in the right-hand side are called the relaxation, convection and anticipation terms respectively.

The model of Karaaslan, Varaiya and Walrand [10], which was proposed as a modification of the model given by (5) is :

$$\begin{aligned} v_i(n+1) &= v_i(n) + \frac{T}{\Delta t}\{V_e[k_i(n)] - v_i(n)\} \\ &\quad + \frac{T}{L_i}\frac{k_{i-1}(n)}{k_i(n)+\kappa'}v_i(n)[\sqrt{v_{i-1}(n)v_i(n)} - v_i(n)] \\ &\quad - \frac{\mu(n)T}{\Delta t L_i}\frac{k_{i+1}(n)-k_i(n)}{k_i(n)+\kappa} \end{aligned} \tag{6}$$

where κ' and κ are positive constants that prevent the convection and anticipation terms from becoming too large and

$$\mu(n) = \begin{cases} \mu_1 \frac{\rho}{k_{jam}-k_{i+1}(n)+\sigma} & if\ k_{i+1}(n) > k_i(n) \\ \mu_2 & otherwise \end{cases} \tag{7}$$

where μ_1, μ_2, ρ and σ are constants to be determined and the equilibrium speed is modeled by

$$V_e(k_i) = v_f(1 - (\frac{k_i}{k_{jam}})^l)^m \tag{8}$$

where v_f, k_{jam}, l and m are constants to be identified for real traffic flow.

The traffic flow models (2) to (8) contain several parameters whose values depend on the traffic flow characteristics that vary according to driving behavior and traffic pattern. One way of choosing these parameters is to use real traffic data to validate the models. A validated model, however, that is accurate for one place at a particular time of the day may not hold in another place at another time. The nonlinear and unpredictable characteristics of traffic flow dynamics make it difficult to have a universal traffic flow model that applies to all traffic situations at all times.

A promising approach to model traffic flow is to use a neural network that is continuously training itself to possible changing patterns of traffic and is therefore adaptive to changes and driving behaviors. Such a neural network model could then be used for control purposes as discussed in the following sections in order to improve

traffic flow characteristics. The general form of the traffic flow models (2) to (6) is used to choose the structure of the ANN.

3 Fundamentals of Artificial Neural Networks

The development of artificial neural networks or connectionist models has been inspired by the nervous system of human brain. An artificial neural network comprises many basic processing elements (PEs) connected in certain parallel structure. Each processing element or neuron is described by a nonlinear algebraic or differential equation. Associated with each interconnection, there is an adjustable parameter or weight which changes according to a certain learning rule. According to their structures, neural networks can be broadly categorized as either feed-forward networks or recurrent networks. Feed-forward networks are also called static networks since the flow of input signal or information is directed to output and no returning paths are allowed. However, in recurrent networks, which are also called dynamic networks, either states or outputs can be fed-back and a current signal is dependent upon the past one. This makes recurrent networks significantly different from feed-forward networks. Once the structure and a learning rule are given, a neural network is completely defined.

Here, we will focus on one of the most popular neural networks called sigmoidal feed-forward networks. The output of the processing element is the nonlinear sigmoidal function of the sum of the inputs and a possible threshold. A sigmoidal function $\sigma(\cdot)$, which is nondecreasing, satisfies the conditions that $\sigma(-\infty) = 0$ and $\sigma(\infty) = 1$. One choice of the smooth sigmoidal functions is expressed by

$$\sigma(x) = \frac{1}{1 + e^{-cx}} \tag{9}$$

where c is a constant determined by the shape of the function.

Thus, the mathematical expression of a processing element with input $x_i, i = 1, \cdots, n$ and output y, shown in Figure 2, is

$$y = \sigma(\sum_{i=1}^{n} w_i x_i + w_{n+1}) \tag{10}$$

where w_i are adjustable weights.

The PEs are arranged in layers with signals flowing forward from input to output. It has been shown by Hornik [6] that multilayer feed-forward networks with as few as one hidden layer are capable of universal approximation in a very precise and satisfactory sense. Shown in Figure 3 is a $1\frac{1}{2}$ layer feed-forward network with p processing elements, the outputs $y_i, i = 1, \cdots, m$ of which each is just a weighted sum of the outputs of the hidden layer. The mathematical expression of this network is given by

$$y_j = \sum_{l=1}^{p} t_{lj}\sigma(\sum_{i=1}^{n} w_{il}x_i + w_{n+1,l}), \quad j = 1, \cdots, m \tag{11}$$

where t_{lj} and w_{il} are adjustable weights.

Let $X = [x_1, \cdots, x_n]^T$, $Y = [y_1, \cdots, y_m]^T$ and $\theta = [w_{11}, \cdots, w_{np}, t_{11}, \cdots, t_{pm}]^T$. Then the input-output relationship of the neural network can be expressed as

$$Y = N(X; \theta) \tag{12}$$

Let $Y_p = [y_{1p}, \cdots, y_{mp}]^T$ be the output vector of an unknown system with the same input $X = [x_1, \cdots, x_n]^T$, i.e.

$$Y_p = F(X, n) \tag{13}$$

where $F(\cdot, \cdot)$ is a completely unknown function. The difference between Y_p and Y is the error given by

$$e \stackrel{\triangle}{=} Y - Y_p = N(X; \theta) - Y_p \tag{14}$$

If we now adjust the weights θ such that $e \to 0$ i.e., $Y \to Y_P$, then the input output characteristics of the unknown system (13) are matched by the neural network (12). The adjustment mechanism for θ may be developed using simple optimization techniques to minimize a certain cost function of e [18, 19].

4 Modeling of Highway Traffic Using Neural Networks

Assuming that there is no on-ramp or off-ramp, the most general form of the density equation in the traffic flow models discussed in section 2 is

$$k_i(n+1) = g_i(k_{i-1}(n), v_{i-1}(n), k_i(n), v_i(n), k_{i+1}(n), v_{i+1}(n)) \tag{15}$$

where $k_i(n)$ is the mean density at section i at time nT and g_i is an unknown nonlinear function. Without loss of generality we express (15) in the form

$$k_i(n+1) = ck_i(n) + f_i(k_{i-1}(n), v_{i-1}(n), k_i(n), v_i(n), k_{i+1}(n), v_{i+1}(n)) \tag{16}$$

where $|c| < 1$ is an arbitrary constant and

$$f_i(n) = g_i(n) - ck_i(n)$$

Our objective is to develop a neural network that identifies the nonlinear function f_i that is used to generate the estimates $\hat{k}_i(n+1)$ that are as close to the measured $k_i(n+1)$ as possible for $i = 1, 2, \cdots, N$. We achieve this objective as follows: Let $N_{f_i}(\cdot; \theta_{f_i})$ be the neural network approximation of the nonlinear function f_i, where θ_{f_i} is a vector of the weights of the network. Then the following model generates the density estimates

$$\hat{k}_i(n+1) = ck_i(n) + N_{f_i}(k_{i-1}(n), v_{i-1}(n), k_i(n), v_i(n), k_{i+1}(n), v_{i+1}(n); \theta_{f_i}(n)) \tag{17}$$

that correspond to the weights $\theta_{f_i}(n)$ at time nT.

The error

$$e_i(n) = \hat{k}_i(n+1) - k_i(n+1) = N_{f_i}(h_i, v_i(n); \theta_{f_i}) - f_i(n) \tag{18}$$

where $h_i = [k_{i-1}(n), v_{i-1}(n), k_i(n), k_{i+1}(n), v_{i+1}(n)]^T$, is a measure of the deviation of the estimated $\hat{k}_i$ from the actual measured k_i at time nT.

The adjustment rule for the weights θ_{f_i} is chosen as [19]

$$\begin{aligned} \mu_i(n+1) &= \theta_{f_i}(n) - \frac{\gamma_0}{\beta_0 + \|\xi_i(n)\|^2}\xi_i(n)e_i(n) \\ \theta_{f_i}(n+1) &= \begin{cases} \mu_i(n+1) & if \quad |\mu_i(n+1)| \le M_{\theta_i} \\ \frac{M_{\theta_i}}{|\mu_i(n+1)|}\mu_i(n+1) & if \quad |\mu_i(n+1)| > M_{\theta_i} \end{cases} \end{aligned} \tag{19}$$

where $0 < \gamma_0 < 2$, $\beta_0 > 0$ and $M_\theta > 0$ are design parameters and

$$\xi_i(n) = \frac{\partial^T N_{f_i}(h_i; \theta_{f_i})}{\partial \theta_{f_i}}$$

We illustrate N_{f_i} in the neural network configuration for section i by Figure 4.

It can be shown [19] that if N_{f_i} is linear with respect to θ_{f_i} and f_i can be parameterized to be of the same form as N_{f_i} with a corresponding unknown $\theta^*_{f_i}$ then (19) guarantees that $e_i(n) \to 0$ as $n \to \infty$.

5 Control of Traffic Flow Using Neural Networks

Based on the neural network techniques described in the previous section, our objective is to design a controller that will generate speed commands to be followed by the vehicles at the various sections of the freeway lane so that a desired traffic flow rate can be achieved by maintaining a desired density profile. The speed commands are generated according to the desired density at each section.

We assume that there exists an inverse mapping ${g_i}^{-1}$ so that from (15) we obtain

$$v_i(n) = {g_i}^{-1}(k_{i-1}(n), v_{i-1}(n), k_i(n), k_i(n+1), k_{i+1}(n), v_{i+1}(n))$$

and

$$k_i(n+1) = g_i(k_{i-1}(n), v_{i-1}(n), k_i(n), {g_i}^{-1}, k_{i+1}(n), v_{i+1}(n))$$

The speed commands to the vehicles at each section i and each time nT are generated as follows: First, a $1\frac{1}{2}$ layer feed-forward network is trained to approximate the inverse mapping ${g_i}^{-1}$ as shown in Figure 5 where

$$h_i = [k_{i-1}(n), v_{i-1}(n), k_i(n), k_{i+1}(n), v_{i+1}(n)]^T$$

and the weights $\theta_{g_i{}^{-1}}$ in $N_{g_i{}^{-1}}(h_i, k_i(n+1); \theta_{g_i{}^{-1}})$ are adjusted according to (19) with different definitions for error signal and sensitivity function which are as follows.

$$\begin{aligned} e_i(n) &= \tilde{v}_i(n) - v_i(n) \\ \xi_i(n) &= \frac{\partial^T N_{g_i{}^{-1}}(h; \theta_{g_i{}^{-1}})}{\partial \theta_{g_i{}^{-1}}} \end{aligned}$$

The adjustment algorithm is listed below:

$$\begin{aligned} \mu_i(n+1) &= \theta_{g_i{}^{-1}}(n) - \frac{\gamma_0}{\beta_0 + \|\xi_i(n)\|^2}\xi_i(n)e_i(n) \\ \theta_{g_i{}^{-1}}(n+1) &= \begin{cases} \mu_i(n+1) & if \quad |\mu_i(n+1)| \le M_{\theta_i} \\ \frac{M_{\theta_i}}{|\mu_i(n+1)|}\mu_i(n+1) & if \quad |\mu_i(n+1)| > M_{\theta_i} \end{cases} \end{aligned} \tag{20}$$

where $0 < \gamma_0 < 2$, $\beta_0 > 0$ and $M_\theta > 0$ are design parameters.

We denote the output of the neural network as $\tilde{v}_i$ given by the expression

$$\tilde{v}_i(n) = N_{g_i{}^{-1}}(k_{i-1}(n), v_{i-1}(n), k_i(n), k_i(n+1), k_{i+1}(n), v_{i+1}(n); \theta_{g_i{}^{-1}})$$

Secondly, assume that the desired density at section i is k_{d_i}. We set the input, $k_i(n+1)$, of $N_{g_i^{-1}}$ to k_{d_i} and denote the output as $\hat{v}_i$. Our controller is shown in Figure 6, where $\hat{v}_i(n)$ is given by

$$\hat{v}_i(n) \quad = \quad N_{g_i^{-1}}(k_{i-1}(n), v_{i-1}(n), k_i(n), k_{d_i}, k_{i+1}(n), v_{i+1}(n); \theta_{g_i^{-1}})$$

It should be noted that even if $N_{g_i^{-1}}$ is perfectly trained, $\hat{v}_i(n)$ is not equal to $v_i(n)$ since k_{d_i} is not necessarily equal to the current $k_i(n+1)$. However, if $\hat{v}_i(n)$ converges to $v_i(n)$, the density k_i is expected to approach k_{d_i}.

The above controller is an open-loop one and cancels the dynamics of the system using feed-forward action. Such controllers are known to have poor robustness properties with respect to modeling errors that are always present in real applications. This drawback of the neural network controller of Figure 6 can be removed using the following approaches:

Approach I. We consider the use of output feedback in Figure 6 to obtain the closed-loop system shown in Figure 7, where F is a linear filter of the form

$$F(e_{ki}(n)) = k_{d_i} + F_c(e_{ki}(n))$$

where $F_c(\cdot)$ is an arbitrary linear filter and $e_{ki}(n) = k_i(n) - k_{d_i}$. Since the neural network controller acts as the inverse model of the traffic flow dynamics, this closed-loop control falls into the class of internal model control(IMC) paradigm [9].

Approach II: Adaptive control is another technique in dealing with uncertainties. Shown in Figure 8 is a system configuration for direct adaptive control. It is built upon the IMC feedback configuration. $F(\cdot)$ is fixed; however, the weights of the neural network $N_{g_i^{-1}}$ or the parameters of the controller in $\theta_{g_i^{-1}}$, are adaptively adjusted based on Adjustment Law 2. Adjustment Law 2 has the same form as (19). The error for Adjustment Law 2 is defined as the difference between the desired density and the output of the forward neural network model, i.e., $\hat{k}_i(n+1) - k_{d_i}$ and the sensitivity function is

$$\xi_i(n) = \frac{\partial^T N(h_i; \theta_{g_i^{-1}}, \theta_{f_i})}{\partial \theta_{g_i^{-1}}}$$

where $N(h_i; \theta_{g_i^{-1}}, \theta_{f_i})$ represents the two $1\frac{1}{2}$ layer neural networks, $N_{g_i^{-1}}$ and N_{f_i}, cascaded together. Adjustment Law 1 provides on-line adaptation and is the same as

the off-line training law (19). However, Adjustment Law 2 assumes that the parameter vector θ_{f_i} has been accurately trained and is kept constant when $\theta_{g_i{-}1}$ is adaptively adjusted. With this assumption, N_{f_i} provides signal paths through θ_{g_i-1} and $\hat{v}(n)$ to $\hat{k}_i(n+1)$ and it allows us to calculate the sensitivity function for Adjustment Law 2. The sensitivity function is calculated using

$$\begin{aligned}\xi_i(n) &= \frac{\partial^T N(h_i;\theta_{g_i{-}1},\theta_{f_i})}{\partial\theta_{g_i{-}1}} \\ &= \frac{\partial^T N(h_i;\theta_{g_i{-}1},\theta_{f_i})}{\partial\hat{v}(n)}\cdot\frac{\partial\hat{v}(n)}{\partial\theta_{g_i{-}1}}\end{aligned}$$

The overall equations of the neural network adaptive controller in Figure 8 are listed below:

$$\begin{aligned}e_{ki}(n) &= k_i(n)-k_{d_i} \\ F(e_{ki}(n)) &= k_{d_i}+F_c(e_{ki}(n)) \\ e_i(n) &= \hat{k}_i(n+1)-k_{d_i} \\ \xi_i(n) &= \frac{\partial^T N(h_i;\theta_{g_i{-}1},\theta_{f_i})}{\partial\hat{v}(n)}\cdot\frac{\partial\hat{v}(n)}{\partial\theta_{g_i{-}1}} \\ \mu_i(n+1) &= \theta_{g_i{-}1}(n)-\frac{\gamma_0}{\beta_0+\|\xi_i(n)\|^2}\xi_i(n)e_i(n) \\ \theta_{g_i{-}1}(n+1) &= \begin{cases}\mu_i(n+1) & if \quad |\mu_i(n+1)|\le M_{\theta_i} \\ \frac{M_{\theta_i}}{|\mu_i(n+1)|}\mu_i(n+1) & if \quad |\mu_i(n+1)|>M_{\theta_i}\end{cases}\end{aligned}$$

where $0<\gamma_0<2$, $\beta_0>0$ and $M_\theta>0$ are design parameters and F_c is a linear filter.

Since $\hat{k}_i(n+1)$ is assumed to be a good estimate for $k_i(n+1)$, as long as $\theta_{g_i{-}1}$ are adjusted such that $\hat{k}_i(n+1)$ is driven to k_{d_i}, $k_i(n+1)$ is expected to track k_{d_i}.

The above controllers are based on heuristics and their stability analysis is not established due to the complexity of the nonlinearities in the traffic flow model and neural networks. Their effectiveness can be evaluated by extensive simulations as discussed in the next section.

6 Simulated Example

6.1 Congestion due to density inhomogeneity

Consider a highway lane that is subdivided into ten sections ($N = 10$) and at certain time instant the density distribution is shown in Figure 9, where sections 6, 7 and 8 have higher densities than the other sections. This inhomogeneity in traffic density is assumed to be caused by an accident at section 8.

The traffic flow instability can be predicted by the model of Karaaslan, Varaiya and Walrand described by equations (2), (3) and (6) to (8) as shown in Figure 10 and Figure 11, where congestion caused by a disturbance due to the accident at section 8 remains and gets worse even though the initial disturbance was removed at $t = 0$. This congestion situation is used as an example for applying the proposed neural controllers. The parameter values in the model used for simulation are: $v_f = 93.1 \;\; km/h$, $k_{jam} = 110 \;\; veh/km$, $l = 1.86$, $m = 4.05$, $\alpha = 0.95$ $\kappa = 40 \;\; veh/km$, $\kappa' = 4 \;\; veh/km$, $\mu_1 = 12 \;\; km^2/h$, $\mu_2 = 6 \;\; km^2/h$, $\rho = 120 \;\; veh/km$, $\sigma = 35 \;\; veh/km$, $\Delta t = 20.4 \;\; seconds$, $L_i = 500 \;\; meters \;\; for \;\; i = 1, 2, \cdots, 10$ and $T = 15 \;\; seconds$. The initial densities and mean speeds at all ten sections of the freeway are listed in Table 1.

6.2 Training of Neural Network Model

Consider a highway lane that is subdivided into ten sections. We assume that all the sections in the freeway are the same and their behavior can be described by the model of Karaaslan, Varaiya and Walrand using equations (2), (3) and (6) to (8). In Figure 4, we use a $1\frac{1}{2}$ layer feed-forward network of ten PEs ($p = 10$) as in Figure 3 for N_{f_i}. 200 sets of training data for the ten-section highway lane (2000 pairs of density-velocity input data and 2000 pairs of output data) are generated according to the model of Karaaslan, Varaiya and Walrand by randomly selecting the initial densities and velocities that distribute uniformly in their possible ranges ($0 < v_i(n) < 130$, $0 < k_i(n) < 110$). The constant in the sigmoidal function (9) is chosen as $c = 0.5$. The parameters in the adjustment law (19) are chosen as: $\gamma_0 = 0.1$, $\beta_0 = 1.0$ and $M_\theta = 10$. We have also arbitrarily chosen $c = 0.5$ in the density dynamic equation

(16). The performance of the learning of a neural network can be evaluated by the mean square error, which is defined by

$$MSE(n) = \frac{1}{n}\sum_{i=1}^{n} e(i)^2 \tag{21}$$

where e is the error signal. As shown in Figure 4, e is defined as $\hat{k}_i(n+1) - k_i(n+1)$. During the course of training, the mean square error is decreasing and approaches a small number. Shown in Figure 12 is the converging mean square error for the network N_{f_i}.

Similarly, we use another $1\frac{1}{2}$ layer feed-forward network of ten PEs for N_{g_i-1} in Figure 5. The same training data used to train N_{f_i} are used to train N_{g_i-1}. The constant in the sigmoidal function (9) is also chosen to be $c = 0.5$. The parameters in the adjustment law (20) are chosen as: $\gamma_0 = 0.1$, $\beta_0 = 1.0$ and $M_\theta = 10$. The error signal used to calculate the mean square error in (21) is defined as $\tilde{v}_i(n) - v_i(n)$. Shown in Figure 13 is the converging mean square error for the network N_{g_i-1}. After 10^6 iterations of training, the network N_{g_i-1} is able to generate the estimates of the mean speed with accuracy. Shown in Figure 14 are a few samples of the output of the trained network N_{g_i-1}. The solid line represents the mean speed generated by the model of Karaaslan, Varaiya and Walrand and the dashed line is the output from the network N_{g_i-1}.

6.3 Open-loop Control

Take the well-trained network N_{g_i-1} as the controller in Figure 6. We assume that the desired density for all the sections is k_d and substitute k_d for k_{d_i} as a input to N_{g_i-1}. The initial conditions are set to be the same as in the uncontrolled case, which has been shown to cause congestion. By assigning $k_d = 35 \;\; veh/km$, the controller generates the speed commands as shown in Figure 15 for vehicles at each section to follow. In the mean time, the traffic flow instability is being removed and the congestion being alleviated. Figure 16 shows that the traffic flow is able to track the desired density accurately in less than 15 minutes.

6.4 Internal Model Control

Assume that the dynamics of the traffic flow described by the model of Karaaslan, Varaiya and Walrand in (3) has changed such that the weighting factor α is 30% smaller than the nominal value of 0.95. In the face of this uncertainty, the open-loop controller is not able to effectively control the traffic flow with the same initial conditions as in the uncontrolled case. However, the robust internal model controller in Figure 7 with

$$F(e_{ki}(n)) = k_d(n) + e_{ki}(n) \cdot (1 - e^{-1})$$

where $e_{ki}(n) = k_i(n) - k_d$, can tolerate the uncertainty. The speed commands generated by the feedback controller are shown in Figure 17. If the commands are followed by the vehicles at each section, the traffic flow will track the desired density pretty accurately as shown in Figure 18.

6.5 Neural Network Adaptive Control

Assume that the parameter vector θ_{g_i-1} for the network N_{g_i-1} in Figure 5 is inaccurately trained or the traffic flow parameters have changed. For the sake of simplicity, in simulation we randomly select θ_{g_i-1} such that each weight in θ_{g_i-1} is either 15% smaller or 15% larger than the nominal value which has been correctly trained for the inverse model N_{g_i-1}. With this uncertainty, the open-loop controller is no longer effective in controlling the traffic flow. However, with the same initial conditions as in the uncontrolled case, the adaptive controller in Figure 8 is able to adjust its parameters in θ_{g_i-1} according to output performance. The speed commands generated by the adaptive controller are shown in Figure 19 and the traffic flow is shown to track the desired density with accuracy in Figure 20.

7 Conclusions

In this paper we consider the use of Artificial Neural Networks (ANNs) for modeling and controlling traffic flow on the macroscopic level. The ANNs consist of $1\frac{1}{2}$ layers and their weights are adjusted using robust adaptive laws developed in the area of adaptive control.

The proposed ANNs structures can be trained to model traffic flow quite accurately. Several controllers are designed based on the ANNs structures and simulated using a nonlinear traffic flow model that describes traffic flow in a single highway lane. The controllers accept measurements of the average density and speed at each section of the lane and each sampling time and generate the appropriate speed commands to be followed by the vehicles. The control objective is to force the actual traffic density to converge to a desired one.

Extensive simulations have been performed to demonstrate the effectiveness of ANNs controllers in managing congestion and improving traffic flow.

The methodology proposed in this paper can be easily extended for a full-scale traffic speed and flow control problem. Traffic on a multiple-lane freeway involves lane changes and on/off ramp metering. The effect of lane changes can be regarded as noise to the traffic density and the problem reduces to the training of neural networks with noisy data. Traffic density also depends on the values of the flow rates of the on/off ramp traffic. In this paper we assume no on/off ramps for the portion of the lane under consideration. Our methodology can be extended to lanes with on/off ramps. In this case a strategy needs to be developed to control the volume of the traffic at the ramps in addition to the control of the traffic density in the lane. This problem is currently under investigation.

References

[1] C. T. Lin, C. H. Hsiao and M. Cassidy, "Application of fuzzy logic and neural networks to automatically detect freeway incidents," *Journal of Transportation Engineering*, vol. 120, pp.753–772, 1994.

[2] M. Cremer and A. D. May, "An extended traffic model for freeway control," *Research Report UCB-ITS-RR-85-7*, 1985.

[3] D. R. Drew, "Deterministic aspects of freeway operations and control," *Highw. Res. Rec.*, vol. 99, pp.48–58, 1965.

[4] H. Greenberg, "An analysis of traffic flow," *Operations Research*, vol. 6, pp.79–85, 1958.

[5] B. Greenshields, "A study in highway capacity," *Proc. Highw. Res. Board*, vol. 14, pp.448–477, 1934.

[6] K. Hornik, "Multilayer feedforward networks are universal approximators," *Neural Networks*, vol 2, pp.359–366, 1989.

[7] P. Ioannou and C. C. Chien, "Autonomous intelligent cruise control," *IEEE Transactions on Vehicular Technology*, vol. 42, pp.657–672, Nov., 1993.

[8] J. Scofer, J. Drake and A. May, "A statistical analysis of speed-density hypothesis," *Proceedings of Third International Symposium on Theory of Traffic Flow*, 1965.

[9] G. Irwin, K. Warwick and K. Hunt, *Neural networks for control and systems*, Peter Peregrinus Ltd., 1992.

[10] U. Karaaslan, P. Varaiya, and J. Walrand, "Two proposals to improve freeway traffic-flow," *preprint*, 1990.

[11] J. J. Lighthill and G. B. Witham, "On kinematic waves ii: A theory of traffic flow on long crowded roads," *Proc. of the Royal Society of London*, series A, vol.229, pp.317–345, 1955.

[12] P. K. Munjal and L. A. Pipes, "Propagation of on-ramp density perturbations on unidirectional and two- and three-lane freeways," *Transportation Research*, vol. 5, pp.241–255, 1971.

[13] K. Narendra and K. Parthasarathy, "Identification and control of dynamical systems using neural networks," *IEEE Transactions on Neural Networks*, vol. 1, pp.4–27, 1990.

[14] M. Papageorgiou, *Applications of automatic control concepts to traffic flow modeling and control*, Springer-Verlag, 1983.

[15] M. Papageorgiou, J. M. Blosseville, and H. Hadj-Salem, "Macroscopic modelling of traffic flow on the boulevard periherique in paris," *Transportation Research*, vol. B23, pp.29–47, 1989.

[16] H. J. Payne, "Models of freeway traffic and control," *Mathematical Models of Public Systems*, Simulation Council Proceedings, pp.51–61, 1971.

[17] L. A. Pipes, "Car-following models and the fundamental diagram of road traffic," *Transportation Research*, vol. 1, pp.21–29, 1967.

[18] M. Polycarpou and P. Ioannou, "Identification and control of nonlinear systems using neural network models: design and stability analysis," *Technical Report 91-09-01, Dept. Elec. Eng. - Systems, University of Southern California*, 1991.

[19] M. Polycarpou and P. Ioannou, "Neural networks and on-line approximators for discrete-time nonlinear system identification," *preprint*, 1991.

[20] W. W. Recker, R. L. Cheu, S. G. Ritchie and B. Bavarian, "Investigation of a neural network model for freeway incident detection," *Artificial Intelligence and Civil and Structural Engineering*, Civil-Comp Press, pp.267–274, 1991.

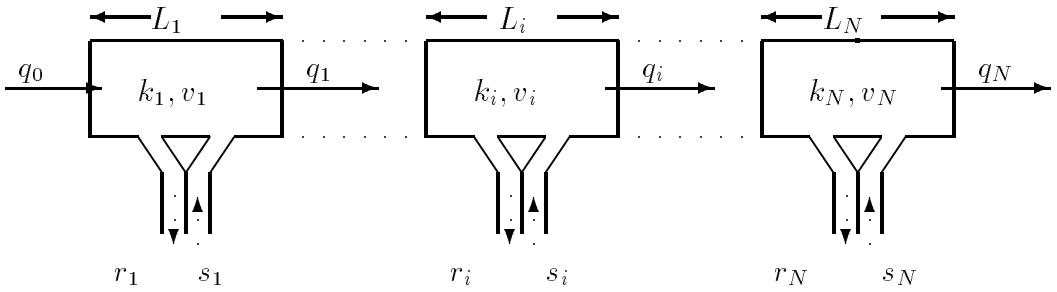

Figure 1: A Highway Lane Subdivided into N Sections

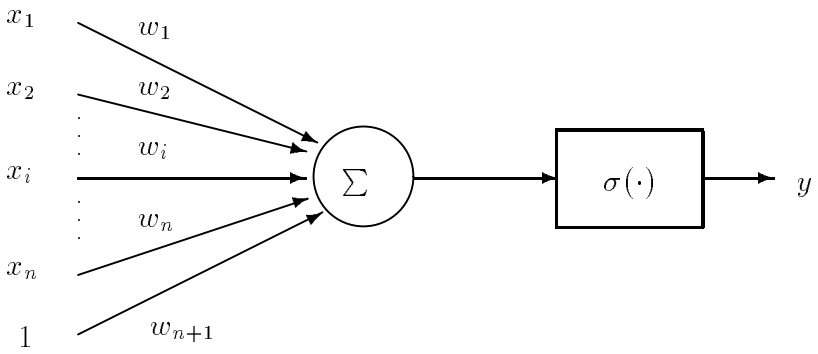

Figure 2: A Processing Element

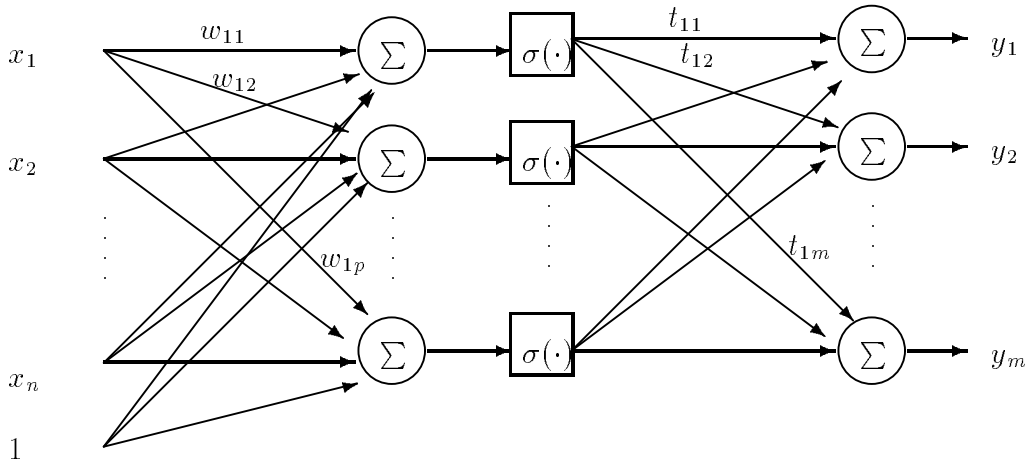

Figure 3: A $1\frac{1}{2}$ Layer Feed-Forward Network

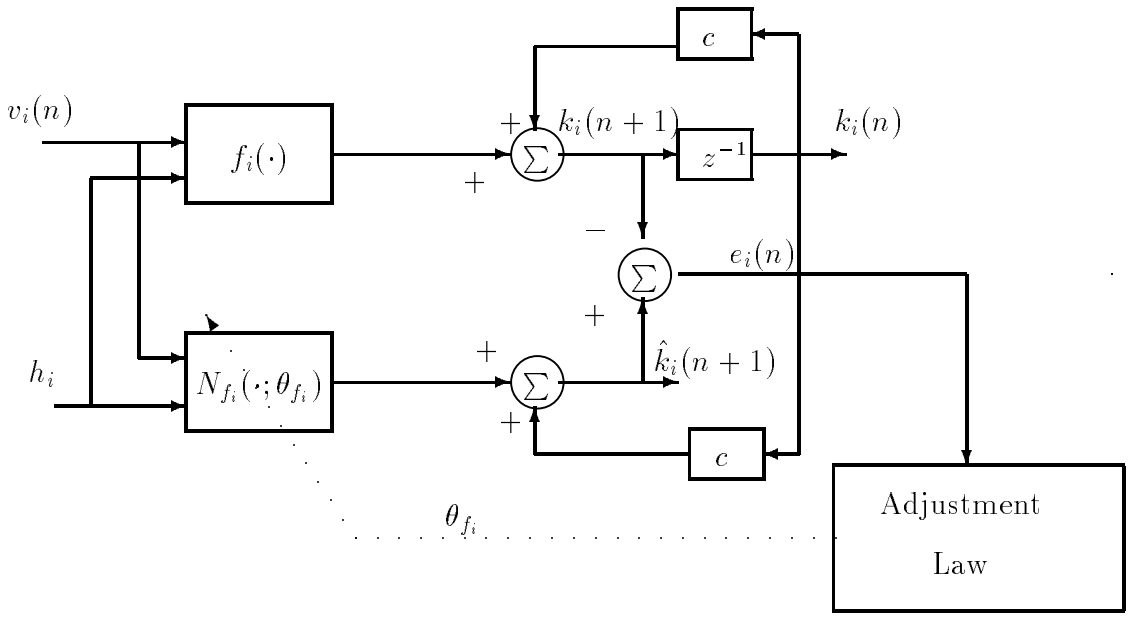

Figure 4: Neural Network Configuration for section i

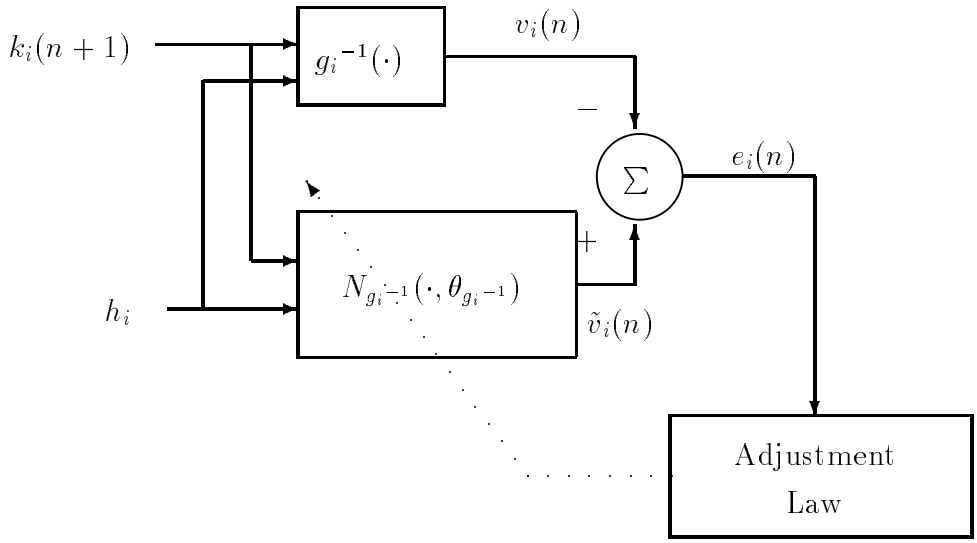

Figure 5: Training scheme for $N_{g_i^{-1}}$

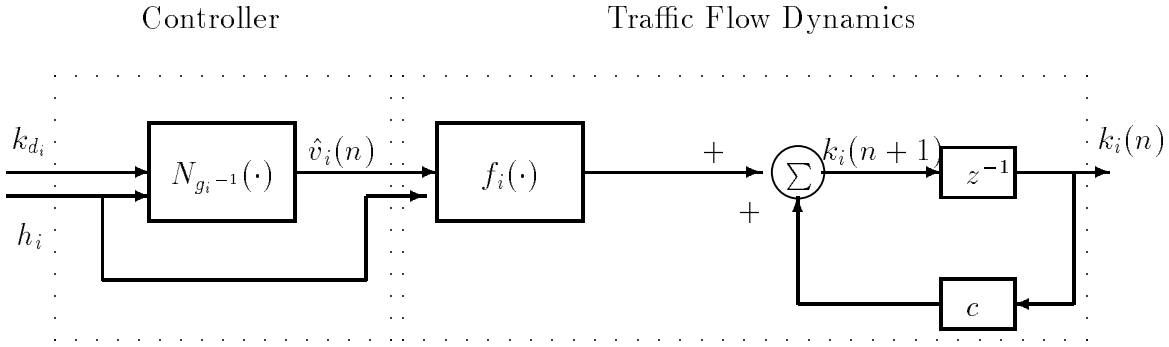

Figure 6: Neural Network Controlled Traffic Flow System

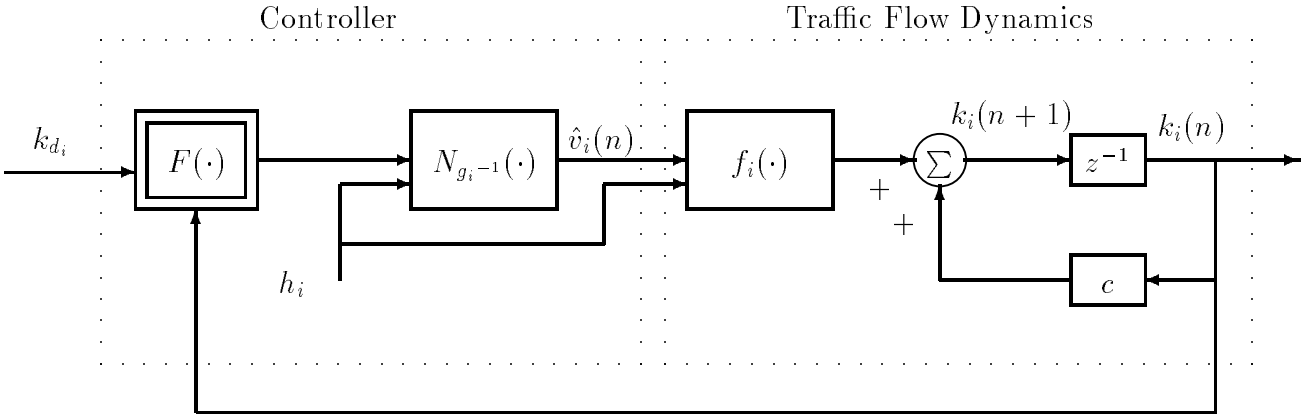

Figure 7: Internal Model Control

Section no. i	1	2	3	4	5	6	7	8	9	10
$k_i(0)$ veh/km	18	18	18	18	18	52	52	52	18	18
$v_i(0)$ km/h	81	81	81	81	81	29	29	29	81	81

Table 1: Initial Conditions of Sectional Density and Speed in A Highway Lane

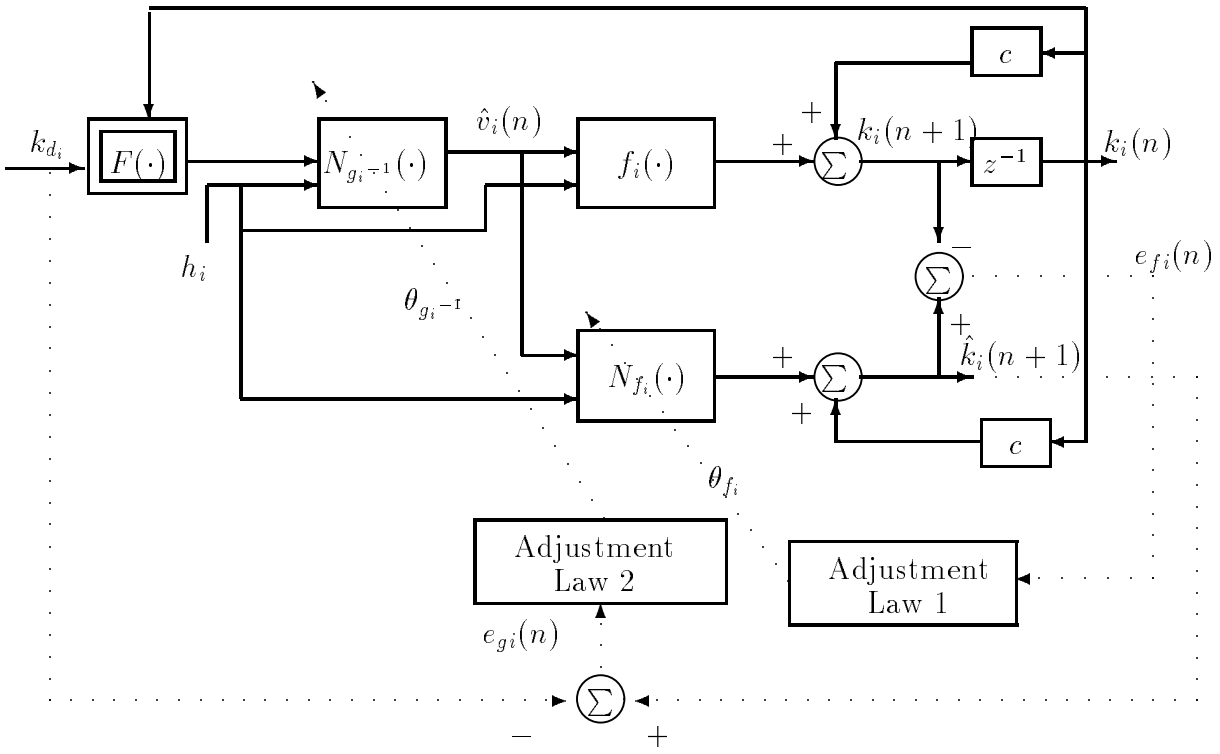

Figure 8: Adaptive Control Using Neural Networks

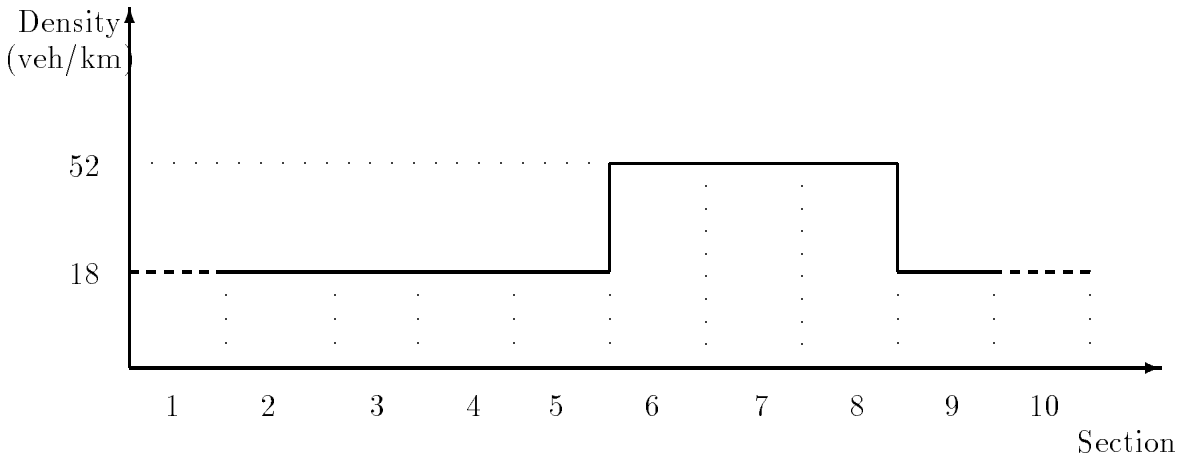

Figure 9: Inhomogeneous Density Profile

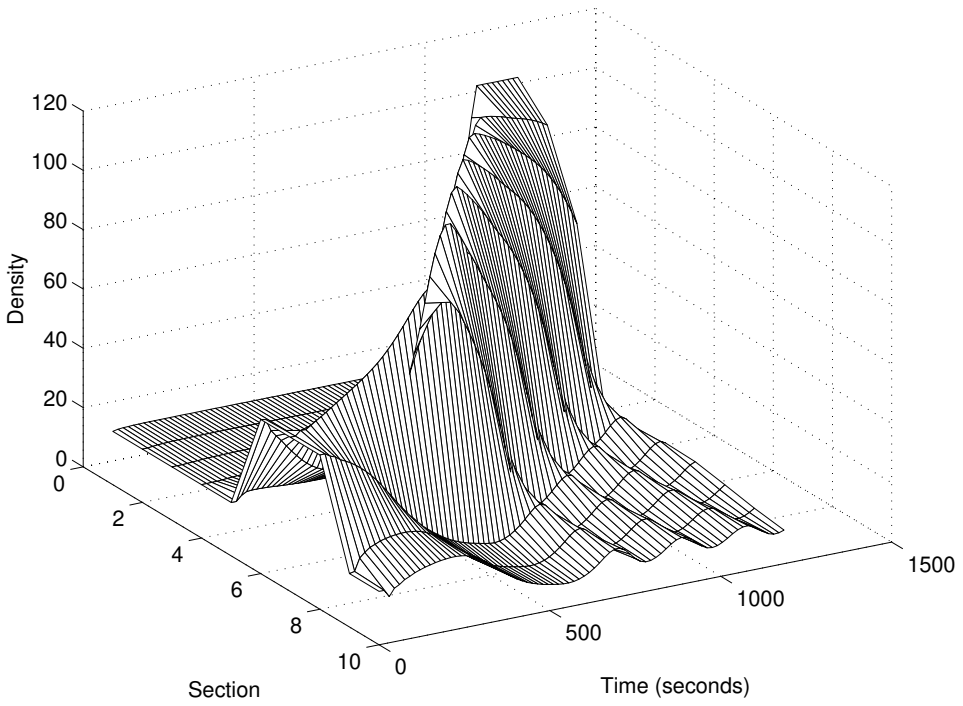

Figure 10: Uncontrolled Density Profile

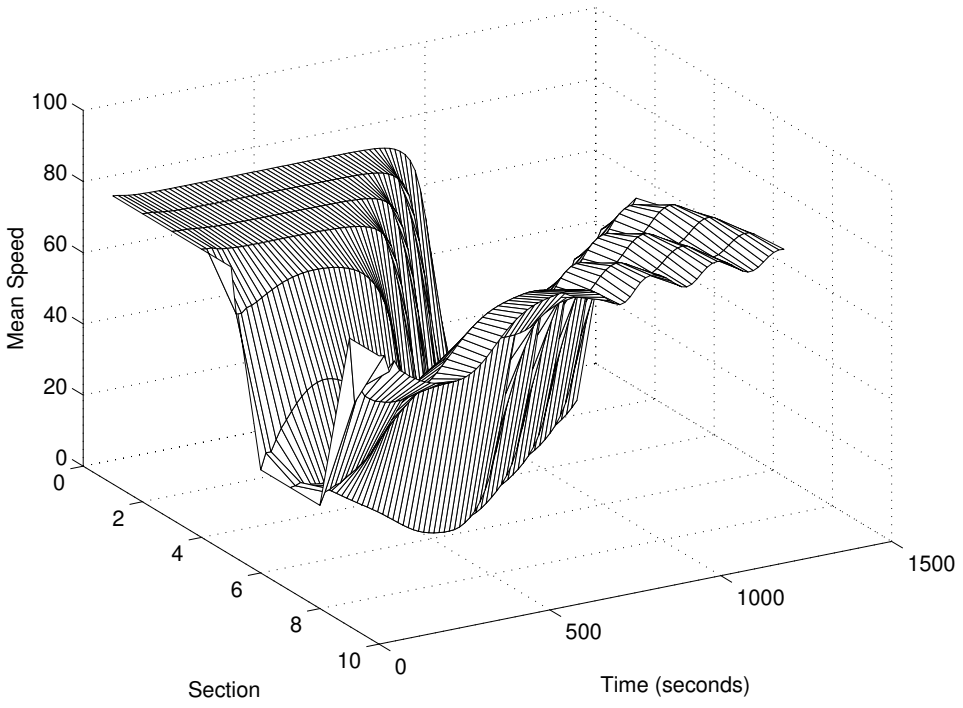

Figure 11: Uncontrolled Mean Speed Profile

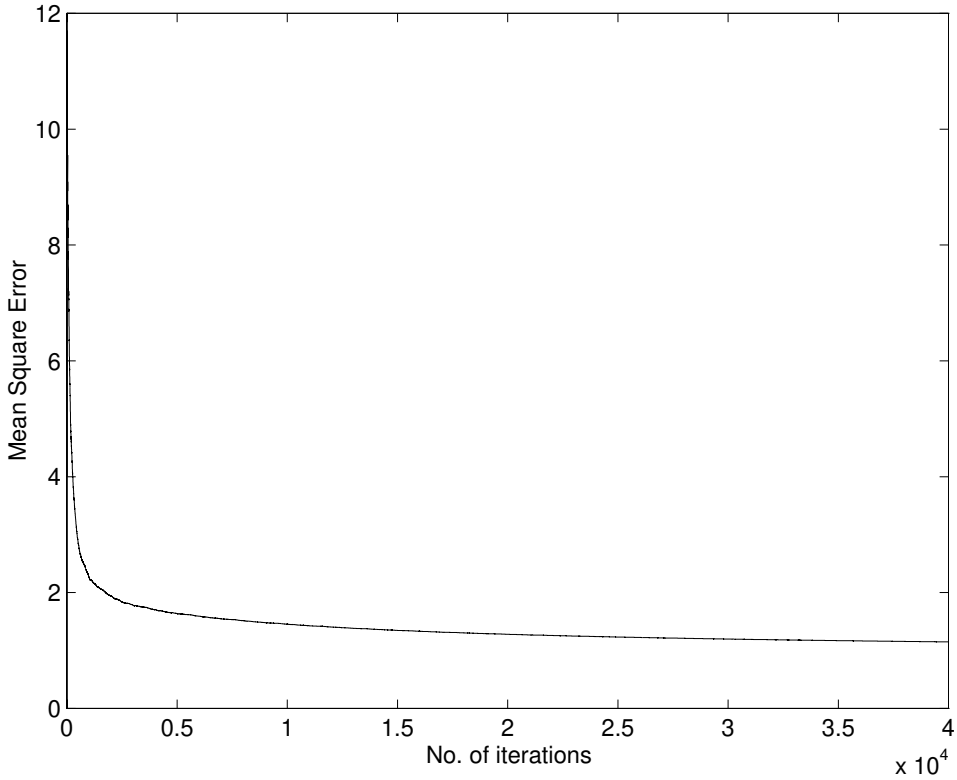

Figure 12: Mean square error during training for N_{f_i}

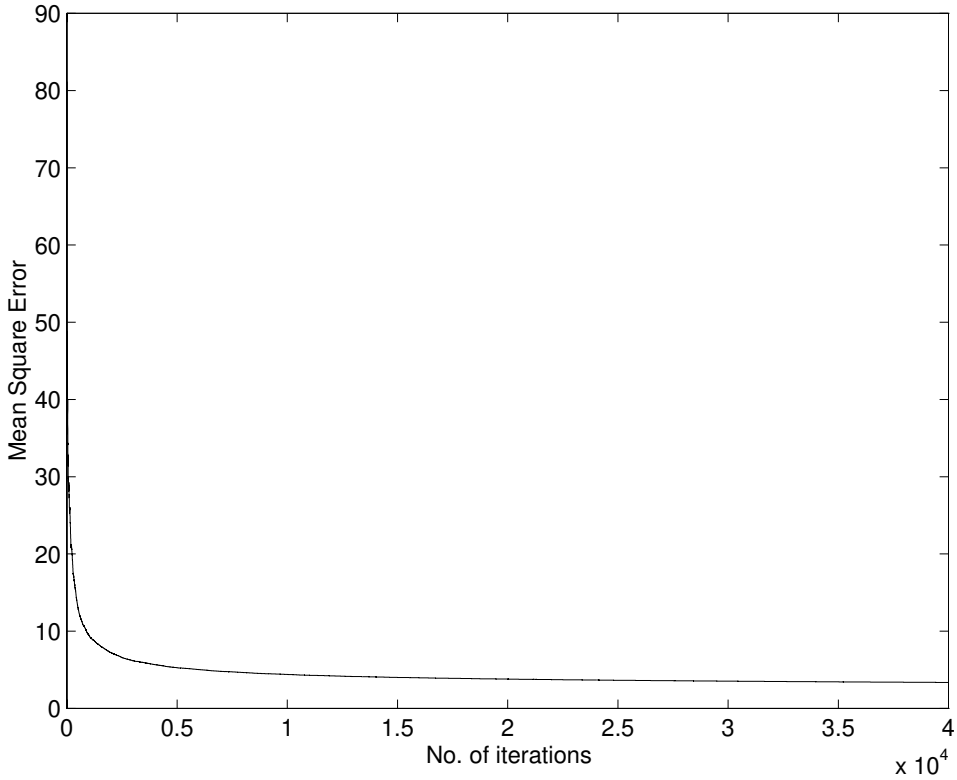

Figure 13: Mean square error during training for N_{g_i-1}

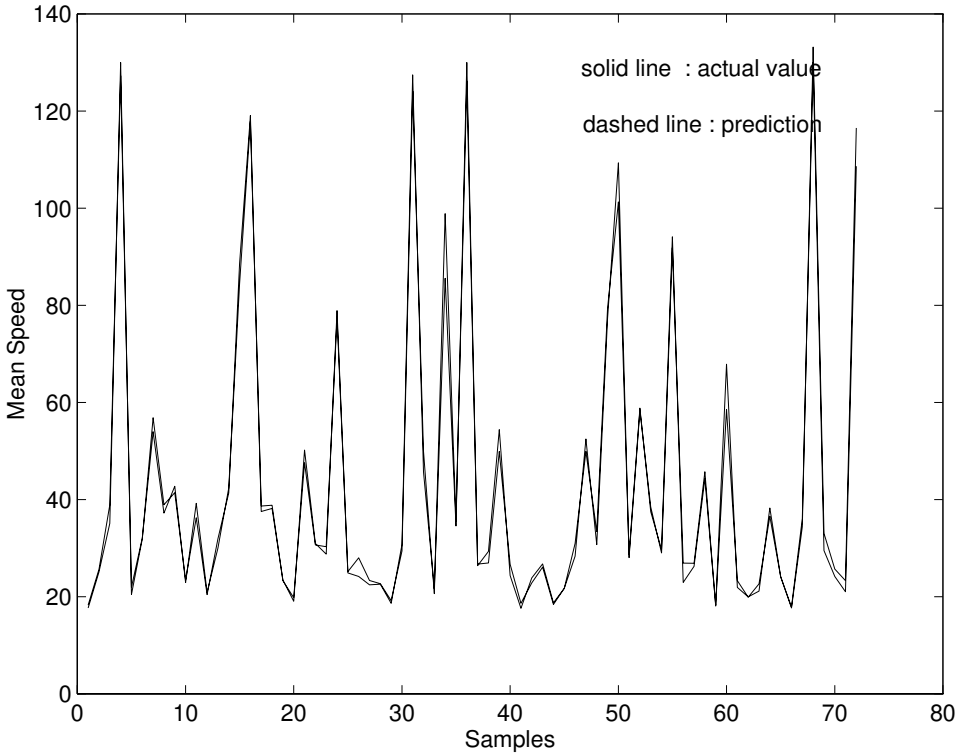

Figure 14: Performance of trained neural network N_{g_i-1}

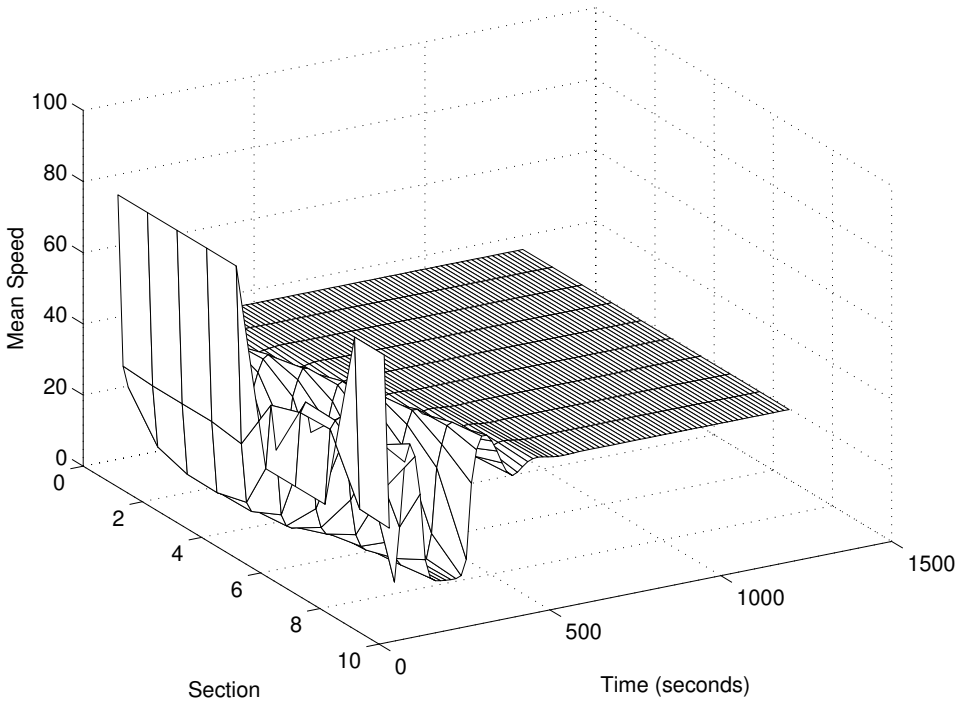

Figure 15: Open-loop Speed Commands : $k_d = 35$

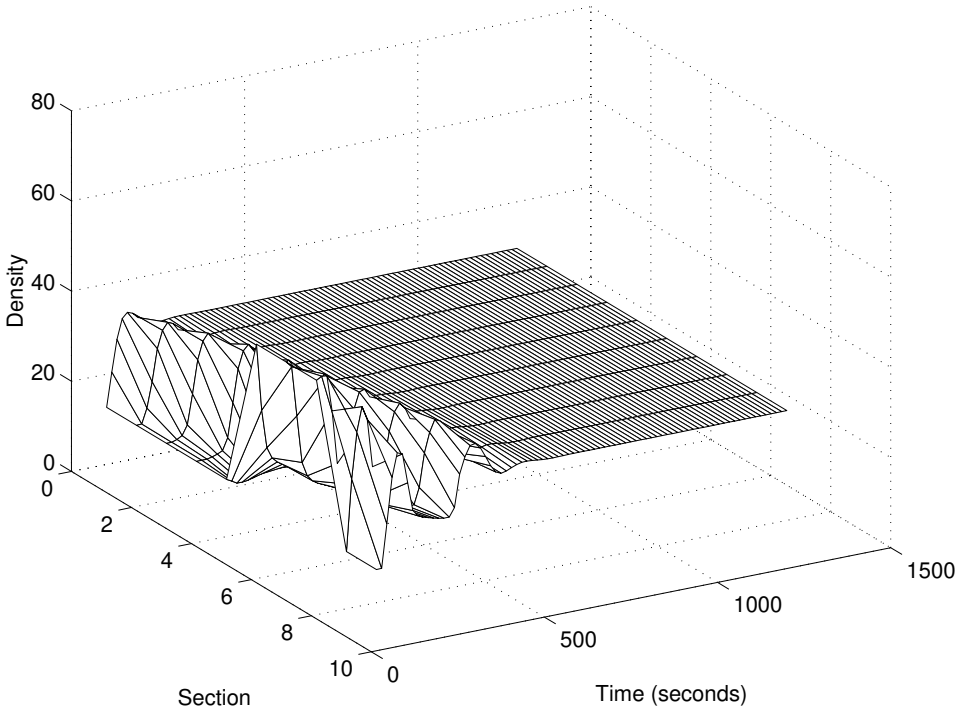

Figure 16: Open-loop Controlled Density Profile: $k_d = 35$

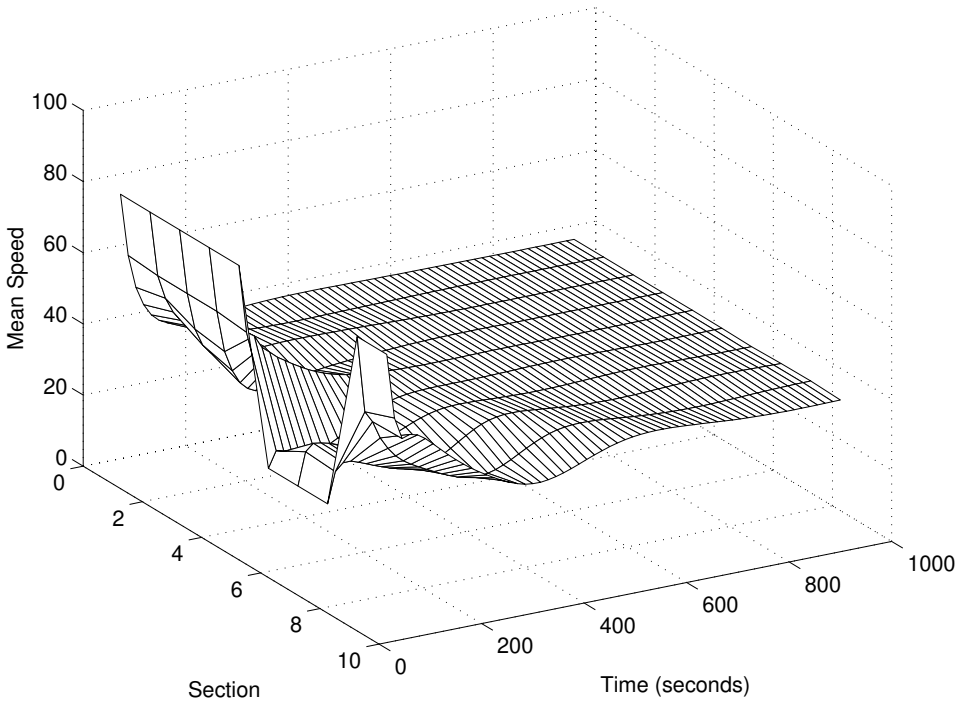

Figure 17: Internal Model Controlled Speed Commands: $k_d = 35$

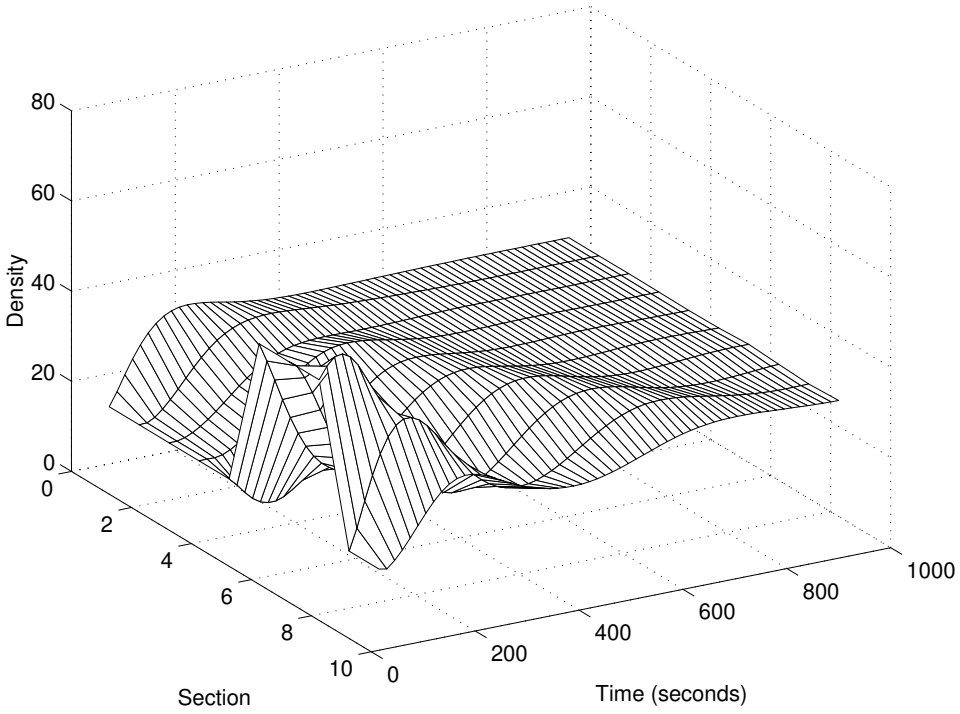

Figure 18: Internal Model Controlled Density Profile: $k_d = 35$

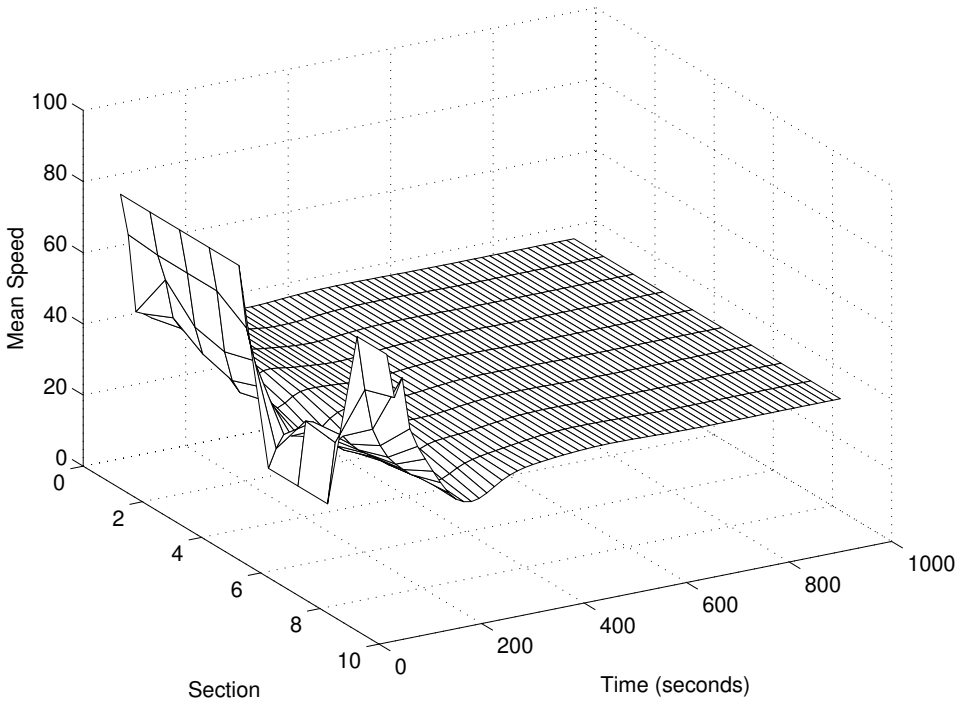

Figure 19: Adaptively Controlled Speed Commands: $k_d = 35$

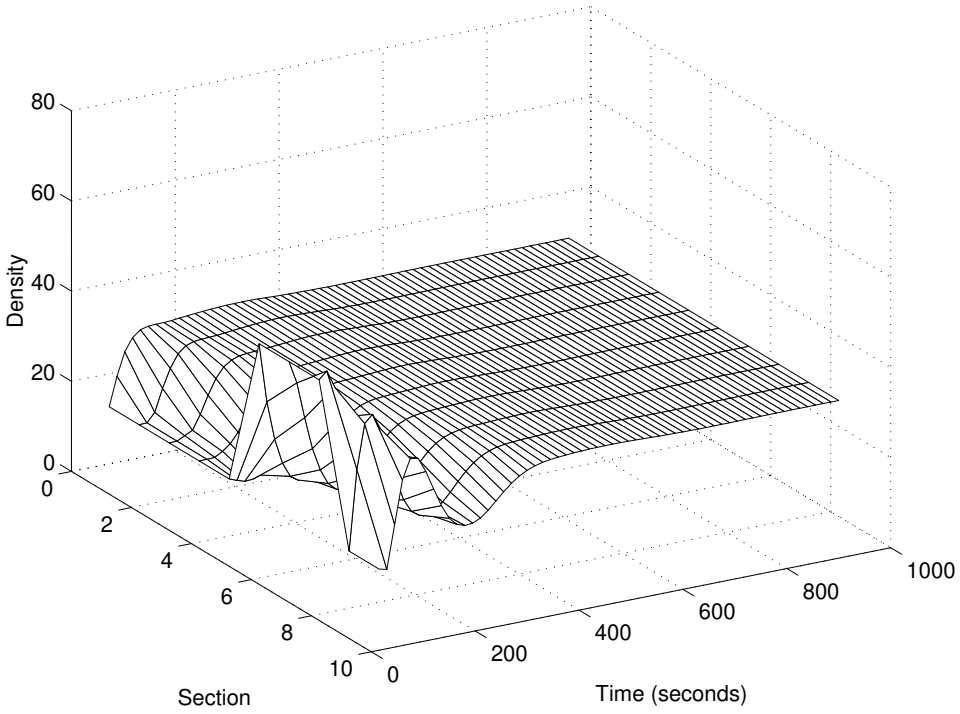

Figure 20: Adaptively Controlled Density Profile: $k_d = 35$

Strategies and Spacing Requirements for Lane Changing and Merging in Automated Highway Systems

Alexander Kanaris, Elias B. Kosmatopoulos, and Petros A. Ioannou

Department of Electrical Engineering — Systems
University of Southern California
Los Angeles, CA 90089
e-mail address: [kosmatop|ioannou]@bode.usc.edu

Abstract

In Automated Highway Systems (AHS) vehicles will be able to follow each other automatically by using their own sensing and control systems, effectively reducing the role of human driver in the operation of the vehicle. Such systems are therefore capable of reducing one source of error, human error, that diminishes the potential capacity of the highways and in the worst case becomes the cause of accidents. Amongst the riskiest maneuvers that the driver has to perform are that of merging into the traffic and that of lane changing. The degree of difficulty and the amount of risk involved in this maneuver depend on the driver performing the maneuver. With AHS, the vehicles in the neat vicinity sense or are notified of the intention of the vehicle to perform the merging or lane changing maneuver. When this intention has been identified, the vehicles that are affected have to increase their relative spacing, in effect to "make space" for the merging vehicle to occupy. How much spacing will be needed, and when and how should the affected vehicles provide that space by adjusting their position and speed is the subject of this study.

In this work, we analyze the problem of collision-free merging and lane changing. We examine various alternative scenaria for merging and lane changing and we present an algorithm for calculating the *Minimum Safety Spacing for Lane Changing (MSSLC)*, that is, we calculate the spacings that the vehicles should have during a merging or lane changing maneuver so that, in the case where one of the vehicles enters in an emergency braking situation, the rest of the vehicles will have enough time and space to stop without any collision taking place. The calculation of the MSSLC's for merging or lane changing maneuver is more complicated than the calculation of the Minimum Safety Spacing for longitudinal vehicle following, since, in the former case we have to take into account the particular lane changing policy of the merging vehicle as well as the effect of combined lateral/longitudinal motion during the lane changing maneuver. The braking profiles of the vehicles involved in an emergency scenario during lane changing maneuver depend on the particular AHS operational concept, i.e., on the degree of communication between the vehicles and between the vehicles and the infrastructure. We consider six different AHS operational concepts; we present the braking profiles of the vehicles for each operational concept and we investigate the effects of the particular operational concept to the MSSLC.

Contents

I. Introduction

Urban highways in many major cities are usually congested and this makes driving difficult and raises the possibility of accidents, especially during merging and lane changing maneuvers. Human drivers engage in information gathering and decision making about driving conditions to determine if and when the conditions are favorable for a lane change. When they decide that the lane change can be successfully completed, they use their signals to notify other vehicles of their intent. Errors might result because the driver failed to collect critical information, or failed to provide a signal, or the other drivers failed to notice and take corrective action, for example to provide additional spacing, when needed. One of the promises of Automated Highway Systems (AHS) is to increase the safety level of driving in highways, and especially the safety of maneuvers like merging and lane changing, by using advanced sensing and control systems to replace the inaccurate human actions. Therefore in AHS vehicles and/or infrastructure should have build in intelligence that allows them, to calculate the spacing requirements for safe merging and lane changing.

Vehicles need to maintain a certain "safety distance" between them, in order to be able to slow down or stop without collision when the leading vehicle performs slow down or stopping maneuver. When another vehicle wants to merge in-between, a spacing equal to the sum of the required safety distance between itself and the merging vehicle and the safety distance required between the merging vehicle and the leading vehicle plus the length of the merging vehicle has to be created. There are several approaches to estimate the required spacing. If the following vehicle has no information about the vehicle class and braking capabilities of the merging vehicle, it has to make worst case assumptions to allow for a large safety margin. Otherwise, extensive communications will be required between the vehicles involved, so that each one can be informed of the vehicle class and braking capabilities of the others. In the latter case, the requirement for a large allowance for a safety margin can be significantly reduced, in effect allowing just enough space for the merging vehicle, so that the spacing between them immediately after the merge is equal to the minimum safety distance calculated for longitudinal vehicle following [3].

The relative speed of the vehicle that intends to merge relative to the speed of the vehicles in the destination lane just prior to the merging is of great importance. The speed can be very different before the merging but it has to be matched after the merge. The speed before the merge is likely not to be the same because the merging vehicle might be accelerating from a ramp or it might be constrained by the speed of the traffic flow in the lane it occupies before merging into the new lane. This imposes additional constraints about the timing of the maneuver and mostly in the amount of additional safety distance that will be required.

In this work, we analyze the problem of collision-free merging and lane changing. We examine various alternative scenaria for merging and lane changing and we present an algorithm for calculating the *Minimum Safety Spacing for Lane Changing (MSSLC)*, that is, we calculate the spacings that the vehicles should have

during a merging or lane changing maneuver so that, in the case where one of the vehicles enters in an emergency braking situation, the rest of the vehicles will have enough time and space to stop without any collision taking place. The calculation of the MSSLC's for the merging or lane changing maneuver is more complicated from the calculation of the Minimum Safety Spacings of the pure longitudinal case, since, in the former case we have to take into account the particular lane changing policy of the merging vehicle as well as the effect of combined lateral/longitudinal motion during the lane changing maneuver. The braking profiles of the vehicles involved in an emergency scenario during lane changing maneuver depend on the particular AHS operational concept, i.e., on the degree of communication between the vehicles and between the vehicles and the infrastructure. We consider six different AHS operational concepts; we present the braking profiles of the vehicles for each operational concept and we investigate the effects of the particular operational concept to the MSSLC.

Due to the similarities between the lane changing and the merging problem, in this work we will consider and analyze only the lane changing problem. The results of this work can be easily extended/modified for the case of merging. Similar studies on the evaluation of safety spacing was performed in [1] for the case of no deceleration or emergencies. As a result the work in [1] leads to the calculation of safety spacing for lane changing under constant speed vehicle movement. In our case, we calculate the intervehicle spacing requirements under possible emergency stopping situations during lane changing.

II. The Lane-Changing Strategies

Consider the five vehicles shown in Figure 1 that will be directly affected when one of them is performing a lane change maneuver; the symbols ℓ_1, f_1, ℓ_2, m and f_2 stand for the leading vehicle in the destination lane, following vehicle in the destination lane, the leading vehicle in the originating lane, the vehicle which must perform the lane-changing (which will be called thereafter as the merging vehicle) and the following vehicle in the originating lane, respectively. Each vehicle has length L_i, $i = \ell_1, f_1, \ell_2, m, f_2$. By assuming a two-dimensional coordinate system as shown in Figure 1, the vehicle's motion can be completely described by the two-dimensional vectors $x^{(i)}, v^{(i)}$, and $a^{(i)}$, $i = \ell_1, f_1, \ell_2, m, f_2$ of position, velocity, and acceleration, respectively. The position of each vehicle is measured with respect to the center of the front end of the vehicle, while the velocity and acceleration are measured with respect to the center of gravity of the vehicle. The first entry of the vectors $x^{(i)}, v^{(i)}, a^{(i)}$ denotes the longitudinal position, velocity, and acceleration, respectively, while the second entry stands for the lateral position, velocity, and acceleration, respectively. Finally, $c^{(i)}$ denotes the distance in the longitudinal direction between the center of the front end and the center of gravity of of the i-th vehicle.

Let d_{ij} denote the intervehicle distance in the longitudinal direction between the vehicles i and j, i.e.,

$$d_{ij} := x_1^{(i)} - x_1^{(j)} - L_i$$

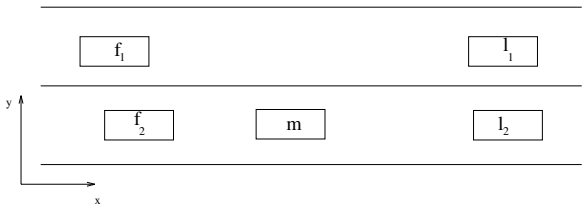

Figure 1: Vehicle about to make a lane change.

Obviously, during a lane changing operation, we are concerned about the longitudinal distances $d_{\ell_1 m}, d_{\ell_2 m}, d_{m f_1}$, $d_{m f_2}$. If one of the above distances measured in the same lane (which will be called thereafter intervehicle spacing) becomes nonpositive then a collision will occur. Moreover, following the work of [3] a lane-changing scenario must be such that it guarantees that no collision occurs if one of the vehicles enters in an emergency braking situation at any point in time before, during and after the end of the maneuver. In other words, during the lane-changing maneuver the intervehicle spacings $d_{\ell_1 m}, d_{\ell_2 m}, d_{m f_1}, d_{m f_2}$ must not only be positive but they must also be large enough so that, in the case where any of the five vehicles enters in an emergency braking situation, the other four vehicles will have sufficient time and spacing to stop without any collision taking place.

Suppose now that at the time-instant $t = 0$ the merging vehicle starts performing the lane change maneuver. There are many alternative lane changing policies for the merging vehicle and the best policy depends on many factors such as relative speed between the originating and destination lane, the spacing between the merging vehicle and the leading vehicle ℓ_2, etc. Despite the differences of the alternative lane changing policies they all can be described as follows: The merging vehicle starts adjusting its longitudinal velocity (by decelerating or accelerating) to make the spacing $d_{\ell_2 m}$ large enough; then it starts adjusting its longitudinal velocity (again by decelerating or accelerating) in order to make its longitudinal velocity equal to the velocity of the destination lane. Let us suppose that the time needed for the merging vehicle to adjust its longitudinal position and velocity is equal to t_{long}. Regarding now the lateral motion of the merging vehicle, at a certain time-instant $t_{lat} \geq 0$ the merging vehicle starts developing a lateral acceleration in order to enter the destination lane. The lateral adjustment of the merging vehicle's motion may start at the same time that the merging vehicle starts adjusting its longitudinal motion (in this case $t_{lat} = 0$), it may start when the merging vehicle has just completed the adjustment of its longitudinal motion (in this case $t_{lat} = t_{long}$), or, it may start any time after the merging vehicle have initiated adjustment of its longitudinal motion (in this case $0 < t_{lat} < t_{long}$). The time-instants t_{long}, t_{lat} as well as the profiles of the longitudinal and lateral accelerations specify the particular lane changing policy. In the next two subsections, we describe the possible profiles of the longitudinal and lateral accelerations of the merging vehicle.

A. The Longitudinal Acceleration Model for the Merging Vehicle

The profile of the longitudinal acceleration of the merging vehicle mainly depends on the relative velocity between the originating and the destination lane. When the destination lane moves faster than the originating one, then the merging vehicle must first decelerate in order to make its spacing with the leading vehicle ℓ_2 large enough for the lane changing maneuver, and then it must accelerate in order to adjust its velocity with the velocity of the destination lane. On the other hand, in the case where the destination lane moves slower than the originating one, then the merging vehicle must first decelerate in order to make its spacing with the leading vehicle ℓ_2 large enough for the lane changing maneuver, and then it may continue decelerating till its velocity becomes equal to the one of the destination lane.

Let V_d and V_o denote the velocity of the destination and originating lane, respectively, and let us examine the acceleration profiles of the merging vehicle in the case where $V_d > V_o$ (i.e., in the case where the destination lane moves faster than the originating one) and $V_d \leq V_o$ (i.e., in the case where the destination lane moves slower than the originating one).

- *The case where* $V_d > V_o$. In this case, the merging vehicle initially decelerates in order to create enough spacing in the originating lane for a safe and collision-free lane changing maneuver. As soon as a sufficient spacing has been created it starts accelerating in order to match its velocity with the velocity V_d of the destination lane. In this work, we will consider a simple model for the longitudinal acceleration profile of the merging vehicle. In particular, we will assume that the merging vehicle's acceleration initially decreases linearly with respect to time until it reaches a limit $-a_{comf}$, where a_{comf} is appropriately chosen to maintain safety and comfort of the passengers in the vehicle. Then, the acceleration remains constant and equal to $-a_{comf}$ until a sufficient spacing has been created in the originating lane and then it switches from decelerating to accelerating. In particular the acceleration starts increasing linearly until it reaches the positive acceleration limit a_{comf}. The acceleration remains constant and equal to a_{comf} for a certain time-interval and then it linearly decelerates to zero in such a way that the merging vehicle's velocity is equal to V_d at the time-instant t_{long}, i.e., at the time-instant that the merging vehicle's acceleration becomes zero.

  Using the above simple model for the longitudinal acceleration profile of the merging vehicle, we can see that the longitudinal acceleration profile, in the case where the destination lane moves faster than the originating one, is the one shown in Figure 2. The constant t_{ch} denotes the time-instant at which the merging vehicle switches from decelerating to accelerating (i.e., t_{ch} denotes the time-instant at which the longitudinal acceleration of the merging vehicle is zero and the vehicle starts accelerating) while the time-constant t_{long} is such that the longitudinal velocity of the merging vehicle equals to the velocity of the destination lane V_d.

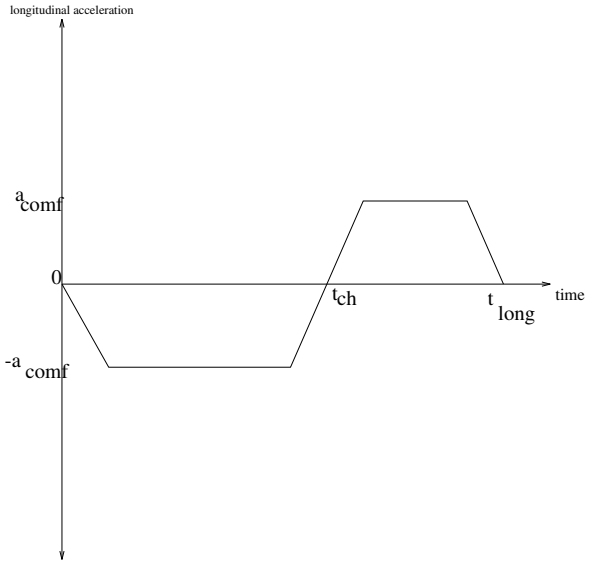

Figure 2: Longitudinal acceleration profile in the case where the destination lane moves faster than the originating one.

- *The case where* $V_d \leq V_o$. In this case, the merging vehicle decelerates in order to both create enough spacing in the originating lane for a safe and collision-free lane changing maneuver and match its velocity with the velocity of V_d of the destination lane. Similarly to the previous case, we will consider a very simple model for the longitudinal acceleration profile of the merging vehicle. In particular, we will consider that the merging vehicle's acceleration initially decreases linearly with respect to time until it reaches a limit $-a_{comf}$, where a_{comf} is appropriately chosen to maintain safety and comfort of the passengers in the vehicle. Then, the acceleration remains constant and equal to $-a_{comf}$ until both a sufficient spacing has been created in the originating lane and the merging vehicle's velocity is very close to V_d. When both the spacing in the originating lane guarantees safe and collision-free lane changing maneuver and the velocity of the merging vehicle is very close to V_d, the acceleration is linearly increased to zero, in such a way that the velocity of the merging vehicle at the time-instant t_{long} (i.e., at the time-instant at which the merging vehicle's acceleration becomes zero) is equal to V_d. The longitudinal acceleration profile, in the case where the destination lane moves slower than the originating one, is shown in Figure 3.

Note that the acceleration profile for the case where $V_d > V_o$ is a general one since we can get the acceleration profile for the case where $V_d \leq V_o$ by setting $t_{ch} = t_{long}$.

Several remarks are in order:

- In the above analysis we made the assumption that the velocities of the leading and following vehicles in the two lanes remain constant and, moreover, the following vehicles have the sampe velocity with that of the corresponding leading vehicle in the same lane. Such an assumption is made for simplicity and in many realistic situations does nto hold. Our results can be easily extended/modified to the case where

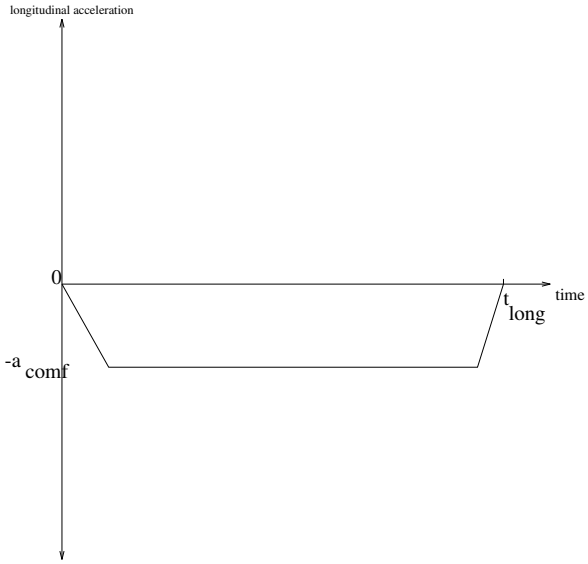

Figure 3: Longitudinal acceleration profile in the case where the destination lane moves slower than the originating one.

the vehicles' velocities do not remain constant, by appropriately modifying the algorithms presented in this paper. In fact, in the case where the velocities of the leading and following vehicles do not remain constant, the acceleration of the merging vehicle can still be assumed that is given by either figure 2 or figure 3, but the constants t_{ch} and t_{long} are chosen based on on-line information about the vehicles' velocities.

- In figures 2 and 3 the merging vehicle is shown to linearly accelerate or decelerate until it reaches a constant acceleration. The slope of such a linear acceleration/deceleration depends on the acceleration characteristics of the vehicle as well as on safety and comfort requirements.

- The results of this paper still hold if we assume a velocity profile for the merging vehicle instead of an acceleration profile. The simplest velocity profile could be the one at which the velocity of the merging vehicle linearly increases until the time-instant t_{ch} and then linearly increases until it becomes equal to V_d at the time-instant t_{long}.

- In the the above analysis we assumed that the following vehicles retain their velocity while the merging vehicle's velocity follows a time-varying trajectory in order to create enough spacing for merging and adjust its velocity. A similar trajectory like the one of the merging vehicle can be assumed for the following vehicles as well, in which case, the following vehicles adjust their velocities and spacings for the lane changing maneuver.

B. The Lateral Acceleration Model for the Merging Vehicle

For the purpose of our analysis, we will use a somewhat simplified model of the lane change maneuver trajectory which assumes a sinusoidal pattern of lateral acceleration. As a first order approximation, the

acceleration of a vehicle during normal lane change maneuvers can be modeled as a sine function of time [2, 5]. The variable parameters of this model are time and distance. The model is symmetric with respect to the direction of lane change, therefore the direction of the change is not a factor. Merging, exiting and weaving have all similar motions in terms of kinematic equations and the same model can be applied for all these cases. According to this model, the lateral acceleration is given by

$$a_{lat} = \begin{cases} \frac{2\pi d_I}{t_{LC}^2} \sin\left(\frac{2\pi}{t_{LC}}(t - t_{lat})\right) & \text{if } t \in [t_{lat}, t_{LC} + t_{lat}] \\ 0 & \text{otherwise} \end{cases} \tag{2.1}$$

where

- a_{lat} is the instantaneous lateral acceleration,
- t_{LC} is the total time to complete the lane change,
- t is the elapsed time,
- d_I is the lateral Intended Lane Change Distance.

Therefore, the lateral peak acceleration A is

$$A = \frac{2\pi d_I}{t_{LC}^2} \tag{2.2}$$

and the lane change frequency is

$$\omega = \frac{2\pi}{t_{LC}}$$

Given the lateral acceleration, the lateral velocity and the lateral distance traveled during a lane change can be derived by successive integration. The assumed sinusoidal acceleration pattern seems to be appropriate for automated lane changing in order to guarantee the comfort of the passengers of the vehicle. This is obvious from the fact that the corresponding jerk function (i.e., the time-derivative of the lateral acceleration) whose value affects passenger comfort does not have any pronounced peaks.

Empirical data collected by photographing several hundreds of lane changes on multi-lane highways [7] has been used to determine the distribution of lateral placement, lane change distance and total lane change time on the lateral acceleration model given by (2.1). The standard lane width on highways is 12 feet and this is the mean value of the d_I, which actually may vary from 9 feet to 15 feet. Total lane change times may vary widely. Lane changes of up to 16 seconds in duration are not outside the normal range, though most lane changes are significantly faster [2]. While the aerial photography method used in determining total lane change time involves a degree of underestimation due to the model used and the resolution limits available, a lower bound of about 2 seconds total lane change time has been determined [7]. The aggressiveness of the lane change depends primarily on the total time t_{LC} taken and also on the lane change distance.

The peak lateral acceleration A can be determined by substituting the d_I for the final distance and t_{LC} for the total time in the equation for A. Thus a range of lateral accelerations from 0.22 ft/sec^2 to 23.55

ft/sec^2 (or, equivalently, from 0.068 g to 0.73 g) has been found. If we assume that a nominal to slow lane change covers 12 feet in 5 seconds we have a peak acceleration of 3 ft/sec^2. The same distance covered in 4 seconds implies a peak acceleration of 4.7 ft/sec^2, while 3 seconds produce acceleration of 8.38 ft/sec^2 and 2.5 seconds produce acceleration of 12 ft/sec^2. It becomes obvious that very fast lane changes involve very large lateral acceleration, while slow lane changes involve negligible lateral acceleration.

C. Safe and Collision-Free Lane Changing Strategies

Using the above two models for the longitudinal and lateral acceleration profiles of the merging vehicle, one can obtain different merging strategies by appropriately chosing the parameters $t_{long}, t_{lat}, t_{ch}, a_{comf}$ and t_{LC}. In other words, a particular choice for these five parameters determines the merging strategy and, moreover, affects the safety of the lane changing maneuver.

We consider a lane changing to be safe and collision-free if there is sufficient spacing between the vehicles involved so that if any of the vehicles performs emergency braking at any time before, during, and after the lane changing all five vehicles could stop without colliding. In this scenario we did not consider the case where a possible collision could be avoided by using both braking and steering. The use of only braking is considered to be a worst case scenario and could lead to larger spacing requirements for collision-free lane change maneuvers. Moreover, this scenario is simpler since the use of both braking and steering for collision avoidance and the resulting spacing requirements for collision-free maneuvers are far more complex.

Since emergency braking can take place any time during a lane change maneuver, we could have a situation where the merging vehicle is decelerating for emergency stop while has both lateral and longitudinal motion. In this case its braking capabilities are limited due to the so-called friction-cycle. The explanation of the braking dynamics during lane change are presented in the following section.

III. Braking During Lane Changing

When a tire is operated under conditions of simultaneous longitudinal and lateral slip, the respective longitudinal and lateral forces depart markedly from those values derived under independent conditions (i.e., the values derived under only longitudinal or only lateral slip). The application of longitudinal slip generally tends to reduce the lateral force at a given slip angle[1] condition. Application of a slip angle reduces the longitudinal force developed under a given braking condition. This behavior can be seen in Figure 4 (taken from [4]).

The general effect on lateral force when braking is applied is illustrated in the traction field of Figure 5 (taken from [4]). The individual curves represent the lateral force at a given slip angle. As the brake force is applied, the lateral force gradually diminishes due to the additional slip induced in the contact area from

[1] *Slip Angle* is defined as the angle between the tire's direction of heading and its direction of travel.

Figure 4: Longitudinal and lateral forces (F_x, F_y) for different slip angles, as a function of longitudinal slip.

Figure 5: Lateral forces versus longitudinal force at constant lateral slip angles.

the braking demand. This type of diagram that displays the tire's traction field is the basis for the *friction circle* concept [4]. The "circle" in most cases is actually an ellipse. Recognizing that the friction limit for a tire, regardless of direction, will be determined by the coefficient of friction multiplied by the load, it is clear that the friction can be used for lateral force or brake (longitudinal) force or a combination of the two. The direction can be positive or negative and this make little difference. *But in no case can the vector total of the two exceed the friction limit.* The limit is therefore a circle (ellipse) in the plane of the lateral and longitudinal forces. The position of the circle in Figure 5 is the friction circle for the positive quadrant of the traction field. The limit is characterized as a friction circle for tires which have effectively the same limits for longitudinal and lateral forces. Certain specialized tires however, may be optimized for lateral traction or braking traction, in which case the limit is not a circle but an ellipse. By making the simplified assumption that the longitudinal and lateral forces F_x and F_y, respectively, during simultaneous longitudinal and lateral slip depend linearly on the longitudinal and lateral accelerations a_x and a_y, respectively, we have that, according to the above analysis regarding the "limited friction circle", the longitudinal and lateral accelerations must satisfy

$$a_x^2 + a_y^2 \leq F_c \tag{3.1}$$

where F_c is a positive constant. It is worth noticing, that in the case of pure longitudinal motion, the maximum longitudinal acceleration of the vehicle a_{max} is larger than $\sqrt{F_c}$. In other words, formula (3.1) applies only for the case of combined longitudinal/lateral braking and not for the case of pure longitudinal braking (in which case $a_y = 0$). The above inequality simply states that braking during combined longitudinal and lateral motion significantly degrades the braking capabilities of the vehicle, and, moreover, the stopping time of the vehicle depends on the time-history of the lateral accelerations; the larger is the lateral acceleration the more distance it takes for the vehicle to stop in the longitudinal direction.

IV. Emergency Braking during Lane Changing

In this section, we analyze the problem of emergency braking during lane changing. More precisely, we consider the problem of analyzing the behavior of the vehicles involved in a lane change maneuver in the case where one of these vehicles enters in an emergency braking situation. A braking scenario, which describes exactly how the vehicles brake, is usually specified by the deceleration profiles of the vehicles as a function of time. The deceleration profile depends, in general, not only on the road conditions and the braking abilities of the vehicle but also on the particular AHS operational concept and the sensors and communication devices that the vehicle is equipped with together with the associated capabilities [3, 6].

Contrary to the longitudinal case where only two vehicles are involved, in the lane changing case we have three different emergency braking scenaria:

1. The case where the vehicle ℓ_1 enters in an emergency braking situation.

2. The case where the vehicle ℓ_2 enters in an emergency braking situation.

3. The case where the merging vehicle m enters in an emergency braking situation.

Since the merging vehicle m is performing a lane changing when the emergency situation takes place, we may have the case where both the following vehicles f_1 and f_2 must enter in an emergency braking situation as well. This is because the merging vehicle is moving in both longitudinal and lateral directions, and therefore we might have the situation where the merging vehicle is in the originating lane when the emergency braking starts and ends up in the destination lane (or somewhere in-between) due to the lateral motion.

In order to simplify our analysis, we will describe only the case where the vehicle ℓ_1 enters in an emergency braking situation. The analysis for the other cases (vehicle ℓ_2 enters in an emergency braking situation, vehicle m enters in an emergency braking situation) are similar. Similarly, we will examine the deceleration profiles only for the case of the following vehicle f_1; the deceleration profiles for the following vehicle f_2 is similar.

Similar to the longitudinal case [3], the deceleration profiles for the vehicles involved in a lane changing maneuver depend on the particular AHS operational concept the vehicles operate under. However, the problem for the case of the lane change maneuver becomes more complicated because of many reasons such as the degraded braking capabilities of the merging vehicle as explained in the previous section. Let us examine the deceleration profiles for each AHS operational concept.

- *Autonomous Vehicles.* A possible AHS concept is the one where the vehicles operate independently, i.e., autonomously, using their own sensors, without any communication between the vehicles. Each vehicle senses its environment, including lane position, adjacent vehicles and obstacles. The infrastructure may provide basic traveler information services, i.e., road conditions and routing information.

  Since, for this particular AHS operational concept, each vehicle relies on its own sensors to determine the motion intentions of the vehicle ahead, we have to consider two different cases depending on whether the merging vehicle position prevents the sensors of the vehicle f_1 from sensing the position of the vehicle ℓ_1: in the first case, the vehicle f_1 can sense the position and relative velocity of the vehicle ℓ_1 since the merging vehicle is either still in the originating lane or, even if part of the vehicle m is already in the destination lane, its body is not in the operational range of the sensors of the vehicle f_1; in other words, in this case the vehicle ℓ_1 is "visible" by the vehicle f_1. The second case, is the case where the vehicle ℓ_1 is not "visible" by the f_1 one, because the merging vehicle prevents the sensors of the vehicle f_1 from sensing the motion of the vehicle ℓ_1. The situation where the vehicle ℓ_1 is "visible" and not "visible" by the vehicle f_1 is illustrated in Figures 6 and 7.

  Let us first analyze the case where the vehicle ℓ_1 is "visible" by the vehicle f_1. In this case, both the merging and the f_1 vehicles are assumed to behave similarly, in the sense that they both detect the

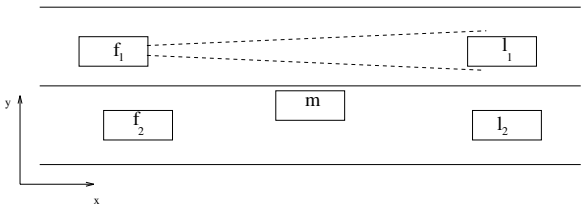

Figure 6: The case where the vehicle ℓ_1 is "visible" by the vehicle f_1.

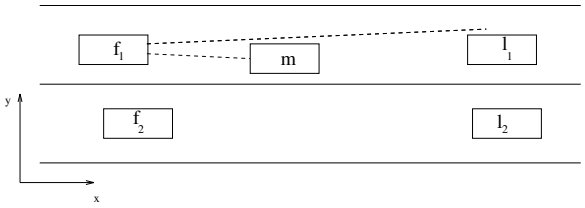

Figure 7: The case where the vehicle ℓ_1 is not "visible" by the vehicle f_1.

emergency braking at the same time. That is, after the vehicle ℓ_1 starts performing emergency braking, the merging and the vehicle f_1, which might have been accelerating initially, start decelerating after a detection and brake actuation delay in an effort to maintain the desired spacing. Since the two vehicles are not aware that the leader is performing emergency braking, they limit their jerks and decelerations in an effort to meet the vehicle control objective and at the same time maintain passenger comfort. The two vehicles detect and initiate emergency braking at possibly different time-instants (since the spacing between the merging vehicle and the vehicle ℓ_1 is less than the spacing between the vehicle f_1 and the vehicle ℓ_1, and thus it is natural to assume that the vehicle f_1 detects the emergency braking after the merging vehicle does). When emergency braking is detected, the passenger comfort is no longer an issue; the vehicles apply the maximum available deceleration in order to minimize the spacing needed for the vehicle to stop. The vehicles apply the maximum available deceleration at minimum time (maximum jerk). Due to the fact that the merging vehicle performs combined longitudinal/lateral braking it is expected (as explained in the previous section) that the maximum available deceleration are less than the ones when the vehicle performs pure longitudinal braking. In our analysis, we used a simplified model in order to incorporate the effect of combined longitudinal/lateral braking in the braking capabilities of the merging vehicle. More precisely, we assumed that if the merging vehicle detects and initiates emergency braking at the time-instant $t_{m_{emerg}}$ and its longitudinal and lateral accelerations at this time instant are $a_1^{(m)}(t_{m_{emerg}})$ and $a_2^{(m)}(t_{m_{emerg}})$, respectively, then both accelerations decrease linearly with respect to time, in such a way that at each time instant $t \geq t_{m_{emerg}}$ they satisfy constraint (3.1). In other words, we have assumed that the longitudinal and lateral accelerations after $t_{m_{emerg}}$ satisfy

$$a_1^{(m)}(t) = \begin{cases} a_1^{(m)}(t_{m_{emerg}}) - J_1[t - t_{m_{emerg}}] & \text{if } |a_1^{(m)}(t)|^2 < F_c \\ \sqrt{F_c} & \text{otherwise} \end{cases} \tag{4.1}$$

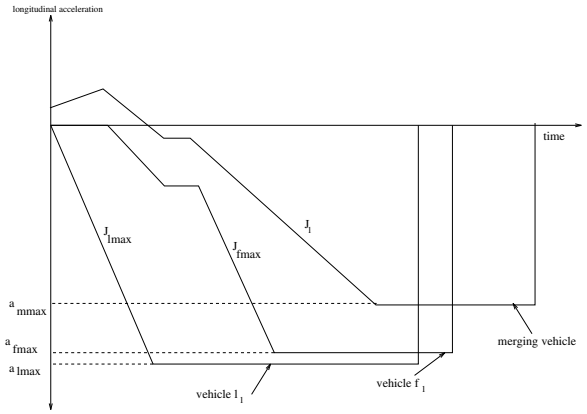

Figure 8: Autonomous Vehicles: The case where the leader is "visible" by the follower.

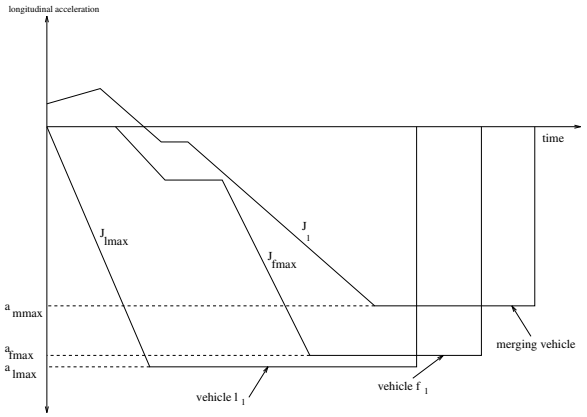

Figure 9: Autonomous Vehicles: The case where the leader is not "visible" by the follower.

$$a_2^{(m)}(t) = \begin{cases} a_2^{(m)}(t_{m_{emerg}}) - J_2[t - t_{m_{emerg}}] & \text{if } v_2^{(m)}(t) > 0 \\ 0 & \text{otherwise} \end{cases} \tag{4.2}$$

where J_1 and J_2 are such that the longitudinal and lateral accelerations $a_1^{(m)}(t)$ and $a_2^{(m)}(t)$ satisfy constraint (3.1) at each $t > t_{m_{emerg}}$. Figure 8 shows the deceleration profiles for the case where the vehicle ℓ_1 is "visible" by the vehicle f_1, where $a_{mmax} = \sqrt{F_c}$.

Let us now analyze the case where the vehicle ℓ_1 is not "visible" by the vehicle f_1. In this case, the deceleration profile for the vehicle f_1 becomes more complicated, while the deceleration profiles of other two vehicles remain the same. The fact, that the sensors of the vehicle f_1 sense only the merging vehicle has the effect the follower to detect the emergency braking situation t_d seconds after the merging vehicle has detected it. The deceleration profiles for the case where the vehicle ℓ_1 is not "visible" by the follower are shown in Figure 9.

- *Free Agents - Infrastructure Supported.* A vehicle is considered a "free agent" if it has the capability to operate autonomously but it is also able to receive communications from other vehicles and from the infrastructure. This implies that the infrastructure may get involved in a supporting role, by issuing warnings and recommendations for desired speed and headways but the infrastructure will not have the

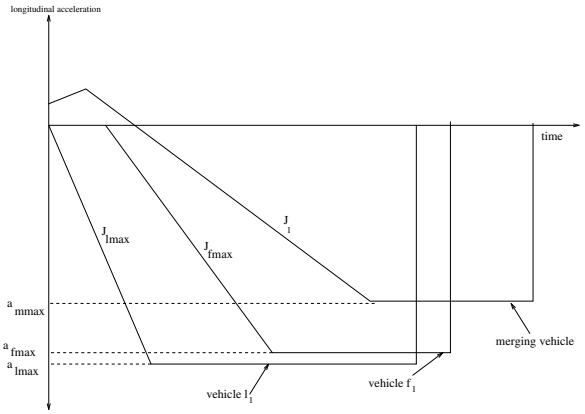

Figure 10: Infrastructure supported free agent vehicles.

authority to issue direct control commands.

Since there exists vehicle to vehicle communication, the leader communicates with the merging vehicle and the merging vehicle, in turn, communicates with the follower, and, therefore, in the case where the leader enters in an emergency braking situation, the merging vehicle and the follower are informed about the emergency braking situation and verify using their own sensors. When the merging and the vehicle f_1 detect that the vehicle ℓ_1 is braking and at the same time receive the information that this is an emergency braking, they bypass the limited jerk/limited braking stage of the autonomous vehicles case. However, as it is shown in Figure 10, there will be a time-delay before the merging vehicle and the follower apply emergency braking. Such a delay is due to the communication delays between the three vehicles and the time needed for the sensors to verify the emergency braking situation. It must expected that the time-delay for the follower to detect and verify emergency braking is larger than the one for the merging vehicle since, similar to the autonomous vehicles case, the vehicle ℓ_1 may be "invisible" from the follower, the follower and the merging vehicle are not at the same lateral position, etc. Finally, the braking capabilities of the merging vehicle will be degraded due to the combined longitudinal/lateral braking. Figure 10 shows the deceleration profiles for the case of infrastructure supported-free agent vehicles. Similar to the autonomous case, the braking capabilities of the merging vehicle will be degraded (see equations (4.1) (4.2)).

- *Free Agents - Infrastructure Managed.* The concept of Free Agents with Infrastructure Management is based on the assumption that the traffic is composed of vehicles acting as free agents while the infrastructure assumes a more active and more complex role in the coordination of the traffic flow and control of vehicles. Each vehicle is able to operate autonomously and uses its sensors to sense its position and environment, including lane position, adjacent vehicles and obstacles. The difference in this centrally managed architecture is that the infrastructure has the ability to send commands to individual vehicles. This is envisioned to be a "request-response" type architecture, in which individual vehicles

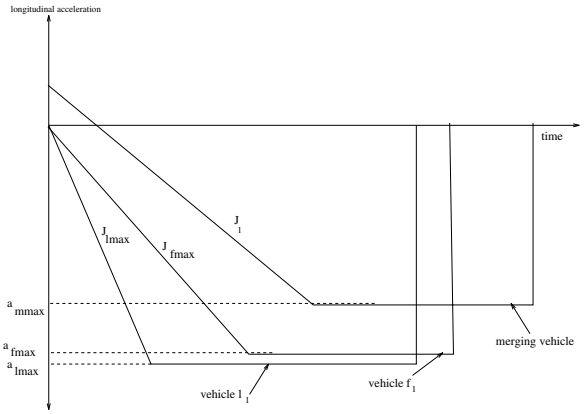

Figure 11: Infrastructure managed free agent vehicles.

ask permission from the infrastructure to perform certain activities and the infrastructure responds by sending commands back to the requesting vehicle and to other vehicles in the neighborhood.

It is expected and assumed that the infrastructure is able to detect emergency situations and whenever it detects such an emergency, the infrastructure will have the responsibility to send an emergency braking command to all the vehicles affected. This concept minimizes the delay in performing emergency braking. The infrastructure may simply issue the command "begin emergency braking now" and all vehicles receiving this will have to apply maximum braking without further delay. This, not only simplifies the task of determining when the vehicle ℓ_1 is performing emergency braking but also minimizes the relative delay in propagating the onset of emergency braking from each vehicle to the vehicle behind, effectively down to zero. In Figure 11, we have plotted the deceleration profiles for the case of free agents with infrastructure management. Notice that the deceleration profiles for the three vehicles will be similar (and moreover the vehicles ℓ_1 and f_1 will stop at the same time-instant in the case where the two vehicles have the same braking capabilities, i.e., in the case where $J_{\ell max} = J_{f max}$ and $a_{\ell max} = a_{f max}$). Similar to the autonomous case, the braking capabilities of the merging vehicle will be degraded (see equations (4.1) (4.2)).

- *Vehicles Platoons without Coordinated Braking.* This concept represents the possibility that the safest and possibly most cost-effective way of achieving maximum capacity is by making platoons of vehicles the basic controlling unit. Platoons are clusters of vehicles with short spacing between individual vehicles in each group and longer spacings between platoons. The characterizing differentiation is the the platoon is to be treated by the infrastructure as an "entity" thereby minimizing some of the need for communicating with and coordinating individual vehicles. The infrastructure does not attempt to control any individual vehicle under normal circumstances, keeping the cost and necessary bandwidth low. The infrastructure is expected to be an intelligent agent which monitors and coordinates the operation of the platoons. Tight coordination is required within the platoon in order to maintain a close

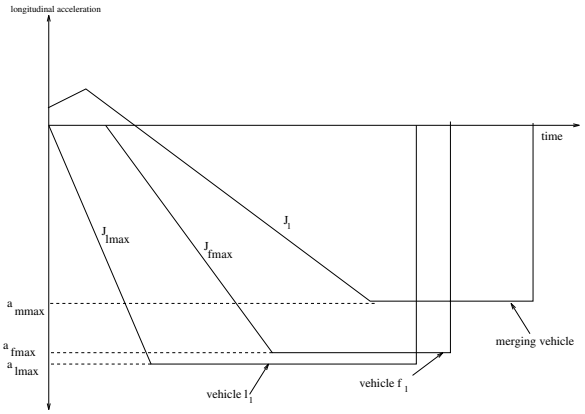

Figure 12: Platoons without coordinated braking.

spacing and this requires that the vehicles must be communicating with each other constantly. The significantly longer inter-platoon spacing is required to guarantee no inter-platoon collisions.

Each vehicle is expected to be equipped with sensors and intelligence to maintain its lane position, sense its immediate surroundings, and perform the functions of merging into and splitting off a platoon. It is not expected to accomplish lane changes, or merging and splitting without the infrastructure's or the platoons entity's help. The main mode of operation of the infrastructure would be of a request-response type. Each platoon's and/or vehicle's request is processed and appropriate commands are sent to the appropriate vehicles/platoons to respond that request. The infrastructure takes a more pro-active role in monitoring traffic flow, broadcasting traffic flow messages, advising lane changes to individual vehicles and platoons in addition to the usual information provider functions.

Once a vehicle has merged into a platoon, the headway maintenance controller must take into account the braking capabilities of the vehicle ahead in order to set an appropriate separation distance that minimizes the possibility of collision. The platoon leader may also provide corrections to the individual intra-platoon headways in order to reduce the possibility of a rear-end collision between two vehicles propagating to the other members of the platoon.

In this concept we assume that no coordination of the braking sequence takes place within a platoon in order to distinguish it from the next one where coordinated braking is employed. Despite the fact that there is no coordinated braking, each vehicle notifies the vehicle behind about its braking capabilities and the magnitude and timing of the braking force used. When the platoon leader detects an emergency, it immediately notifies the vehicle that follows. There will be a delay while the message propagates from each vehicle to the vehicle behind, as well as an actuation delay. The deceleration profiles for the case of platoons without coordinated braking is shown in Figure 12. Notice that the merging vehicle's profile is slightly different than the one of the vehicle f_1, due to the degraded braking capabilities of the merging vehicle.

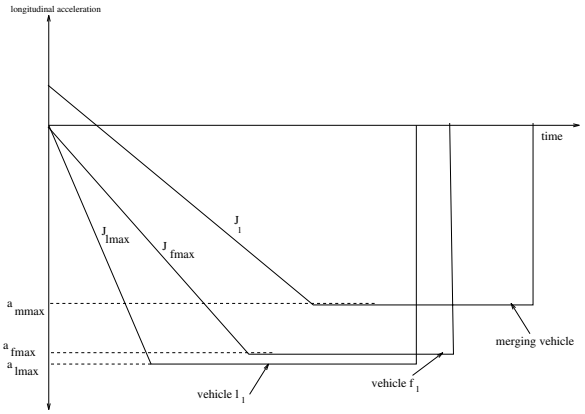

Figure 13: Platoons with coordinated braking and no delay.

- *Vehicles Platoons with Coordinated Braking.* The platooning concept with coordinated braking is based on the concept of maximizing capacity by carefully coordinating the timing and degree of braking among the vehicles participating in a platoon entity. This allows the minimization of spacing between vehicles without compromising safety. During a braking maneuver the platoon leader may dictate a braking sequence to be followed by each vehicle so that the maneuver is performed without any intra-platoon collision. Such a sequence may require the last vehicle to brake first followed by the second last vehicle, etc.

  In platooning with coordinating braking we assume that the platoon leader assumes the primary responsibility of detecting emergencies and notifying each and every vehicle in the platoon. This notification takes place through a network style vehicle to vehicle communication system that minimizes the communication delays. The platoon leader notifies all the vehicles in the platoon about the magnitude of the braking force that is to be applied and also the exact time this is to be applied. This architecture, not only eliminates the need for each vehicle to detect the magnitude of the braking and if the braking should be limited or emergency braking, but also can adjust the onset of emergency braking for an effective 0 seconds relative delay, or even to an artificial negative relative delay. The brake actuation delay can be completely compensated for and it is not affecting the scenario as long as it is approximately the same for each vehicle. Figure 13 shows the deceleration profiles for the case of platooning with coordinated braking and no delays.

V. Safe Spacing for Lane Changing

Consider again the five vehicles involved in a lane changing maneuver as shown in Figure 1. For simplicity, we will assume that during the lane change maneuver the leading and following vehicles ℓ_1, ℓ_2, f_1, f_2 travel with constant velocities unless an emergency braking happens. Suppose that the j-th vehicle (where $j \in \{\ell_1, \ell_2, m\}$) enters in emergency braking situation at the time-instant t_s. Then, we have that the longitudinal and lateral

accelerations of the five vehicles are as follows

$$a_1^{(i)}(t;t_s) = \begin{cases} 0 & \text{if } t < t_s \\ \bar{a}_1^{(i)}(t;j) & \text{otherwise} \end{cases} \qquad i \in \{\ell_1, \ell_2, f_1, f_2\} \tag{5.1}$$

$$a_2^{(i)}(t) = 0, \ \forall t, \qquad i \in \{\ell_1, \ell_2, f_1, f_2\} \tag{5.2}$$

$$a_1^{(m)}(t;t_s) = \begin{cases} \tilde{a}_1^{(m)}(t) & \text{if } t < t_s \\ \bar{a}_1^{(m)}(t;j) & \text{otherwise} \end{cases} \tag{5.3}$$

$$a_2^{(m)}(t;t_s) = \begin{cases} \tilde{a}_2^{(m)}(t) & \text{if } t < t_{m_{emerg}} \\ \bar{a}_2^{(m)}(t;j) & \text{otherwise} \end{cases} \tag{5.4}$$

where $\bar{a}_1^{(i)}(t;j), i \in \{\ell_1, \ell_2, f_1, f_2\}$ is the deceleration profile of the i-th vehicle in the case where the j-th vehicle performs an emergency braking as described in the previous section, $\tilde{a}_1^{(m)}(t)$, $\tilde{a}_2^{(m)}(t)$ denote the longitudinal and lateral, respectively, acceleration models for the merging vehicle when it performs the lane changing maneuver, and $\tilde{a}_1^{(m)}(t;j)$, $\tilde{a}_2^{(m)}(t;j)$ denote the longitudinal and lateral, respectively, deceleration profiles of the merging vehicle in the case where the j-th vehicle performs an emergency braking as described in the previous section. More precisely, the longitudinal acceleration $\tilde{a}_1^{(m)}(t)$ is given in Figures 2 and 3, depending on whether the destination lane moves faster than the originating one, the lateral acceleration $\tilde{a}_2^{(m)}(t)$ is the sinusoidal function given in equation (2.1) and finally the longitudinal and lateral decelerations $\tilde{a}_1^{(m)}(t;j)$, $\tilde{a}_2^{(m)}(t;j)$ are given in equations (4.1) and (4.2), respectively. Finally note that $t_{m_{emerg}}$ is equal to $t_s + t_d$, where t_d denotes the time needed for the merging vehicle to detect and initiate emergency braking.

Based on the above equations, we can calculate the position and velocity of the vehicle i, $i \in \{\ell_1, \ell_2, m, f_1, f_2\}$ as follows

$$x^{(i)}(t) = x^{(i)}(0) + \int_0^t v^{(i)}(\tau)d\tau \tag{5.5}$$

$$v^{(i)}(t) = v^{(i)}(0) + \int_0^t a^{(i)}(\tau)d\tau \tag{5.6}$$

where $x^{(i)}(0), v^{(i)}(0)$ denote the initial position and velocity of the vehicle, respectively.

If the initial intervehicle spacings are large enough, then there would be no collision in the case of emergency braking during the lane change maneuver. For a given lane changing policy and a given AHS operational concept, we would like to calculate the minimum value of the initial intervehicle spacing for which there will be no collision. We refer to this value as the *Minimum Safety Spacing during Lane Changing - (MSSLC)* between those two vehicles. Note that we are interested in the following intervehicle distances $d_{\ell_1 f_1}, d_{\ell_1 m}, d_{\ell_2 f_2}, d_{\ell_2, m}, d_{m f_1}$ and $d_{m f_2}$.

Our approach in calculating the MSSLC is as follows: let us consider the intervehicle spacing d_{kh} where d_{kh} is one of the spacings of interest $d_{\ell_1 f_1}, d_{\ell_1 m}, d_{\ell_2 f_2}, d_{\ell_2, m}, d_{m f_1}$ and $d_{m f_2}$. Suppose now that each of the five vehicles travels in the freeway alone, i.e., assume that the rest four vehicles are absent. Let $T_s^{(h)}(t_s;j)$ be the *stopping time* of the h-th vehicle in the case where the j-th vehicle $j \in \{\ell_1, \ell_2, m\}$ starts an emergency braking

at $t = t_s$, i.e., $T_s^{(h)}(t_s; j)$ is the time at which the h-th vehicle velocity is zero. Note now that a collision occurs if the following holds: there exists a time instant $t_c \in [0, {}_s^{(h)}(t_s; j)]$ such that $d_{kh}(t_c)$ is negative and moreover the lateral positions of the vehicles k and h satisfy $|x_2^{(k)}(t_c) - x_2^{(h)}(t_c)| < L_{lat}^{kh}$; here L_{lat}^{kh} is defined as follows: suppose that the two vehicles k and h are in two adjacent lanes and their longitudinal positions are the same. Then L_{lat}^{kh} denotes the minimum lateral distance of the vehicles k and h such that if the lateral distance between these two vehicles is larger than L_{lat}^{kh} then the two vehicle do not collide. The definition of the constant L_{lat}^{kh} is necessary because we may have the case where the spacing d_{hk} is negative at a given time-instant but a collision does not occur because the two vehicles are in two different lanes (or their lateral distance is large enough) at this time-instant. In order to incorporate the case where the two vehicles have large enough lateral distance we define the variable $\mathcal{I}_{hk}$ as follows: $\mathcal{I}_{hk} = 1$ if $|x_2^{(k)} - x_2^{(h)}| < L_{lat}^{kh}$ and $\mathcal{I}_{hk} = 0$, otherwise. Then, the MSSLC for the spacing d_{kh} is defined as follows

$$D_{min}^{kh} = - \min_{t_s \in [0, t_{LC}], j \in \{\ell_1, \ell_2, m\}} \left\{ \min_{t \in [0, T_s^{(h)}(t_s, j)]} \{ I_{hk}(t) \cdot d_{kh}(t), 0 \} \right\} \tag{5.7}$$

In other words, D_{min}^{kh} is equal to the maximum distance by which the vehicle h would overtake vehicle k, for all possible different emergency braking situations, in the case where the two vehicles travel alone. $D_{min}^{kh} < 0$ implies that a collision occurs, while $D_{min}^{kh} = 0$ implies that the initial spacing between the vehicles k and h is such that there will be no collision in the case where any of the vehicles ℓ_1, ℓ_2, m at any time-instant during the lane change maneuver enters in an emergency braking situation.

We employ a exhaustive search technique in order to calculate the MSSLCs D_{min}^{kh}, i.e., we calculate the intervehicle spacings for all the possible cases of emergency braking situation as it is demonstrated in the following algorithm

Algorithm for the Calculation of MSSLCs

1. **Choose** the sampling time interval Δt.

2. **Specify** the velocities in originating lane V_o and in destination lane V_d, the initial positions of the vehicles, and the intended lane change distance d_I. For each vehicle $j \in \{\ell_1, \ell_2, m, f_1, f_2\}$, specify the maximum available acceleration a_{jmax} and jerk J_{jmax}; specify the friction limit constant F_c for the merging vehicle. Finally, specify the deceleration profiles of the five vehicles based on the analysis of section IV, the constants L_{lat}^{kh} and the time constant t_d such that $t_{m_{emerg}} = t_s + t_d$.

3. **Specify the Merging Strategy**: Choose the parameters $t_{long}, t_{lat}, t_{ch}, t_{LC}$ and a_{comf} that determine the merging strategy.

4. **FOR** all $D_{min}^{kh} \in \{D_{min}^{\ell_1,f_1}, D_{min}^{\ell_1,m}, D_{min}^{\ell_2,f_2}, D_{min}^{\ell_2,m}, D_{min}^{m,f_1}, D_{min}^{m,f_2}\}$ **DO**

   (a) Set $D_{min}^{kh} = 0$.

   (b) **FOR** all $j \in \{\ell_1, \ell_2, m\}$ **DO**

      i. **FOR** all $t_s \in \{0, \Delta t, 2\Delta t, \ldots, t_{LC}\}$ **DO**

         A. Set $t = 0$.

         B. Calculate $a^k(t)$ and $a^h(t)$, based on equations (5.1)-(5.4).

         C. Update $v^{(k)}, v^{(h)}, x^{(k)}, x^{(h)}$ based on equations (5.5), (5.6), i.e., set

$$v^{(i)}(t+\Delta t) = v^{(i)}(t) + \int_t^{t+\Delta t} a^{(i)}(\tau)d\tau,\ i = k, h$$

$$x^{(i)}(t+\Delta t) = x^{(i)}(t) + \int_t^{t+\Delta t} v^{(i)}(\tau)d\tau,\ i = k, h$$

         D. **IF** $D_{min}^{kh} > -I_{hk}(t+\Delta t) \cdot d_{kh}(t+\Delta t)$ **THEN** set

$$D_{min}^{kh} = -I_{hk}(t+\Delta t) \cdot d_{kh}(t+\Delta t)$$

         E. **IF** $v^{(h)}(t+\Delta t) > 0$ **THEN** set $t = t + \Delta t$ and **GOTO STEP B**
         OTHERWISE set $T_s^{(h)}(t_s, j) = t + \Delta t$ and **ENDFOR**

   (c) **ENDFOR**

5. **ENDFOR**

VI. Simulations

We used the algorithm presented in the previous section in order to calculate the Minimum Safety Distances for different conditions during a lane changing maneuver. Only the case of autonomous vehicles was considered; for simplicity all the five vehicles was assumed to have the same characteristics and performance. More precisely, we considered five vehicles with length 5 meters, and maximum deceleration (during braking) and jerk equal to $0.5g$ and 50 m/sec^3, respectively. The constant F_c for the merging vehicle was set equal to 0.25. In the case where one of the leading vehicles enters in an emergency braking situation, we assumed that the merging vehicle needs a time of 0.3 seconds to start decelerating and a time of 1 second to confirm the emergency braking and 0.3 seconds to start performing emergency braking. For the two following vehicles, we assumed the same time-delays in the case where the emergency-braking leading vehicle is "visible" and in the case where it is not visible we assumed that the following vehicle needs 2 seconds to start decelerating, 1 second to confirm the emergency braking and and 0.3 seconds to start performing emergency braking. The constants L_{lat}^{kh} were all set equal to 2 meters.

Regarding now the particular lane changing policy of the merging vehicle we choose the various parameters as follows: In order to simplify the problem we assumed that the time (delay) needed for the merging vehicle to switch from a_{comf} deceleration/acceleration to 0 or a_{comf} acceleration/deceleration was negligible (i.e. this time was set equal to zero in the simulations). Moreover, we set $t_{lat} = t_{ch} = 0$ and tried different values for the a_{comf} in order to cover many possible cases of different lane changing maneuver strategies.

We run three different simulations. In all three simulations we calculated the MSSLC functions for the case where the speed in the destination and originating lane covers the range between 10 and 30 m/sec. In the first simulation we set $a_{comf} = 0.1g$ and the time t_{LC} needed for the lane changing maneuver to be completed was set equal to 5 seconds. In the second simulation, we increased a_{comf} to $0.3g$ and we kept $t_{LC} = 5$ seconds. In the third simulation we set a_{comf} equal to $0.1g$ and we increased t_{LC} to 10 seconds.

Figures 14-17 plot the MSSLC values versus relative speed between the originating and the destination lanes for the three different simulations while Figures 18-21 plot the worst case emergency braking time for the various intervehicle spacings versus the the relative speed $V_d - V_o$ between the two lanes for the three different simulations. By "worst case emergency braking time" for a particular intervehicle spacing between two vehicles and given velocities in the two lanes, we define the time-instant which is such that, if an emergency braking starts at this instant, then the required safety spacing for the particular two vehicles is the maximum. Note that at each figure more than one points (i.e., more than one MSSLC) correspond to each relative speed point; those MSSLC points correspond to different absolute speed values. For example, when the relative speed is -5 the various MSSLC points that correspond to this relative speed are for the cases where $(V_o = 30, V_d = 25)$, $(V_o = 28, V_d = 23)$, $(V_o = 26, V_d = 21)$, etc. The points that correspond to

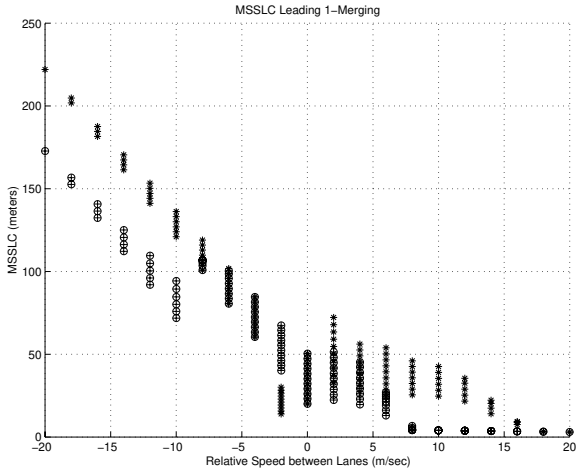

Figure 14: MSSLC for the spacing between the Vehicle ℓ_1 and the Merging Vehicle versus Relative Speed between Lanes ($\circ$: $a_{comf} = 0.1g$ and $t_{LC} = 5$ seconds; $\star$: $a_{comf} = 0.3g$ and $t_{LC} = 5$ seconds; $+$: $a_{comf} = 0.1g$ and $t_{LC} = 10$ seconds).

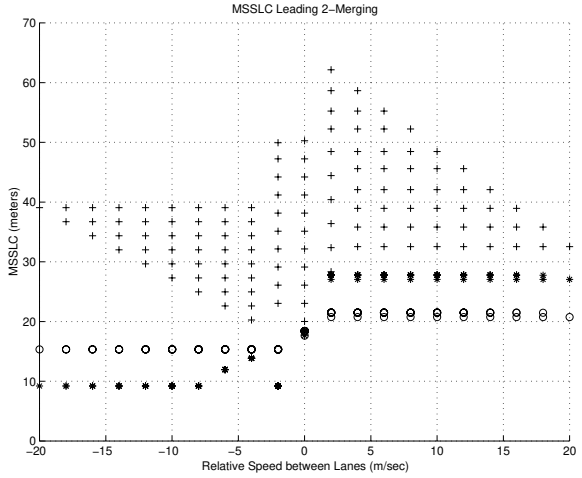

Figure 15: MSSLC for the spacing between the Vehicle ℓ_2 and the Merging Vehicle versus Relative Speed between Lanes ($\circ$: $a_{comf} = 0.1g$ and $t_{LC} = 5$ seconds; $\star$: $a_{comf} = 0.3g$ and $t_{LC} = 5$ seconds; $+$: $a_{comf} = 0.1g$ and $t_{LC} = 10$ seconds).

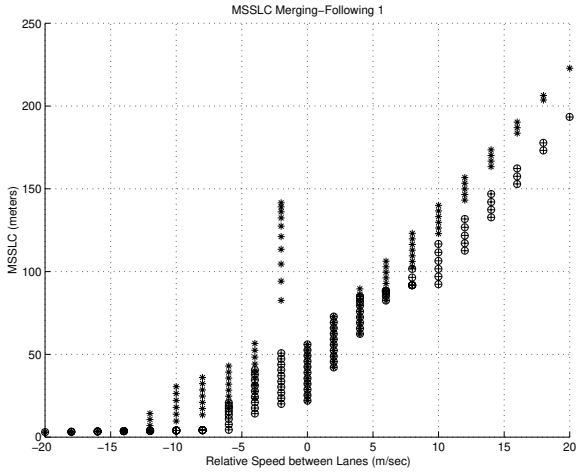

Figure 16: MSSLC for the spacing between the Merging Vehicle and the Vehicle f_1 versus Relative Speed between Lanes ($\circ$: $a_{comf} = 0.1g$ and $t_{LC} = 5$ seconds; $\star$: $a_{comf} = 0.3g$ and $t_{LC} = 5$ seconds; $+$: $a_{comf} = 0.1g$ and $t_{LC} = 10$ seconds).

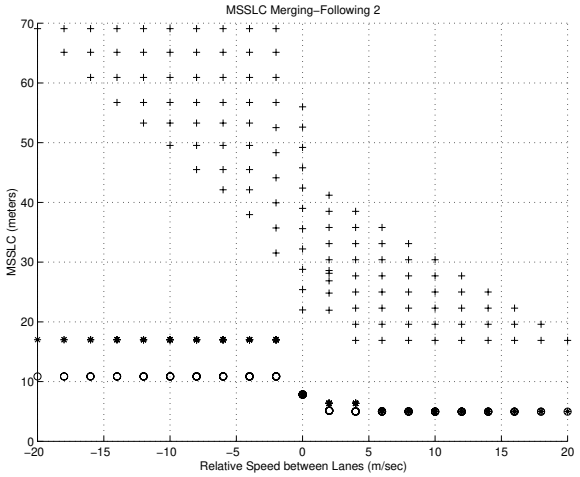

Figure 17: MSSLC for the spacing between the Merging Vehicle and the Vehicle f_2 versus Relative Speed between Lanes ($\circ$: $a_{comf} = 0.1g$ and $t_{LC} = 5$ seconds; $\star$: $a_{comf} = 0.3g$ and $t_{LC} = 5$ seconds; $+$: $a_{comf} = 0.1g$ and $t_{LC} = 10$ seconds).

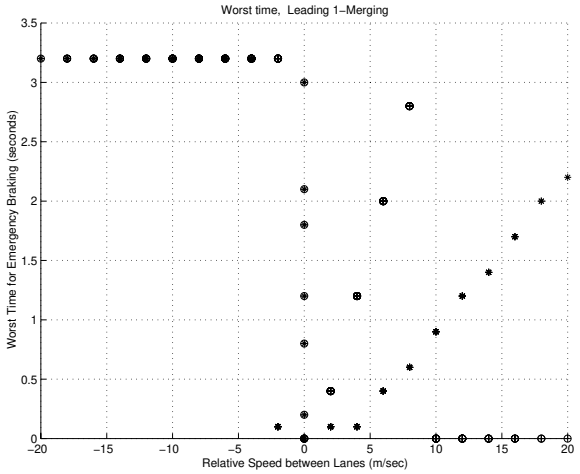

Figure 18: Worst case emergency braking time for the spacing between the Vehicle ℓ_1 and the Merging Vehicle versus Relative Speed between Lanes ($\circ$: $a_{comf} = 0.1g$ and $t_{LC} = 5$ seconds; $\star$: $a_{comf} = 0.3g$ and $t_{LC} = 5$ seconds; $+$: $a_{comf} = 0.1g$ and $t_{LC} = 10$ seconds).

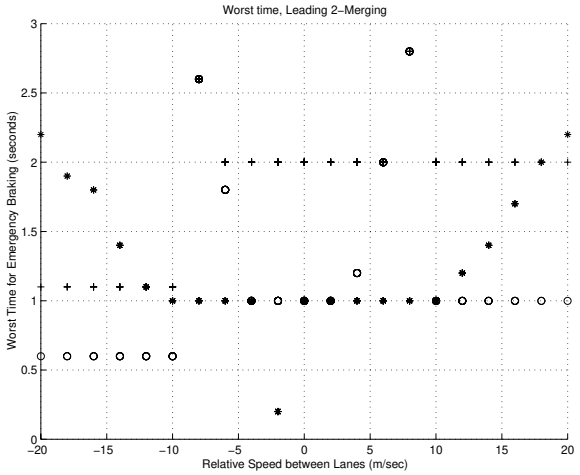

Figure 19: Worst case emergency braking time for the spacing between the Vehicle ℓ_2 and the Merging Vehicle versus Relative Speed between Lanes ($\circ$: $a_{comf} = 0.1g$ and $t_{LC} = 5$ seconds; $\star$: $a_{comf} = 0.3g$ and $t_{LC} = 5$ seconds; $+$: $a_{comf} = 0.1g$ and $t_{LC} = 10$ seconds).

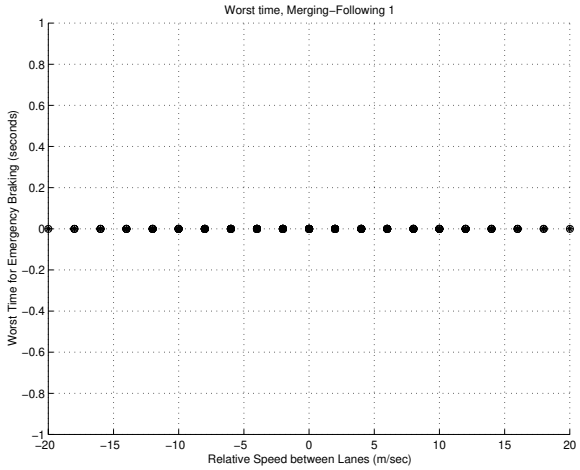

Figure 20: Worst case emergency braking time for the spacing between the Merging Vehicle and the Vehicle f_1 versus Relative Speed between Lanes ($\circ$: $a_{comf} = 0.1g$ and $t_{LC} = 5$ seconds; $\star$: $a_{comf} = 0.3g$ and $t_{LC} = 5$ seconds; $+$: $a_{comf} = 0.1g$ and $t_{LC} = 10$ seconds).

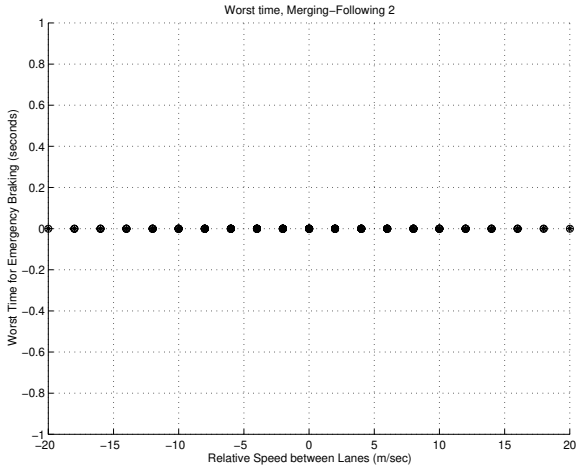

Figure 21: Worst case emergency braking time for the spacing between the Merging Vehicle and the Vehicle f_2 versus Relative Speed between Lanes ($\circ$: $a_{comf} = 0.1g$ and $t_{LC} = 5$ seconds; $\star$: $a_{comf} = 0.3g$ and $t_{LC} = 5$ seconds; $+$: $a_{comf} = 0.1g$ and $t_{LC} = 10$ seconds).

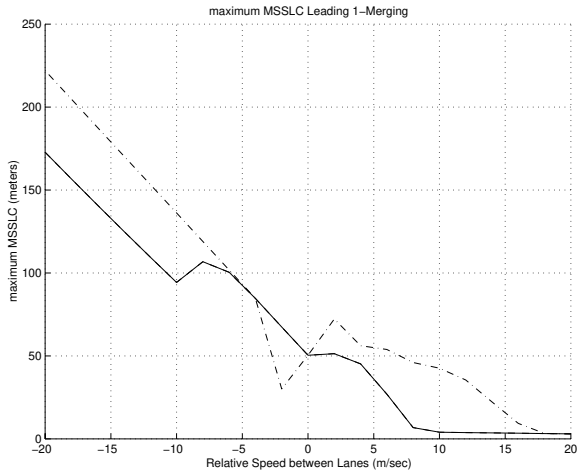

Figure 22: Maximum MSSLC for the spacing between the Vehicle ℓ_1 and the Merging Vehicle versus Relative Speed between Lanes (solid curve: $a_{comf} = 0.1g$ and $t_{LC} = 5$ seconds; dash-dotted curve: $a_{comf} = 0.3g$ and $t_{LC} = 5$ seconds; dashed curve: $a_{comf} = 0.1g$ and $t_{LC} = 10$ seconds).

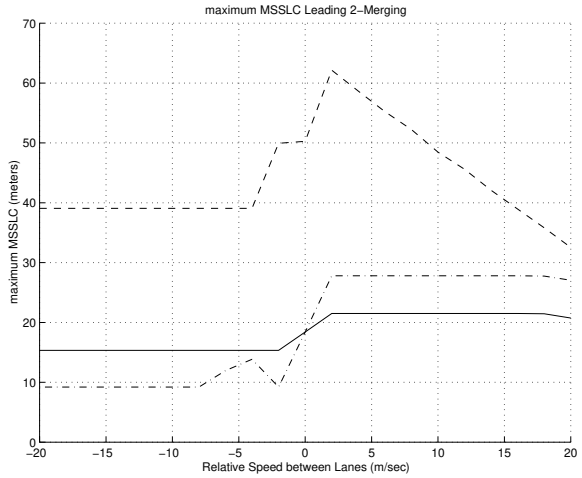

Figure 23: Maximum MSSLC for the spacing between the Vehicle ℓ_2 and the Merging Vehicle versus Relative Speed between Lanes (solid curve: $a_{comf} = 0.1g$ and $t_{LC} = 5$ seconds; dash-dotted curve: $a_{comf} = 0.3g$ and $t_{LC} = 5$ seconds; dashed curve: $a_{comf} = 0.1g$ and $t_{LC} = 10$ seconds).

the highest MSSLCs are the points that correspond to the highest absolute speed values. In Figures 22-25, we plot the Maximum MSSLC's versus relative speed between the two lanes, where by Maximum MSSLC we mean the maximum MSSLC that corresponds to a given relative speed point.

By observing the Figures 14-25, we can see that

- The MSSLC for the spacing between the leading vehicle in the destination lane and the merging vehicle increases very fast as the relative speed between the originating and the destination lane increases. On the other hand, the MSSLC for the spacing between the merging vehicle and the following vehicle in the destination lane increases very fast as the relative speed between the originating and the destination lane decreases, while the spacings between the merging vehicle and the leading and following vehicle in the originating lane remain small. Moreover, for $a_{comf} = 0.1$, the spacings between the merging vehicle and the leading and following vehicle in the originating lane remain almost constant as soon as the sign

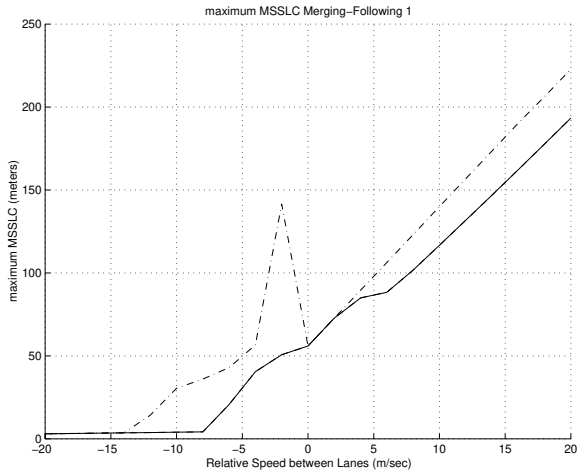

Figure 24: Maximum MSSLC for the spacing between the Merging Vehicle and the Vehicle f_1 versus Relative Speed between Lanes (solid curve: $a_{comf} = 0.1g$ and $t_{LC} = 5$ seconds; dash-dotted curve: $a_{comf} = 0.3g$ and $t_{LC} = 5$ seconds; dashed curve: $a_{comf} = 0.1g$ and $t_{LC} = 10$ seconds).

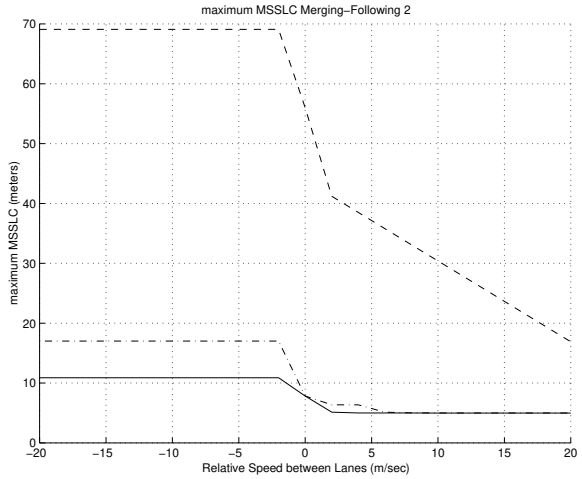

Figure 25: Maximum MSSLC for the spacing between the Merging Vehicle and the Vehicle f_2 versus Relative Speed between Lanes (solid curve: $a_{comf} = 0.1g$ and $t_{LC} = 5$ seconds; dash-dotted curve: $a_{comf} = 0.3g$ and $t_{LC} = 5$ seconds; dashed curve: $a_{comf} = 0.1g$ and $t_{LC} = 10$ seconds).

of the relative speed between the two lanes remains constant.

- The magnitude of the "control variable" a_{comf} affects significantly the MSSLC. In general, as can be seen in figures 14-17, the more aggressive is the adjustment in the longitudinal direction (i.e., the larger is a_{comf}), the larger are the safety spacings required.

- The "aggressiveness" of the lane change maneuver specified by the magnitude of the variable t_{LC} does not affect the MSSLC for the spacings between the merging vehicle and the vehicles in the originating lane, but affects considerably the MSSLC for the spacings between the merging vehicle and the vehicles in the originating lane. For instance, the MSSLC's for the spacings between the merging vehicle and the vehicles in the originating lane are in the range $4m - 30m$ in the case where $t_{LC} = 5$ seconds and they increase considerably (in the range $16m - 70m$) in the case where $t_{LC} = 10$ seconds.

- The main factor that affects the MSSLC is the relative speed between the two lanes. In general, the smaller is the relative speed between the two lanes the less is the required safety spacing.

- The sensitivity of the MSSLC with respect to the absolute speed of the two lanes is large. As it can be seen in the figures 14-17, for a given relative speed between the two lanes the MSSLC obtained for high absolute speeds is sometimes up to 50 meters larger than the MSSLC obtained for the same relative speed but for low absolute speeds. On the contrary, the worst case emergency braking time is not affected by the absolute speed, as it can be seen in Figures 18-21.

- The worst time for an emergency braking heavily depends on the relative speed between the two lanes as well. Moreover, the worst case emergency braking time for a particular spacing between two vehicles as a function of the relative speed between the two lanes, differs a lot with the worst case emergency braking time of the spacing between two other vehicles. Therefore, we cannot specify (given the lane changing policy and the relative speed between the two lanes) a particular time-instant of the lane-changing maneuver as the most "dangerous" for en emergency braking situation, i.e., as the time-instant at which an emergency braking will produce the worst results.

VII. Conclusions

In this work, we analyzed the problem of collision-free merging and lane changing. We examined various alternative scenaria for merging and lane changing and we presented an algorithm for calculating the *Minimum Safety Spacings for Lane Changing (MSSLC)*. The calculation of the MSSLC's for the merging or lane changing maneuver is more complicated from the calculation of the minimum safety spacings of the pure longitudinal case, since, in the former case we have to take into account the particular lane changing policy of the merging vehicle as well as the effect of combined lateral/longitudinal motion during the lane changing

maneuver. The braking profiles of the vehicles involved in a lane changing maneuver depend on the particular AHS operational concept, i.e., on the degree of communication between the vehicles and between the vehicles and the infrastructure. We considered six different AHS operational concepts; we presented the braking profiles of the vehicles for each operational concept and we investigated the effects of the particular operational concept to the MSSLC.

References

[1] J. L. Bascunana, "Analysis of lane change crash avoidance," *Systems and Issues in ITS*, (SP-1106), 1997.

[2] K. Enke, "Possibilities for improving safety within the driver vehicle environment control loop," *7th International Technical Conference on Experimental Safety Vehicles*, Washington, DC, National Highway Traffic Safety Administration, 1979.

[3] P. A. Ioannou, A. Kanaris, and F.-S. Ho, "Spacing and capacity evaluations for different AHS concepts," *Technical Report*, University of Southern California, 1995.

[4] T.D. Gillespie, *Fundamentals of Vehicle Dynamics*. Published by the SAE, 1992.

[5] S.E. Shladover, C.A. Desoer, J.K. Hedrick, M. Tomizuka, J. Walrand, W.B. Zhang, D.McMahon, and S. Sheikholeslam, "Automatic vehicle control development in the PATH program," *IEEE Transactions on Vehicular Technology*, vol. 40, pp. 114-130, 1991.

[6] Y. Sun and P.A. Ioannou, "A handbook for inter-vehicle spacing in vehicle following," *California PATH Research Report*, UCB-ITS-PRR-95-1, University of Southern California, 1995.

[7] R.D. Worall and A.G.R. Bullen, "An empirical analysis of lane changing on multilane highways," *Highway Research Board*, vol. 303, pp. 30-43, 1970.